

UNCLASSIFIED

AD NUMBER

ADC032302

LIMITATION CHANGES

TO:

Approved for public release; distribution is unlimited.

FROM:

Distribution authorized to DoD only; Specific Authority; 31 DEC 1983. Other requests shall be referred to Defense Advanced Research Projects Agency, Arlington, VA 22209.

AUTHORITY

darpa ltr, 1 may 1985

THIS PAGE IS UNCLASSIFIED

UNCLASSIFIED

AD NUMBER	
ADC032302	
CLASSIFICATION CHANGES	
TO:	UNCLASSIFIED
FROM:	CONFIDENTIAL
LIMITATION CHANGES	
TO: Distribution authorized to DoD only; Specific Authority; 31 DEC 1983. Other requests shall be referred to Defense Advanced Research Projects Agency, Arlington, VA 22209.	
FROM: DTIC Classified Users Only. Controlling DoD Organizaion: Defense Advanced Research Projects Agency, Washington, DC 22301. Dec 1977.	
AUTHORITY	
31 Dec 1983, per document markings; 31 Dec 1983, DoDI 5253.24	

THIS PAGE IS UNCLASSIFIED

AD C 032302

AUTHORITY: DARPA

1tr, 1 MAY 85



CONFIDENTIAL

0

AD C 032302

M-6

Los Alamos Scientific Laboratory
Los Alamos, New Mexico

A STUDY OF THE FORMATION AND PENETRATION
OF METAL JETS FROM TAPERED LINER EXPLOSIVE SYSTEMS (U)

DARPA Order Number 2993

containing #
(W 7405-ENG-36)

Final Report for the Period

January 1, 1976 to September 30, 1977

December 1977

DTIC FILE COPY

DTIC
ELECTE
AUG 30 1983
S D D

CONFIDENTIAL

83 08 19 501

CONFIDENTIAL

M-6

Los Alamos Scientific Laboratory
Los Alamos, New Mexico

A STUDY OF THE FORMATION AND PENETRATION
OF METAL JETS FROM TAPERED LINER EXPLOSIVE SYSTEMS (U)

DARPA Order Number 2993

Contract #
(W 7405-ENG-36)

Final Report for the Period

January 1, 1976 to September 30, 1977

December 1977

LASL Work Done By:

S. P. Marsh
R. L. Burback
J. M. Dickinson
J. L. Parkinson
J. M. Walsh

Report Written By:

S. P. Marsh
S. P. Marsh

Distribution:

Approved By:

Defense Advanced Research Projects Agency
1400 Wilson Blvd.
Arlington, VA 22209
Attn: Mr. Fred A. Koether
3 copies to the Director through
Program Management
2 copies to Dr. Ernest F. Blase

Director
USA Ballistic Research Laboratories
Attn: Security Officer
Aberdeen Proving Ground, MD 21005
for A. M. Dietrich
R. N. Thorn /S. D. Gardner, DIR-0, MS-100
A. D. McGuire, DIR-0, MS-120
W. E. Deal/B. G. Craig, M-DO, MS-682
E. Eyster/M. L. Brooks/L. W. Hantel, WX-DO, MS-686
R. D. Baker, CMB-DO, MS-756
Report Library, ISD-4, MS-362
S. P. Marsh, M-6, MS-970.

John W. Hopson
J. W. Hopson

Accession For	
NTIS GRA&I	<input type="checkbox"/>
DTIC TAB	<input checked="" type="checkbox"/>
Unannounced	<input type="checkbox"/>
Justification	
By	
Distribution/	
Availability Codes	
Dist	Avail and/or Special
9	

NATIONAL SECURITY
INFORMATION

Unauthorized Disclosure Subject to
Criminal Sanctions

Classified By: 00054

EXCLUDED FROM AUTOMATIC
DECLASSIFICATION
EXEMPTED FROM
DECLASSIFICATION
EXEMPTED FROM
DECLASSIFICATION
DECLASSIFIED ON DECEMBER 31, 1983.

Classified by
M-6 Group Leader

CONFIDENTIAL

TECHNICAL REPORT SUMMARY

1. Technical Problem

The objective of this study was to determine the phenomenology of a 76.2-mm diameter, tapered liner, shaped charge and to design a liner that would have a high penetration into hardened steel billets at a standoff of 2 meters.

2. General Methodology

Metals and contours for the tapered liners were varied and the performance of the shaped charges were monitored with a framing camera, flash x-rays, and penetration into hardened 4340 steel targets. The performance of the tapered liner charges was also studied by running calculations using the two-dimensional hydrodynamic code HELP.

3. Technical Results

Hydrodynamic calculations are necessary to design liner contours to avoid jet formation "pinch off" and radial instability of the jet and to assure a low liner collapse phase velocity and large jet mass.

Liners fabricated from annealed copper and tantalum form jets which undergo brittle fracture or nonuniform elongation. Sintering these metals does not eliminate the problem. Liners made of eutectic alloys of lead/tin and gold/germanium form jets which do not reduce to small diameter during elongation. Depleted uranium liners do form highly penetrating jets which elongate uniformly to small diameter.

4. DOD Implications

Depleted uranium can be used to form highly penetrating, pyrophoric jets in tapered liner charges which is not possible in conical systems.

CONFIDENTIAL

UNCLASSIFIED

M-6
Page 3

(This page is unclassified)

5. Implications for Further Research

Evidence was obtained that closer tolerances in depleted uranium tapered liner charges would make significant improvement in jet penetration. A study of this improvement would be valuable to the military.

CONFIDENTIAL

(This page is unclassified)

UNCLASSIFIED

ABSTRACT

↙ Calculational and experimental studies have been done on 76.2-mm diameter, tapered liner shaped charges to understand their phenomenology and to design a liner that would have a high penetration into hardened steel billets at 2 meters standoff. Rules governing the design of tapered liner contours affecting the liner collapse position and the collapse phase velocity are given. Tests of unsintered and sintered liners of copper and tantalum and tests of liners of eutectic alloys of Pb/Sn and Au/Ge produced jets which did not elongate properly nor reduce to uniform, small diameters. A design for a depleted uranium liner was tested which did elongate properly and had a high penetration into the target. ↘

A STUDY OF THE FORMATION AND PENETRATION
OF METAL JETS FROM TAPERED LINER EXPLOSIVE SYSTEMS (U)

I. INTRODUCTION

The standard method of producing armor-penetrating jets has been by means of shaped charges containing metal-lined conical cavities. Although it has been known for over 20 years that a jet could be formed by the explosive collapse of a metal-lined rounded cavity (herein called a tapered liner charge or TLC), no studies have been done to determine the characteristics of these jets and the effects of varying the cavity shape and the thickness profile of the tapered metal liner.

In this study several parameters in tapered liner charges were varied to study their effect on the formation and performance of the resulting jet. These parameters were liner metal, liner porosity, and liner contour. In addition, a system was designed to maximize mass in the jet, kinetic energy of the jet, and radial stability in an effort to achieve the maximum penetration of a hardened steel target at a standoff of two meters for use in the ATAADS application.

II. SCOPE OF STUDY

Fifty-six different TLC's were studied. Of this total, twelve designs were studied using both hydrodynamic calculations and experiments to compare the results of both methods. Thirty-two designs were studied with hydrodynamic calculations only. These were primarily systems in which continuous liner variations were made in an attempt to find optimum performance. And twelve designs were studied using experiments only. These were designs having a greater departure from others that had been studied up till then.

III. DESCRIPTION OF TAPERED LINER CHARGES (TLC'S) AND THEIR VARIATIONS

The dimensions and materials used for the three configurations of TLC's studied are given in Appendix A. The high explosive charges were cased in mild steel cylinders having a wall thickness of 3.2 mm. The detonator was placed in the center of the back face of the charge and the tapered liner was located in a cavity on the opposite face. A 6.4-mm-thick mild steel flange is also located on this face and extends 3 mm inside of the inner surface of the liner.

Six different liner materials were studied. These were copper, tantalum, uranium (D-38), lead/tin eutectic alloy, gold/germanium eutectic alloy, and free-cutting brass. These are described in Table I. Most copper liners were fully annealed but one experiment was performed with fully hardened copper. Calculations were run on copper and tantalum liners with porosities of 4% and 8% each and experiments were done on all but the tantalum liner with 4% porosity. Three tests were done using a brass liner. Eutectic alloys were selected for liner material tests because their low melting points caused them to melt on the first shock from the high explosive and to remain melted (or partially melted) on release to zero pressure along their isentropes.

Hydrodynamic calculations were run to study variations of the inner and outer contours of unsintered copper and tantalum, D-38, and both eutectic alloys with experiments being done on a few selected designs. Calculations were also run on the specific contours chosen to be tested in experiments on sintered copper and tantalum liners. Twelve experiments were performed using copper, brass, and Pb/Sn eutectic liners to test designs for which no calculations were run. These were primarily departures from the more usual liner contours studied up till that time. The method used in designing contours is given in a following section.

Variations were made in both the dimensions and materials of the high explosives used in the shaped charges. Changes in the high explosive were made primarily for the purpose of facilitating fabrication and thus significantly reducing the unit cost of the charges rather than for making a controlled study of the effect of these changes. Machined PBX-9501 (a pressed, bonded explosive containing 95 wt% HMX, 2.5 wt% nitroplasticizer, and 2.5 wt% estane) was used in 11 experiments and a combination of composition B-3 and composition C-4 was used in the remaining 13 experiments. One calculation was performed using a shortened cylinder of 9501 (76.2 mm) to determine its effect on liner collapse.

IV. HYDRODYNAMIC CALCULATIONS

The HELP code is a multi-material Eulerian program for compressible, elastic-plastic fluid flows in two space dimensions and time. It was written by Systems, Science, and Software in 1970 and has been in use at LASL since 1975.

HELP deviates from the pure Eulerian model by employing massless tracer particles to track material interfaces and free surfaces. This Lagrangian-type definition of moving surfaces allows the tracing of material flow without sacrificing the capability of treating extreme distortions.

In addition to the tracer particles the HELP code also contains sliplines, a high explosive detonation model, and a very versatile setup generator.

V. METHOD FOR OBTAINING LINER CONTOURS

In designing deep contours a small computer modeling code CONTOUR was used. Its usage depended on having the results of a two-dimensional hydrodynamic calculation on which to normalize. This was accomplished as follows. The mass trajectories and collapse timing of the inner surface of the liner was determined from a HELP run. The code CONTOUR determined the kinetic energy imparted to each mass element and the angle between the normal to the

inner surface and the velocity vector for each mass element (see Fig. 1). Then, having these values, the desired trajectories and collapse times were input into CONTOUR from which variations on the original contours were calculated to approximate these new trajectory and collapse conditions in the next hydrodynamic iteration. The use of this program was only partially successful because successive iterations would develop unexplained thick regions on the outer contour within 10-15 degrees of the axis of symmetry and consequently convergence of the contour design to the desired hydrodynamic performance would sometimes not occur. In these cases the outer contour was approximated in this region.

Because the boundaries of the mass elements were surfaces of cones whose apex was on the axis of symmetry and lying in the equatorial plane of the liner, CONTOUR could not be used to design liners that were relatively shallow (the polar radius being considerably smaller than the equatorial radius). In this case the velocity vector of a mass element makes a large angle with the element boundaries. The kinetic energy of the element is very poorly handled for this case, and the CONTOUR-HELP iterations become nonconvergent.

Consequently, a different method was used to design the shallow liners in which no iterations on contour designs were performed. This method assumes that the velocity vector of a mass element is normal to the inner surface of the element. If points are selected along the axis to which the velocity vectors of the various mass elements should be directed for proper liner performance, this determines the contour of the inner surface (see Fig. 2). Because no collapse timing enters this method, it does not determine the outer contour of the liner. It was specified in a similar manner requiring

the inner and outer contours to have the same center of curvature at the pole and that the equatorial thickness be one-half the polar thickness. The r, θ coordinates for the contours studied are given in Appendix B.

VI. EXPERIMENTAL PROGRAM

Data were obtained on tests of the TLC's with 1) a framing camera to record the early motion of the liner if permitted by its condition, 2) flash x radiography to determine the condition and velocity of the jet, and 3) target penetration at a standoff of 2 meters.

Framing camera records were obtained with either a Beckman-Whitley Model 189 or a Cordin Model 120 framing camera. These have comparable resolutions and were operated at framing rates of 1 μ s/frame in all cases. The tapered liners were illuminated with explosively shocked gas boxes containing mixtures of argon and xenon. The position of the inner surface of the liner was obtained by observing the position of coordinates painted on this surface with respect to a fixed transparent grid of points placed in front of the moving liner. These data were analysed by means of the code, HAT.

Flash radiographs of the jets in motion were taken with two 480 keV remote x-ray heads of Hewlett-Packard flash x-ray units, which have x-ray pulse durations of 20-30 ns. Kodak XR-5 film and Radelin TI-3 intensifying screens were used in screen-film-screen combinations. The source-film distance was 4.3 meters and the jet-film distance was 0.3 meters. The film and screen were protected by a 12.7-mm-thick plate of 6061 aluminum. In most cases, the first x ray was triggered 150 μ s after the detonator signal and the second x ray was triggered 8-10 μ s after the first.

The targets used to test for jet penetration were 4340 steel cylinders, 150 mm long and 150 mm in diameter. They were hardened uniformly to BHN 308 \pm 9 using a process supplied by R. L. Woodall of Firestone Tire and Rubber Company,

modified slightly because of the limitations of available equipment (see Appendix C). In all experiments the targets had a standoff of 2.0 meters, which is 26.3 charge diameters. The reasons for this standoff was to permit x radiographs to be made of the undisturbed jets and to simulate the ATAADS requirements in which this standoff penetration capability is necessary.

VII. CALCULATIONAL AND EXPERIMENTAL RESULTS

A complete presentation of the calculational and experimental results for each shaped charge is given in Appendix D and a summary of these results appears in Tables II and III.

A. Comparison of Calculations and Experiments

The liner collapse phase of a number of the systems was investigated using both calculations and framing camera to compare the results obtained by each. The systems in which these comparisons can be made in Appendix D are TLC-6, 7, 23, 24, 37 and 38.

It can be seen that differences exist in both the inner liner contours and the trajectories of fixed points on the inner liner surfaces. These differences in the contour positions are less than 1 mm over the experimental range corresponding to time differences of less than 0.3 μ s, which is small compared to the time required for the liner to collapse. The angular differences in the initial trajectories are less than 4 degrees with the linear displacement growing to 1.5 mm at later times on one of the trajectories in TLC-38. In general the agreement was much better than this.

An attempt was made to reduce the differences in the contours and trajectories by including the detonator booster charge in the calculation. This system is TLC-37 and the corresponding system with no booster is TLC-6. It

can be seen in Fig. 4 that the agreement between the contours of the calculation and experiment improves when the booster charge is included. However, the trajectories are not improved by this change. All other problems were run with no booster charge because the study was nearly completed when this improvement was found. Additional attempts at minimizing calculational and experimental differences were made by varying the effective charge length and the equation of state of both the HE and liner without success. At the present time we do not know why this disparity exists unless it can be related to the accuracy of the positioning of the detonator on the back of the charge or the bowing of the transparent grid by helium pressure in the liner at the time of the experiment. These possibilities have not been investigated.

The importance of contour and trajectory differences is perhaps indicated by comparing the jet tip velocity, radial stability, and mass-velocity distribution from both calculations and experiments even though it is not known how well these jet properties would agree if there was no disagreement in the contours and trajectories. The comparison of tip velocity and mass for velocity over 3 km/s can be made in Table III for those systems in which jet properties were obtained in both calculations and experiments.

In general, tip velocities are in reasonable agreement with the experimental values averaging 5% higher than the calculations. But the radial stability of the jet does not agree well (see Appendix D) especially for the deep liner designs in which the calculated trajectories show radial divergence not seen in the radiographs. Most of the calculations for deep liners show some outward component of velocity yet radial instability of the body of the jet (excluding the tip) can only be definitely identified in two radiographs, TLC-43 and 53. An imperfection in the fabrication of the D-38 liner of TLC-43

is thought responsible for its instability. No tensile strength (only shear strength) is used in the HELP calculations which may account for the jet rebounding radially outward if any outward radial velocity component exists.

The calculated total mass traveling above a velocity of 3 km/s averages about 70% of the corresponding experimental value. (See Appendix D for the method used to determine the masses and velocities of the jets.) It is not understood how a difference of this magnitude could result from the differences in the calculated and experimental liner contours and trajectories. However, it is possible that the assumption of crystal density and cylindrical symmetry for the jet mass may not be valid. The mass difference is too large to account for entirely in this way. As more experience was gained in conducting the experiments, the agreement between calculated and experimental masses improved. It is also significant that the slope of the experimental mass-velocity distribution in these jets agrees reasonably well with the calculations. In spite of these differences, the HELP code gives good insight into the collapse dynamics of the liners and the jet formation.

B. Contour Variations

Calculations were run on shaped charges having different liner contours producing varying effects on the collapse dynamics and the resulting jet. Because of the infinite number of contours that are possible for a tapered liner charge, this cannot be considered an exhaustive study in any sense; however, some observations can be made. These are summarized below and discussed in the following paragraphs.

1. Thinning a liner increases its collapse velocity although a maximum must exist in the kinetic energy vs liner thickness function.
2. Liners whose mass near the equator arrives at the axis before the mass near the pole can "pinchoff" jet formation.

3. Decreasing the collapse phase velocity from 5 to less than 3 km/s in a deep liner (one whose polar radius exceeds its equatorial radius)
 - a) decreases its tip velocity and b) improves mass uniformity in the jet.
4. Increasing the collapse distance by moving the focal point of liner collapse away from the liner pole
 - a) improves jet radial stability and b) decreases the velocity gradient with an accompanying decrease in mass having velocity greater than 5 km/s and an increase in mass having velocity greater than 1 km/s.

1. Collapse Velocity

Calculations were run with copper, tantalum, D-38, and Pb/Sn alloy liners, varying their thicknesses but keeping the outer pole height constant. The maximum kinetic plus internal energy of each liner was obtained and is plotted as a function of polar thickness in Fig. 3. The total kinetic energy of the jet and the kinetic energy for that mass having velocity greater than 3 km/s are also shown. It can be seen that the liner and jet energies increase as the polar thickness decreases. Although no maximum is obtained over this range of polar thickness one must exist because as the thickness approaches zero the total energy must vanish. Because there is more scatter in the jet kinetic energy distribution than there is in the total liner energy distribution the kinetic energy must be more dependent on the liner contour variations.

2. Equatorial Pinchoff

Several calculations were performed with liners that were thin enough in a region near the equator that the mass from that region collapsed (arrived

at the axis) before mass that was near the pole. The result of this is the pinching off of the polar mass, which prevents the normal formation of a jet. Evidence of this is the deceleration of liner mass at the pole. For examples of this see TLC-8, 15, and 16.

3. Collapse Phase Velocity

The term "collapse phase velocity" refers to the velocity of the focal point of liner collapse. This point is determined by extrapolating the early and more linear portions of the liner trajectories to the axis of symmetry. The consideration of this velocity was useful in improving the design of liner contours.

Systems whose collapse phase velocity is high (greater than 5 km/s) or whose collapse is nearly simultaneous (within 0.5 μ s) to a point (within several millimeters) have common jet formation characteristics (Table II). Radiographs show a small amount of mass in the front half of the jet compared to the mass in the back half. Further, these systems are very sensitive to manufacturing tolerances because the jets are generally very nonlinear. (See TLC-5, 6, 7, 23, and 24.)

Systems whose collapse phase velocity is low (3 km/s or less) have collapse focal points which extend over longer distances and have jets with a more even distribution of mass along their length. They appear to be less sensitive to manufacturing tolerances because of their greater linearity. The mass-velocity gradients in these systems are lower and they have lower jet tip velocities. (See TLC-18, 28, 38, 39, 41, 42, and 43.)

4. Collapse Distance

The distance from the equator to the focal point of collapse for liner mass in the vicinity of the pole will be called "collapse distance". Although its influence cannot be separated completely from the collapse phase velocity,

the effect of extreme variations in collapse distance can be seen. The shallow liners are those having a large collapse distance.

The HELP calculations show a more radially stable jet for large collapse distances (see TLC-32 to 36). For these systems there is no radially outward component of the jet velocity whereas for systems with short collapse distances even quite stable systems (those with a collapse phase velocity less than 3 km/s) can have some outward component visible in the calculated trajectories (see TLC-28, 29, and 30) although there are some systems which have none (see TLC-39, 40, and 41).

Both calculations and radiographs indicate the larger collapse distance to be associated with smaller tip velocities and smaller velocity gradients in the jet, similar to the effect of low collapse phase velocities (see TLC-32 to 36).

C. Liner Metal Variations

The metals used for liners in this study can be divided into two groups, those which remain solid and those which liquify during collapse. With the exception of two metals, all of the jets appear to have remained in the solid state. The indication that this is true is best shown by viewing the radiographs of the four jets of eutectic alloys, which could not have been solid because the internal energy of the initial high explosive shock is adequate to liquify or partially liquify them at the foot of the release isentropes. These jets have diffuse edges different from all of the other jets and this is considered to be evidence of the liquid phase of the jet. The radiographic appearance of a jet in a mixed phase is not known but possibly would have an appearance similar to a liquid jet.

Annealed copper did not perform well in forming elongating ductile jets in tapered liner charges. Although in most cases there is a region near the

front of the jet, which appears to undergo ductile elongation in the radiographs, there is a larger diameter region toward the back of the jet, which either undergoes brittle fracture rather than drawing out to a long, small diameter rod (see TLC-5, 6, and 7), or which shows lumps of copper which are not drawing out although the adjacent mass appears ductile (see TLC-38).

Two causes for this different behavior between the front and back of copper jets were considered, the variation in strain rate and the variation of temperature (or internal energy) along the jet. The velocity along the jet for system TLC-6, a system manifesting this front-to-back ductility problem, is shown in Fig. 5. A constant velocity gradient is seen to exist so the strain rate is uniform along the jet and this cannot explain the jet behavior. Two variations were made in the copper liners to study the effect of changing the internal energy of the jet. A fully hardened copper liner was fabricated and fired in a system identical to one in which an annealed copper liner had been used (see TLC-31 and 44). The plastic work done on the hardened copper during its collapse increased its temperature (an undetermined amount) above that of the annealed liner. However, no difference in ductile behavior can be seen in the two radiographs for these systems. In the second variation, two sintered copper liners having 4% and 8% porosity (in the annealed state) were fired in a system manifesting the ductility problem when annealed copper having no porosity was used. (See TLC-7, 23, and 24 which have 0, 4, and 8% porosity, respectively.) Additional internal energy is now put into the liners by virtue of the collapse of the voids by the initial shocks from the explosive. This increases the liner temperatures by about 150 and 400 K for the liners having 4% and 8% porosity, respectively. Differences appear in the jet radiographs but the changes are in the ductile part of the jet rather than in the nonductile region. The ductile region appears to

undergo a finer particulation for the sintered copper but the nonductile region still appears nonductile and undergoes brittle fracture as can be seen from the large irregular pieces. Consequently, neither strain rate nor internal energy can be shown to be causing the problem in these copper jets.

Tantalum exhibits the same ductility problem shown by copper (see TLC-39). Sintering tantalum to 8% porosity again did not remove the problem although some improvement resulted. (see TLC-41),

Uranium (D-38) appeared to undergo ductile elongation in both of the systems in which it was used (TLC-42 and 43). It can be seen to elongate to a thin rod with a diameter of 1 mm near the tip in TLC-42. Particulation is just beginning near the tip of the jet.

Radiographs of free machining brass jets (TLC-50, 51, and 52) indicate a fine particulation which may be related to separation along intergrain boundaries in the metal. There is no indication of ductile drawing of the jet however.

Eutectic alloys of Pb/Sn and Au/Ge were designed and fired to determine whether the ductility problem manifested in copper and tantalum jets could be solved by using liquid jets (see TLC 18, 53, 54, and 28). The jets elongate with no evidence of either the lumps or brittle fracture manifested in copper and tantalum. However, the lack of tensile strength apparently prevents the jets from reducing to a uniform, small diameter in these particular designs.

D. HE System Variations

Three different main explosive charges were used in these systems (see Appendix A). The first two had PBX-9501 with lengths of 120 and 76 mm. The short charge was used only in TLC-56 for which only a calculation was done. The third HE system was a combination of composition B-3 and composition C-4 in which composition C-4 was packed around the outer contour of the liner until

there was a thickness of 25 mm of explosive over the liner pole. A cylinder of composition B-3 was then placed in contact with the back face of composition C-4 to complete the main charge. The C-J pressures were approximately 38 and 29 GPa in the PBX-9501 and comp B/C systems, respectively.

Calculations were run on systems having total charge lengths of 120 mm and 76 mm. The comparison of liner collapse for these calculations is shown in Fig. 6. The mass velocities vary the most at the pole with the collapse time increasing for the shorter HE systems which resulted in pinchoff in this case. It appears from this that the collapse phase velocity can be modified with charge length and that perhaps a charge length can be found which will create the desired collapse phasing of a hemispherical liner.

E. Energy Efficiency

The calculated total energy of the liners (kinetic and internal) are given in Table III along with the jet kinetic energies (for all mass and for mass having velocity greater than 3 km/s). Approximately 70 to 90% of the liner energy is converted into kinetic energy of the total jet mass. Approximately 45 to 60% of the liner energy is converted into kinetic energy of that jet mass having velocity greater than 3 km/s. This mass is approximately 10 to 20% of the total liner mass.

F. Target Penetration

Most of the jets formed in TLC systems were nonlinear and consequently had poor penetration in hardened steel targets. These penetrations varied from just a few millimeters for TLC-28 and 51 to over 70 mm for TLC-38, 39, 41, and 42. The most successful penetration was achieved with the D-38 jet from TLC-42 in which 155 mm of steel was penetrated.

The volumes of these penetrations were also highly variable. A volume could not be assigned to the penetrations of the poorly formed jets in TLC-5, 6, 7, 18, 23, 24, and 28. However, in later designs the volumes clustered mainly between 15 and 20 cm³. The largest volume obtained was 23.3 cm³, which was achieved with the jet from the hardened copper liner. Using a constant value for the jet kinetic energy per unit volume of penetrations listed in Table III a correlation of volume with calculated jet energy was attempted. Because of jet nonlinearity a correlation was not found.

G. Precision of Manufacture

The shaped charges reported here cannot be considered precision shaped charges. The tolerances on the liner and HE contours for charges containing PBX-9501 were ± 0.03 mm in the X and Z coordinates, which were machined on tape-controlled milling machines. The clearance allowed for the cement layer bonding the liner to the charge was approximately 0.10 mm. In the comp B/C systems the liner machining tolerance was ± 0.06 mm. This resulted from approximating the contoured surfaces by machining a series of 2 to 5 spherical zones on the liner faces (depending on its nonsphericity) using a manually controlled milling machine. The remaining HE and case machining tolerances were approximately ± 0.03 mm for both the PBX-9501 and comp B/C systems.

H. Jet History in TLC Systems

Jet formation in conical systems is a continuing process as various parts of the liner arrive at the axis of the charge. It is approximated in calculations as a steady-state process. However, in tapered liner charges the jets arrive at their final mass-velocity profiles just 2 to 4 μ s after collapse and thus are much more rapidly formed than in conical systems.

Whereas the breakup of a jet from a conical system is approximated as being simultaneous, jet breakup in a TLC system is much slower with breakup toward the tip occurring considerably earlier than breakup toward the base of the jet. This can be observed clearly in TLC-38 and 42. However, experiments do not give an understanding of why this occurs.

VIII. CONCLUSIONS

Calculational and experimental studies have been made on tapered liner charges to develop long standoff penetration capability and to understand the phenomenology of these systems. Variations were made in liner materials and liner contours for 76.2-mm-diameter systems producing the following results.

1. During liner collapse, hydrodynamic calculations (HELP) agree with framing camera results within 1 mm in liner positions and within 4 deg in liner trajectories, which is sufficiently close for the calculations to be useful in liner design.
2. Following jet formation, HELP calculations indicate a jet tip velocity approximately 95% of the radiographic value and jet masses which average approximately 70% of the radiographic value.
3. Hydrodynamic calculations are necessary to design liner contours for the following reasons: a) to avoid equatorial pinchoff of the liner mass during collapse, b) to assure a liner collapse phase velocity of less than 3 km/s, required for good jet mass distribution, c) to avoid jets which have a large outward radial velocity component, and d) to maximize jet mass traveling greater than a given specified velocity.
4. Liners fabricated from annealed copper and tantalum do not undergo uniform ductile elongation in jets, exhibiting lumps or brittle fracture in some regions of the jets. Sintering these metals did

not correct this problem. Liners fabricated from eutectic alloys form diffuse jets which do not reduce to small diameter during elongation. Liners fabricated from depleted uranium have produced jets which undergo ductile elongation resulting in diameters of 1-2 mm prior to particulation.

5. Of the total energy imparted to the liner (300-350 kJ) approximately 80% appears as kinetic energy of the total jet mass and approximately 50% appears as kinetic energy of that jet mass having a velocity of 3 km/s or greater. This mass is approximately 10 to 20% of the total liner mass.
6. Maximum penetration achieved for jets into 4340 steel (hardened to BHN 300) at a standoff of 26 charge diameters was 0.94, 1.36, and 2.03 charge diameters for copper, tantalum, and depleted uranium, respectively. These penetrations were limited primarily by the extent of elongation of the jet mass. The maximum hole volumes achieved were about 20 cm³.
7. Nonprecision shaped charges were used in obtaining the above results. No components had fabrication tolerances less than ± 0.03 mm in any dimension.

TABLE I. Description of Liner Metals

Metal	Composition	Condition	Porosity	Density
			(%)	(g/cm ³)
copper	copper	annealed	0	8.92
copper	copper	fully hard	0	8.90
copper	copper	annealed	4	8.56
copper	copper	annealed	8	8.21
tantalum	tantalum	annealed	0	16.65
tantalum	tantalum	annealed	4	15.98
tantalum	tantalum	annealed	8	15.32
uranium	uranium	annealed	0	18.95
Pb/Sn eutectic	Pb-62 wt% Sn	as-cast	0	8.43
Au/Ge eutectic	Au-12 wt% Ge	as-cast	0	14.6
brass (capra-360)	Cu-35.5 wt% Zn 3 wt% Pb	half hard	0	8.45

TABLE II. Tapered Liner Charge Parameters

TLC No.	HE System	Contour	Metal	Liner		Mass (g)	HELP	HELP
				Pole Ht. (mm)	Pole Tk. (mm)		Collapse Position (mm)	Collapse Phase Vel. (km/s)
1	A	1	Cu	33	6	85	0	9
2	A	2	Cu	35	6	87	0	s ^a
3	A	3	Cu	35	4.5	58	-3	i ^b
4	A	4	Cu	30	4	43	0	s
5	A	5	Cu	35	6	91	0	9
6	A	6	Cu	35	4	68	0	5
7	A	7	Cu	35	8	104	0	s
8	A	8	D-38	35	2	93	1	i
9	A	9	D-38	35	4	176	-2	s
10	A	10	D-38	35	6	241	-1	s
11	A	11	D-38	35	8	288	0	s
12*	A	12	D-38	35	1	53	-	-
13	A	13	D-38	35	2	106	2	i
14	A	14	D-38	35	4	206	3	i
15	A	15	D-38	35	2	93	1	s
16	A	16	D-38	35	2	98	1	s
17	A	17	D-38	35	2	107	3	s
18	A	7	Pb/Sn	35	8	99	0	2
19	A	18	Pb/Sn	35	8	89	0	i
20	A	19	Pb/Sn	35	8	84	8	i
21	A	20	Pb/Sn	35	8	105	4	i
22	A	21	Au/Ge	31	4	81	-1	14
23	A	7	Cu, 4%	35	8	100	0	s
24	A	7	Cu, 8%	35	8	96	0	s
25	A	22	Au/Ge	31	4	114	-1	3
26	A	23	Au/Ge	31	4	104	-2	i
27	A	24	Au/Ge	31	4	123	-2	3
28	A	25	Au/Ge	31	4	163	-3	2
29	A	26	Au/Ge	31	4	180	-2	3
30	A	24	Ta	31	4	141	-2	3
31	C	34	Cu	35	6	154	3	-
32	A	27	Ta	18	4	212	20	-
33	A	28	Ta	15.4	2	87	20	-
34	A	29	Ta	21.5	4	211	10	-
35	A	30	Ta	16.6	2	87	10	-
36	A	31	Ta	19.5	2	99	10	-
37	A	6	Cu	35	4	68	0	-
38	C	32	Cu	35	4	120	0	-
39	A	33	Ta	35	2	117	-4	-
40	A	33	Ta, 4%	35	2	112	-4	-
41	A	33	Ta, 8%	35	2	107	-3	-
42	A	33	D-38	35	2	133	-3	-
43	A	31	D-38	19.5	2	113	15	-
44	C	34	Cu, hard	35	6	154	-	-
45	C	27	Cu	18	4	114	-	-

TABLE II. Tapered Liner Charge Parameters

TLC No.	HE System	Contour	Metal	Liner			HELP Collapse	HELP Collapse
				Pole Ht. (mm)	Pole Tk. (mm)	Mass (g)	Position (mm)	Phase Vel. (km/s)
46	C	28	Cu	15.4	2	46	-	-
47	C	29	Cu	21.5	4	113	-	-
48	C	30	Cu	16.6	2	47	-	-
49	C	31	Cu	19.5	2	53	-	-
50	C	35	Brass	35	8	76	-	-
51	C	36	Brass	35	8	122	-	-
52	C	25	Brass	31	4	94	-	-
53	C	29	Pb/Sn	21.5	4	107	-	-
54	C	32	Pb/Sn	35	4	111	-	-
55	A	6	Cu**	35	4	68	0	-
56	B	6	Cu	35	4	68	-2	-

* Calculation unstable

** No shear strength

a Near-simultaneous collapse to a point

b Irregular collapse phase velocity

TABLE III. Tapered Liner Charge Results

TLC No.	Jet Tip Velocity		Mj (v>3 km/s)		Calculated Energies			KE _{jet} / E _{liner} tot.		Target Penetration	
	Calc. (km/s)	Exp. (km/s)	Calc. (g)	Exp. (g)	E _{liner} tot. (kJ)	KE _{jet} tot. (kJ)	KE _{jet} v>3 (kJ)	KE _{jet} / E _{liner} tot.	KE _{jet} v>3 / E _{liner} tot.	Depth (mm)	Vol. (cm ³)
1	14.4		9.3		298	235	162	0.79	0.54		
2	11.5		11.6		320	229	160	.72	.50		
3	13.8		13.3		322	222	165	.69	.51		
4	9.8		9.5		241	168	129	.70	.54		
5	13.3	11.0	11.9	16.1	323	252	174	.78	.54	40	-
6	13.3	9.4	17.9	9.8	349	297	235	.85	.67	7	-
7	12.7	12.3	10.3	24.8	293	225	144	.77	.49	17	-
8	-				351						
9	-				306						
10	-				251						
11	-				211						
12	-				-						
13	11.8		13.2		355	272	219	.77	.62		
14	8.2		7.6		286	171	69	.60	.24		
15	13.0		14.3		349	284	194	.81	.56		
16	10.4		11.9		343	260	152	.76	.44		
17	14.0		12.1		341	254	147	.74	.43		
18	10.1	8.9	12.4	-	311	219	147	.70	.47	8	-
19	20.5		14.0		316	234	167	.74	.53		
20	13.3		11.1		318	243	164	.76	.52		
21	7.2		11.9		301	221	147	.73	.49		
22	14.1		9.9		272	199	120	.73	.44		
23	14.7	8.6	10.5	9.6	301	225	148	.75	.49	23	-
24	14.6	9.2	10.0	-	310	229	149	.74	.48	21	-
25	11.3		9.9		280	221	148	.79	.53		
26	6.8		12.5		282	208	129	.74	.46		
27	8.8		13.2		289	228	152	.79	.53		
28	8.1	7.3	13.2	-	281	220	123	.78	.44	3	-
29	8.0		11.1		270	192	99	.71	.37		
30	7.6		11.9		270	197	114	.73	.42		

TABLE III. Tapered Liner Charge Results

TLC No.	Jet Tip Velocity		Mj (v>3 km/s)		Calculated Energies		KE _{jet} tot.		KE _{jet} tot.		Target Penetration	
	Calc. (km/s)	Exp. (km/s)	Calc. (g)	Exp. (g)	E _{liner} tot. (kJ)	KE _{jet} tot. (kJ)	KE _{jet} tot. (kJ)	E _{liner} tot.	KE _{jet} tot. E _{liner}	KE _{jet} tot. E _{liner}	Depth (mm)	Vol. (cm ³)
31	-	-	-	16.2	204	161	0	.79	0		46	16.1
32	2.4	-	0	-	254	242	68	.93	.27			
33	4.2	-	12.2	-	215	176	0	.82	0			
34	3.0	-	0	-	257	240	76	.93	.30			
35	4.3	-	12.9	-	269	245	95	.91	.35			
36	4.3	-	16.3	-	333	267	186	.80	.56			
37	13.9	-	13.7	-	224	208	118	.93	.53			
38	5.4	5.8	15.5	18.4	340	257	158	.76	.46		72	21.0
39	6.0	6.2	20.3	31.5	347	260	169	.75	.49		86	21.5
40	6.1	-	21.8	-	355	261	172	.74	.48			
41	6.1	6.7	21.8	34.2	337	246	148	.73	.44		104	23.1
42	6.2	6.4	19.3	37.4	265	215	74	.81	.28		155	19.0
43	4.3	4.9	12.0	16.7							50	11.3
44	-	4.6	-	13.2							31	23.3
45	-	4.4	-	1.9							24	15.3
46	-	5.6	-	6.4							32	15.6
47	-	3.8	-	6.5							32	13.0
48	-	5.4	-	13.1							23	16.3
49	-	4.6	-	8.4							27	16.0
50	-	-	-	-							11	-
51	-	-	-	-							2	-
52	-	8.9	-	-							50	8.7
53	-	5.2	-	-							33	3.2
54	-	6.8	-	-							26	4.8
55	16.9	-	16.1	-	350	292	226	.83	.65			
56	-	-	-	-	272							

UNCLASSIFIED

Fig. 1. Mass element parameters determined by CONTOUR code. The angle β between the velocity \vec{V} and the normal \vec{N} and the kinetic energy of each mass element are determined by CONTOUR and are used in determining modifications to these contours.

UNCLASSIFIED

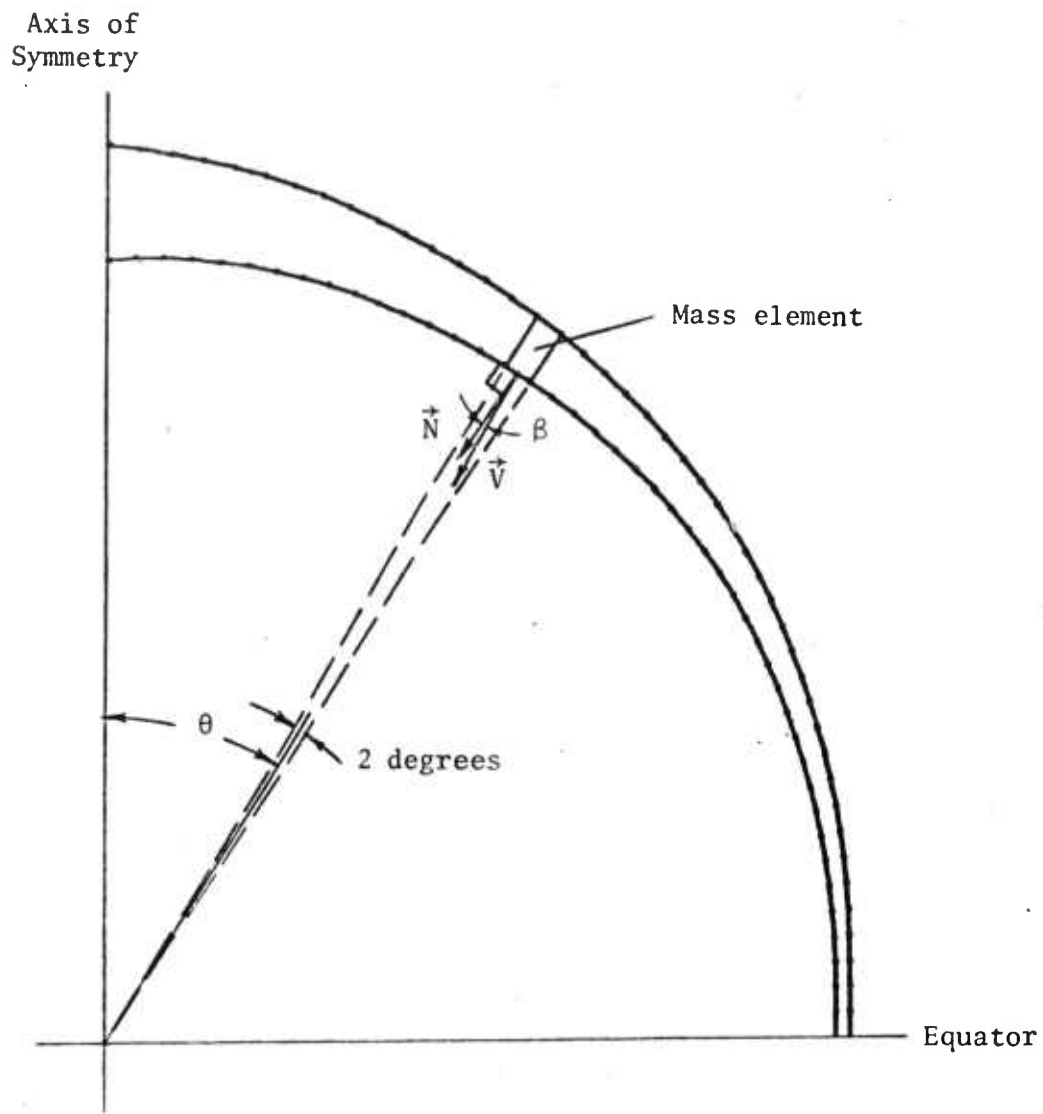


Fig. 2. Determination of shallow liner contours. The inner contour was determined by varying the radius of curvature continuously (and linearly with the polar angle θ) from the pole to the equator. The locus of the center of curvature is indicated and was determined by the position of liner collapse desired at any polar angle. The outer contour was determined in a similar way with the center of curvature being the same as the inner contour at the pole and the center of curvature at the equator determined by the requirement that the equatorial liner thickness be one-half of the polar thickness.

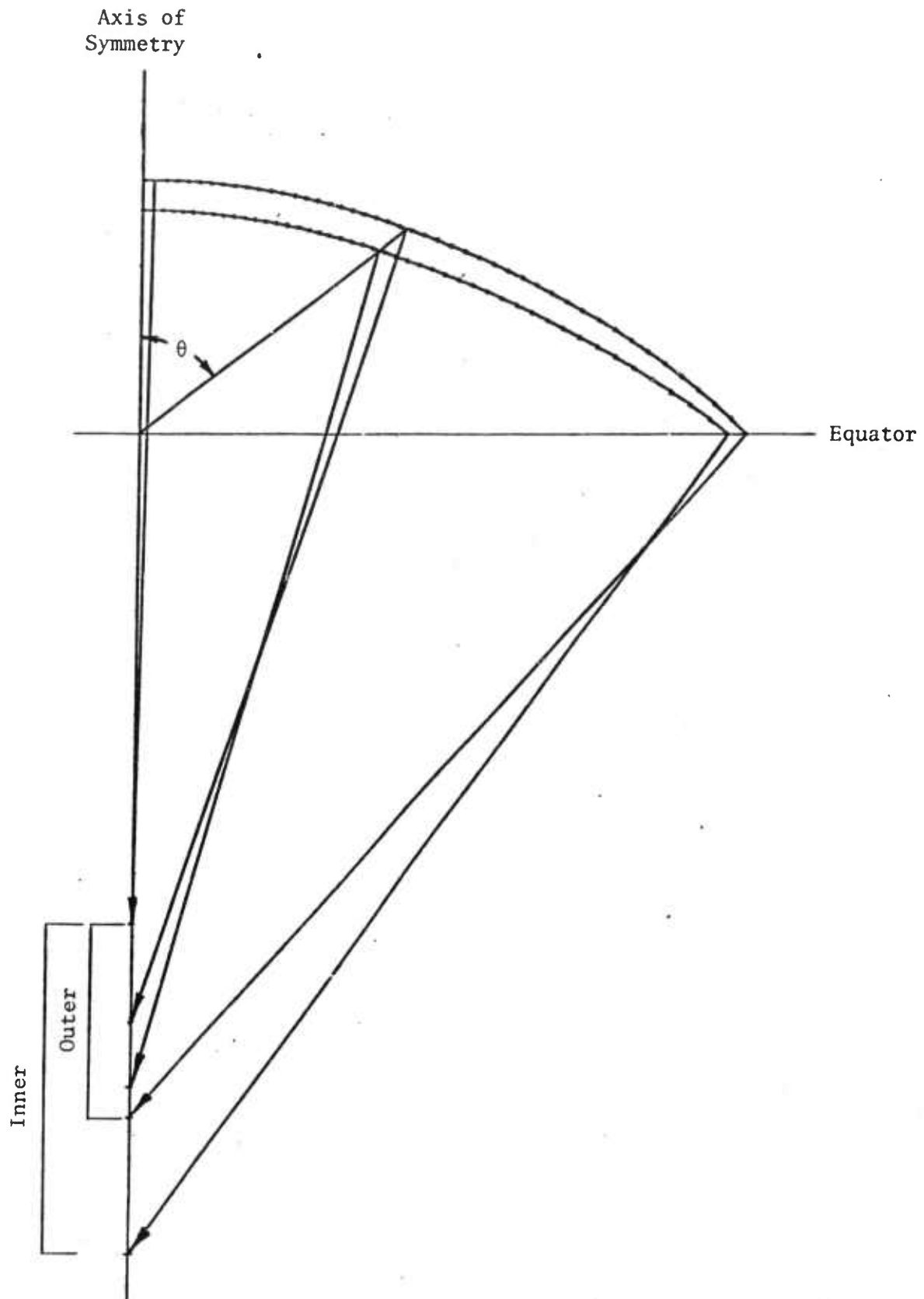


Fig. 3. Liner and jet energy variation with polar thickness. The maximum total energy of the liner (o), kinetic energy of the jet (Δ), and kinetic energy of the jet mass having velocity greater than 3 km/s (\square) are shown as functions of polar liner thickness (D-38 mass equivalent). All systems are included that have an outer pole height of 35 mm with high explosive system A.

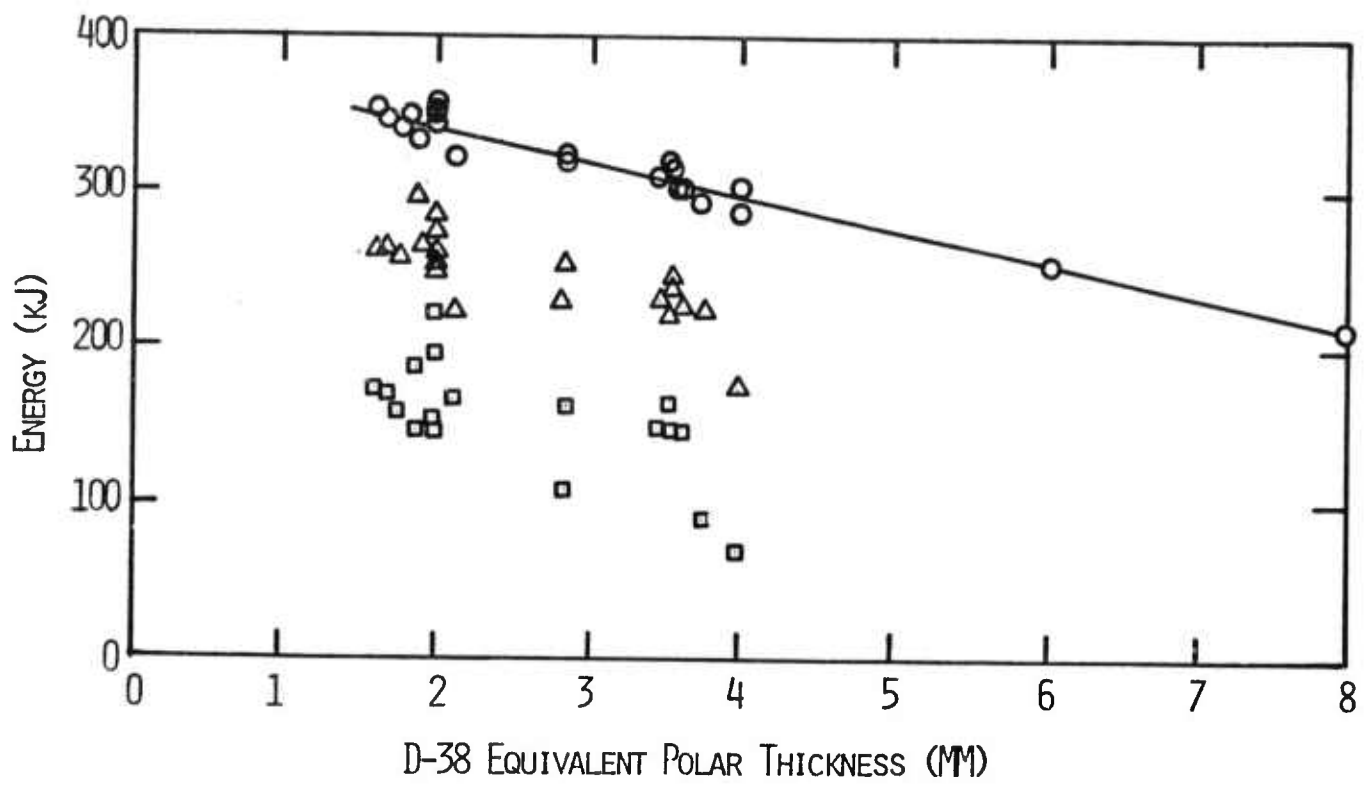


Fig. 4. Hydrodynamic calculations of TLC-6 and TLC-37 compared with experiment.

TLC-6 (+) and TLC-37 (X) were calculated without and with a detonator booster charge, respectively. The experiment (O), which contained a booster, yields contours (isochrones) which agree better with TLC-37. The mass trajectories of the calculations are about the same over the range of the experiment and agree equally well with it. The plotted time intervals of the calculations and experiment were 2 and 1 μ s, respectively.

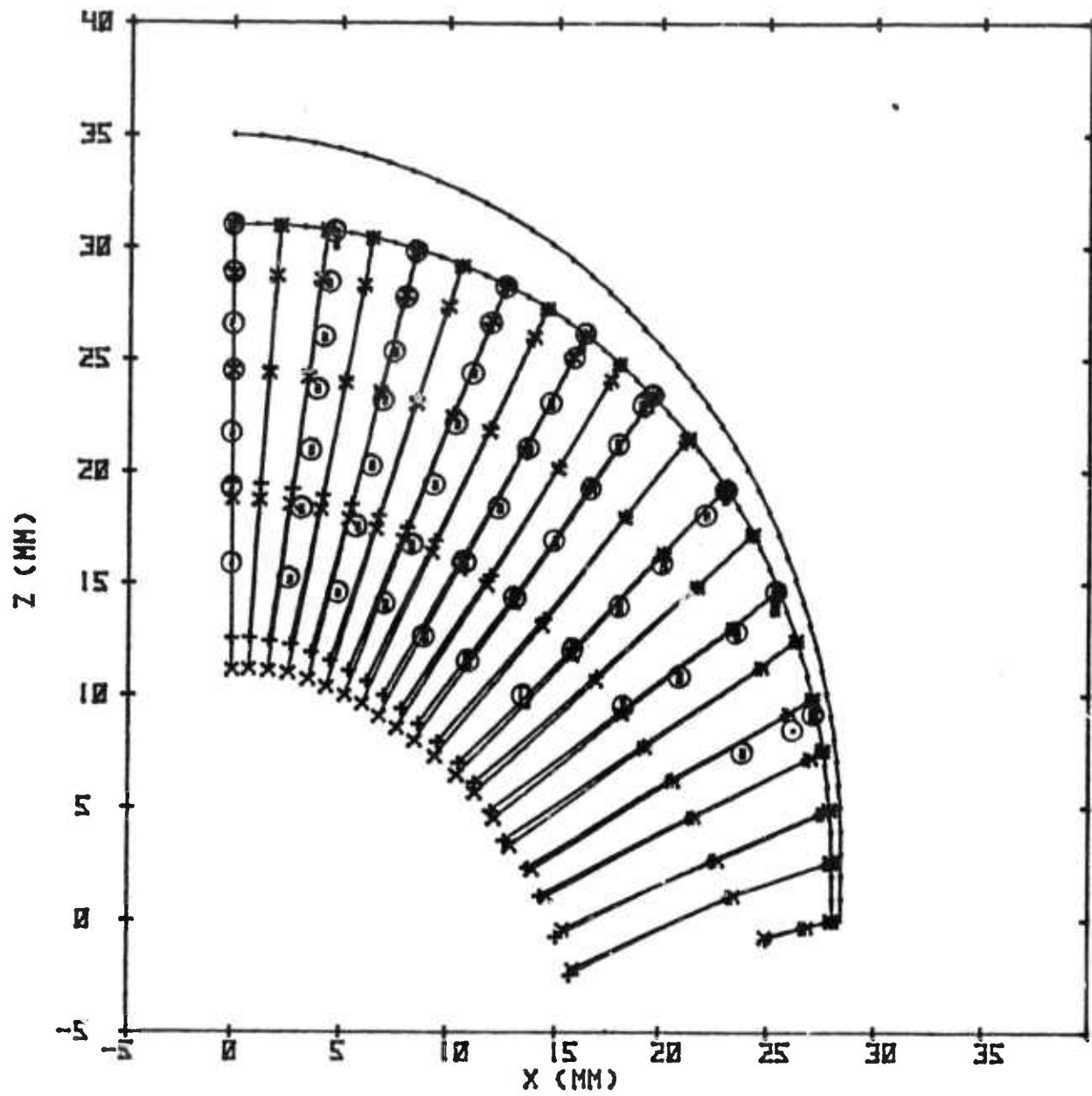


Fig. 5. Elongation of jet for TLC-6. The velocity of the jet particles is a linear function of the distance from the liner equator. Thus the velocity gradient and strain rate are constant along the jet.

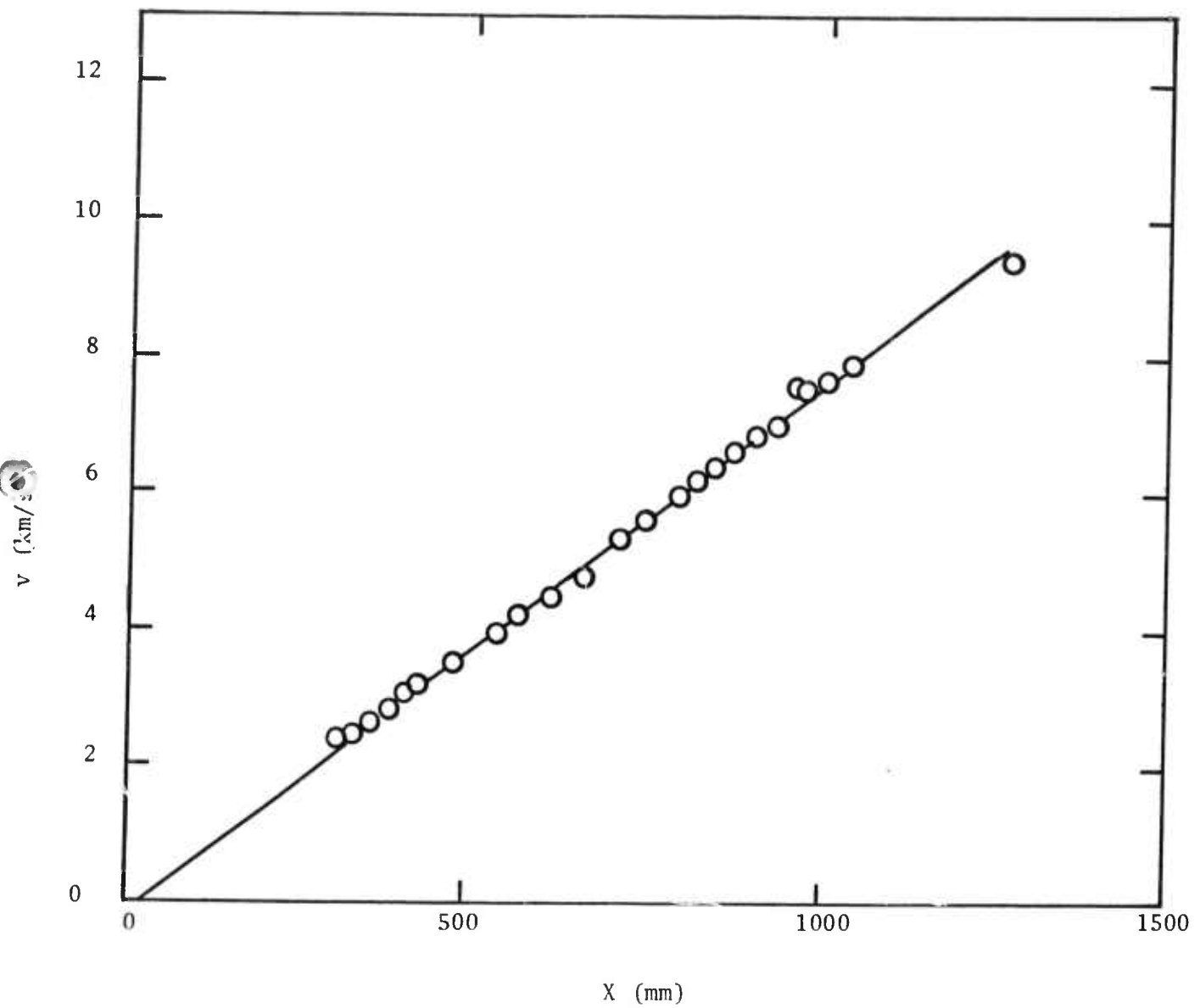
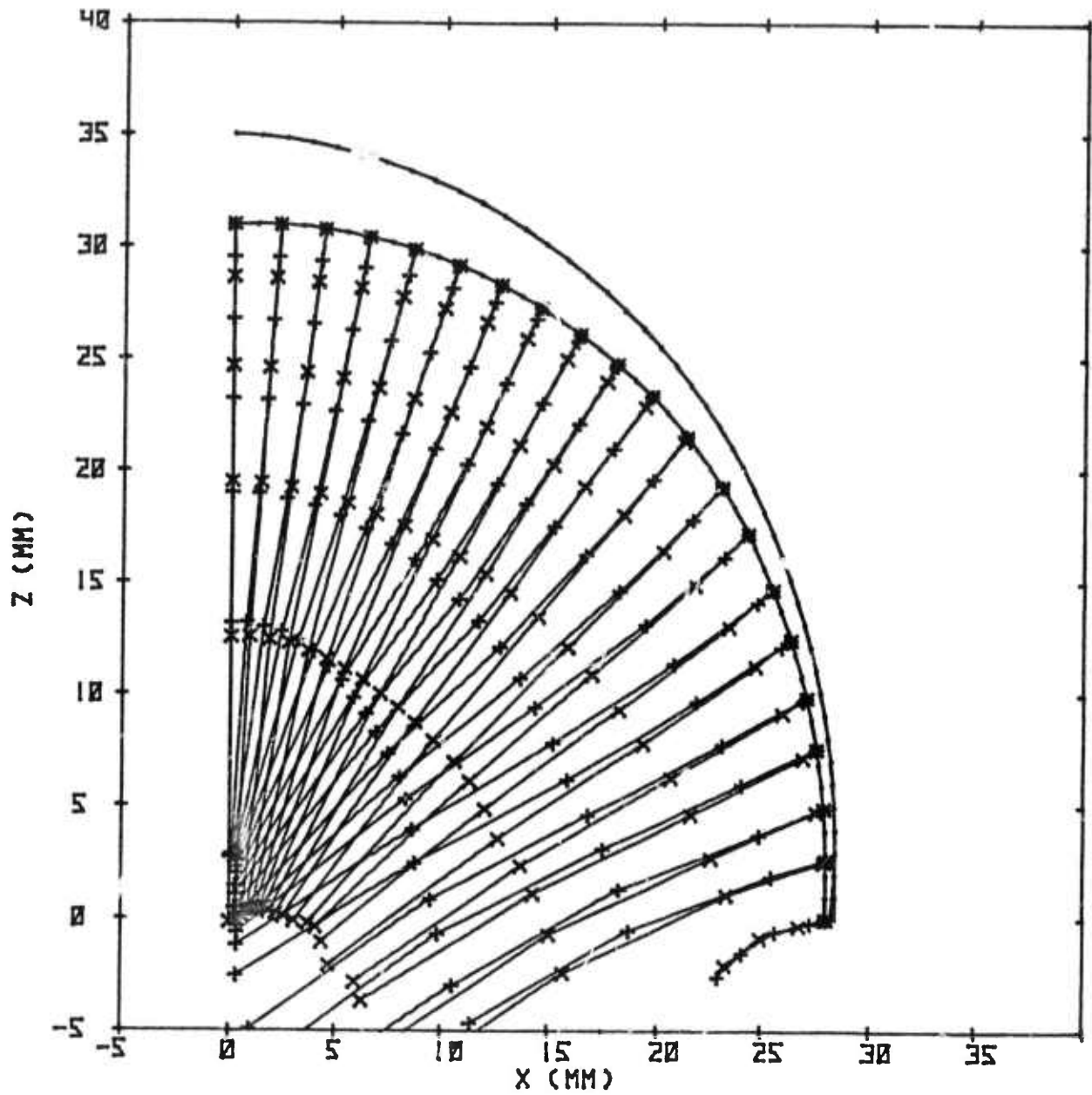


Fig. 6. Inner liner contour isochrones and trajectories for different charge lengths. The contours are plotted at 2 μ s intervals for TLC-6 (X) and TLC-56 (+), which have 85 mm and 41.2 mm of PBX-9501 over their poles, respectively. The equatorial regions move at approximately the same velocity because the effective explosive thickness is unchanged in this region. The polar region for TLC-56 moves more slowly because of the thinner HE, which results in pinchoff.



APPENDIX A. High Explosive Systems Used in Tapered Liner Charges

Three high explosive systems (Systems A, B, and C) were used in the tapered liner charges which were studied. They are shown in Figs. A-1, A-2, and A-3 with the materials and dimensions indicated. The detonators, which are not shown, were centered on-axis on the top face of the charges.

UNCLASSIFIED

Fig. A-1. High explosive system A. This high energy system uses the explosive PBX-9501. It is confined in a mild steel case over its entire length and has a confinement ring on the face of the charge.

UNCLASSIFIED

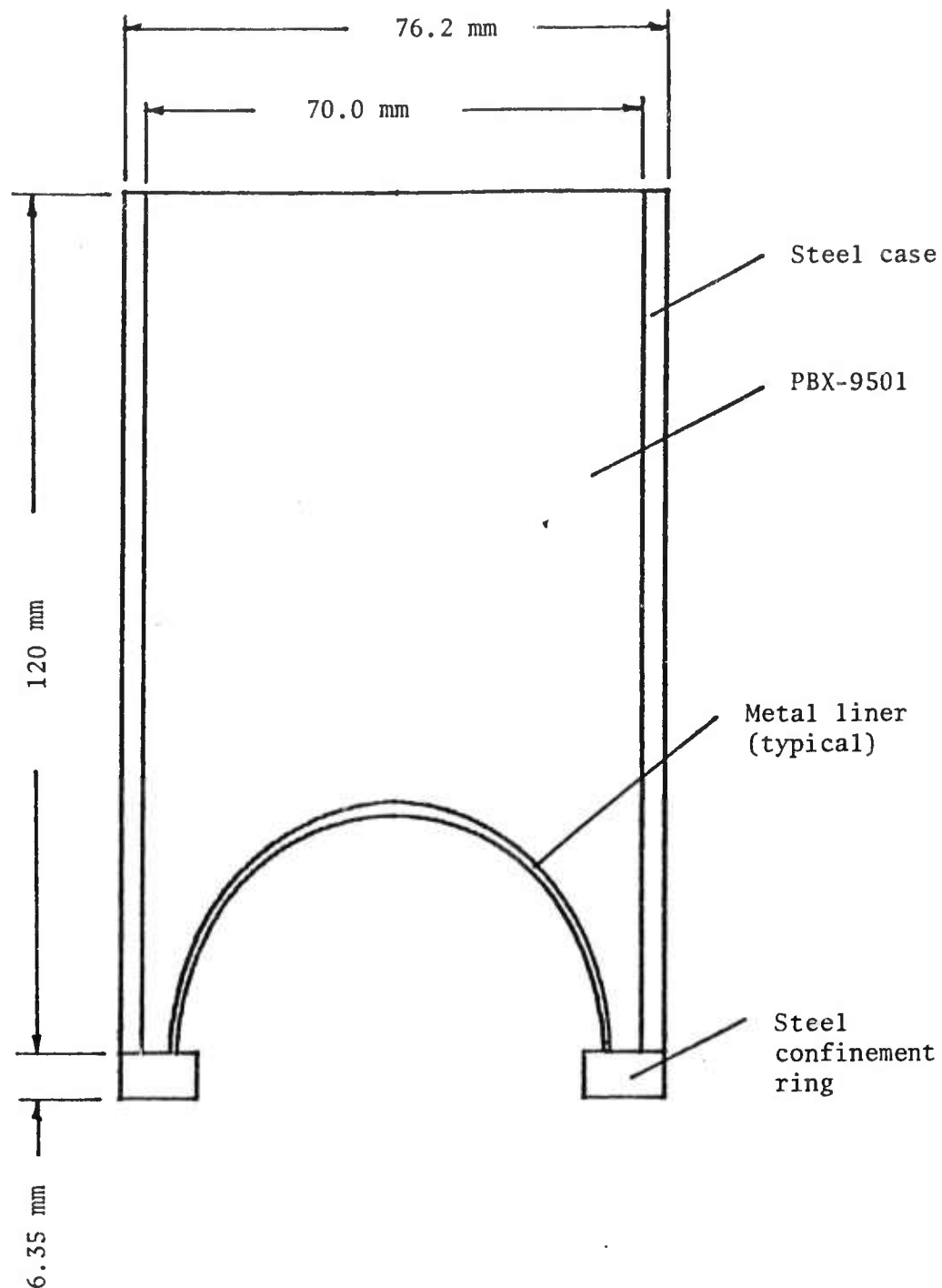


Fig. A-2. High explosive system B. This is a shortened version of
high explosive system A.

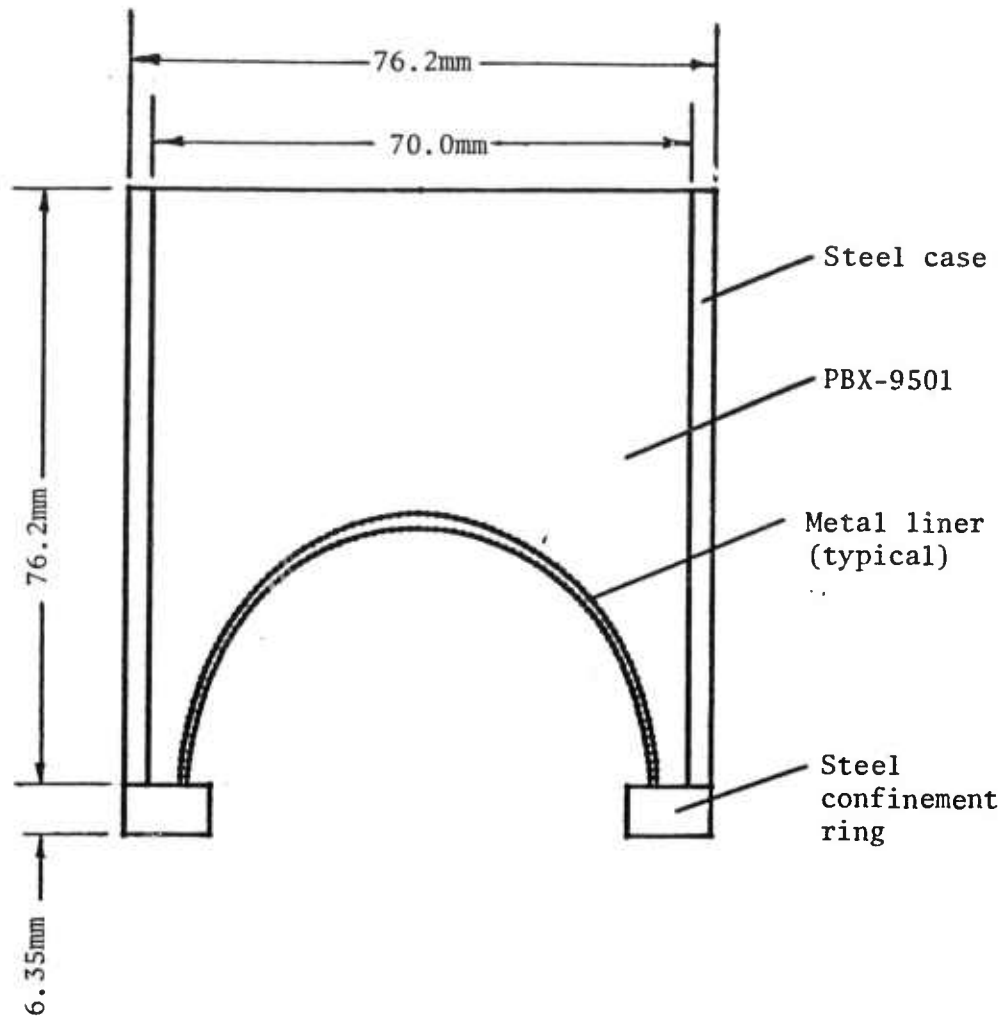
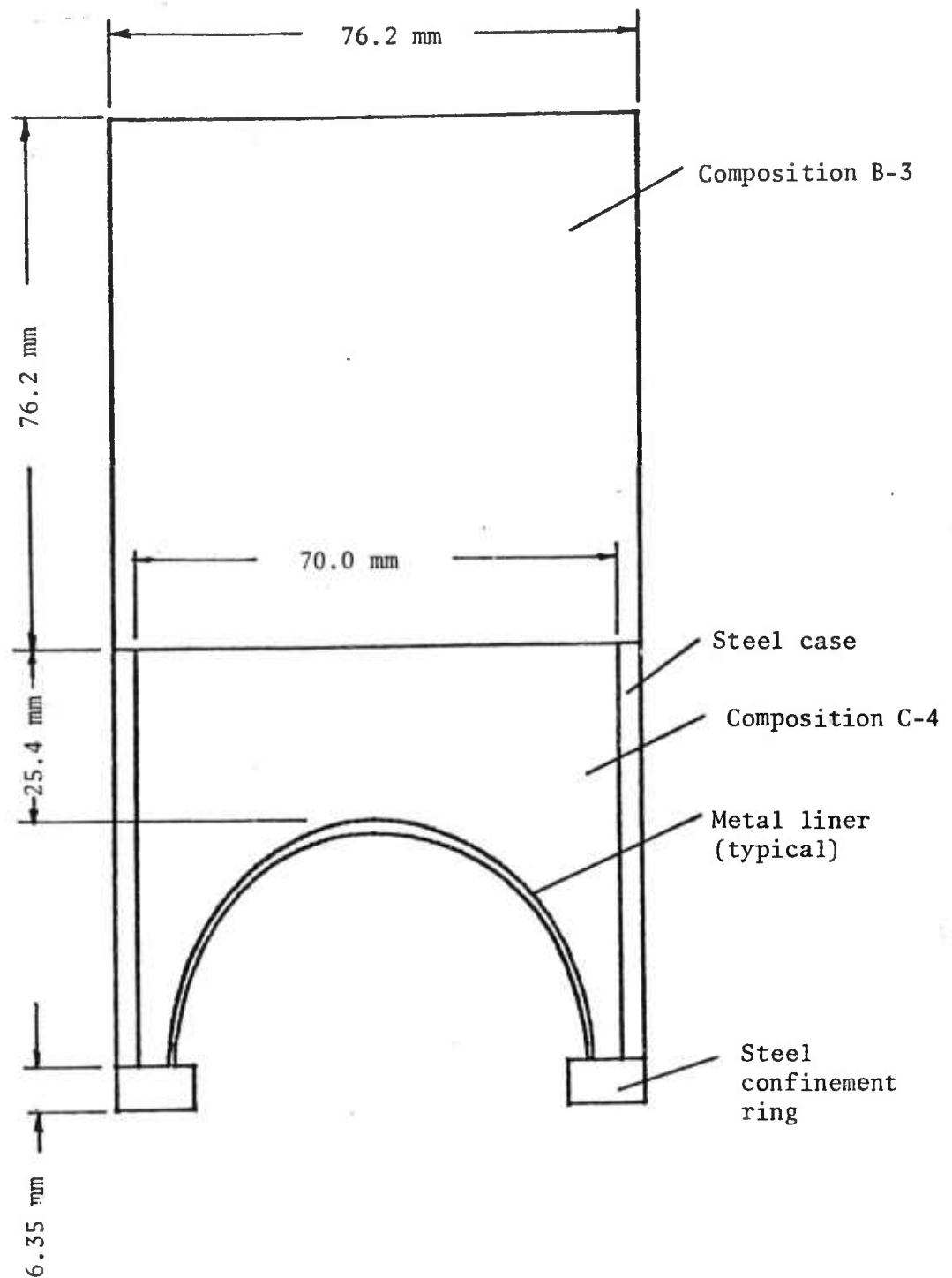


Fig. A-3. High explosive system C. This low energy system uses the explosive composition B-3 and hand-packed plastic explosive composition C-4. Only the composition C-4 explosive is confined in a mild steel case. A confinement ring is used on the face of this charge.



APPENDIX B. Liner Contours

The 36 different sets of liner contours which were studied are numbered sequentially in Table B-1. The contours are given in polar coordinates (r, θ) with the origin in the equatorial plane of the liner.

TABLE B-I. LINER CONTOURS FOR TAPERED LINER CHARGES

POLAR ANGLE	CONTOUR NO. 1		CONTOUR NO. 2		CONTOUR NO. 3		CONTOUR NO. 4	
	OUTER RADIUS	INNER RADIUS	OUTER RADIUS	INNER RADIUS	OUTER RADIUS	INNER RADIUS	OUTER RADIUS	INNER RADIUS
DEG	MM	MM	MM	MM	MM	MM	MM	MM
0	33.00	27.00	35.00	29.00	35.00	30.50	30.00	26.00
2	32.90	27.04	34.88	29.05	34.90	30.54	29.93	26.03
4	32.79	27.07	34.75	29.09	34.79	30.57	29.85	26.04
6	32.66	27.09	34.60	29.12	34.67	30.59	29.76	26.06
8	32.52	27.11	34.44	29.14	34.53	30.60	29.65	26.06
10	32.36	27.13	34.27	29.16	34.38	30.60	29.53	26.06
12	32.19	27.13	34.09	29.16	34.22	30.59	29.41	26.05
14	32.01	27.13	33.90	29.16	34.05	30.57	29.27	26.03
16	31.82	27.12	33.70	29.15	33.87	30.55	29.13	26.01
18	31.63	27.11	33.50	29.13	33.68	30.52	28.97	25.98
20	31.42	27.09	33.28	29.10	33.49	30.48	28.81	25.95
22	31.21	27.06	33.06	29.07	33.28	30.43	28.64	25.91
24	31.00	27.02	32.83	29.03	33.07	30.37	28.47	25.86
26	30.78	26.98	32.60	28.98	32.86	30.31	28.29	25.81
28	30.55	26.94	32.36	28.93	32.64	30.24	28.11	25.76
30	30.33	26.88	32.13	28.87	32.42	30.16	27.92	25.69
32	30.10	26.82	31.88	28.80	32.19	30.08	27.73	25.63
34	29.87	26.76	31.64	28.73	31.97	29.99	27.53	25.56
36	29.65	26.69	31.40	28.65	31.74	29.90	27.34	25.48
38	29.42	26.61	31.16	28.56	31.51	29.79	27.14	25.39
40	29.19	26.53	30.91	28.46	31.27	29.67	26.94	25.30
42	28.97	26.44	30.66	28.35	31.03	29.55	26.73	25.20
44	28.74	26.35	30.40	28.24	30.79	29.41	26.52	25.09
46	28.52	26.26	30.14	28.11	30.54	29.27	26.31	24.97
48	28.30	26.16	29.89	27.97	30.30	29.11	26.09	24.84
50	28.09	26.05	29.63	27.83	30.05	28.95	25.87	24.71
52	27.87	25.94	29.38	27.67	29.80	28.78	25.66	24.57
54	27.66	25.83	29.11	27.51	29.55	28.60	25.44	24.42
56	27.46	25.72	28.86	27.34	29.29	28.41	25.21	24.27
58	27.26	25.60	28.60	27.16	29.04	28.20	24.99	24.11
60	27.06	25.48	28.34	26.98	28.78	28.02	24.77	23.95
62	26.86	25.36	28.08	26.79	28.53	27.82	24.55	23.78
64	26.67	25.23	27.82	26.59	28.28	27.61	24.32	23.61
66	26.48	25.10	27.56	26.40	28.02	27.40	24.09	23.43
68	26.30	24.98	27.31	26.19	27.77	27.18	23.86	23.25
70	26.12	24.85	27.05	25.99	27.52	26.96	23.64	23.07
72	25.94	24.72	26.80	25.78	27.26	26.74	23.41	22.89
74	25.77	24.59	26.55	25.57	27.01	26.52	23.19	22.70
76	25.60	24.45	26.30	25.35	26.76	26.30	22.97	22.51
78	25.43	24.32	26.09	25.15	26.55	26.09	22.79	22.33
80	25.27	24.19	25.92	24.98	26.37	25.91	22.64	22.13
82	25.13	24.05	25.77	24.84	26.22	25.77	22.51	22.06
84	25.02	23.95	25.66	24.73	26.11	25.66	22.41	21.96
86	24.95	23.88	25.58	24.66	26.03	25.58	22.35	21.89
88	24.90	23.83	25.54	24.61	25.98	25.53	22.31	21.85
90	24.89	23.82	25.52	24.60	25.97	25.52	22.29	21.84

TABLE B-I. (CONTINUED)

POLAR ANGLE	CONTOUR NO. 5		CONTOUR NO. 6		CONTOUR NO. 7		CONTOUR NO. 8	
	OUTER RADIUS	INNER RADIUS	OUTER RADIUS	INNER RADIUS	OUTER RADIUS	INNER RADIUS	OUTER RADIUS	INNER RADIUS
DEG	MM	MM	MM	MM	MM	MM	MM	MM
0	35.00	29.00	35.00	31.00	35.00	27.00	35.00	33.00
2	34.89	29.04	34.95	31.03	34.67	27.09	34.99	33.01
4	34.75	29.08	34.89	31.05	34.39	27.16	34.98	33.03
6	34.60	29.10	34.82	31.07	34.12	27.20	34.97	33.05
8	34.44	29.12	34.74	31.09	33.86	27.22	34.94	33.07
10	34.26	29.14	34.64	31.10	33.60	27.24	34.91	33.08
12	34.08	29.14	34.53	31.11	33.34	27.24	34.88	33.08
14	33.89	29.14	34.42	31.11	33.09	27.24	34.83	33.08
16	33.70	29.13	34.29	31.10	32.84	27.23	34.78	33.07
18	33.51	29.12	34.17	31.08	32.60	27.22	34.72	33.06
20	33.31	29.10	34.02	31.06	32.34	27.19	34.65	33.04
22	33.09	29.07	33.87	31.03	32.07	27.17	34.56	33.01
24	32.87	29.03	33.71	31.00	31.81	27.13	34.48	32.98
26	32.66	28.99	33.55	30.96	31.56	27.09	34.38	32.94
28	32.44	28.95	33.39	30.91	31.31	27.05	34.29	32.89
30	32.22	28.90	33.21	30.86	31.05	27.00	34.16	32.84
32	31.99	28.84	33.03	30.80	30.80	26.95	34.05	32.78
34	31.76	28.78	32.84	30.73	30.54	26.89	33.91	32.71
36	31.54	28.71	32.65	30.67	30.30	26.83	33.79	32.64
38	31.33	28.64	32.47	30.59	30.07	26.76	33.64	32.56
40	31.11	28.57	32.29	30.51	29.85	26.69	33.51	32.48
42	30.90	28.49	32.10	30.43	29.62	26.62	33.36	32.39
44	30.69	28.40	31.91	30.34	29.41	26.54	33.22	32.30
46	30.49	28.32	31.73	30.24	29.20	26.46	33.06	32.20
48	30.28	28.22	31.54	30.14	28.99	26.38	32.90	32.09
50	30.08	28.13	31.35	30.04	28.78	26.29	32.74	31.98
52	29.88	28.03	31.16	29.93	28.57	26.20	32.57	31.86
54	29.68	27.92	30.97	29.81	28.37	26.11	32.41	31.74
56	29.47	27.82	30.78	29.70	28.16	26.02	32.25	31.61
58	29.27	27.71	30.59	29.58	27.96	25.92	32.09	31.48
60	29.08	27.60	30.40	29.46	27.76	25.82	31.89	31.35
62	28.89	27.49	30.22	29.34	27.56	25.73	31.72	31.21
64	28.70	27.39	30.05	29.22	27.38	25.63	31.56	31.08
66	28.53	27.28	29.88	29.10	27.20	25.54	31.39	30.95
68	28.36	27.18	29.71	28.99	27.04	25.45	31.24	30.82
70	28.20	27.08	29.56	28.87	26.87	25.37	31.08	30.70
72	28.04	26.99	29.41	28.77	26.72	25.29	30.94	30.57
74	27.89	26.90	29.26	28.66	26.56	25.21	30.79	30.45
76	27.75	26.81	29.12	28.56	26.42	25.13	30.66	30.34
78	27.62	26.73	28.99	28.46	26.28	25.07	30.53	30.23
80	27.49	26.65	28.87	28.37	26.15	25.00	30.41	30.12
82	27.36	26.57	28.75	28.28	26.01	24.94	30.28	30.02
84	27.24	26.50	28.63	28.19	25.90	24.88	30.17	29.91
86	27.16	26.43	28.54	28.11	25.82	24.82	30.08	29.82
88	27.11	26.39	28.49	28.06	25.78	24.77	30.02	29.77
90	27.09	26.37	28.47	28.04	25.76	24.76	30.00	29.75

TABLE B-I. (CONTINUED)

POLAR ANGLE	CONTOUR NO. 9		CONTOUR NO. 10		CONTOUR NO. 11		CONTOUR NO. 12	
	OUTER RADIUS	INNER RADIUS	OUTER RADIUS	INNER RADIUS	OUTER RADIUS	INNER RADIUS	OUTER RADIUS	INNER RADIUS
DEG	MM	MM	MM	MM	MM	MM	MM	MM
0	35.00	31.00	35.00	29.00	35.00	27.00	35.00	34.00
2	34.96	31.02	34.90	29.04	34.79	27.06	35.00	34.01
4	34.91	31.05	34.79	29.07	34.59	27.11	35.01	34.02
6	34.85	31.07	34.68	29.09	34.39	27.14	35.01	34.04
8	34.79	31.08	34.55	29.11	34.19	27.16	35.00	34.05
10	34.71	31.09	34.41	29.13	33.98	27.18	34.99	34.06
12	34.62	31.10	34.27	29.13	33.77	27.18	34.98	34.06
14	34.53	31.10	34.12	29.13	33.57	27.18	34.95	34.06
16	34.43	31.09	33.97	29.12	33.37	27.17	34.92	34.05
18	34.32	31.08	33.81	29.11	33.15	27.16	34.87	34.03
20	34.19	31.05	33.62	29.09	32.91	27.14	34.82	34.01
22	34.05	31.03	33.41	29.06	32.64	27.11	34.77	33.98
24	33.90	30.99	33.21	29.02	32.39	27.07	34.70	33.95
26	33.75	30.95	33.01	28.98	32.14	27.04	34.63	33.91
28	33.60	30.91	32.81	28.94	31.90	26.99	34.56	33.87
30	33.43	30.86	32.59	28.89	31.65	26.94	34.48	33.82
32	33.26	30.80	32.37	28.83	31.39	26.89	34.40	33.77
34	33.08	30.73	32.15	28.77	31.14	26.83	34.31	33.72
36	32.90	30.66	31.94	28.70	30.90	26.77	34.23	33.66
38	32.72	30.59	31.73	28.63	30.67	26.70	34.14	33.60
40	32.54	30.51	31.52	28.56	30.44	26.64	34.04	33.54
42	32.36	30.43	31.31	28.48	30.22	26.56	33.94	33.47
44	32.17	30.34	31.11	28.40	30.00	26.49	33.84	33.39
46	31.99	30.24	30.90	28.31	29.79	26.41	33.73	33.30
48	31.80	30.14	30.70	28.22	29.57	26.33	33.61	33.20
50	31.61	30.04	30.49	28.12	29.36	26.24	33.48	33.10
52	31.42	29.93	30.29	28.02	29.15	26.15	33.34	32.97
54	31.23	29.81	30.09	27.92	28.95	26.05	33.18	32.81
56	31.04	29.70	29.88	27.81	28.73	25.96	32.98	32.63
58	30.84	29.58	29.68	27.70	28.52	25.86	32.76	32.43
60	30.66	29.45	29.48	27.59	28.32	25.76	32.53	32.21
62	30.47	29.33	29.28	27.48	28.12	25.67	32.28	31.98
64	30.29	29.21	29.09	27.38	27.93	25.57	32.03	31.74
66	30.12	29.10	28.92	27.27	27.75	25.48	31.77	31.49
68	29.95	28.98	28.74	27.17	27.58	25.39	31.50	31.24
70	29.79	28.87	28.58	27.07	27.41	25.31	31.24	30.98
72	29.63	28.76	28.42	26.98	27.24	25.23	30.98	30.72
74	29.49	28.65	28.26	26.88	27.08	25.15	30.71	30.47
76	29.34	28.55	28.12	26.80	26.93	25.07	30.45	30.21
78	29.21	28.46	27.98	26.71	26.79	25.00	30.21	29.97
80	29.08	28.36	27.84	26.63	26.65	24.94	30.00	29.76
82	28.95	28.27	27.70	26.56	26.50	24.87	29.84	29.60
84	28.83	28.19	27.58	26.48	26.39	24.81	29.71	29.47
86	28.74	28.10	27.50	26.41	26.31	24.75	29.62	29.38
88	28.69	28.05	27.45	26.36	26.26	24.70	29.56	29.33
90	28.67	28.04	27.43	26.35	26.25	24.69	29.55	29.31

TABLE B-I. (CONTINUED)

POLAR ANGLE	CONTOUR OUTER RADIUS	NO. 13 INNER RADIUS	CONTOUR OUTER RADIUS	NO. 14 INNER RADIUS	CONTOUR OUTER RADIUS	NO. 15 INNER RADIUS	CONTOUR OUTER RADIUS	NO. 16 INNER RADIUS
DEG	MM	MM	MM	MM	MM	MM	MM	MM
0	35.00	33.00	35.00	31.00	35.00	33.00	35.00	33.00
2	35.00	33.01	34.99	31.01	34.99	33.01	34.99	33.01
4	34.99	33.02	34.96	31.03	34.98	33.03	34.98	33.03
6	34.98	33.04	34.90	31.05	34.96	33.05	34.96	33.05
8	34.96	33.05	34.84	31.06	34.94	33.06	34.94	33.06
10	34.93	33.06	34.77	31.07	34.91	33.07	34.92	33.07
12	34.89	33.07	34.68	31.07	34.87	33.08	34.88	33.08
14	34.84	33.06	34.58	31.07	34.82	33.08	34.84	33.08
16	34.79	33.05	34.48	31.06	34.77	33.08	34.79	33.08
18	34.73	33.03	34.37	31.04	34.71	33.07	34.73	33.07
20	34.65	33.01	34.23	31.02	34.64	33.06	34.67	33.06
22	34.56	32.98	34.07	30.99	34.57	33.04	34.61	33.04
24	34.46	32.95	33.91	30.95	34.50	33.01	34.53	33.01
26	34.36	32.91	33.75	30.92	34.42	32.98	34.45	32.98
28	34.26	32.87	33.59	30.88	34.33	32.94	34.37	32.94
30	34.15	32.82	33.42	30.83	34.22	32.90	34.27	32.90
32	34.04	32.77	33.25	30.78	34.11	32.85	34.16	32.85
34	33.92	32.72	33.08	30.73	34.00	32.79	34.04	32.79
36	33.81	32.67	32.92	30.68	33.88	32.73	33.92	32.73
38	33.70	32.61	32.78	30.62	33.75	32.66	33.80	32.66
40	33.58	32.54	32.63	30.56	33.62	32.59	33.67	32.59
42	33.46	32.47	32.48	30.49	33.49	32.51	33.53	32.51
44	33.34	32.40	32.34	30.42	33.35	32.42	33.39	32.43
46	33.22	32.31	32.19	30.34	33.20	32.33	33.25	32.33
48	33.08	32.22	32.04	30.26	33.05	32.23	33.10	32.24
50	32.94	32.11	31.90	30.16	32.90	32.13	32.94	32.13
52	32.80	31.99	31.76	30.06	32.74	32.02	32.78	32.02
54	32.64	31.85	31.63	29.93	32.58	31.90	32.62	31.90
56	32.45	31.67	31.45	29.77	32.41	31.78	32.45	31.78
58	32.23	31.48	31.25	29.59	32.25	31.66	32.29	31.66
60	32.00	31.27	31.02	29.40	32.08	31.53	32.12	31.53
62	31.75	31.04	30.78	29.20	31.92	31.41	31.95	31.41
64	31.49	30.81	30.53	28.99	31.76	31.28	31.79	31.28
66	31.24	30.58	30.29	28.77	31.60	31.16	31.63	31.16
68	30.98	30.34	30.04	28.56	31.45	31.03	31.48	31.03
70	30.72	30.09	29.80	28.34	31.30	30.91	31.33	30.91
72	30.47	29.85	29.56	28.12	31.15	30.79	31.18	30.79
74	30.21	29.60	29.32	27.90	31.01	30.67	31.04	30.67
76	29.96	29.36	29.09	27.68	30.88	30.56	30.91	30.56
78	29.72	29.12	28.86	27.46	30.75	30.45	30.78	30.45
80	29.52	28.93	28.66	27.27	30.63	30.34	30.66	30.34
82	29.36	28.77	28.51	27.12	30.51	30.24	30.54	30.24
84	29.23	28.64	28.38	27.01	30.39	30.14	30.42	30.14
86	29.14	28.56	28.30	26.93	30.30	30.05	30.33	30.05
88	29.09	28.51	28.25	26.88	30.24	29.99	30.27	29.99
90	29.07	28.49	28.23	26.86	30.22	29.97	30.25	29.97

TABLE B-I. (CONTINUED)

POLAR ANGLE	CONTOUR OUTER RADIUS	NO. 17 INNER RADIUS	CONTOUR OUTER RADIUS	NO. 18 INNER RADIUS	CONTOUR OUTER RADIUS	NO. 19 INNER RADIUS	CONTOUR OUTER RADIUS	NO. 20 INNER RADIUS
DEG	MM	MM	MM	MM	MM	MM	MM	MM
0	35.00	33.00	35.00	27.00	35.00	27.00	35.00	27.00
2	34.99	33.01	34.65	27.07	34.63	27.07	34.87	27.03
4	34.98	33.03	34.31	27.13	34.24	27.14	34.72	27.04
6	34.96	33.05	33.98	27.18	33.87	27.19	34.56	27.06
8	34.95	33.06	33.64	27.21	33.49	27.22	34.38	27.08
10	34.93	33.07	33.32	27.23	33.11	27.25	34.17	27.09
12	34.91	33.08	33.02	27.24	32.77	27.26	33.94	27.10
14	34.87	33.08	32.77	27.24	32.47	27.25	33.72	27.10
16	34.83	33.08	32.50	27.23	32.16	27.24	33.47	27.09
18	34.78	33.07	32.22	27.21	31.81	27.23	33.25	27.07
20	34.73	33.06	31.93	27.19	31.49	27.21	32.97	27.05
22	34.67	33.04	31.66	27.16	31.23	27.18	32.71	27.03
24	34.61	33.01	31.41	27.13	31.00	27.15	32.42	27.00
26	34.53	32.98	31.18	27.10	30.81	27.12	32.15	26.97
28	34.45	32.95	30.94	27.06	30.63	27.09	31.88	26.92
30	34.35	32.90	30.72	27.02	30.42	27.04	31.58	26.88
32	34.25	32.85	30.49	26.97	30.22	26.99	31.29	26.83
34	34.13	32.80	30.29	26.92	30.04	26.94	30.99	26.77
36	34.02	32.73	30.09	26.86	29.86	26.88	30.67	26.71
38	33.89	32.67	29.90	26.80	29.69	26.81	30.40	26.64
40	33.76	32.59	29.72	26.74	29.49	26.73	30.13	26.57
42	33.63	32.51	29.54	26.67	29.30	26.64	29.84	26.50
44	33.49	32.43	29.35	26.60	29.11	26.55	29.57	26.43
46	33.34	32.34	29.15	26.52	28.91	26.45	29.32	26.34
48	33.19	32.24	28.95	26.43	28.67	26.35	29.05	26.25
50	33.04	32.13	28.75	26.34	28.44	26.25	28.78	26.16
52	32.88	32.02	28.54	26.25	28.21	26.14	28.53	26.07
54	32.71	31.90	28.32	26.16	27.97	26.04	28.28	25.96
56	32.54	31.78	28.10	26.06	27.74	25.95	28.03	25.87
58	32.37	31.66	27.89	25.97	27.52	25.86	27.78	25.76
60	32.20	31.53	27.68	25.88	27.35	25.80	27.54	25.66
62	32.03	31.41	27.48	25.80	27.25	25.75	27.31	25.55
64	31.87	31.28	27.28	25.72	27.16	25.72	27.11	25.45
66	31.71	31.15	27.11	25.66	27.08	25.71	26.91	25.35
68	31.55	31.03	26.94	25.61	27.02	25.72	26.69	25.25
70	31.40	30.91	26.80	25.57	26.98	25.74	26.53	25.15
72	31.25	30.79	26.67	25.54	26.96	25.78	26.34	25.06
74	31.11	30.67	26.56	25.51	26.94	25.83	26.16	24.96
76	30.97	30.56	26.45	25.49	26.95	25.89	26.00	24.88
78	30.84	30.45	26.36	25.48	26.96	25.96	25.85	24.79
80	30.72	30.34	26.27	25.46	26.98	26.03	25.71	24.71
82	30.60	30.23	26.19	25.44	27.01	26.11	25.57	24.63
84	30.47	30.13	26.10	25.42	27.04	26.20	25.46	24.55
86	30.38	30.04	26.02	25.40	27.06	26.28	25.38	24.48
88	30.32	29.98	25.97	25.38	27.07	26.38	25.34	24.44
90	30.30	29.96	25.96	25.36	27.22	26.49	25.32	24.42

TABLE B-I. (CONTINUED)

POLAR ANGLE	CONTOUR OUTER RADIUS	NO. 21 INNER RADIUS	CONTOUR OUTER RADIUS	NO. 22 INNER RADIUS	CONTOUR OUTER RADIUS	NO. 23 INNER RADIUS	CONTOUR OUTER RADIUS	NO. 24 INNER RADIUS
DEG	MM	MM	MM	MM	MM	MM	MM	MM
0	31.00	27.00	31.00	27.00	31.00	27.00	31.00	27.00
2	30.88	27.09	30.98	27.00	30.99	27.00	30.98	27.00
4	30.78	27.16	30.94	27.00	30.95	27.00	30.95	27.00
6	30.66	27.20	30.88	27.00	30.90	27.01	30.89	27.01
8	30.54	27.22	30.80	27.00	30.83	27.01	30.82	27.01
10	30.42	27.24	30.70	27.00	30.74	27.02	30.73	27.02
12	30.29	27.24	30.58	27.00	30.63	27.02	30.63	27.02
14	30.17	27.24	30.44	27.00	30.51	27.03	30.50	27.03
16	30.04	27.23	30.30	26.99	30.37	27.03	30.36	27.03
18	29.91	27.22	30.15	26.98	30.21	27.03	30.20	27.03
20	29.77	27.19	30.00	26.96	30.02	27.02	30.02	27.02
22	29.62	27.17	29.86	26.93	29.85	27.00	29.86	27.00
24	29.47	27.13	29.71	26.89	29.71	26.97	29.71	26.97
26	29.33	27.09	29.56	26.85	29.57	26.94	29.57	26.94
28	29.18	27.05	29.41	26.81	29.42	26.91	29.42	26.91
30	29.03	27.00	29.25	26.76	29.28	26.87	29.28	26.87
32	28.88	26.95	29.10	26.71	29.14	26.83	29.14	26.83
34	28.72	26.89	28.95	26.65	29.00	26.78	29.00	26.78
36	28.57	26.83	28.80	26.59	28.87	26.73	28.87	26.72
38	28.42	26.76	28.65	26.52	28.74	26.66	28.74	26.66
40	28.27	26.69	28.51	26.45	28.60	26.60	28.60	26.59
42	28.12	26.62	28.36	26.38	28.46	26.52	28.46	26.52
44	27.98	26.54	28.22	26.30	28.31	26.44	28.31	26.44
46	27.83	26.46	28.07	26.22	28.17	26.36	28.17	26.36
48	27.69	26.38	27.92	26.14	28.04	26.28	28.04	26.28
50	27.54	26.29	27.77	26.05	27.91	26.20	27.91	26.20
52	27.39	26.20	27.62	25.96	27.77	26.11	27.77	26.11
54	27.24	26.11	27.47	25.87	27.62	26.02	27.62	26.02
56	27.09	26.02	27.32	25.78	27.47	25.93	27.49	25.93
58	26.94	25.92	27.18	25.68	27.33	25.83	27.37	25.84
60	26.79	25.82	27.04	25.58	27.18	25.74	27.27	25.76
62	26.65	25.73	26.90	25.49	27.05	25.66	27.19	25.69
64	26.51	25.63	26.78	25.39	26.91	25.57	27.12	25.64
66	26.37	25.54	26.65	25.30	26.76	25.50	27.06	25.60
68	26.25	25.45	26.54	25.21	26.60	25.43	27.01	25.50
70	26.12	25.37	26.42	25.13	26.47	25.38	27.02	25.50
72	26.01	25.29	26.31	25.05	26.35	25.32	27.04	25.61
74	25.89	25.21	26.21	24.97	26.21	25.27	27.08	25.65
76	25.78	25.13	26.11	24.89	26.07	25.21	27.14	25.71
78	25.68	25.07	26.01	24.83	25.92	25.16	27.22	25.79
80	25.58	25.00	25.91	24.76	25.79	25.10	27.32	25.89
82	25.48	24.94	25.81	24.70	25.66	25.04	27.44	26.01
84	25.39	24.88	25.72	24.64	25.55	24.97	27.59	26.16
86	25.32	24.82	25.65	24.58	25.47	24.91	27.75	26.32
88	25.28	24.77	25.60	24.54	25.42	24.89	27.91	26.48
90	25.26	24.76	25.59	24.52	25.41	24.89	28.07	26.64

TABLE B-1. (CONTINUED)

POLAR ANGLE	CONTOUR OUTER RADIUS	NO. 25 INNER RADIUS	CONTOUR OUTER RADIUS	NO. 26 INNER RADIUS	CONTOUR OUTER RADIUS	NO. 27 INNER RADIUS	CONTOUR OUTER RADIUS	NO. 28 INNER RADIUS
DEG	MM	MM	MM	MM	MM	MM	MM	MM
0	31.00	27.00	31.00	27.00	18.00	14.00	15.40	13.41
2	30.98	27.00	30.98	27.00	18.01	14.00	15.41	13.41
4	30.94	27.00	30.93	27.00	18.02	14.01	15.42	13.43
6	30.89	27.00	30.89	27.00	18.05	14.02	15.45	13.45
8	30.81	27.01	30.80	27.01	18.09	14.04	15.49	13.49
10	30.73	27.01	30.73	27.01	18.14	14.06	15.54	13.53
12	30.62	27.02	30.61	27.02	18.20	14.11	15.60	13.59
14	30.50	27.02	30.50	27.02	18.28	14.18	15.67	13.65
16	30.35	27.03	30.34	27.03	18.37	14.26	15.75	13.73
18	30.19	27.02	30.18	27.01	18.47	14.35	15.84	13.82
20	30.02	27.01	30.02	27.00	18.58	14.46	15.95	13.92
22	29.86	26.99	29.86	26.98	18.70	14.57	16.07	14.03
24	29.71	26.97	29.71	26.97	18.84	14.70	16.20	14.15
26	29.56	26.93	29.55	26.92	18.99	14.83	16.34	14.29
28	29.42	26.90	29.42	26.89	19.15	14.98	16.50	14.44
30	29.28	26.85	29.28	26.83	19.32	15.14	16.67	14.60
32	29.13	26.80	29.12	26.77	19.52	15.31	16.85	14.77
34	28.99	26.73	28.98	26.68	19.73	15.50	17.05	14.96
36	28.86	26.65	28.85	26.58	19.96	15.69	17.26	15.17
38	28.71	26.56	28.68	26.46	20.20	15.90	17.49	15.39
40	28.55	26.46	28.50	26.33	20.46	16.12	17.74	15.62
42	28.37	26.34	28.28	26.16	20.73	16.35	18.00	15.88
44	28.19	26.22	28.07	26.00	21.02	16.60	18.27	16.15
46	28.02	26.08	27.87	25.80	21.32	16.86	18.57	16.44
48	27.85	25.95	27.66	25.62	21.63	17.14	18.88	16.75
50	27.67	25.80	27.43	25.40	21.96	17.44	19.22	17.08
52	27.48	25.65	27.19	25.19	22.31	17.77	19.57	17.43
54	27.29	25.49	26.96	24.96	22.67	18.13	19.94	17.80
56	27.10	25.33	26.71	24.73	23.05	18.51	20.34	18.20
58	26.93	25.16	26.49	24.48	23.45	18.91	20.75	18.62
60	26.79	25.01	26.31	24.26	23.86	19.34	21.19	19.07
62	26.69	24.88	26.19	24.07	24.29	19.79	21.65	19.55
64	26.62	24.77	26.12	23.90	24.74	20.27	22.14	20.05
66	26.58	24.68	26.10	23.76	25.20	20.78	22.65	20.59
68	26.60	24.63	26.19	23.68	25.68	21.31	23.19	21.16
70	26.68	24.60	26.34	23.62	26.18	21.88	23.76	21.76
72	26.84	24.61	26.64	23.61	26.71	22.47	24.35	22.40
74	26.96	24.65	26.84	23.65	27.25	23.10	24.97	23.08
76	27.18	24.74	27.18	23.77	27.82	23.78	25.62	23.79
78	27.46	24.87	27.46	23.95	28.41	24.50	26.30	24.55
80	27.84	25.05	27.84	24.21	29.02	25.26	27.01	25.34
82	28.24	25.30	28.24	24.59	29.64	26.10	27.75	26.18
84	28.78	25.61	28.78	25.06	30.28	26.99	28.51	27.07
86	29.40	25.98	29.40	25.64	30.94	27.94	29.31	28.00
88	30.12	26.42	30.12	26.36	31.61	28.94	30.14	28.98
90	31.16	26.91	31.16	27.18	32.30	30.00	31.00	30.00

TABLE B-I. (CONTINUED)

POLAR ANGLE	CONTOUR OUTER RADIUS	NO. 29 INNER RADIUS	CONTOUR OUTER RADIUS	NO. 30 INNER RADIUS	CONTOUR OUTER RADIUS	NO. 31 INNER RADIUS	CONTOUR OUTER RADIUS	NO. 32 INNER RADIUS
DEG	MM	MM	MM	MM	MM	MM	MM	MM
0	21.47	17.48	16.64	14.64	19.49	17.48	35.00	31.00
2	21.47	17.49	16.65	14.64	19.49	17.49	34.95	31.03
4	21.49	17.50	16.66	14.65	19.50	17.50	34.89	31.05
6	21.51	17.52	16.68	14.67	19.52	17.52	34.82	31.07
8	21.54	17.55	16.71	14.70	19.55	17.55	34.74	31.09
10	21.58	17.59	16.75	14.74	19.59	17.59	34.64	31.10
12	21.62	17.63	16.79	14.78	19.64	17.63	34.53	31.11
14	21.68	17.69	16.85	14.83	19.69	17.69	34.41	31.11
16	21.75	17.75	16.91	14.90	19.76	17.75	34.29	31.10
18	21.82	17.82	16.99	14.97	19.83	17.82	34.16	31.08
20	21.91	17.91	17.07	15.05	19.92	17.91	34.04	31.06
22	22.00	18.00	17.17	15.15	20.01	18.00	33.92	31.03
24	22.10	18.11	17.28	15.25	20.12	18.11	33.81	30.99
26	22.22	18.22	17.40	15.36	20.23	18.22	33.69	30.95
28	22.34	18.35	17.53	15.49	20.36	18.35	33.57	30.90
30	22.48	18.48	17.67	15.63	20.49	18.48	33.45	30.84
32	22.62	18.63	17.82	15.78	20.64	18.63	33.32	30.77
34	22.78	18.79	17.99	15.95	20.80	18.79	33.18	30.70
36	22.94	18.96	18.17	16.12	20.97	18.96	33.05	30.63
38	23.12	19.15	18.36	16.32	21.15	19.15	32.93	30.54
40	23.31	19.34	18.57	16.52	21.35	19.34	32.80	30.46
42	23.51	19.56	18.80	16.75	21.55	19.56	32.68	30.37
44	23.72	19.78	19.04	16.99	21.77	19.78	32.55	30.27
46	23.94	20.02	19.30	17.24	22.00	20.02	32.43	30.18
48	24.18	20.27	19.57	17.52	22.25	20.27	32.31	30.08
50	24.42	20.54	19.86	17.81	22.51	20.54	32.18	29.97
52	24.68	20.83	20.17	18.13	22.78	20.83	32.06	29.87
54	24.95	21.13	20.50	18.46	23.07	21.13	31.94	29.76
56	25.23	21.45	20.85	18.82	23.37	21.45	31.81	29.66
58	25.53	21.78	21.22	19.20	23.69	21.78	31.69	29.55
60	25.84	22.14	21.62	19.61	24.02	22.14	31.58	29.45
62	26.16	22.51	22.04	20.05	24.37	22.51	31.47	29.36
64	26.49	22.90	22.48	20.51	24.73	22.90	31.37	29.28
66	26.84	23.32	22.95	21.00	25.11	23.32	31.28	29.20
68	27.20	23.75	23.44	21.52	25.51	23.75	31.20	29.13
70	27.58	24.20	23.96	22.08	25.92	24.20	31.14	29.08
72	27.96	24.67	24.51	22.67	26.35	24.67	31.08	29.03
74	28.36	25.17	25.09	23.30	26.80	25.17	31.03	29.00
76	28.77	25.69	25.71	23.97	27.27	25.69	31.00	28.99
78	29.20	26.24	26.36	24.68	27.75	26.24	30.98	28.98
80	29.64	26.80	27.04	25.44	28.25	26.80	30.97	28.99
82	30.09	27.39	27.75	26.25	28.76	27.39	30.97	29.02
84	30.55	28.01	28.51	27.10	29.30	28.01	30.98	29.06
86	31.02	28.65	29.30	28.01	29.85	28.65	30.97	29.12
88	31.51	29.31	30.13	28.98	30.42	29.31	30.95	29.18
90	32.00	30.00	31.00	30.00	31.00	30.00	30.93	29.26

TABLE B-I. (CONTINUED)

POLAR ANGLE	CONTOUR OUTER RADIUS	NO. 33 INNER RADIUS	CONTOUR OUTER RADIUS	NO. 34 INNER RADIUS	CONTOUR OUTER RADIUS	NO. 35 INNER RADIUS	CONTOUR OUTER RADIUS	NO. 36 INNER RADIUS
DEG	MM	MM	MM	MM	MM	MM	MM	MM
0	35.00	33.00	35.00	29.00	35.00	27.00	35.00	27.00
2	34.95	32.99	34.88	29.04	34.48	27.10	34.84	27.05
4	34.89	32.97	34.74	29.08	34.01	27.18	34.69	27.11
6	34.82	32.95	34.59	29.11	33.60	27.24	34.53	27.16
8	34.74	32.91	34.43	29.13	33.22	27.27	34.37	27.21
10	34.64	32.87	34.26	29.14	32.86	27.29	34.22	27.26
12	34.53	32.82	34.07	29.15	32.55	27.30	34.06	27.31
14	34.41	32.76	33.88	29.15	32.28	27.30	33.92	27.37
16	34.29	32.69	33.69	29.14	32.01	27.29	33.78	27.43
18	34.16	32.62	33.51	29.12	31.74	27.28	33.65	27.49
20	34.04	32.55	33.34	29.10	31.48	27.25	33.53	27.56
22	33.92	32.48	33.18	29.07	31.25	27.22	33.41	27.62
24	33.81	32.40	33.04	29.04	31.02	27.19	33.29	27.69
26	33.69	32.32	32.90	28.99	30.80	27.15	33.17	27.76
28	33.57	32.24	32.77	28.95	30.58	27.10	33.04	27.83
30	33.45	32.14	32.62	28.89	30.36	27.04	32.90	27.90
32	33.32	32.05	32.48	28.83	30.14	26.98	32.75	27.97
34	33.18	31.94	32.33	28.76	29.92	26.91	32.59	28.04
36	33.06	31.84	32.20	28.69	29.71	26.83	32.44	28.11
38	32.93	31.74	32.08	28.62	29.50	26.74	32.30	28.18
40	32.80	31.63	31.95	28.54	29.29	26.64	32.16	28.25
42	32.68	31.52	31.83	28.45	29.08	26.53	32.02	28.32
44	32.55	31.41	31.72	28.37	28.85	26.41	31.89	28.39
46	32.43	31.30	31.61	28.28	28.62	26.28	31.76	28.46
48	32.31	31.19	31.51	28.19	28.37	26.15	31.63	28.53
50	32.18	31.08	31.40	28.10	28.12	26.00	31.51	28.59
52	32.06	30.96	31.30	28.01	27.85	25.84	31.38	28.65
54	31.94	30.85	31.20	27.92	27.58	25.67	31.26	28.72
56	31.81	30.74	31.09	27.83	27.29	25.50	31.14	28.77
58	31.69	30.62	30.99	27.74	27.01	25.33	31.03	28.83
60	31.58	30.52	30.90	27.65	26.72	25.15	30.92	28.89
62	31.47	30.42	30.81	27.58	26.44	24.98	30.82	28.95
64	31.37	30.32	30.73	27.51	26.17	24.81	30.73	29.01
66	31.28	30.24	30.66	27.44	25.90	24.64	30.66	29.08
68	31.20	30.17	30.60	27.39	25.64	24.48	30.59	29.14
70	31.14	30.11	30.55	27.35	25.39	24.32	30.54	29.21
72	31.08	30.06	30.51	27.32	25.15	24.17	30.49	29.28
74	31.03	30.02	30.48	27.30	24.92	24.02	30.46	29.36
76	31.00	29.99	30.46	27.30	24.70	23.86	30.43	29.44
78	30.98	29.98	30.45	27.31	24.50	23.71	30.42	29.52
80	30.98	29.99	30.46	27.34	24.34	23.55	30.42	29.60
82	30.97	30.00	30.46	27.38	24.20	23.42	30.42	29.68
84	30.98	30.02	30.46	27.43	24.10	23.32	30.42	29.76
86	30.97	30.05	30.45	27.49	24.02	23.25	30.43	29.85
88	30.95	30.07	30.39	27.57	23.98	23.21	30.43	29.93
90	30.93	30.09	30.38	27.66	23.97	23.19	30.45	30.01

APPENDIX C. Hardening Schedule for 4340 Steel

The following heat-treat formula was used to harden 4340 steel cylinders uniformly to a hardness of BHN 308±9.

1. Preheat 2 - 3 hours at 1200° F (649°C)
2. Heat 1 - 2 hours at 1500° F (816°C)
3. Quench in oil, Gulf Super-Quench 70, and agitate 30 - 45 minutes or that time required to reduce the temperature of steel cylinder to less than 300° F (149° C).
4. Temper at 1000° F (538° C) for 5 hours.

APPENDIX D. Results for Each TLC System

The calculational and/or experimental results for each TLC system studied are given. If a radiograph was obtained a print of it is given showing the general features of the jet.

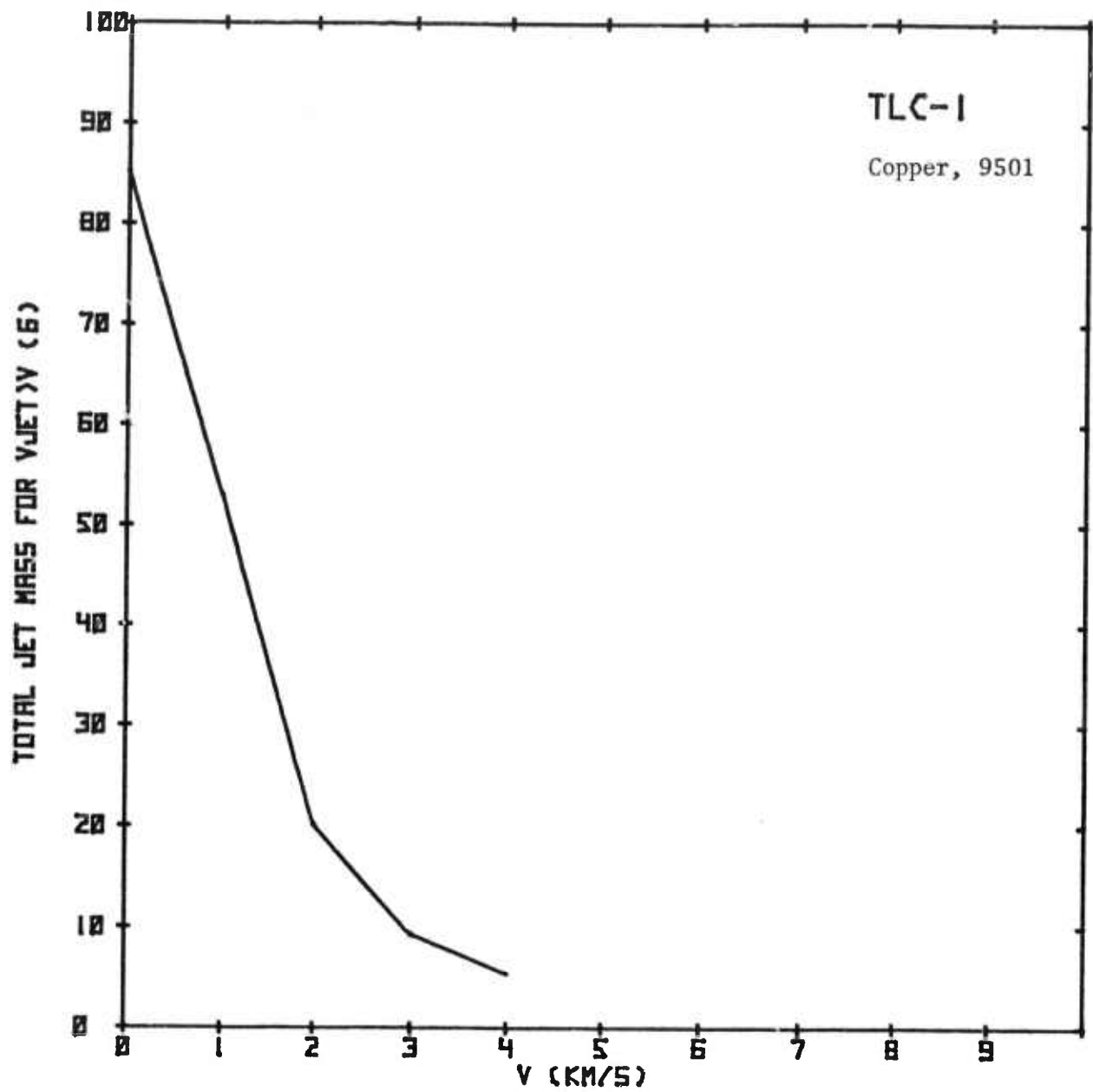
A plot is given for the total jet mass having velocity greater than v as a function of the velocity v . The masses were found by measuring the size of each particle on the radiograph and using the assumption of cylindrical symmetry and crystal density for each particle. The agreement between the experimental values (X) and calculated values (obtained from HELP) can be observed for those systems in which each was obtained.

Another plot shows the original contours of the liner as well as the trajectories of points on its inner surface. The axis of cylindrical symmetry is the vertical axis through the origin. The horizontal plane through the origin, normal to the Z -axis, is the equatorial plane of the liner. Again the degree of agreement between the experimental values (\square) and calculated values can be seen for those systems on which each was obtained. The size of the rectangle representing experimental values is an indication of the experimental standard deviation in both X and Z coordinates. The calculated trajectories (obtained from HELP) are shown without symbols. The experimental values are shown as far as the liner motion could be observed with the framing camera. The calculated values are generally shown as far as is required to obtain the degree of radial stability of the jet. Radial instability is inferred from the presence of an outward velocity component in the jet profile. Pinch-off of the jet during liner collapse is inferred from both the early collapse of the equatorial region of the liner and the resulting deceleration of the jet mass near the axis.

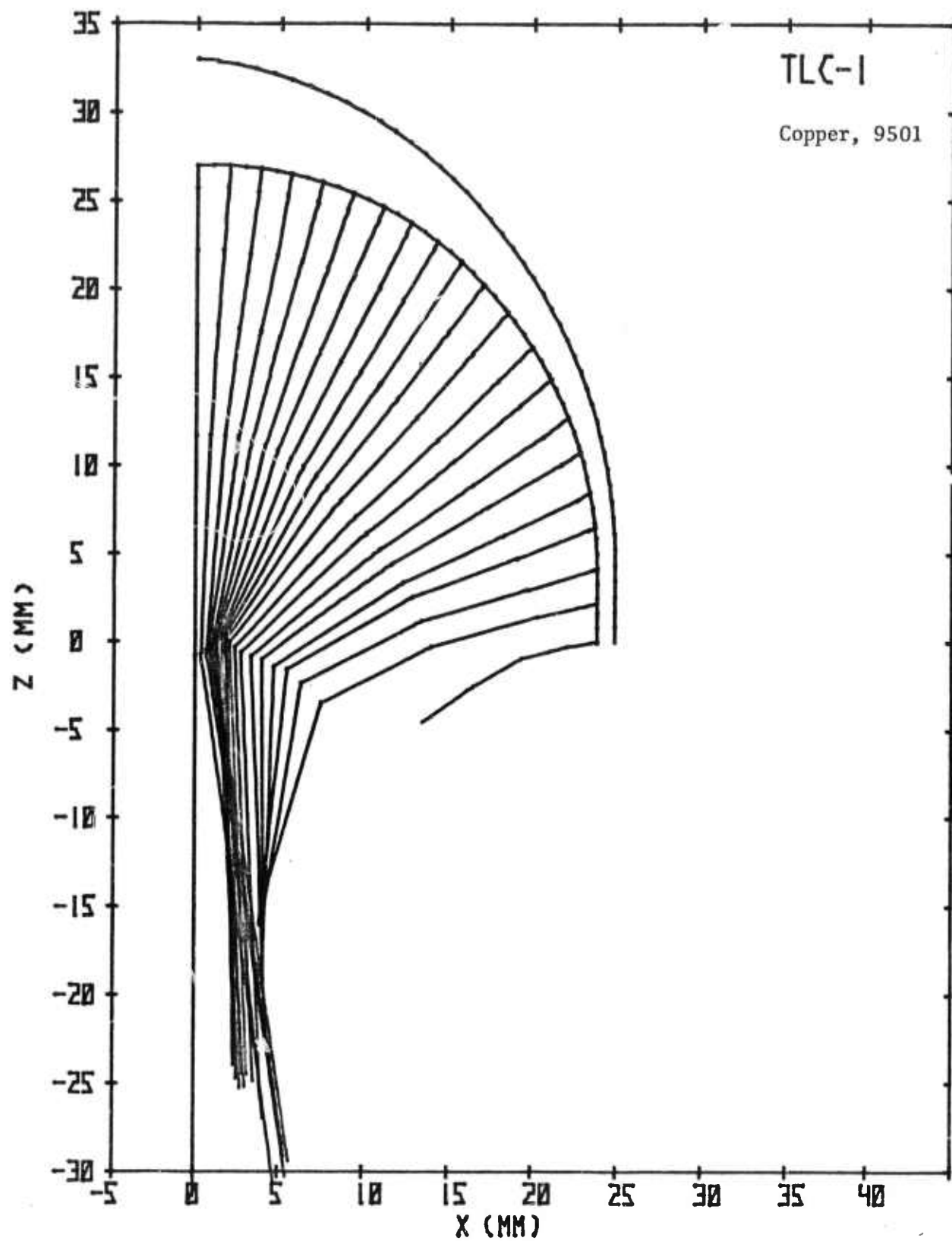
The liner and high explosive materials are given on each plot.

Space fiducials are seen as rods extending up from the bottom edge of the radiographs. They were located at 500 and 1000 mm from the equator of the liner. The equator of the liner was located at the origin of the meter stick or at the left edge of the radiograph if the meter stick is not visible. Jet velocities were obtained from the displacement of the jet image on the radiographs and the measured delay time between the two x-ray exposures. If only one image is shown on the radiograph the time of jet formation (at the liner equator) as obtained from a HELP calculation is used to obtain the jet velocities.

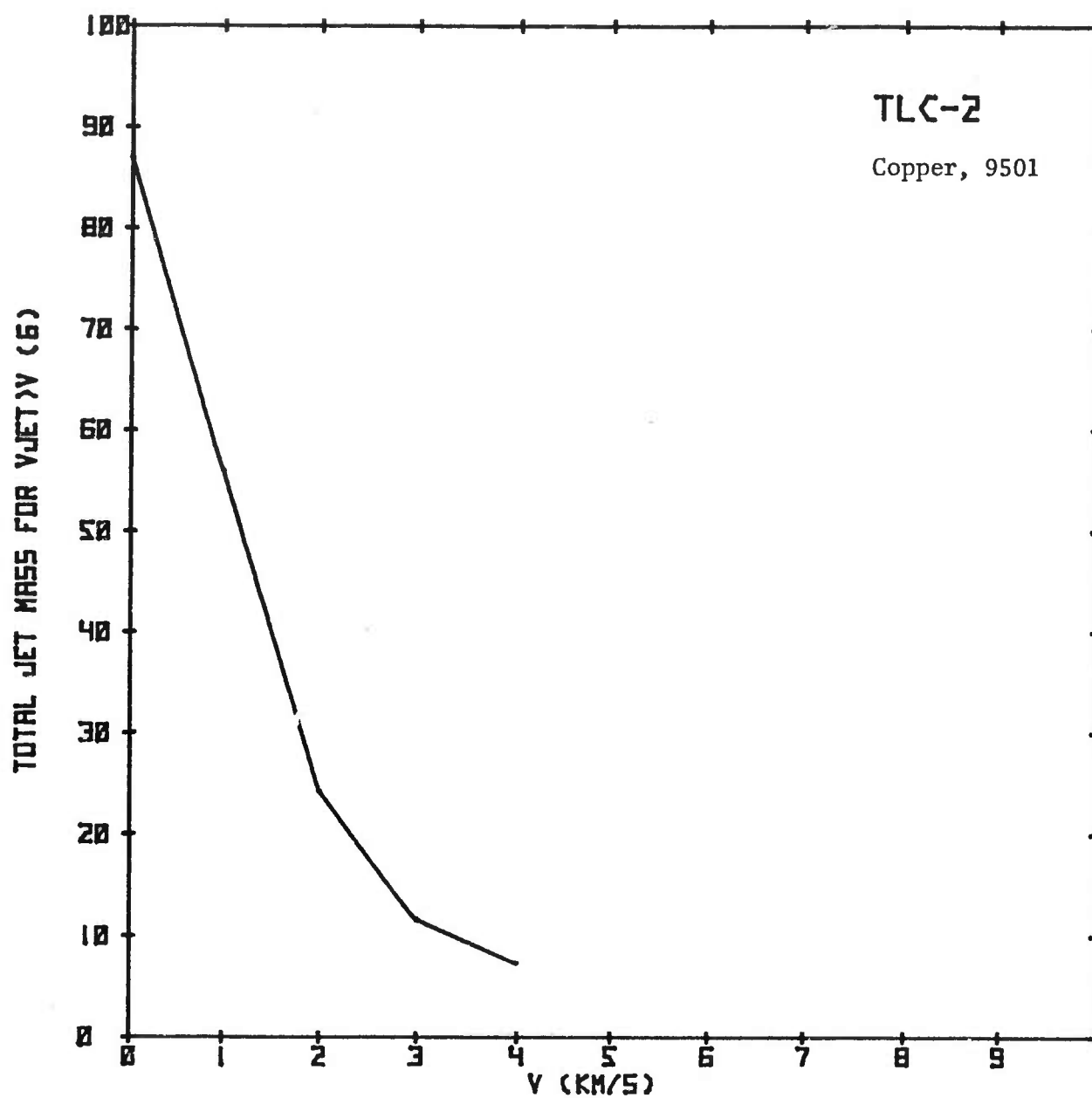
UNCLASSIFIED



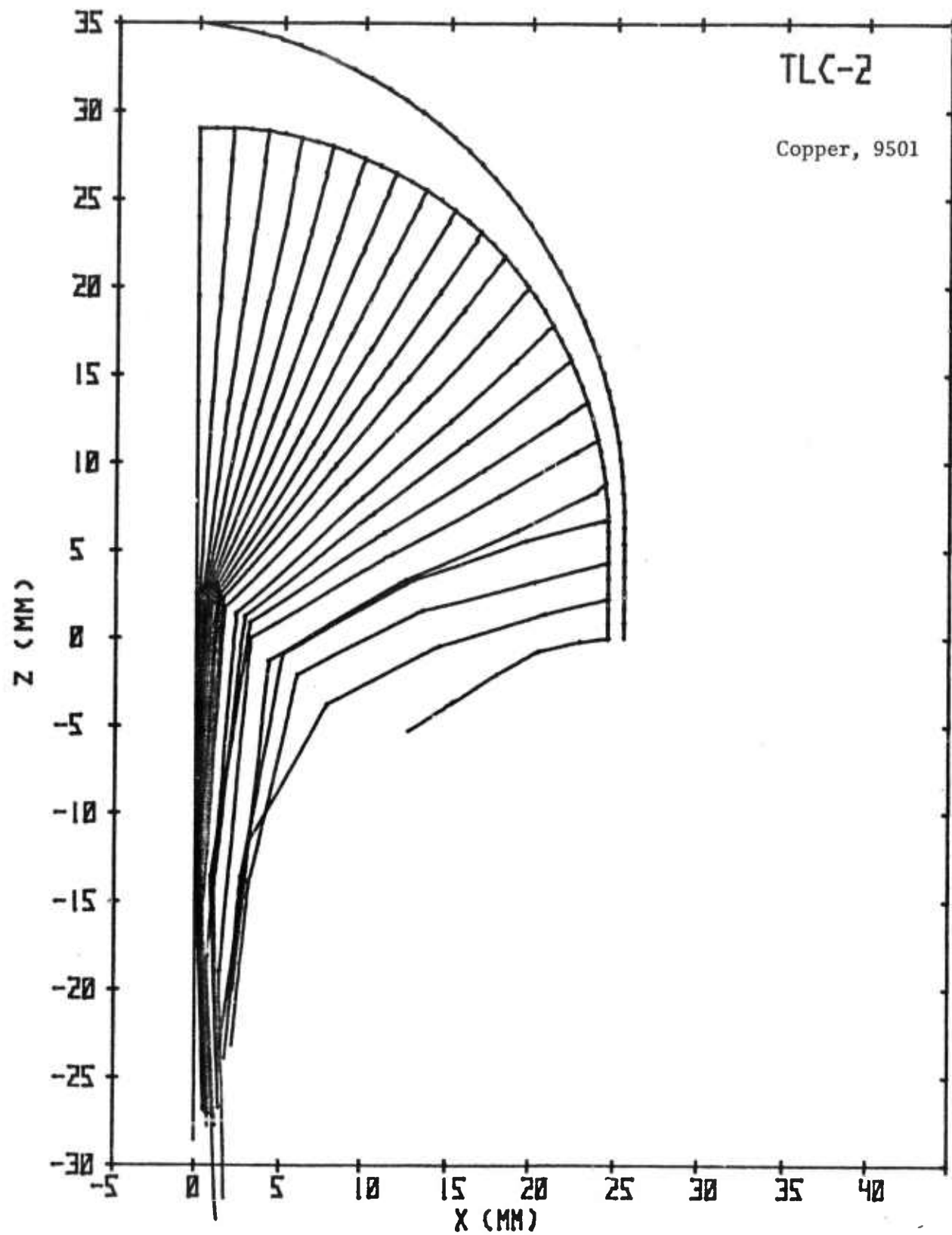
UNCLASSIFIED



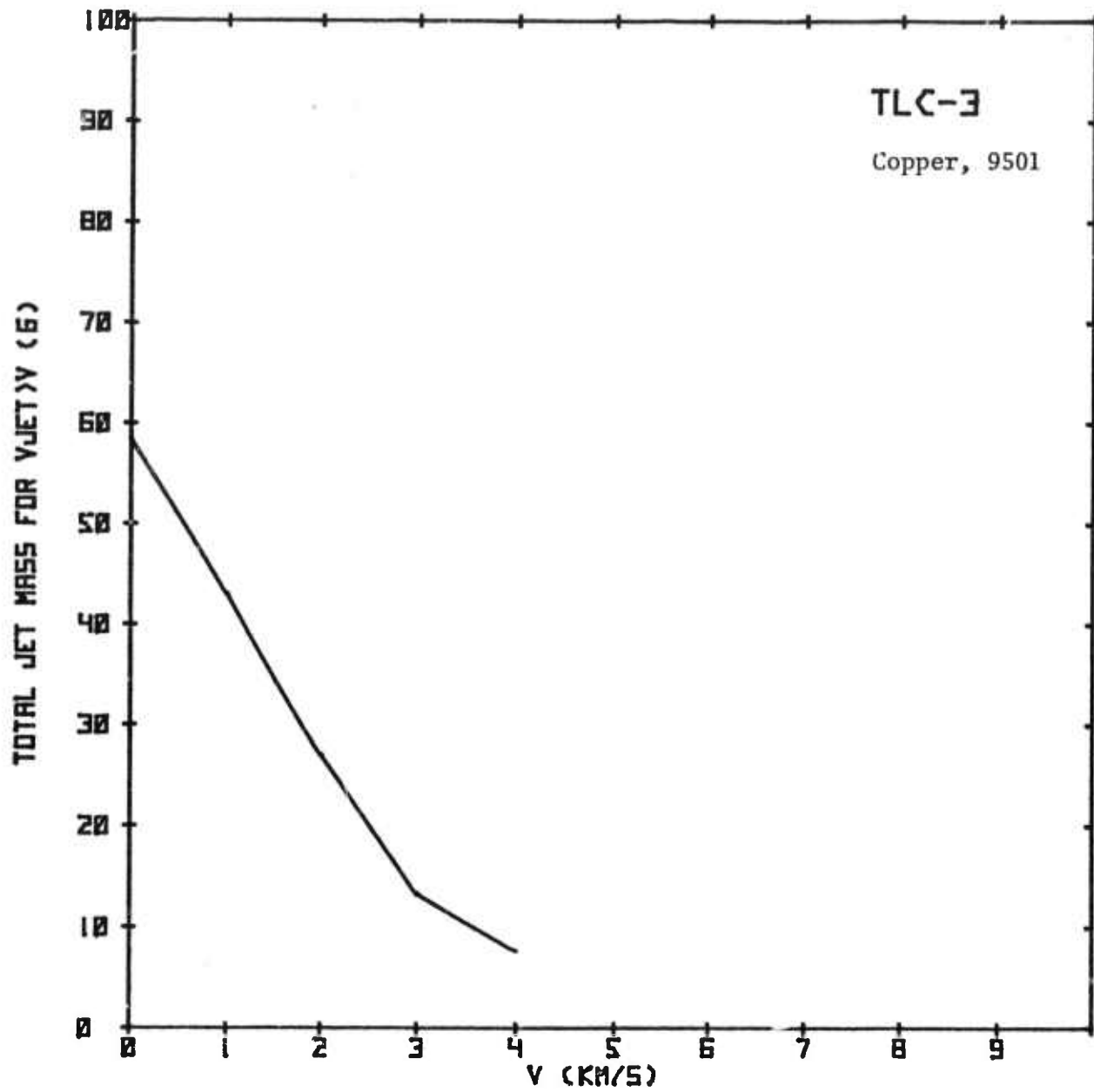
UNCLASSIFIED



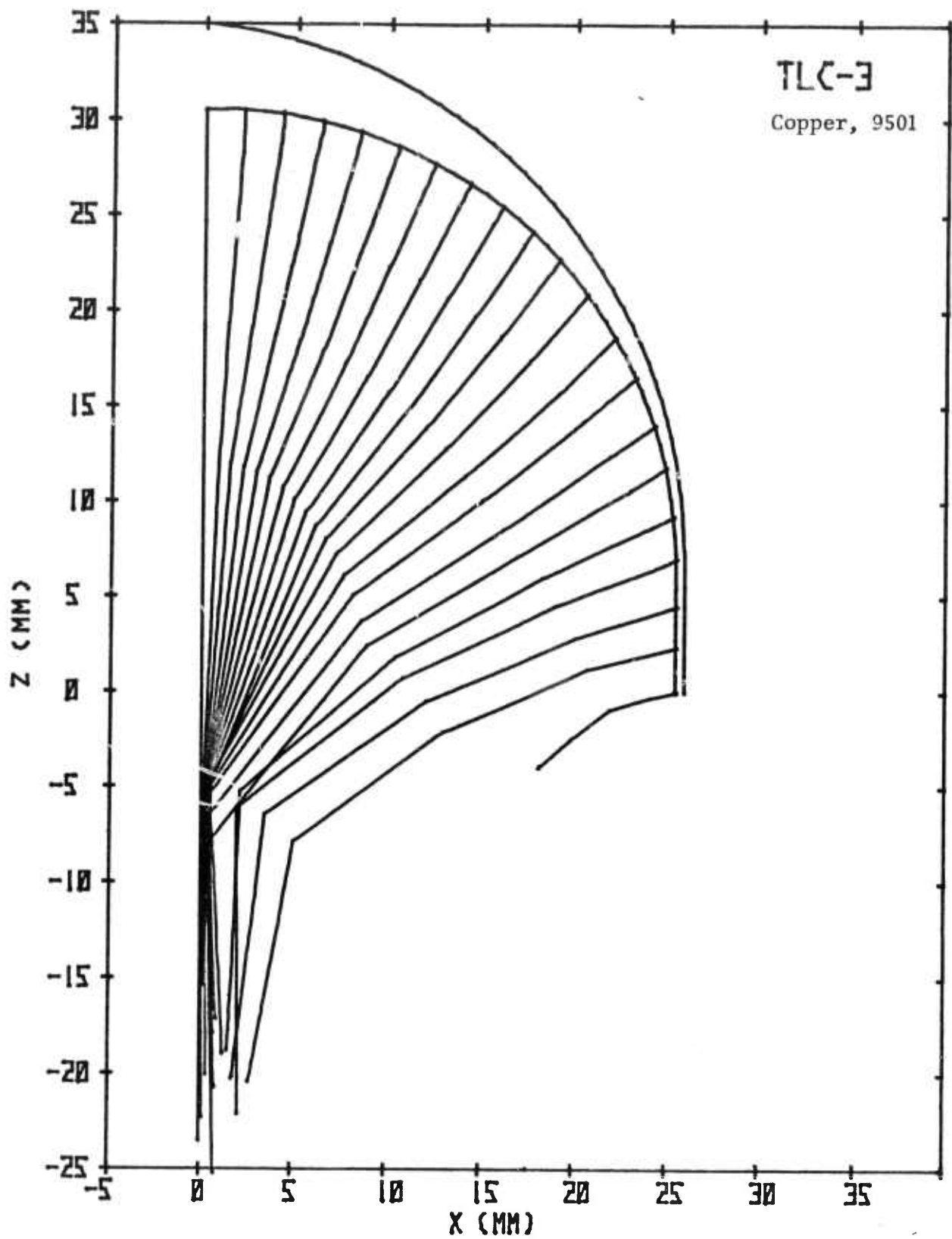
UNCLASSIFIED



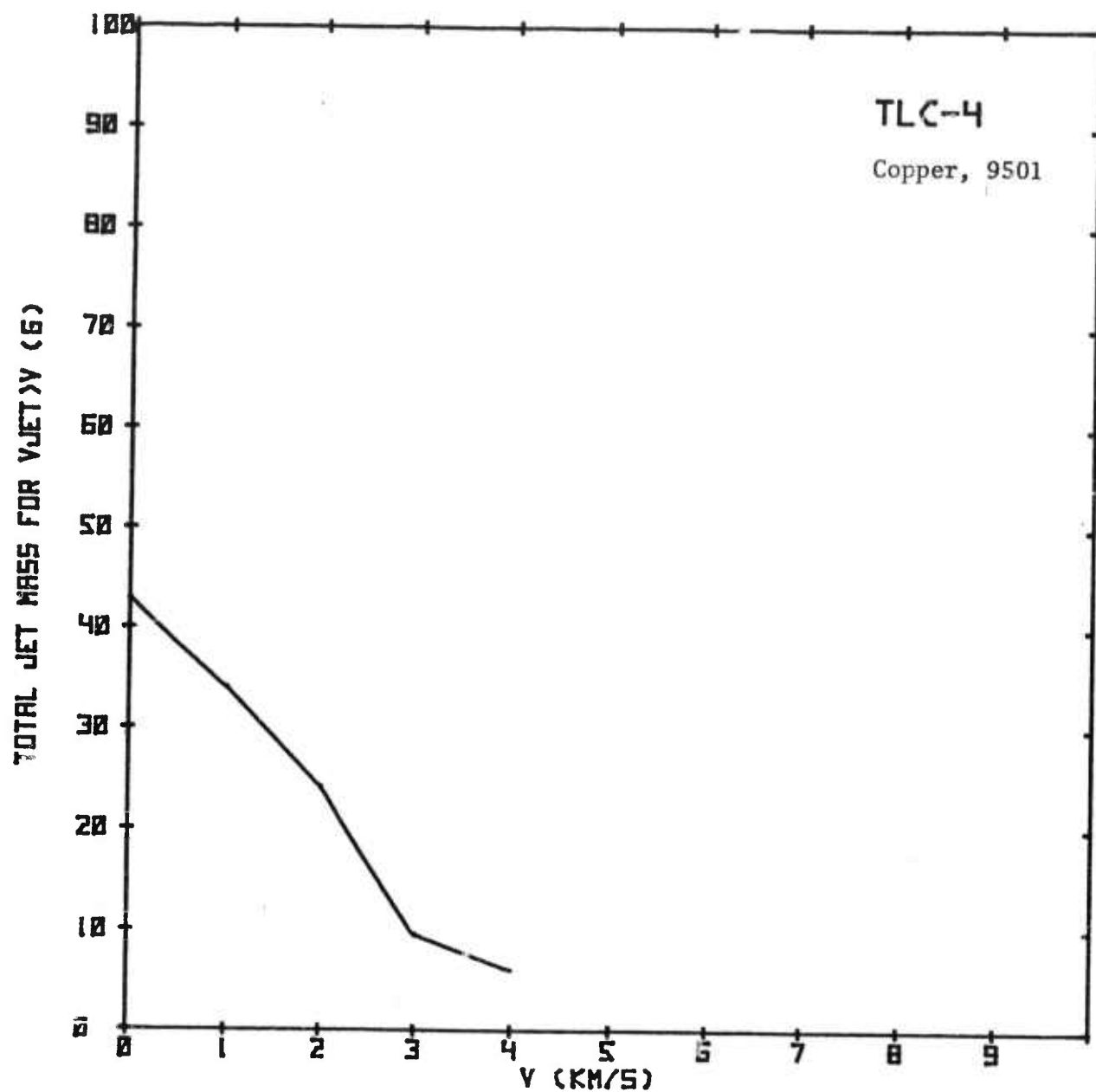
UNCLASSIFIED



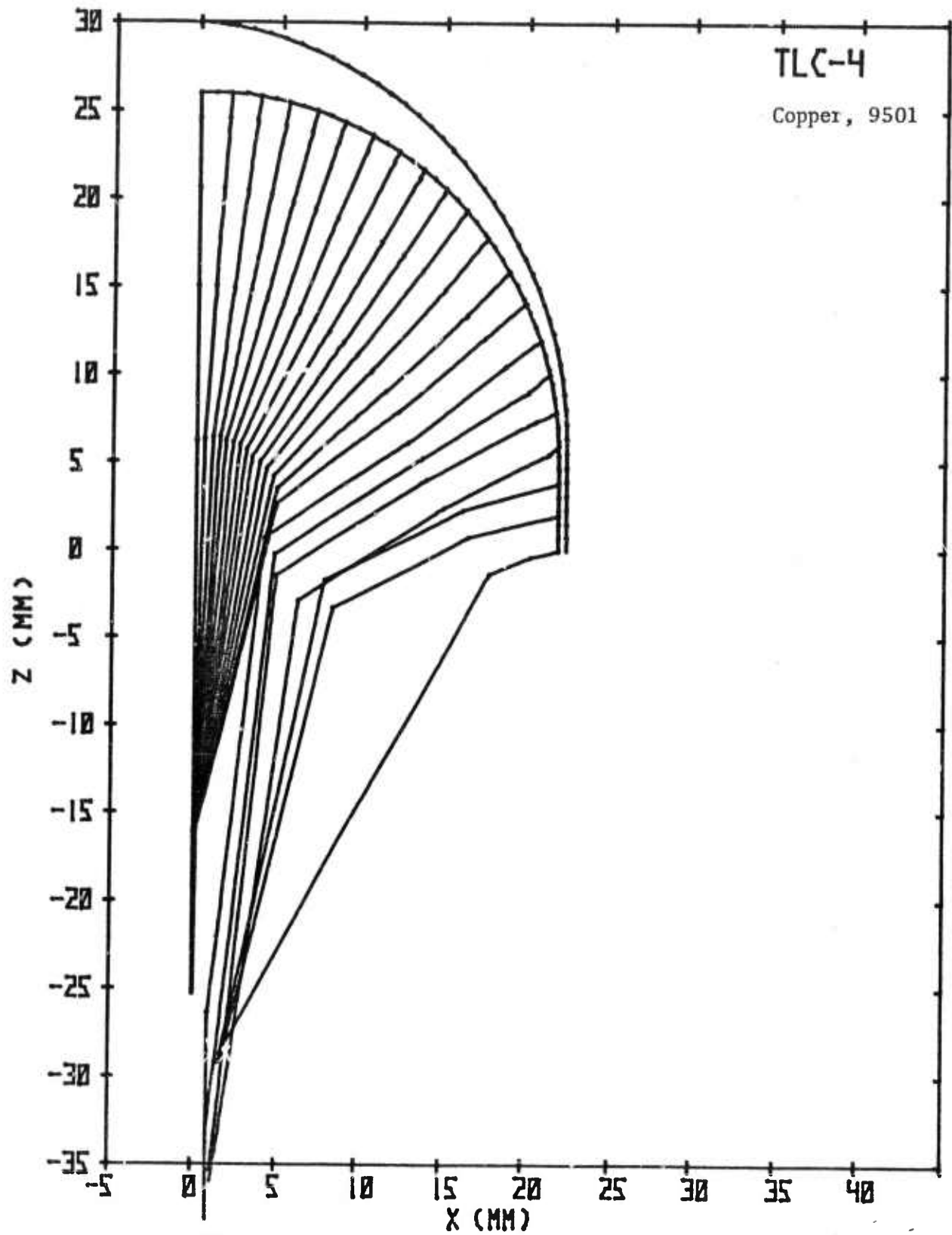
UNCLASSIFIED

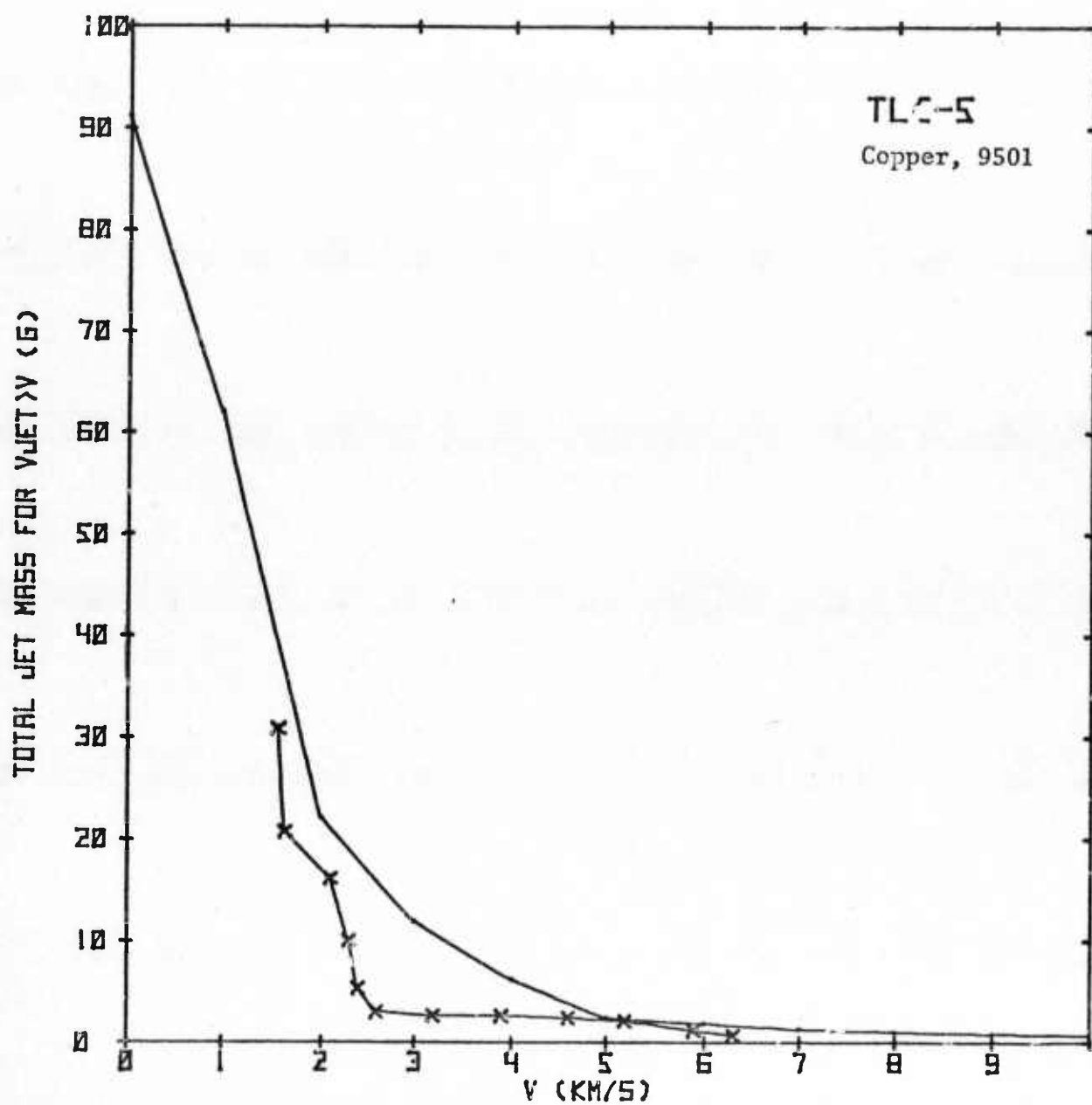
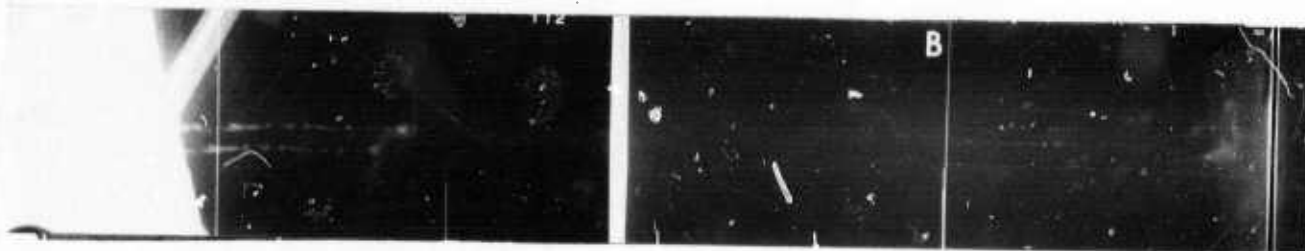


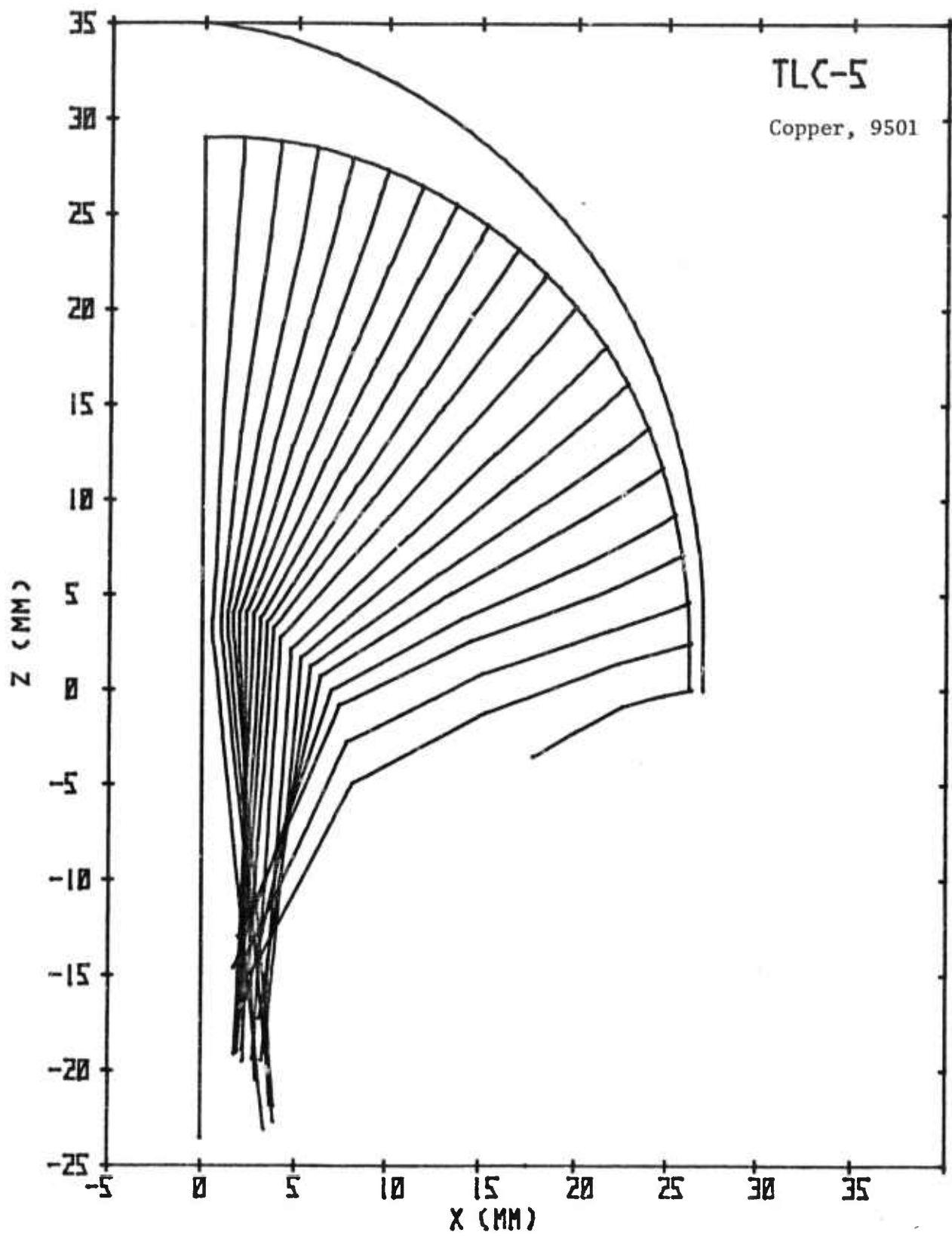
UNCLASSIFIED

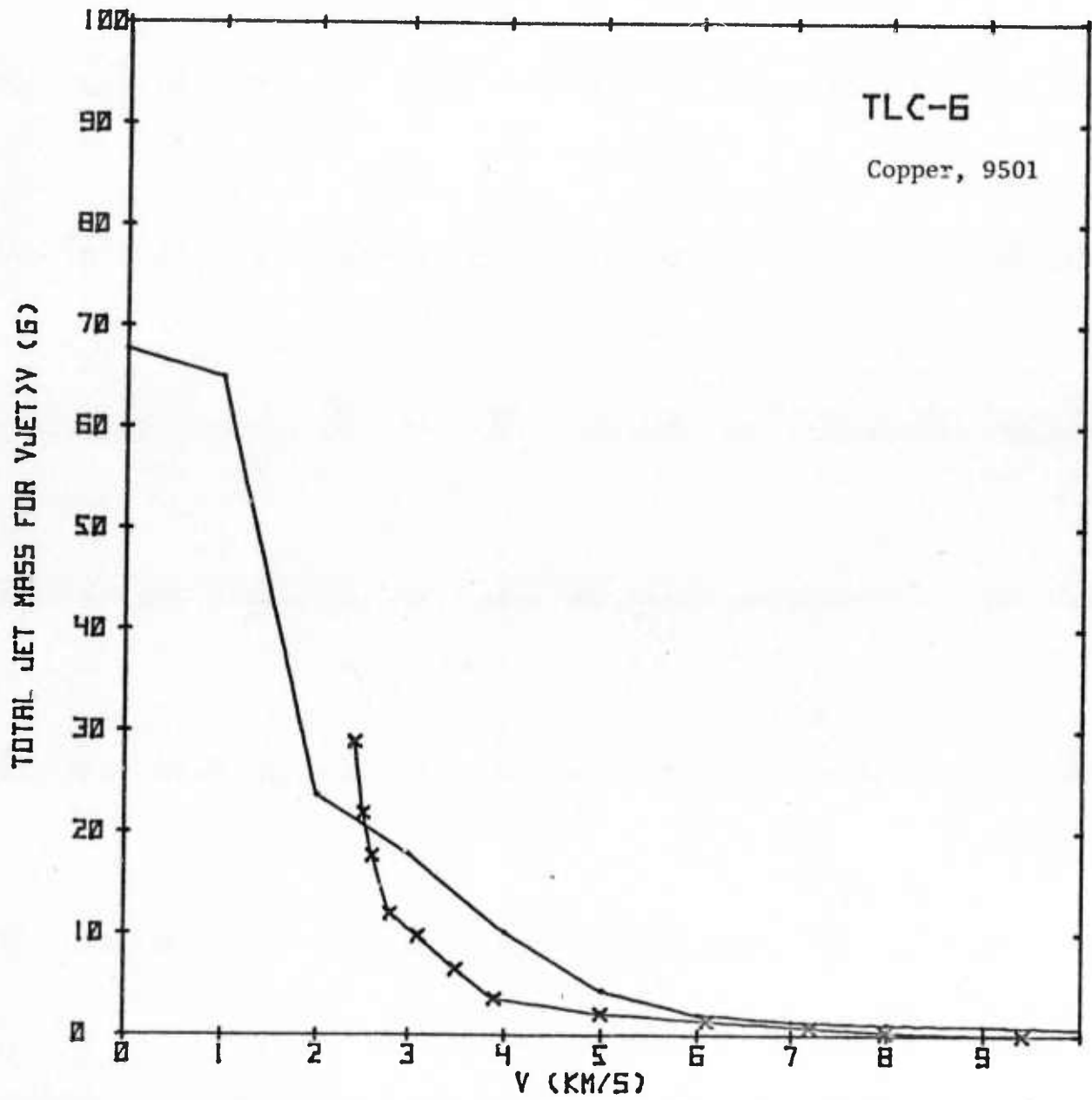


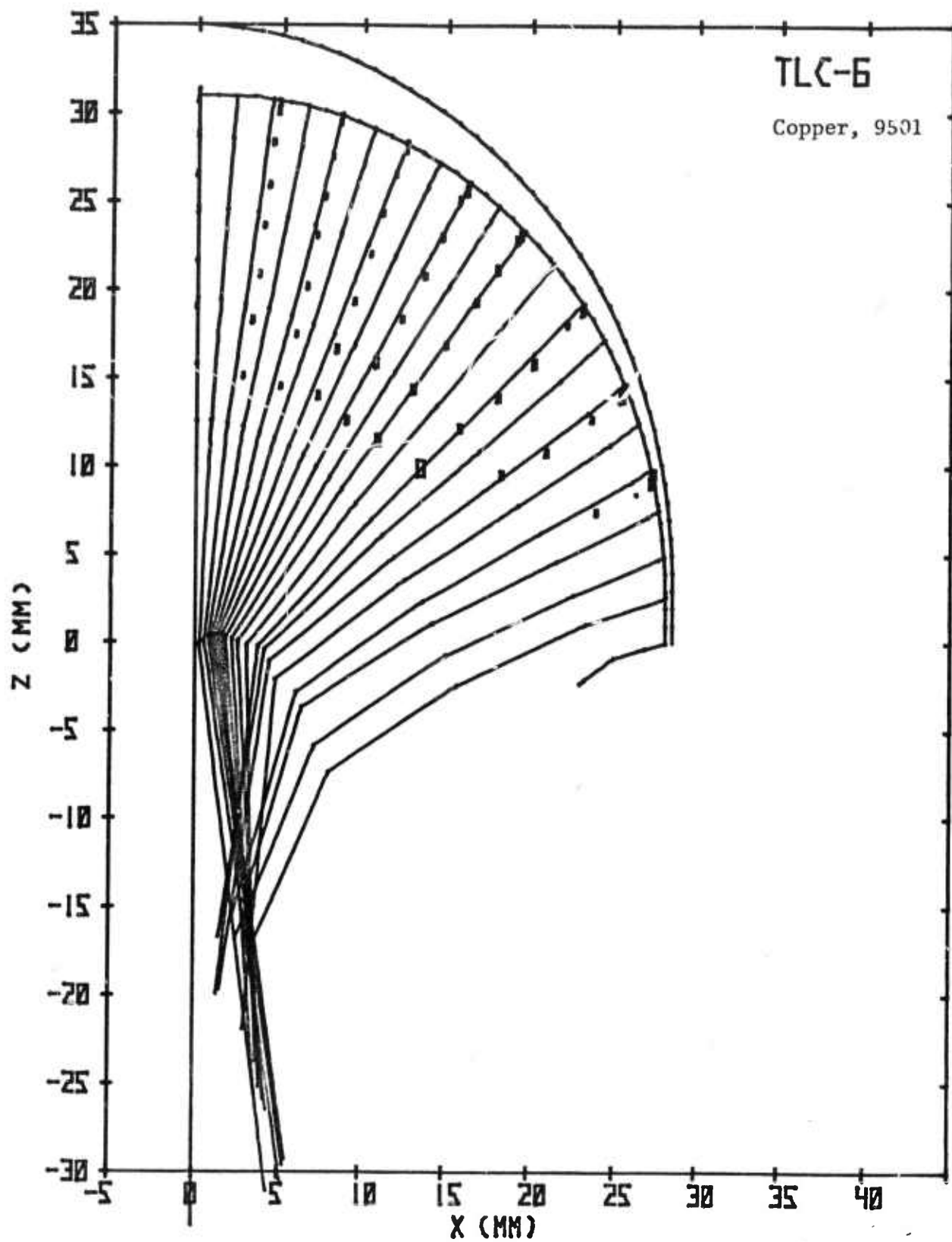
UNCLASSIFIED



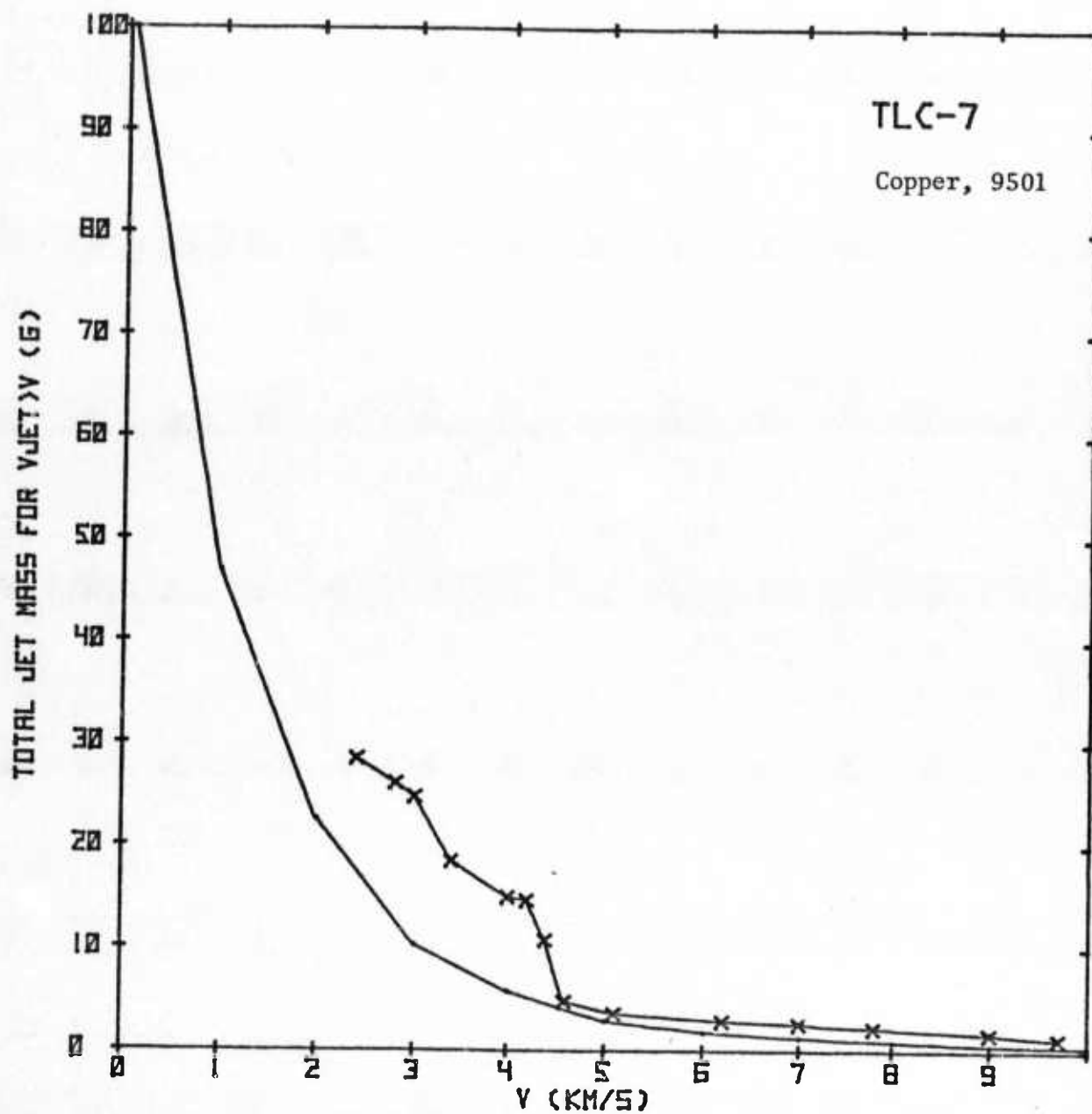
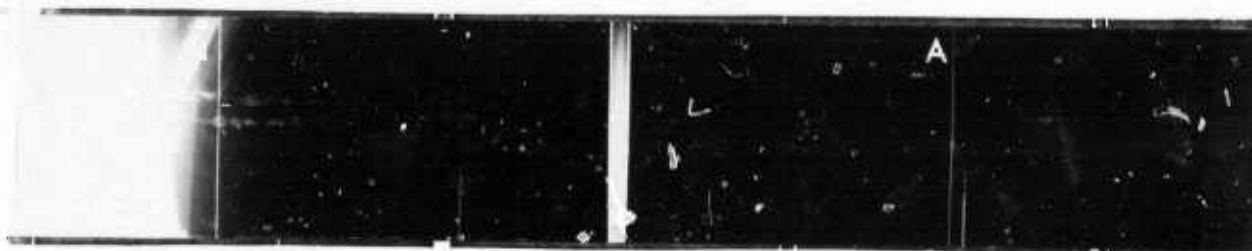




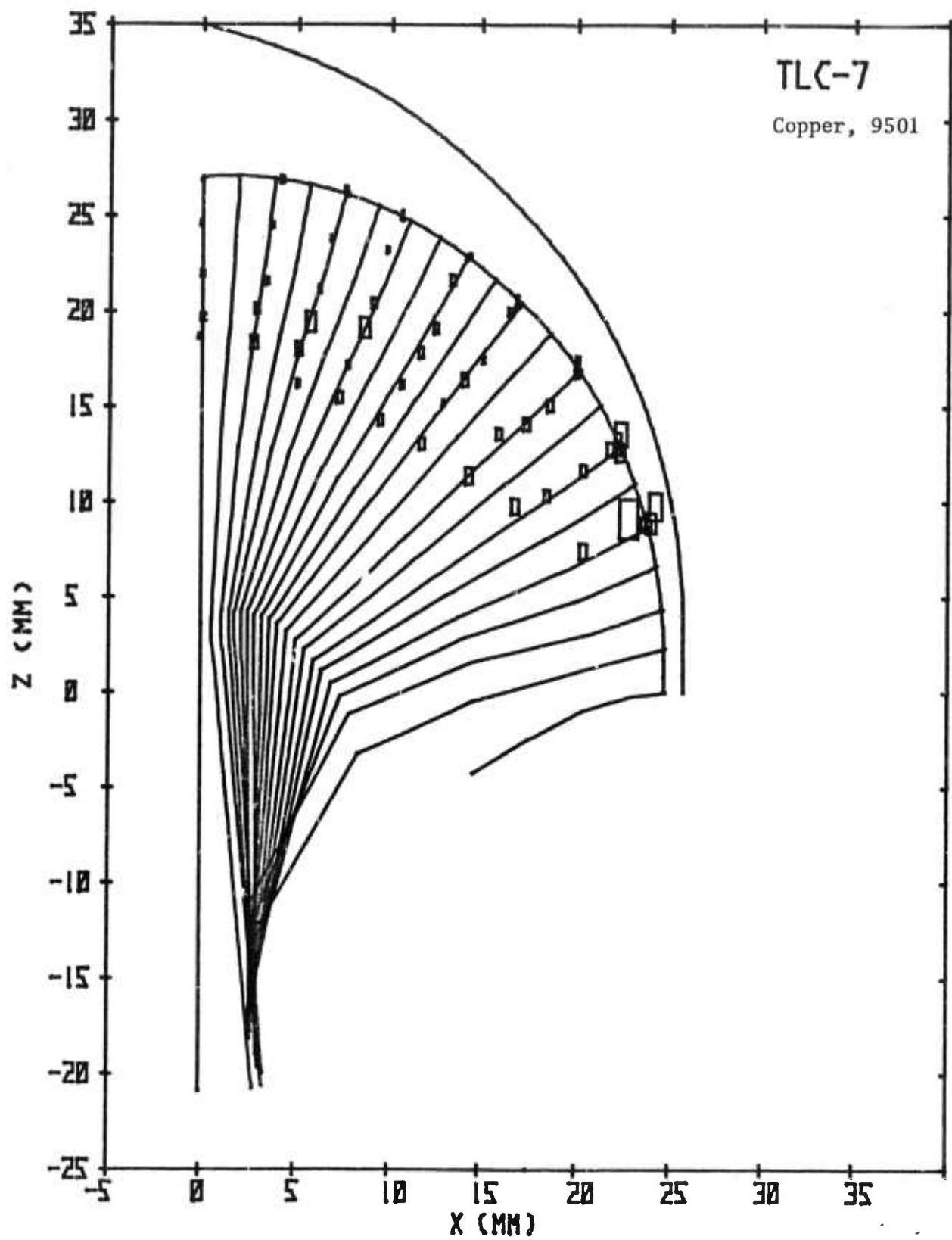


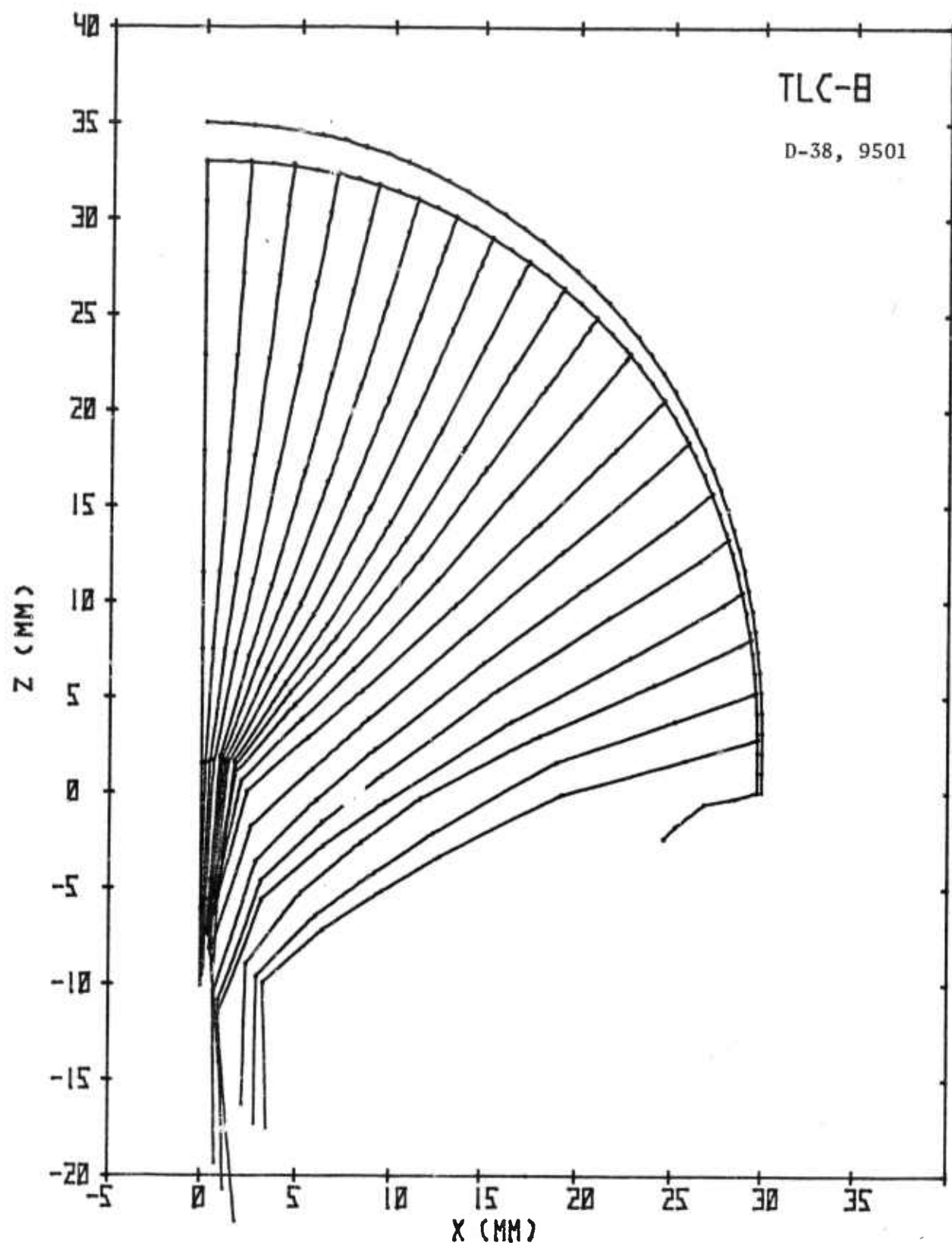


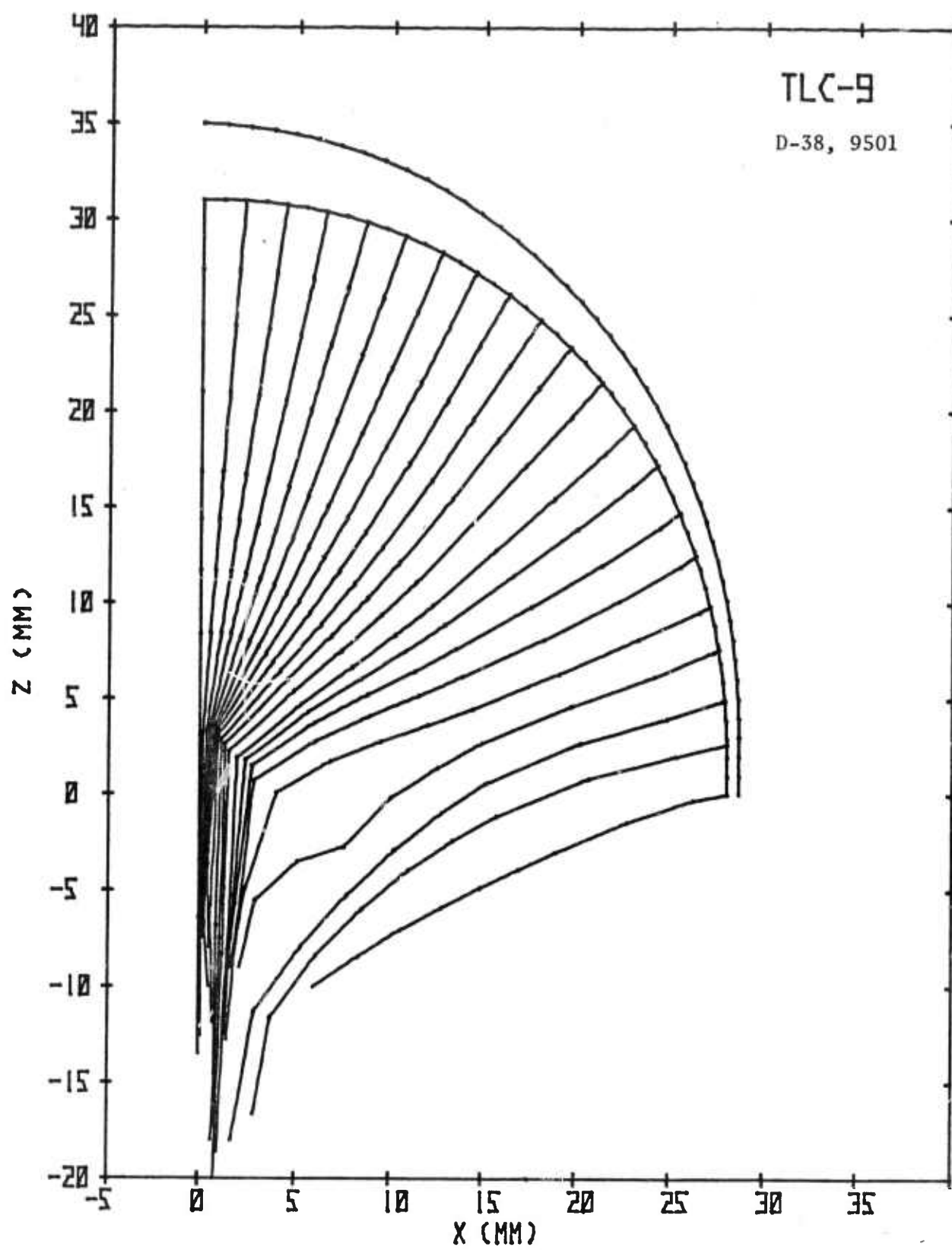
UNCLASSIFIED

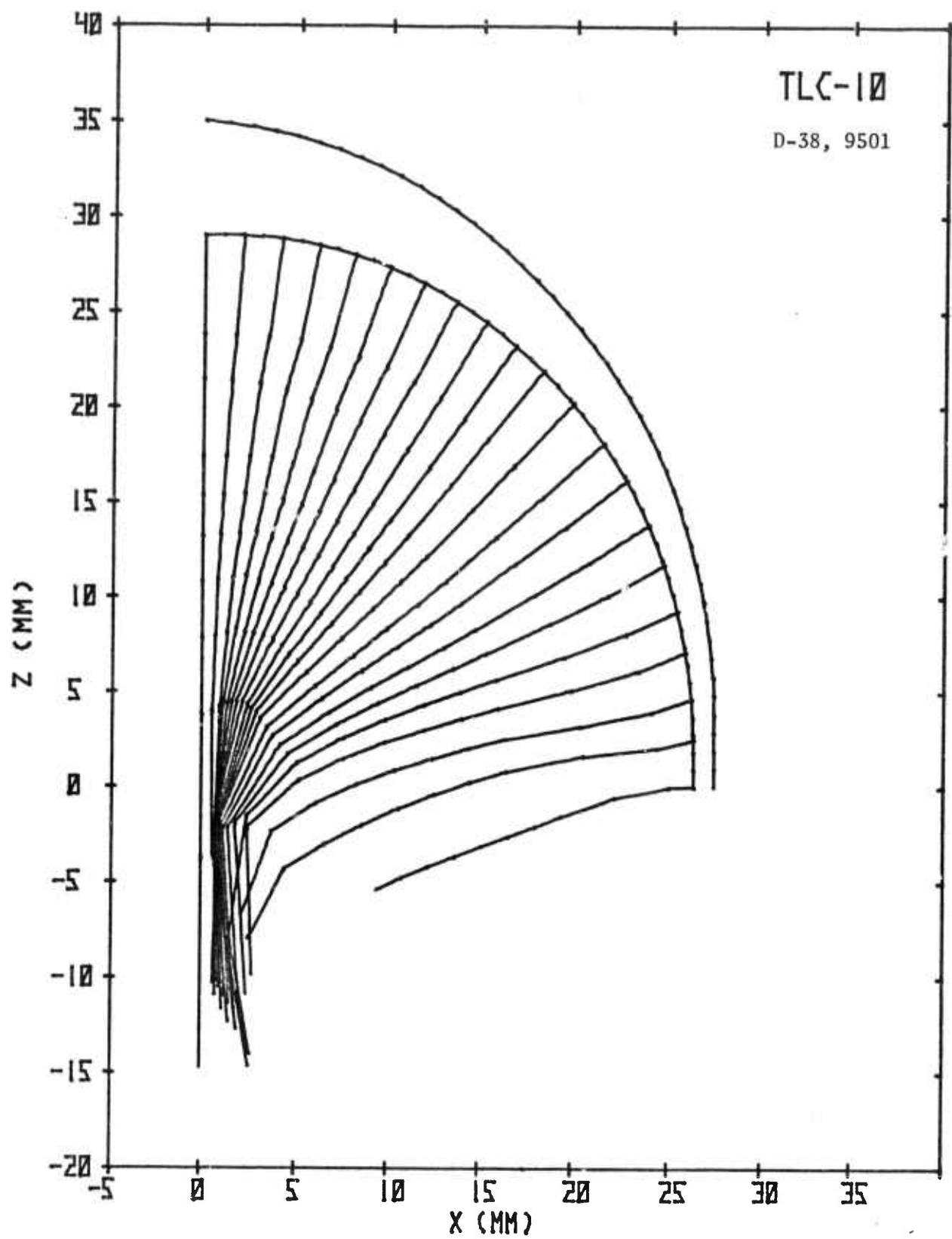


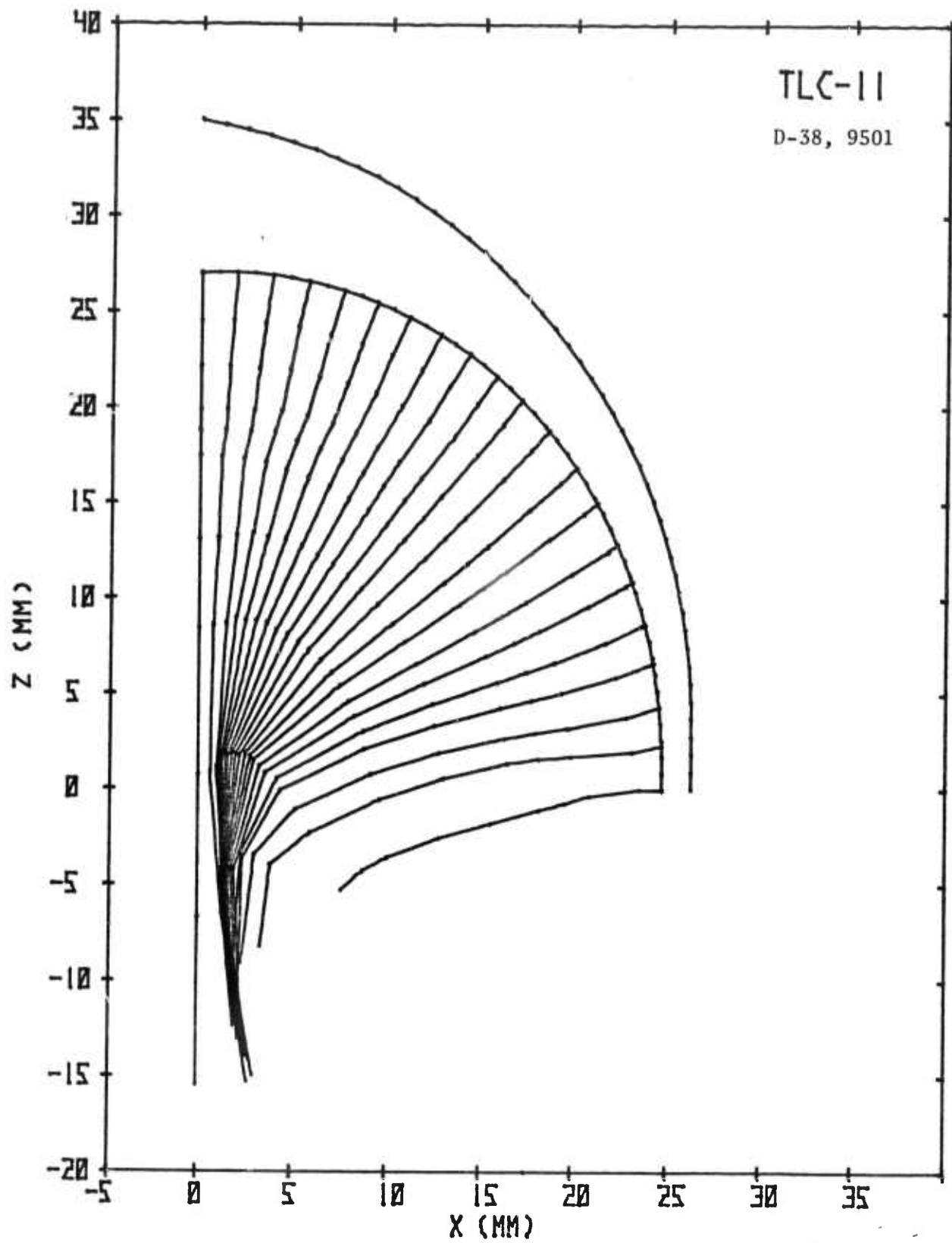
UNCLASSIFIED

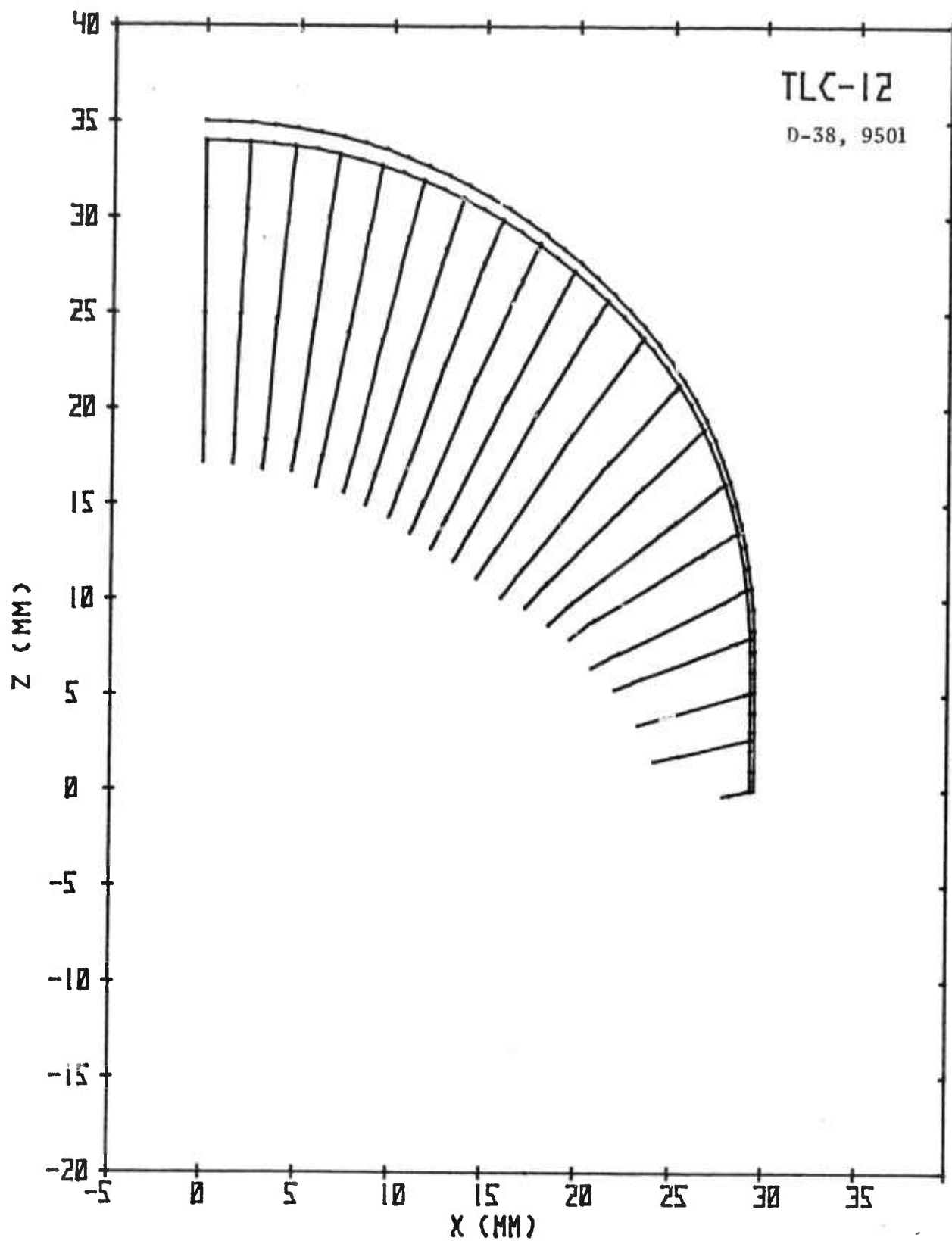


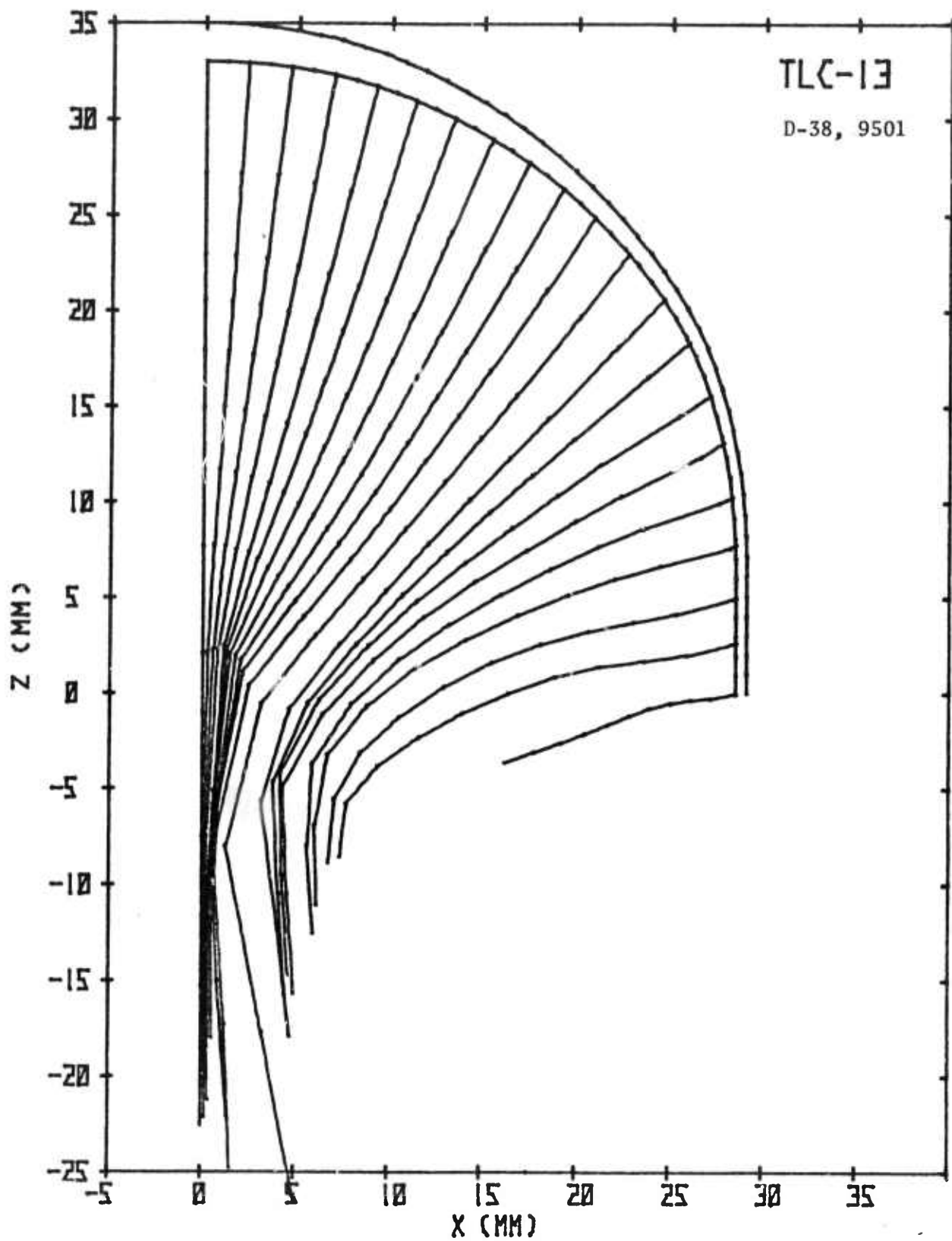


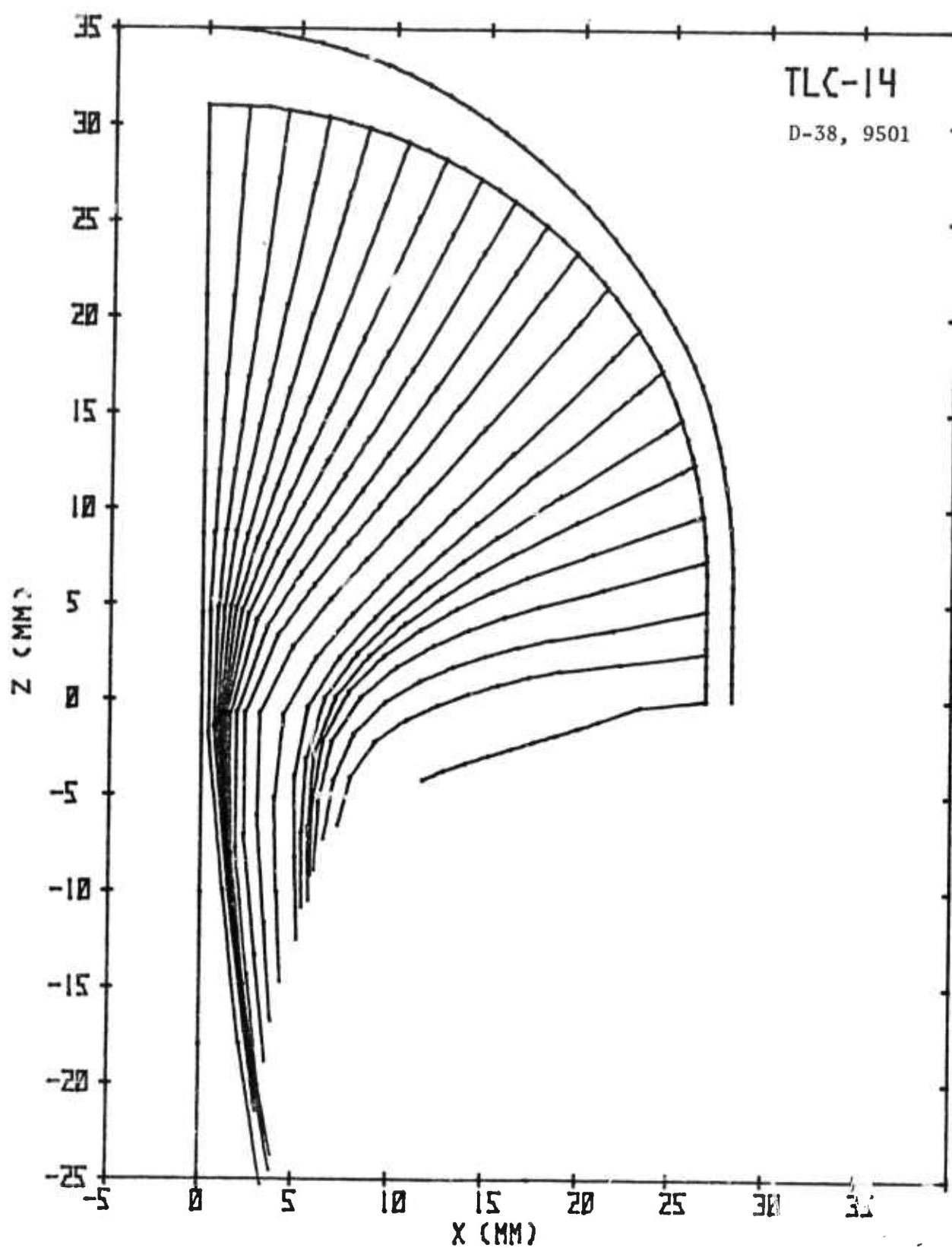




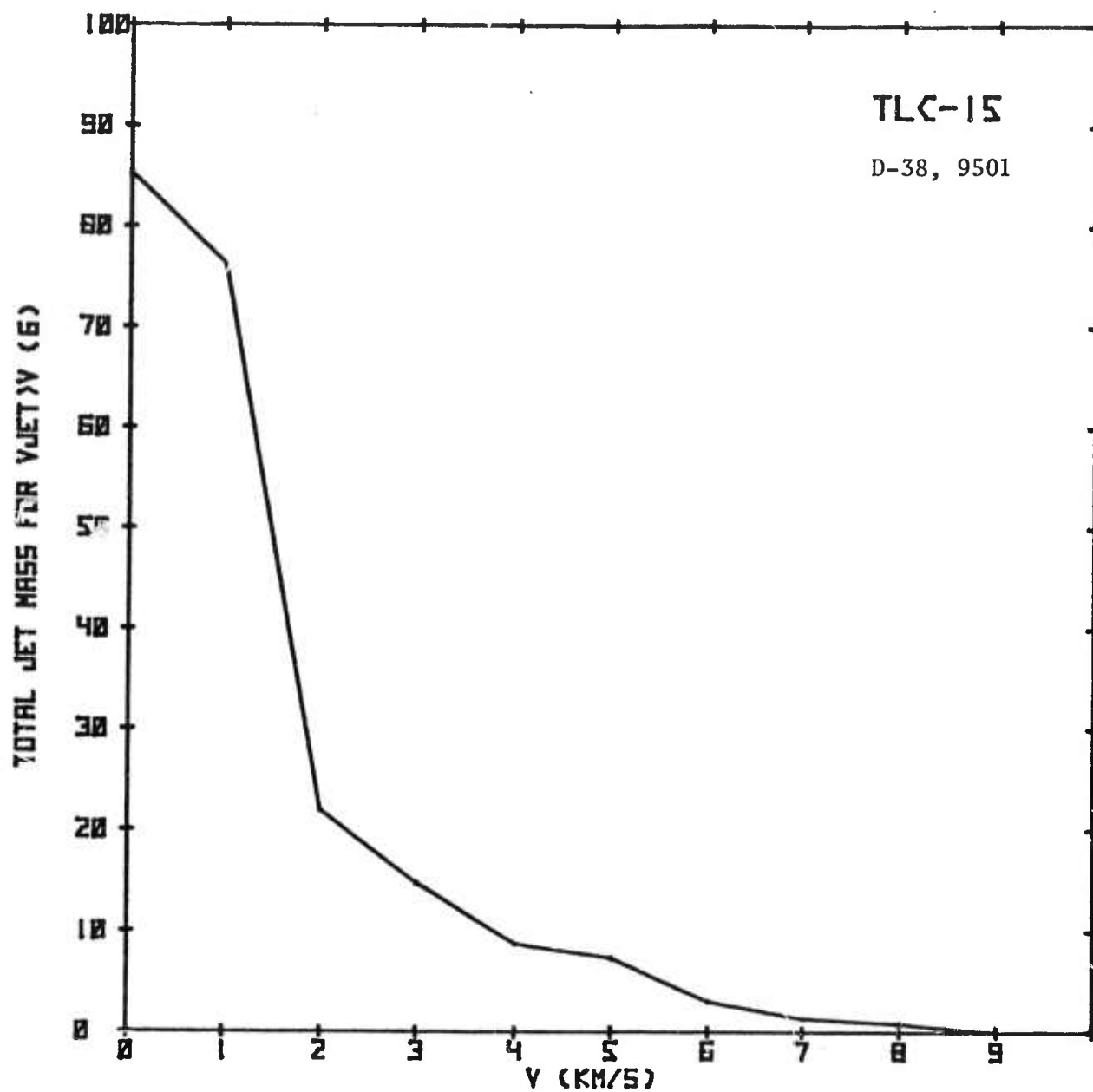




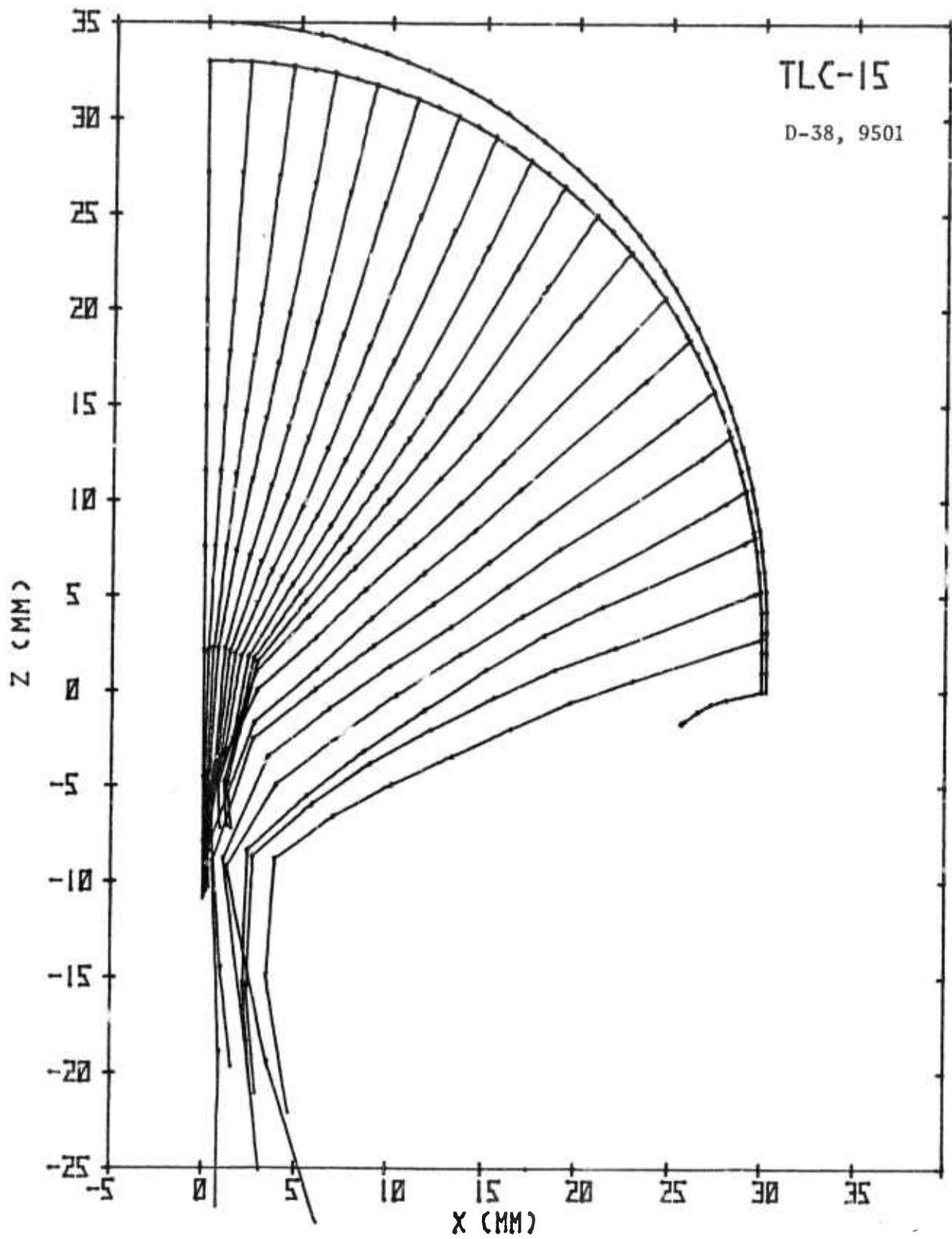




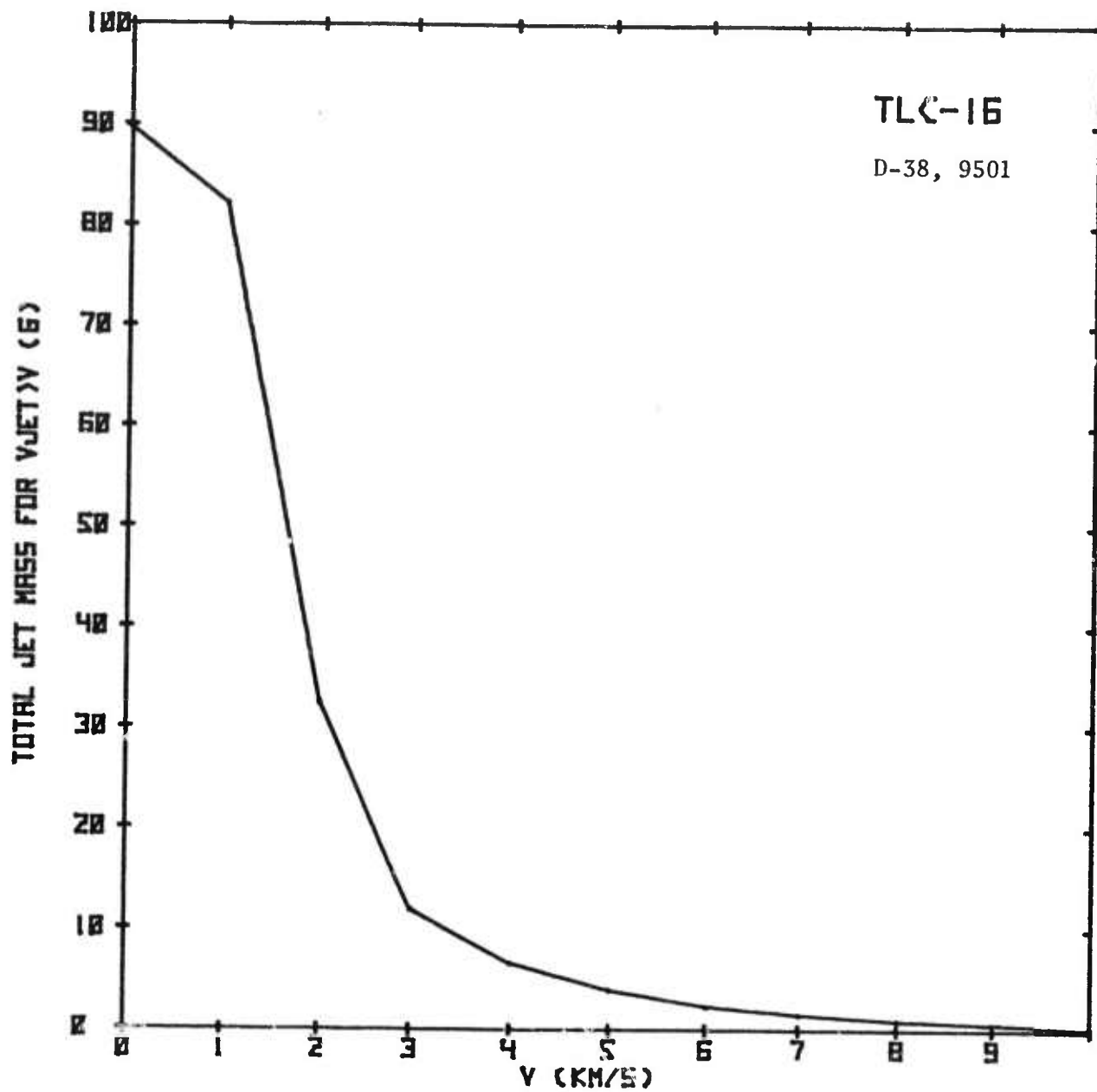
UNCLASSIFIED



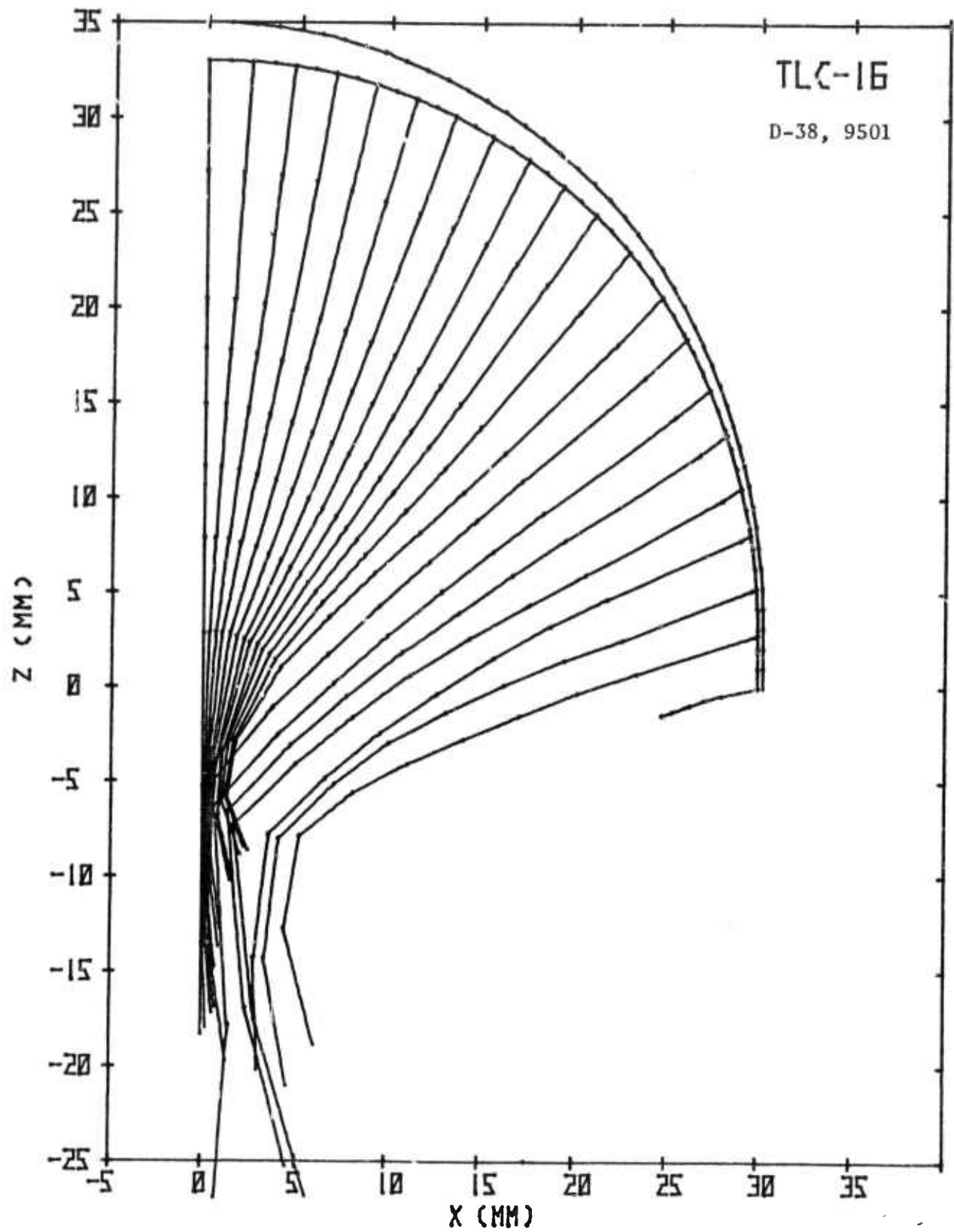
UNCLASSIFIED



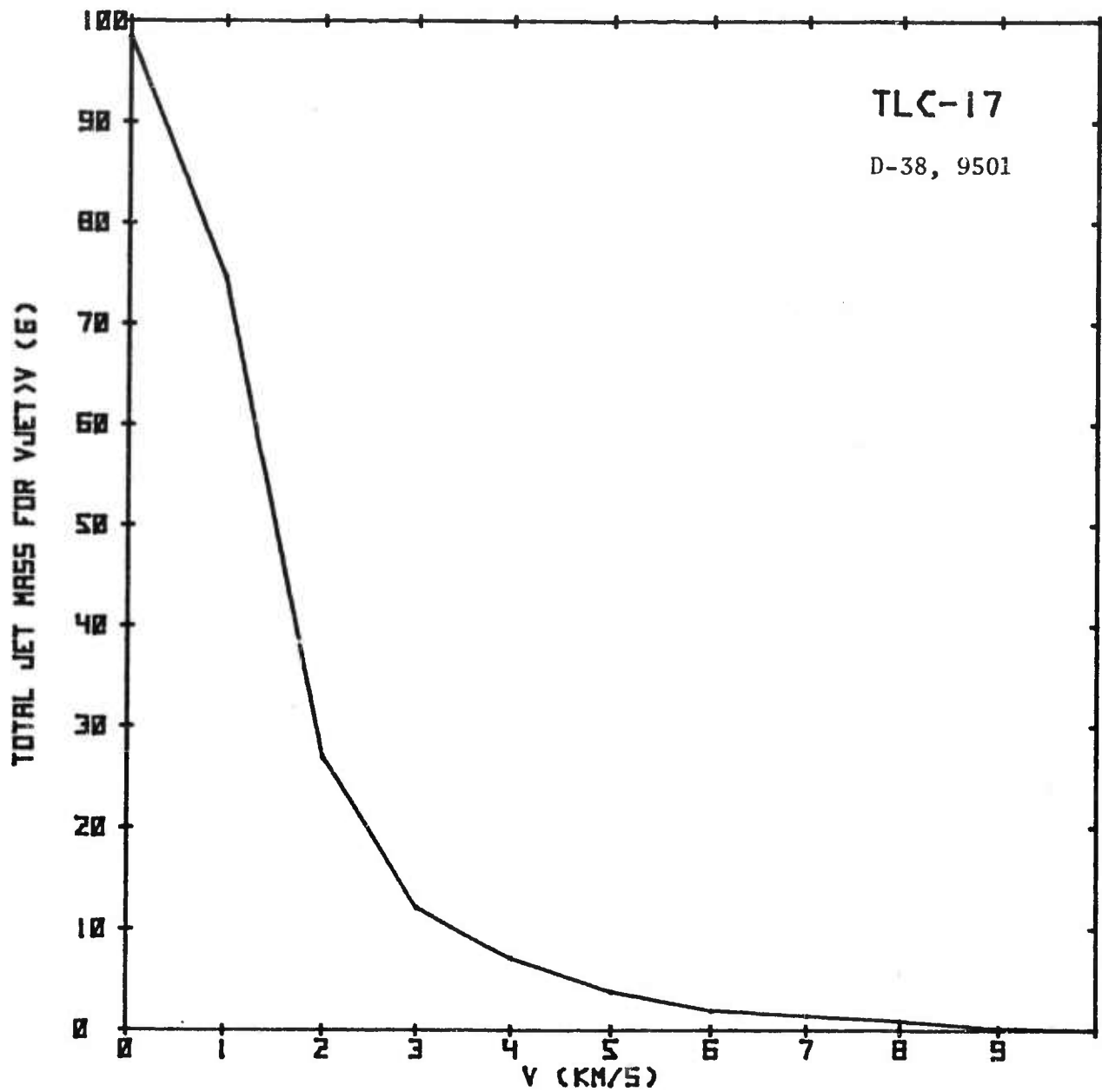
UNCLASSIFIED



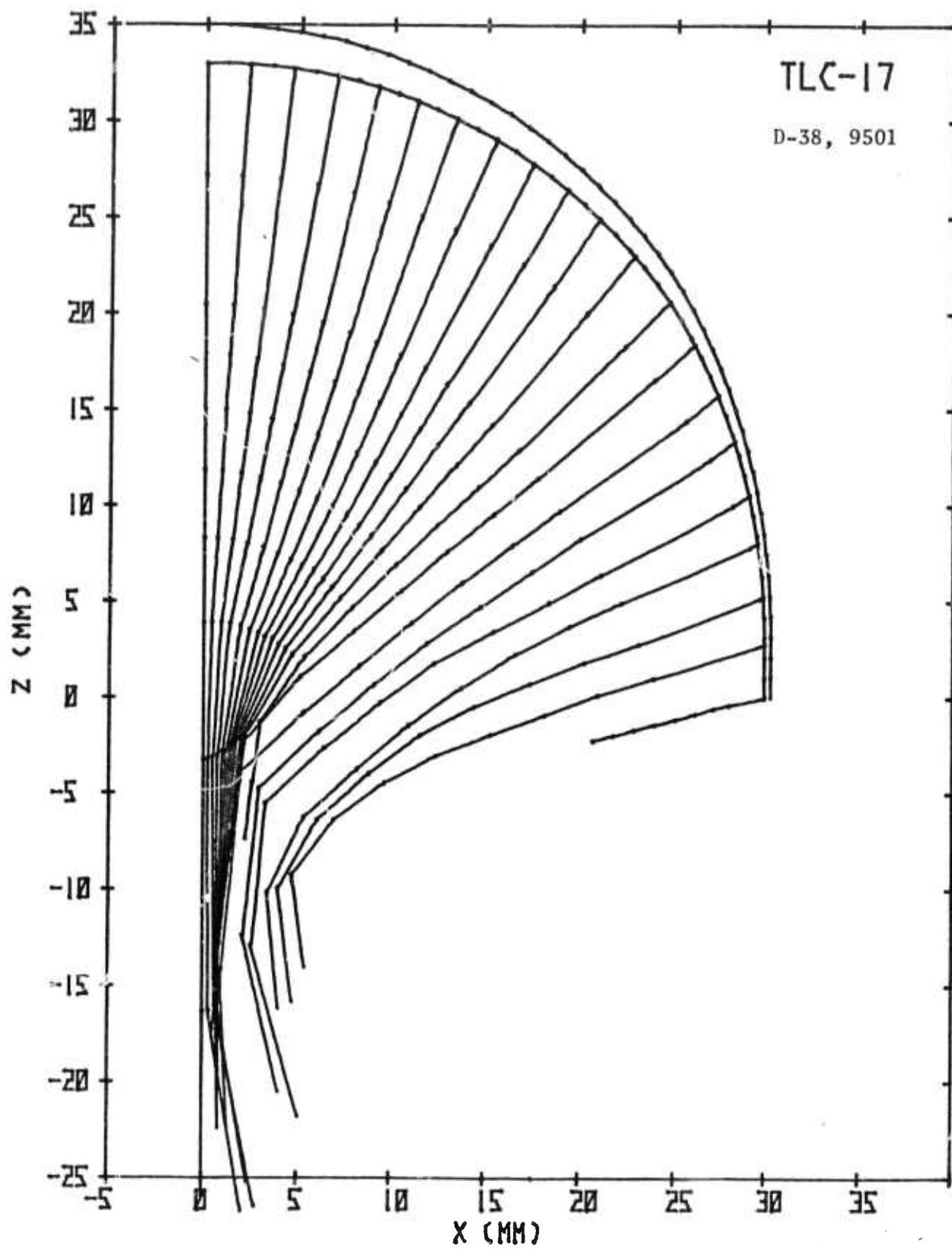
UNCLASSIFIED



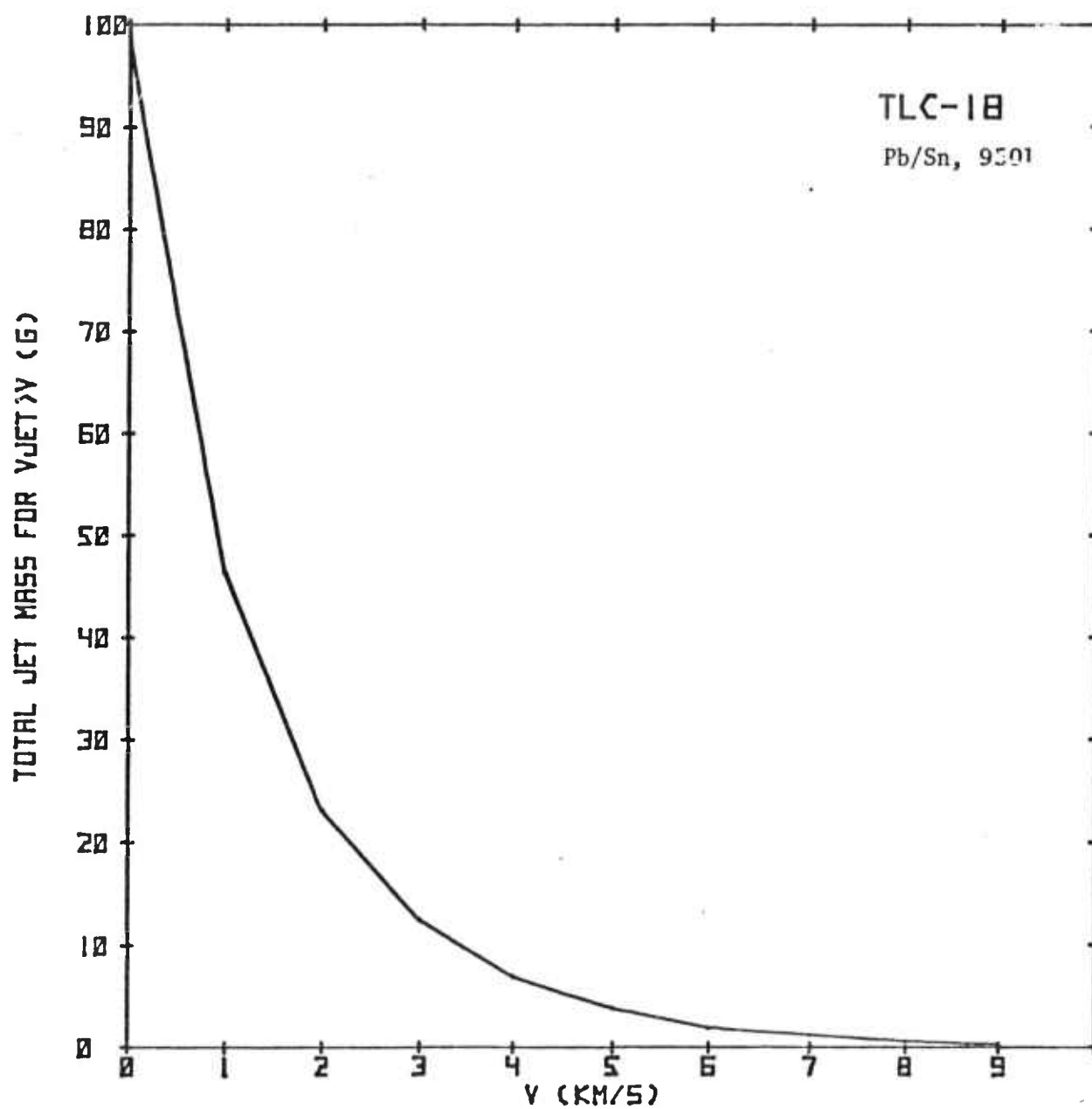
UNCLASSIFIED



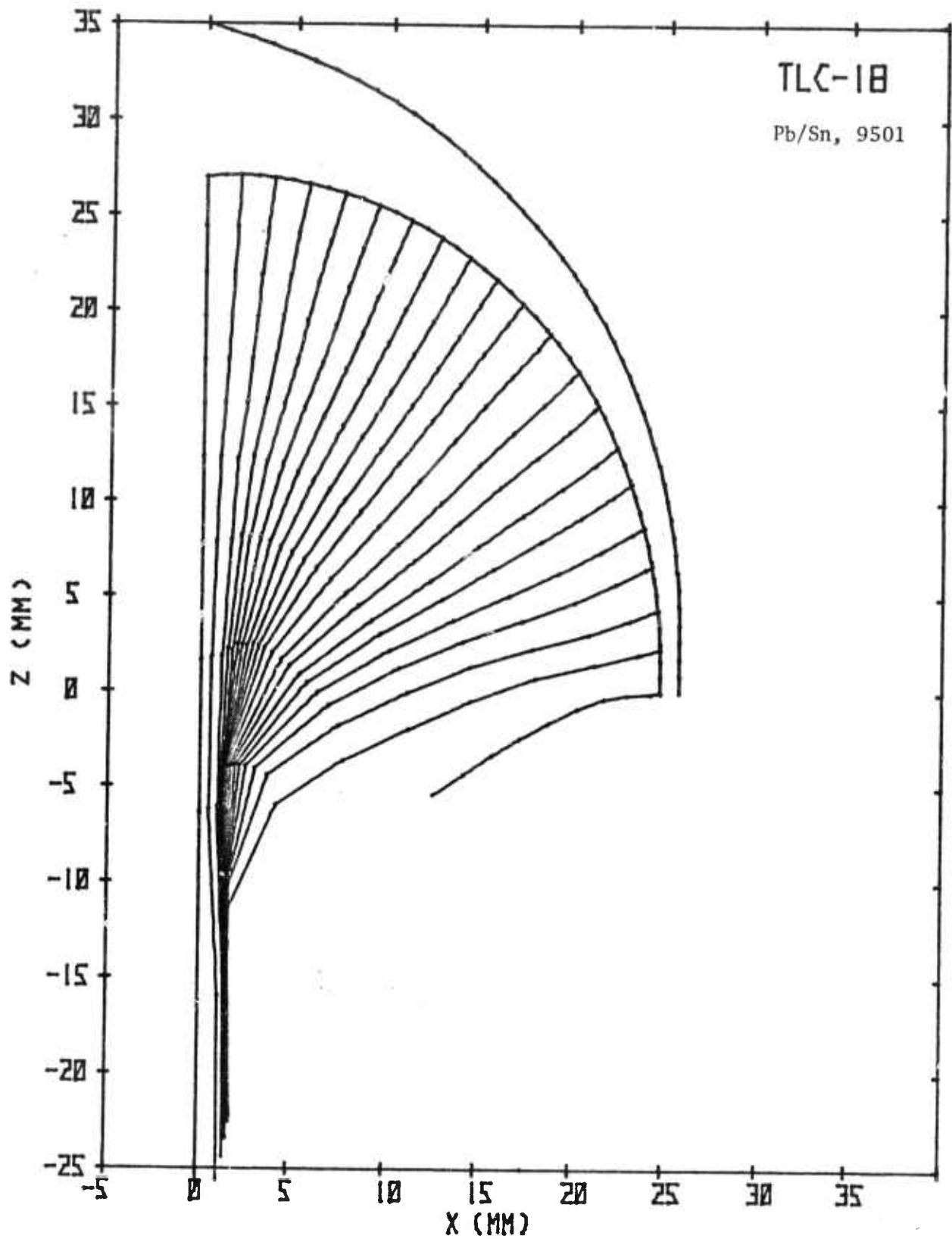
UNCLASSIFIED



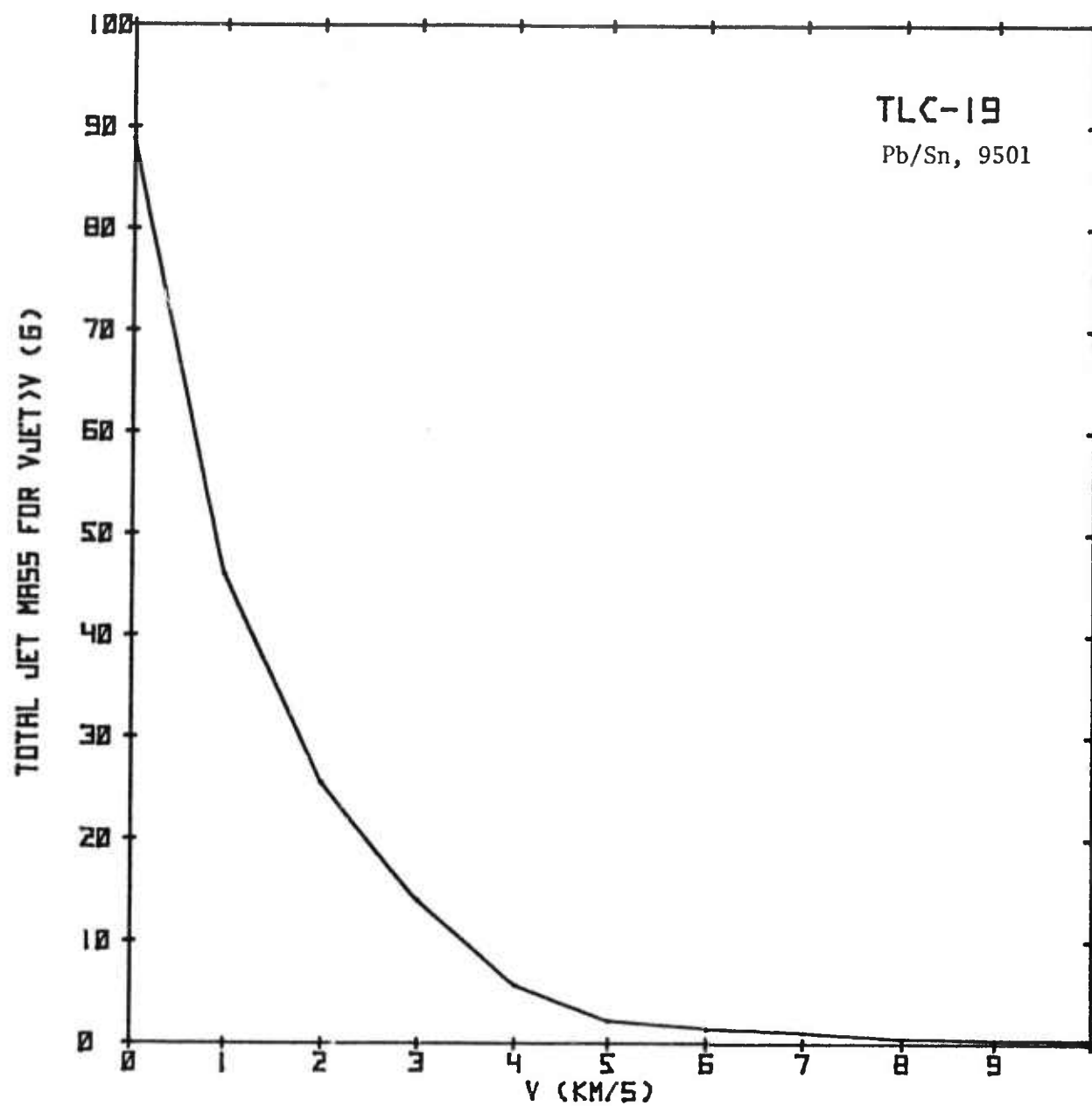
UNCLASSIFIED



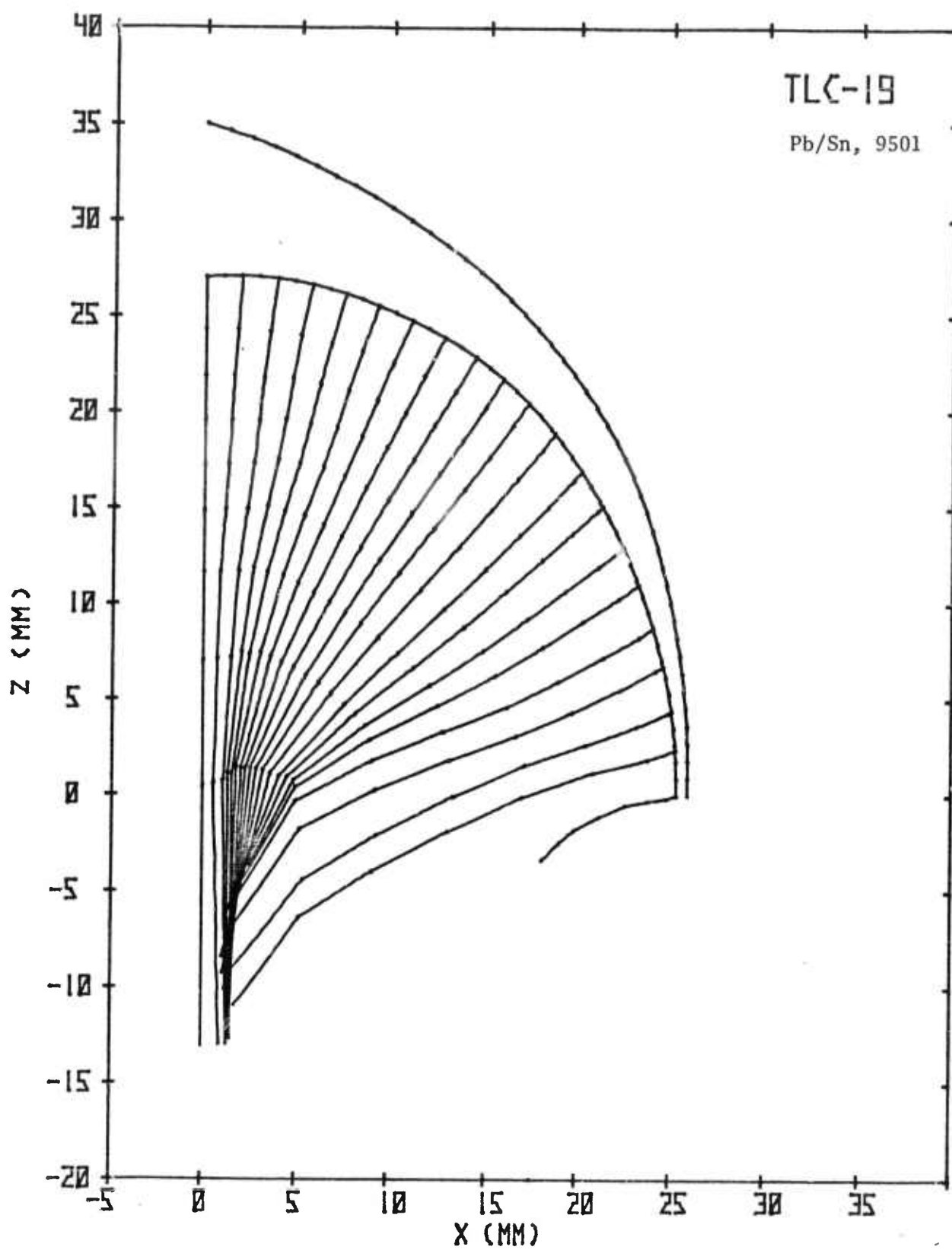
UNCLASSIFIED



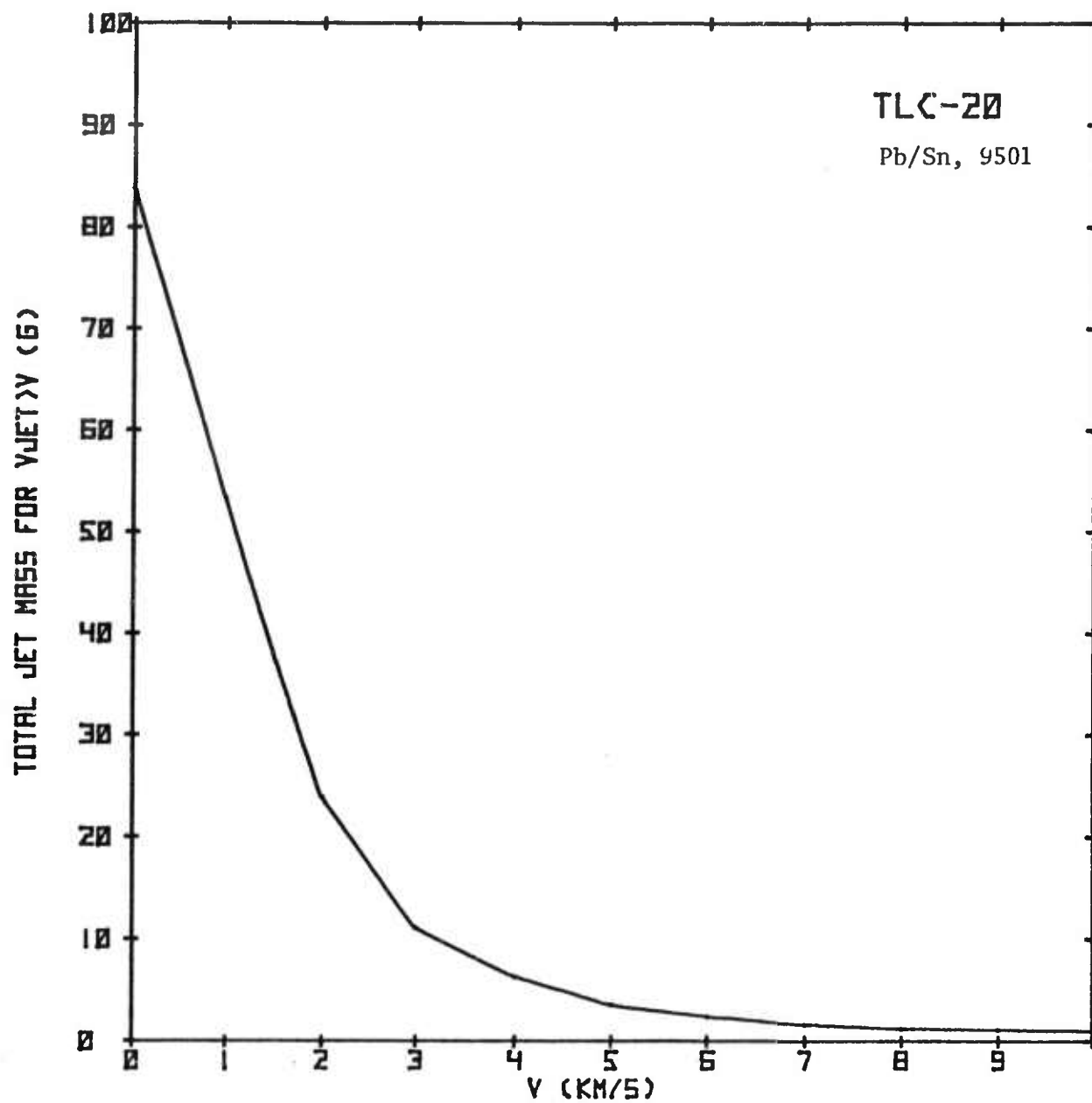
UNCLASSIFIED



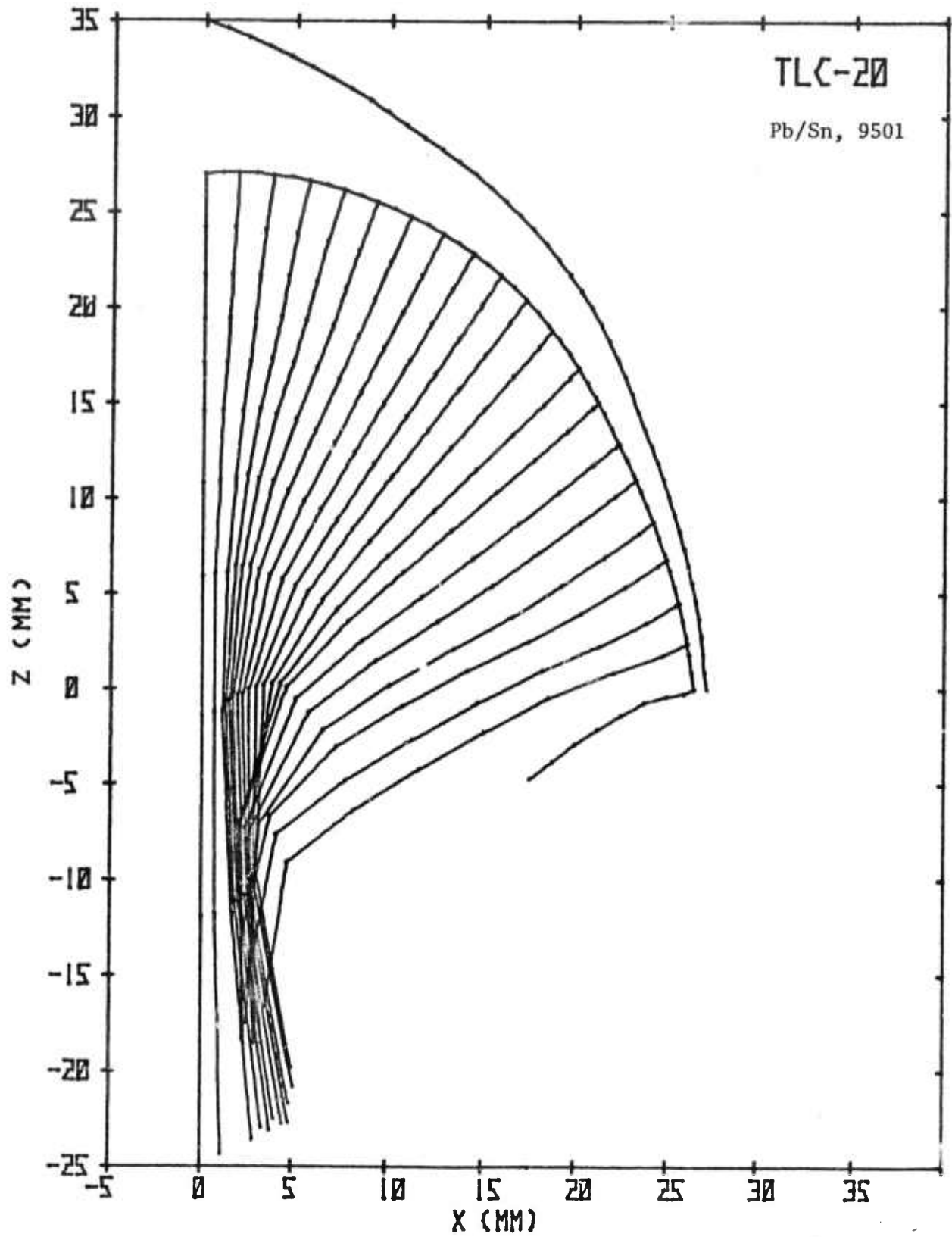
UNCLASSIFIED



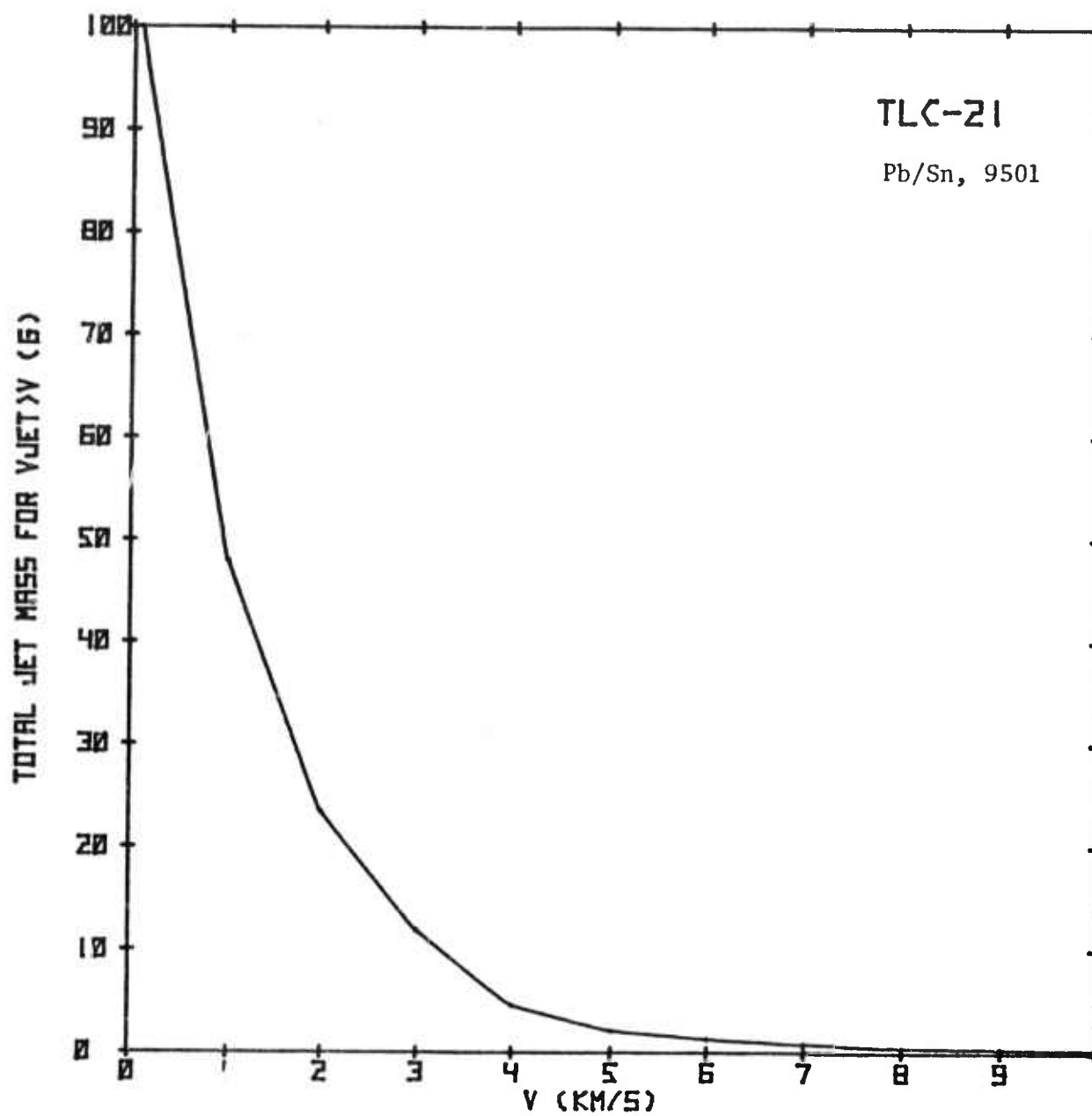
UNCLASSIFIED



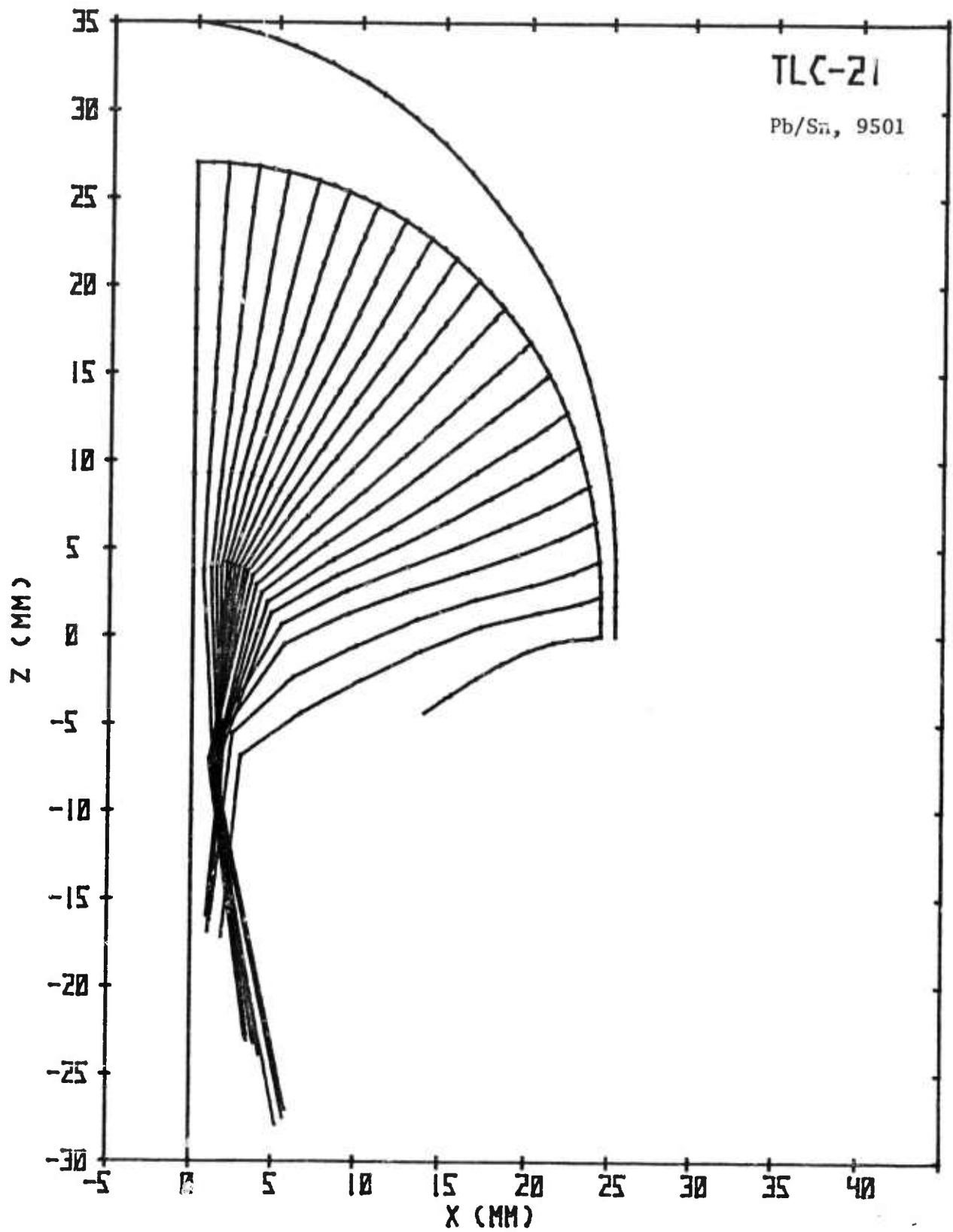
UNCLASSIFIED



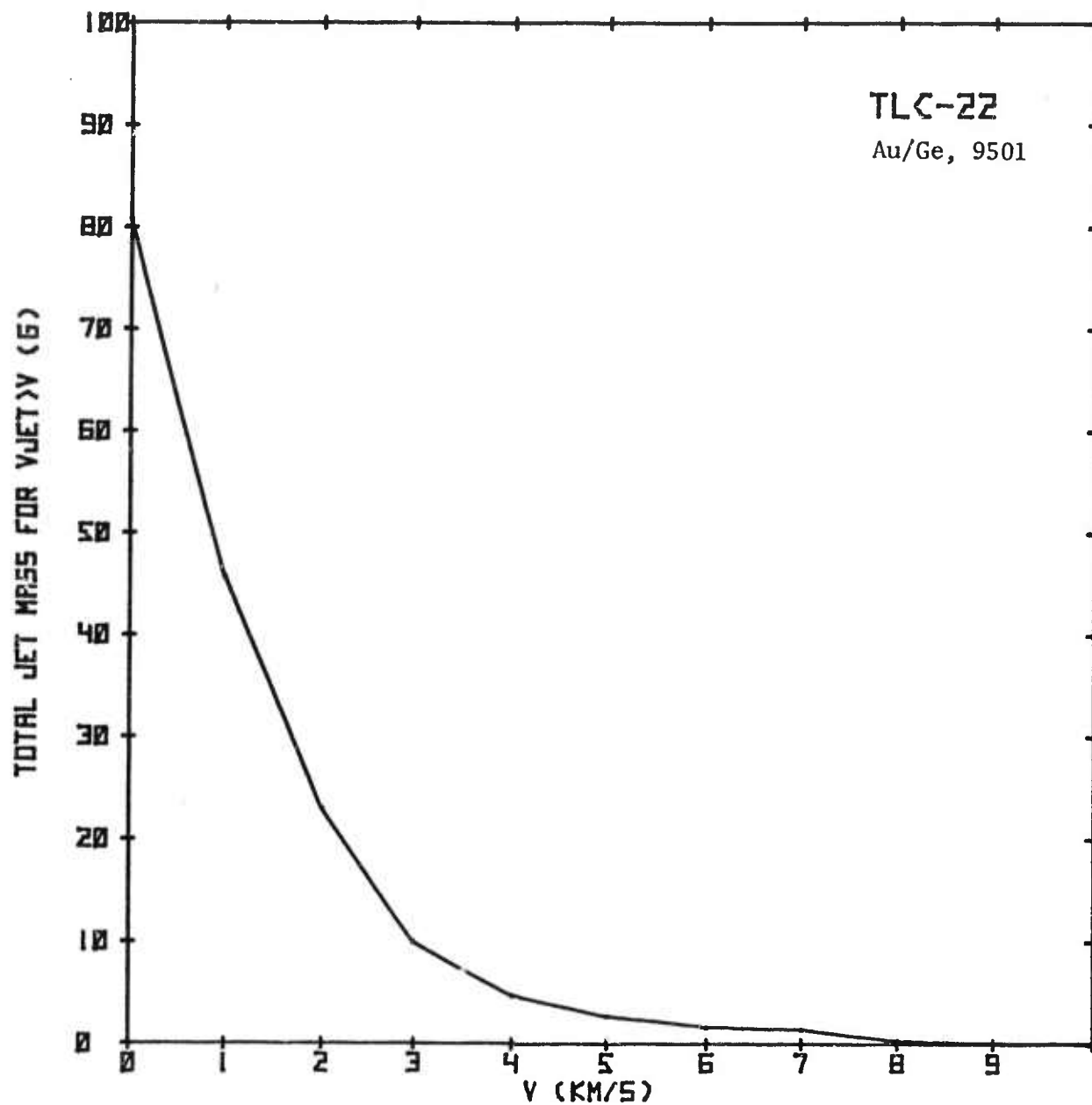
UNCLASSIFIED



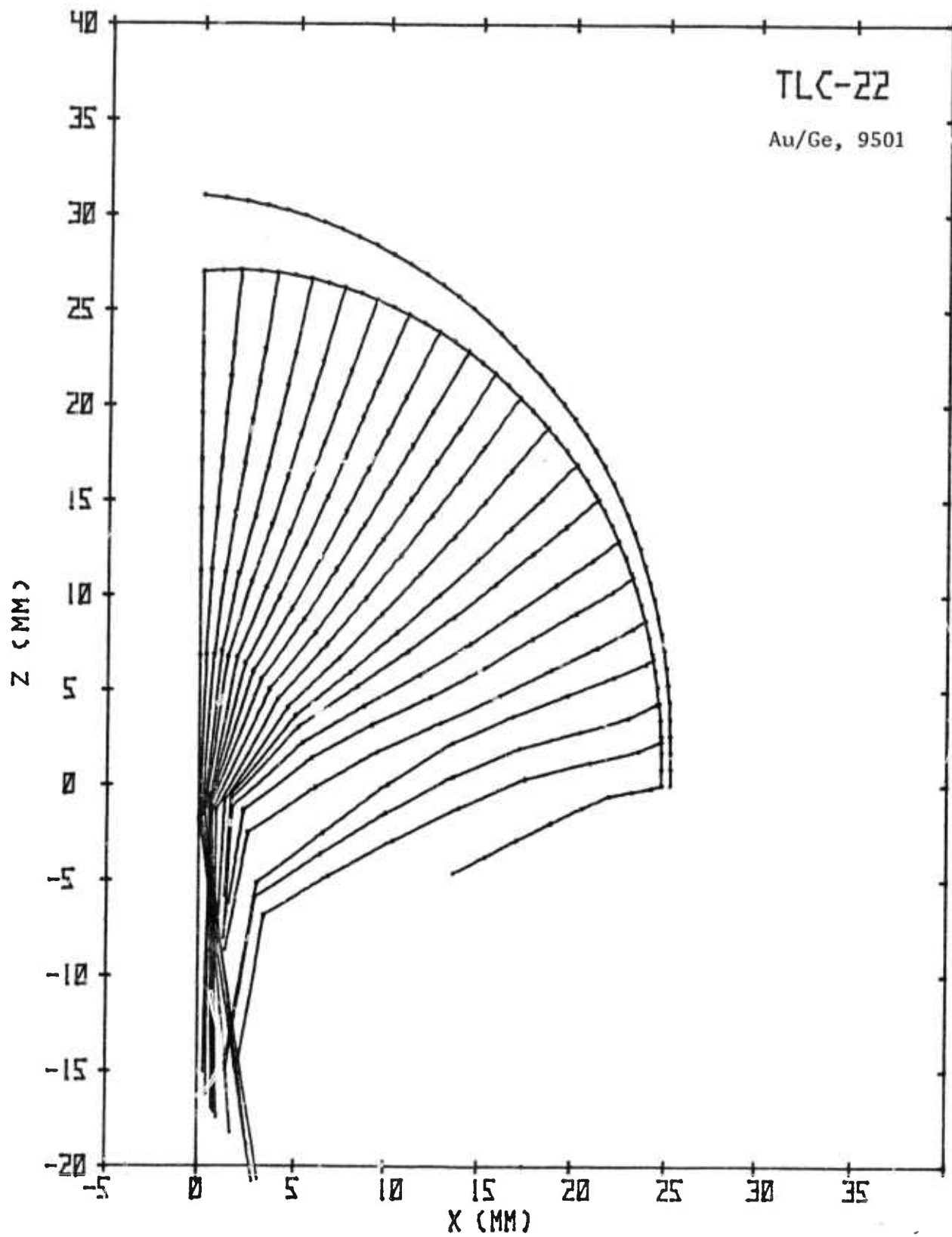
UNCLASSIFIED



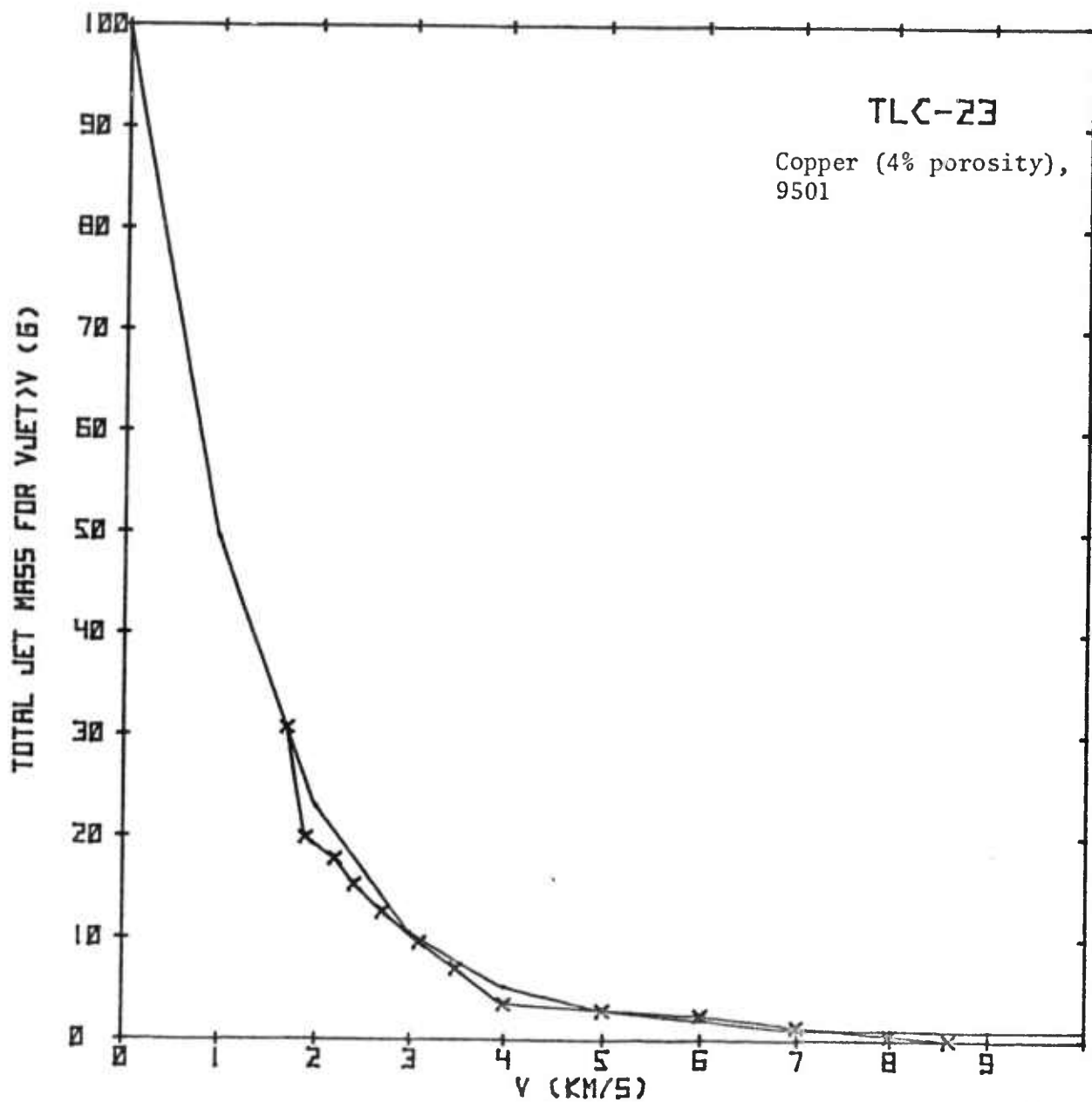
UNCLASSIFIED



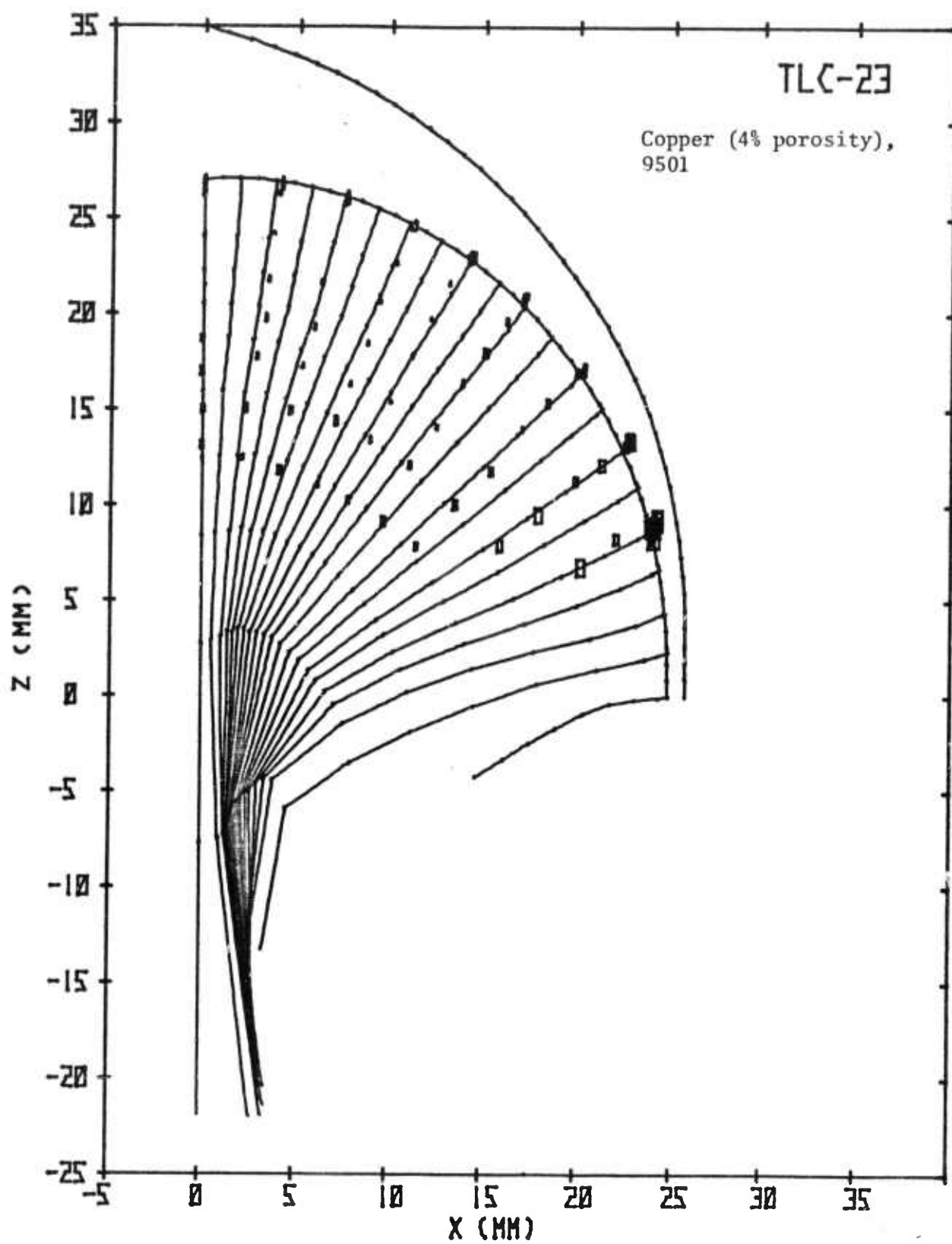
UNCLASSIFIED



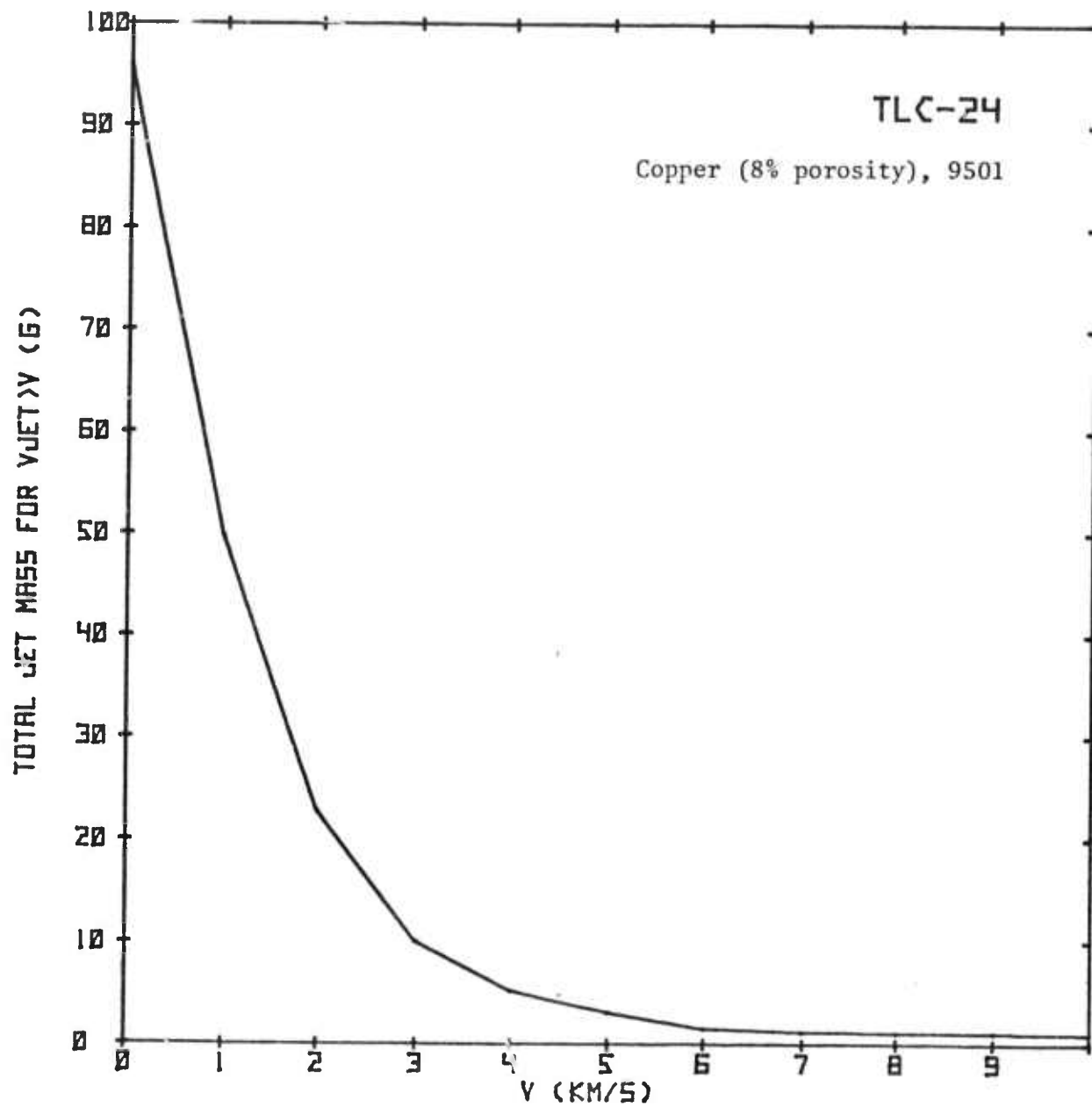
UNCLASSIFIED



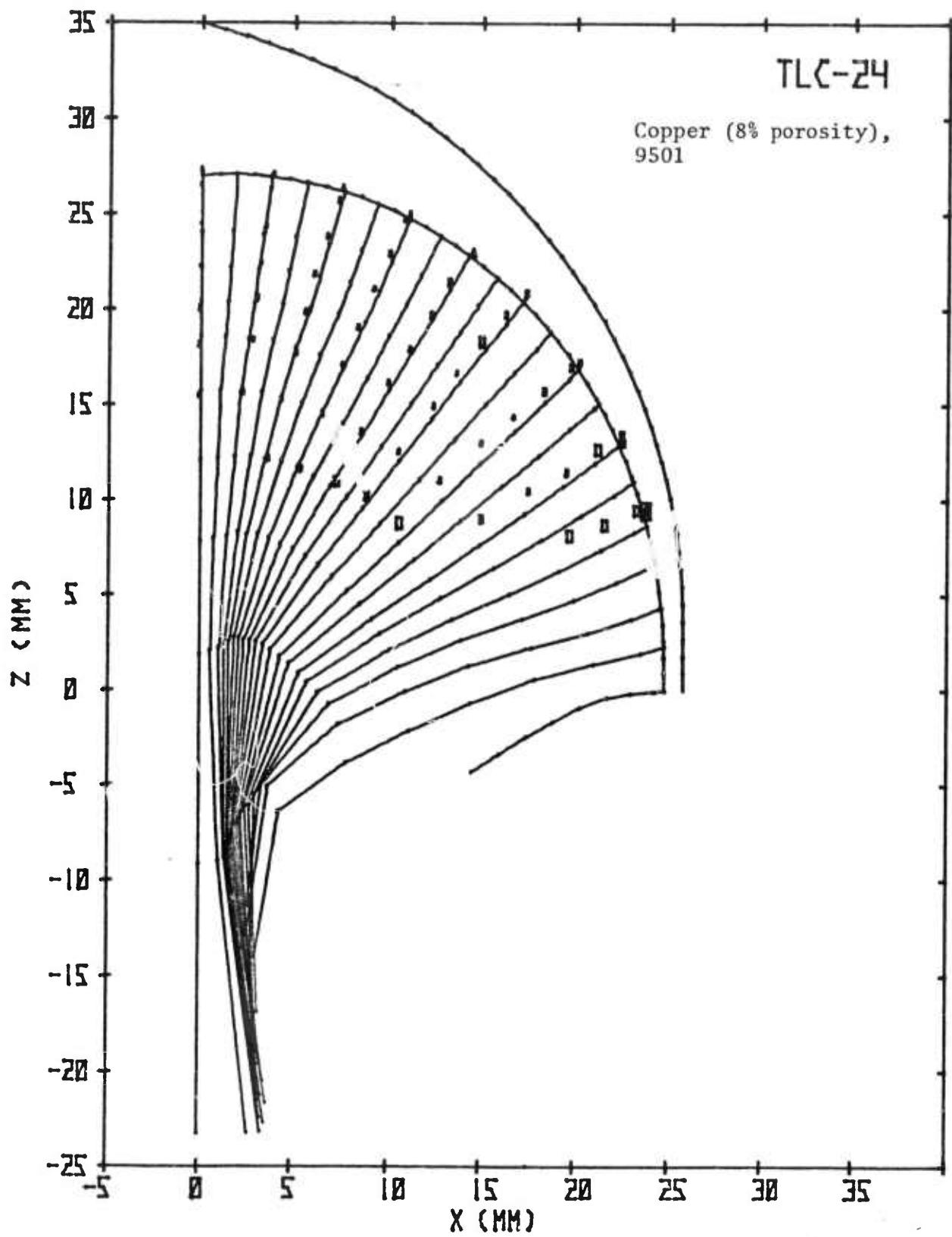
UNCLASSIFIED



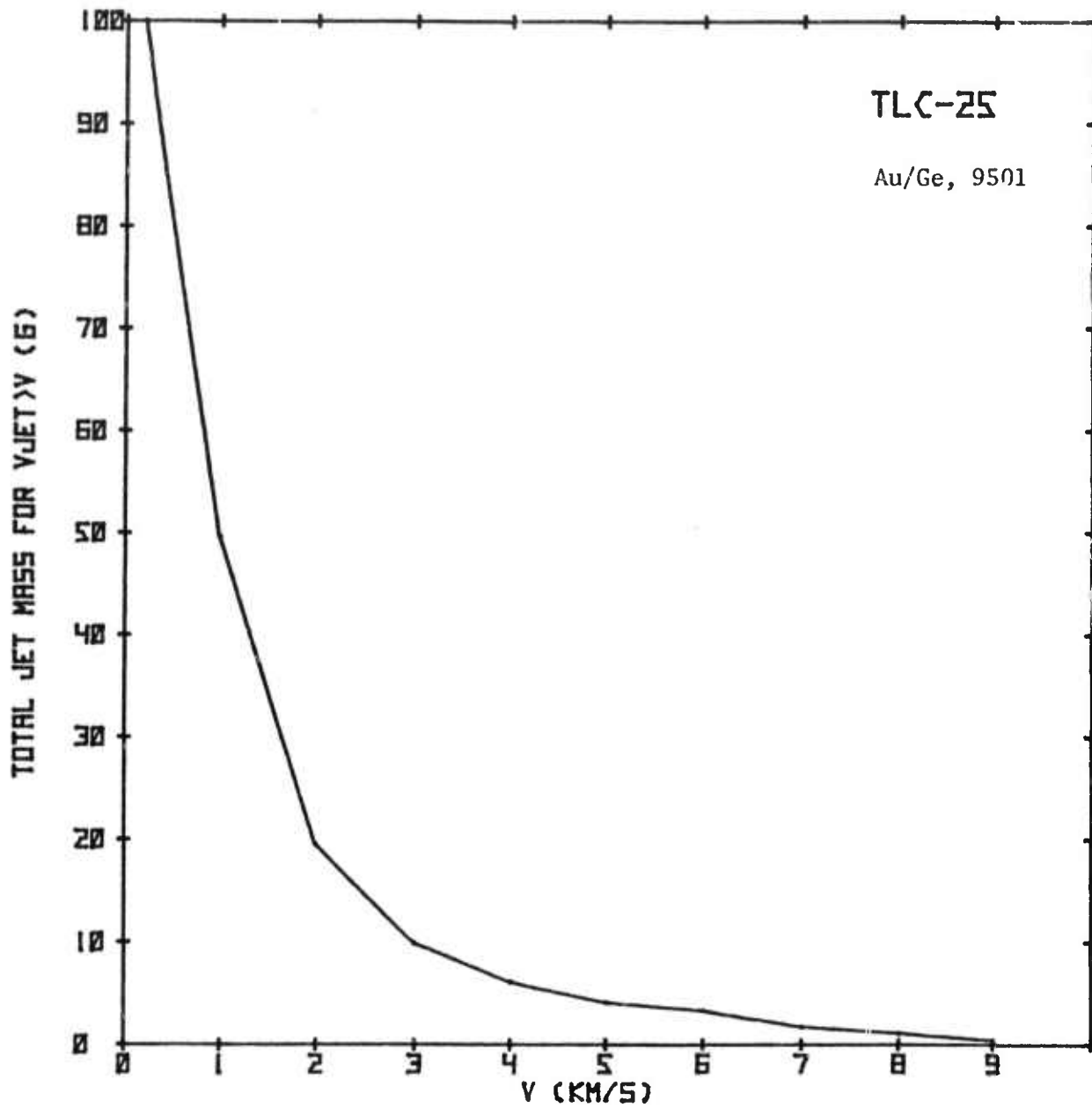
UNCLASSIFIED



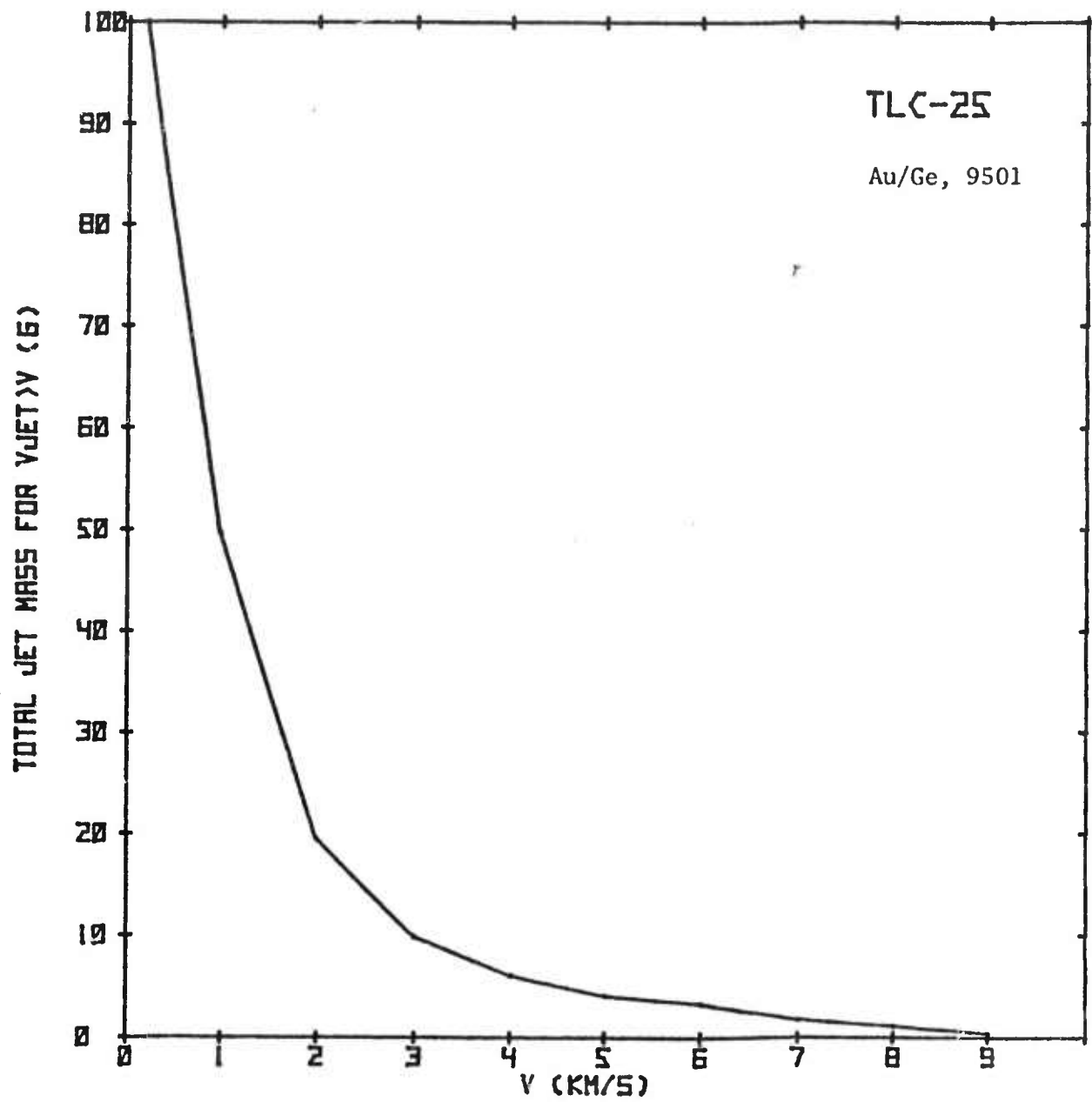
UNCLASSIFIED

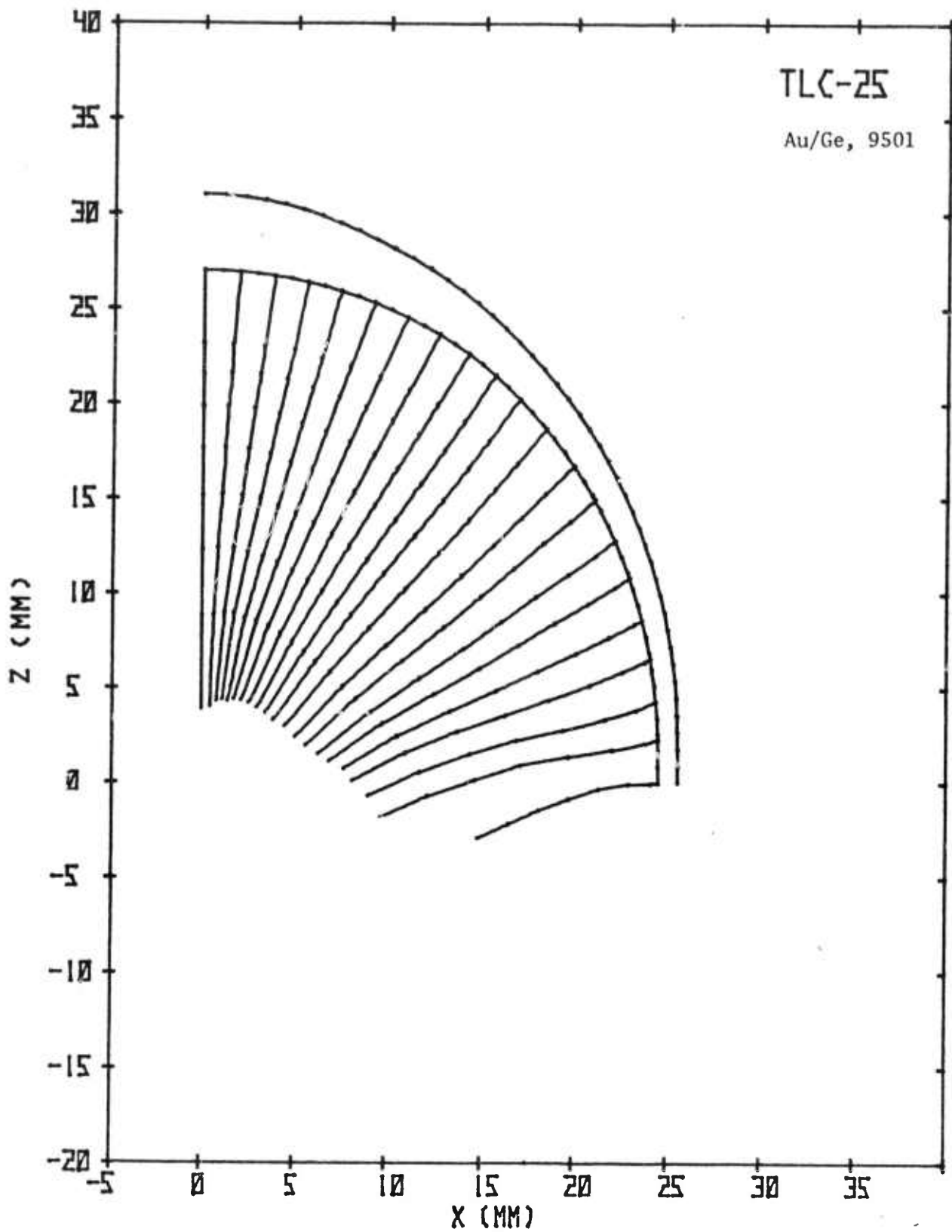


UNCLASSIFIED

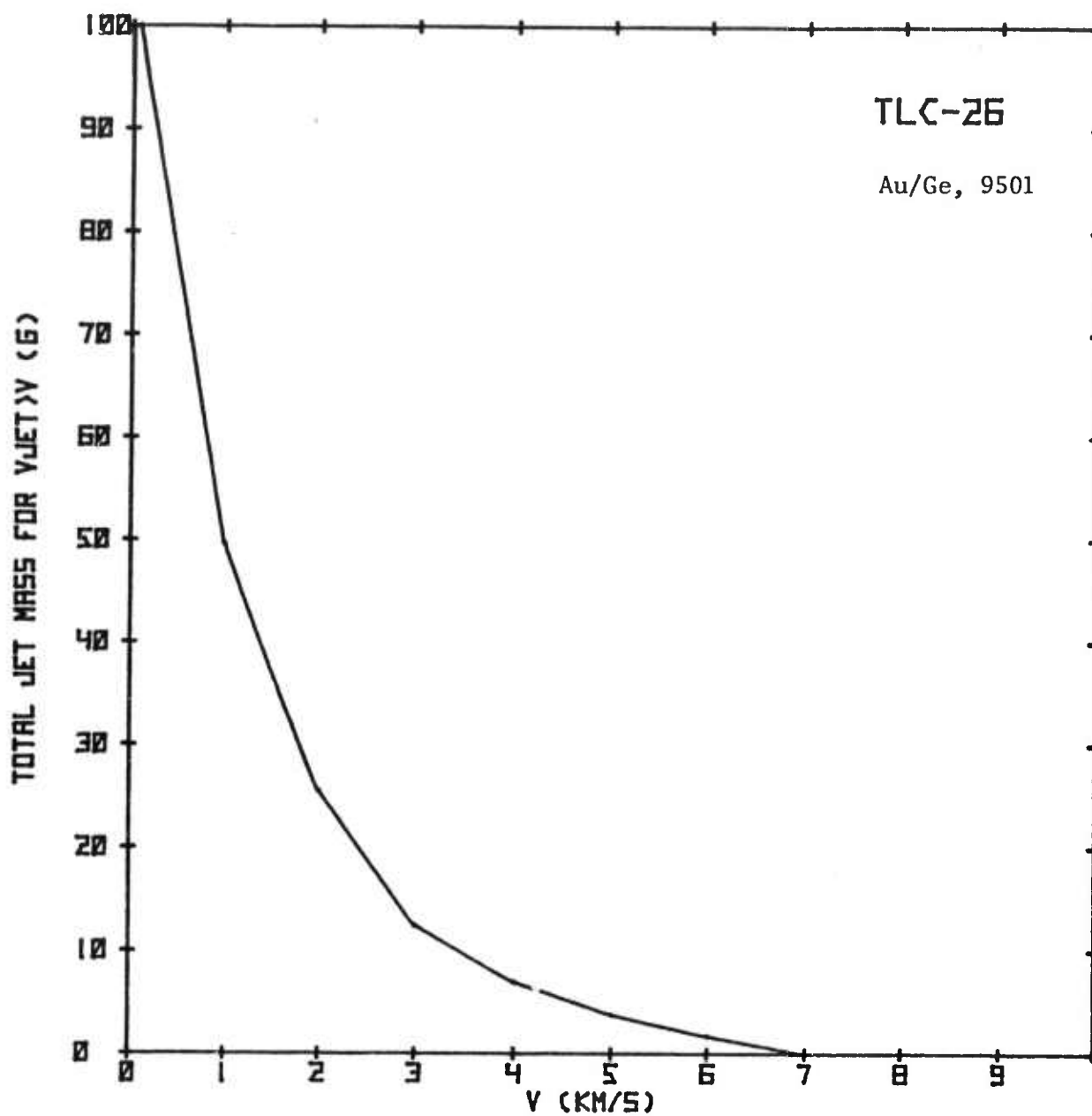


UNCLASSIFIED

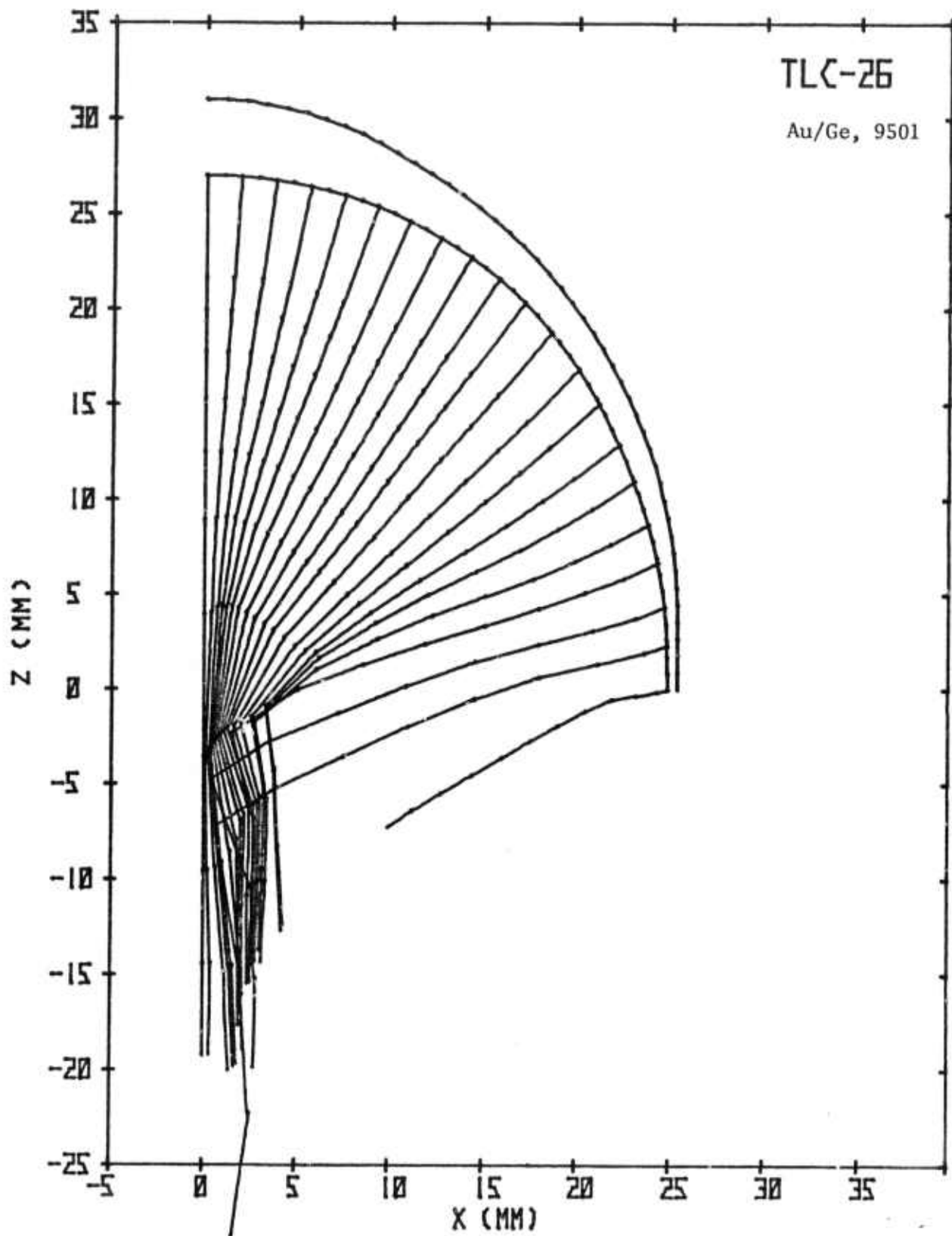




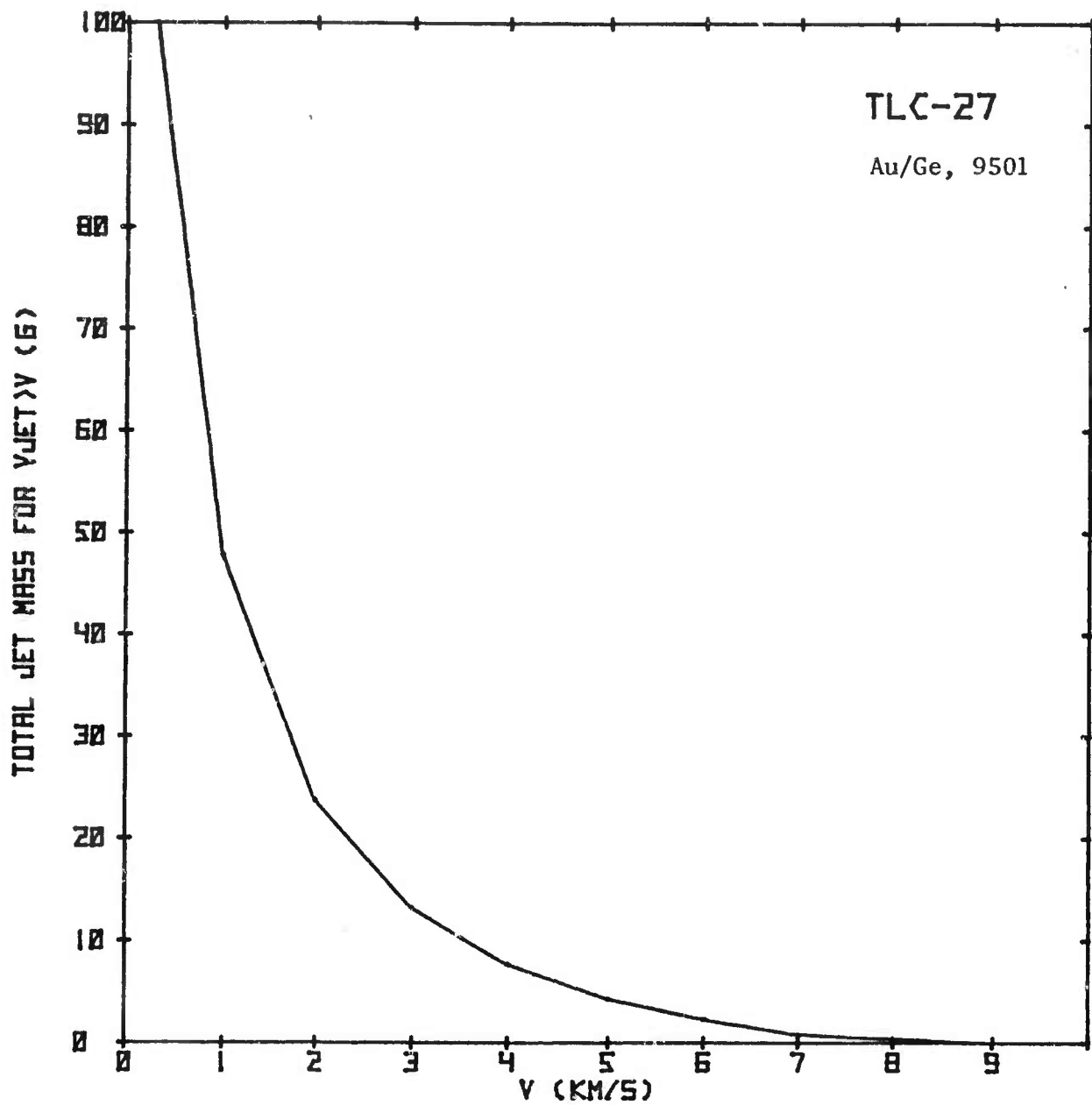
UNCLASSIFIED



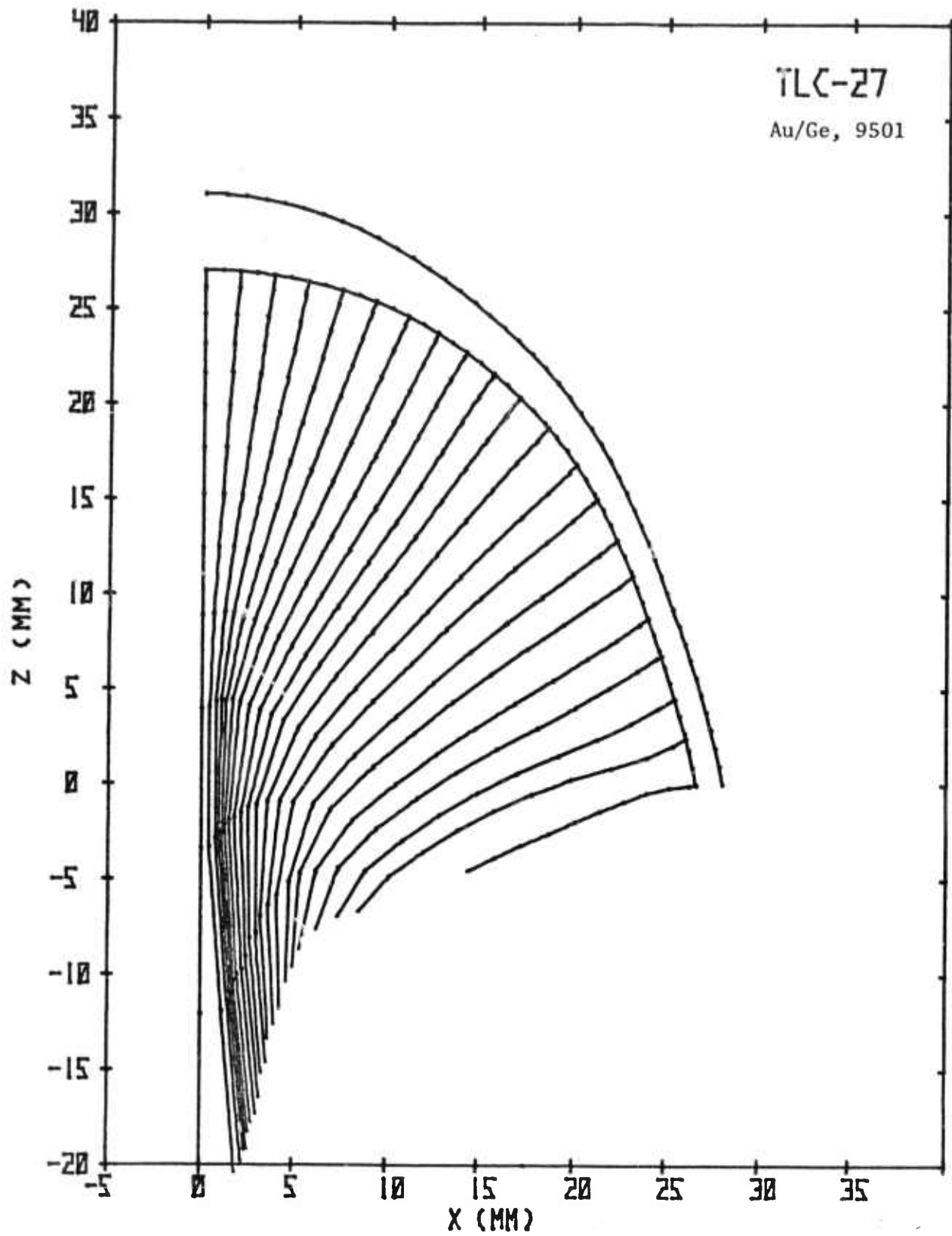
UNCLASSIFIED



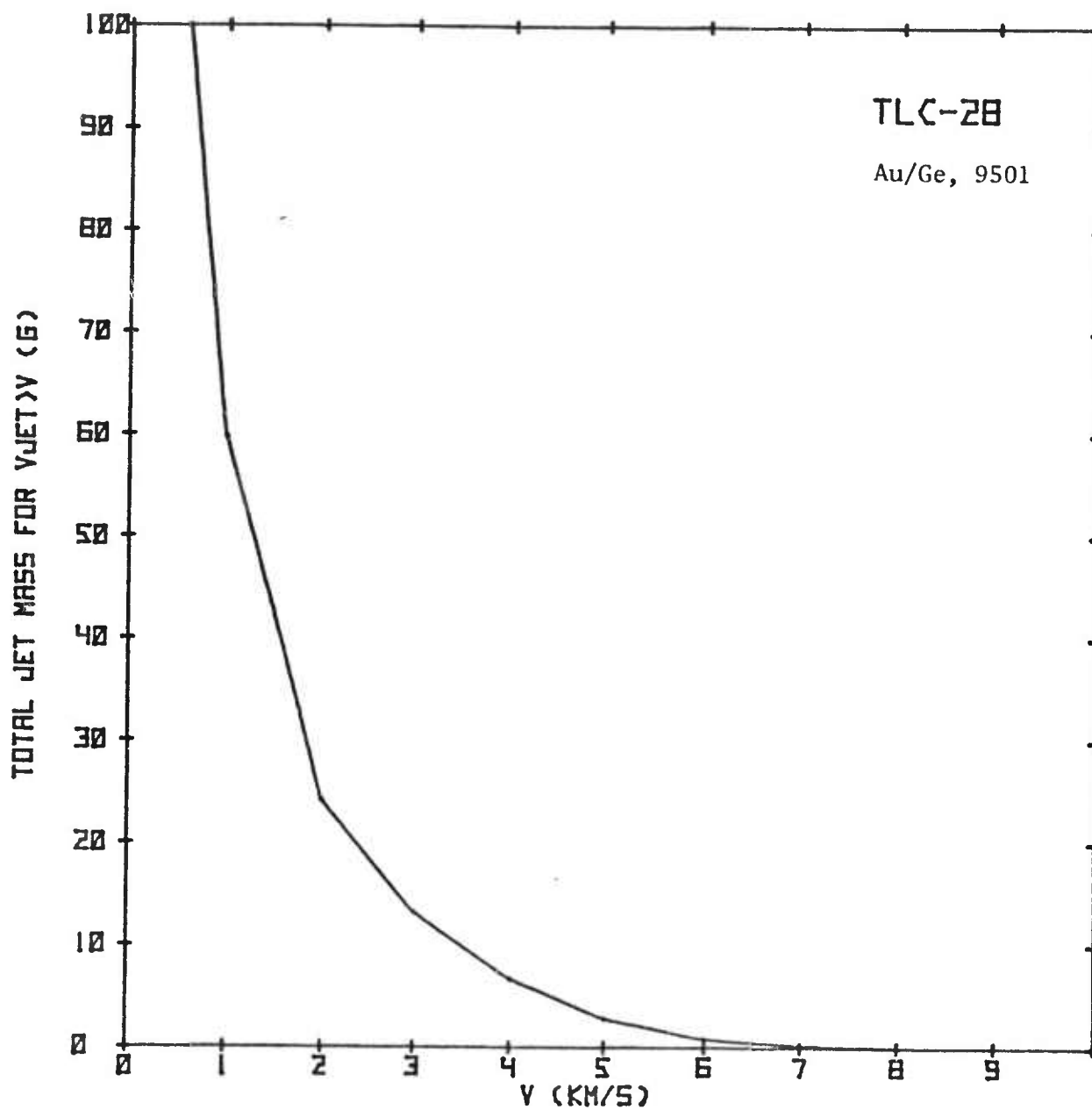
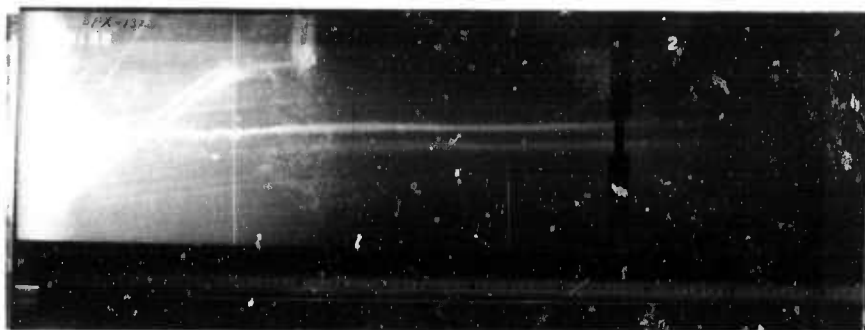
UNCLASSIFIED



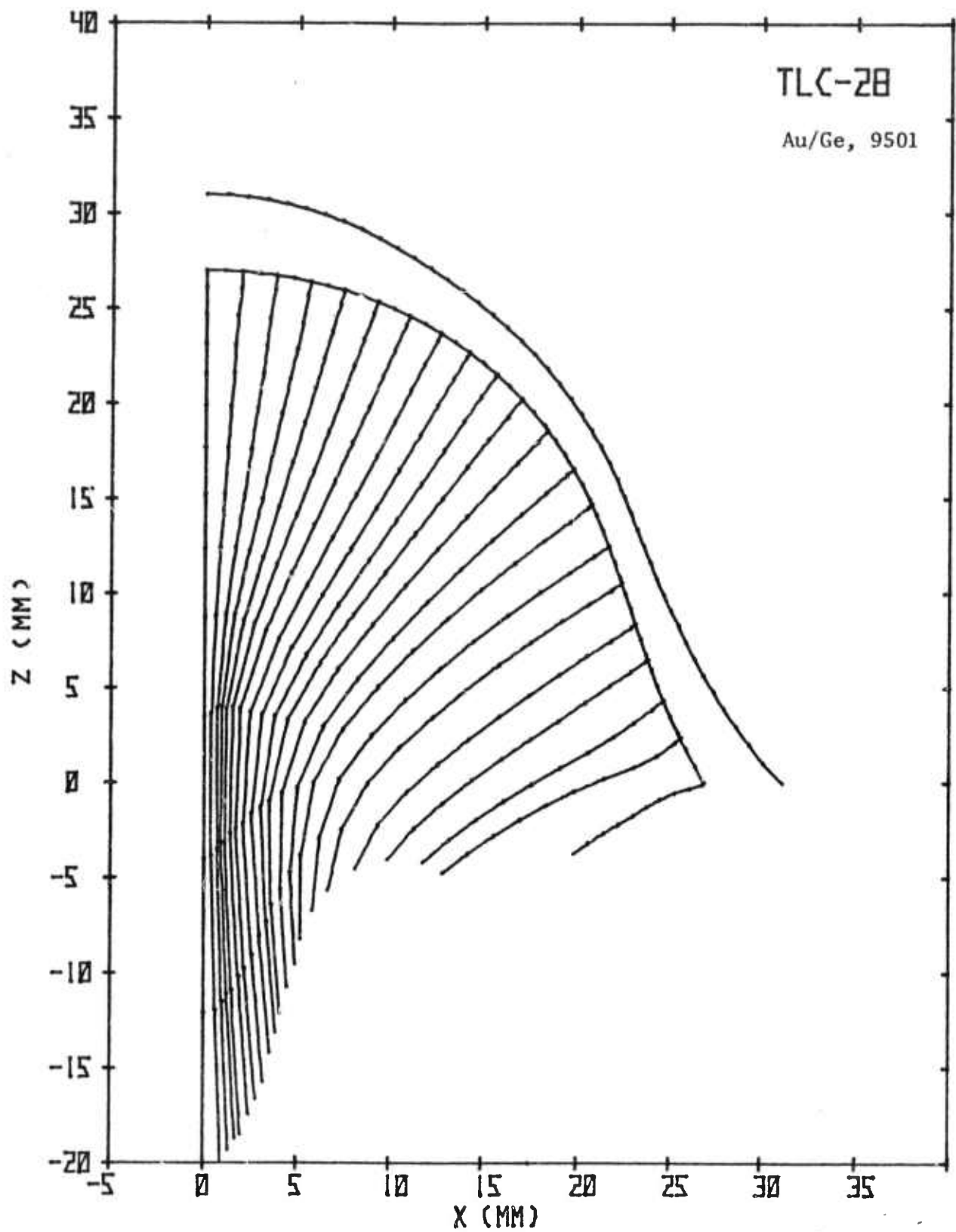
UNCLASSIFIED



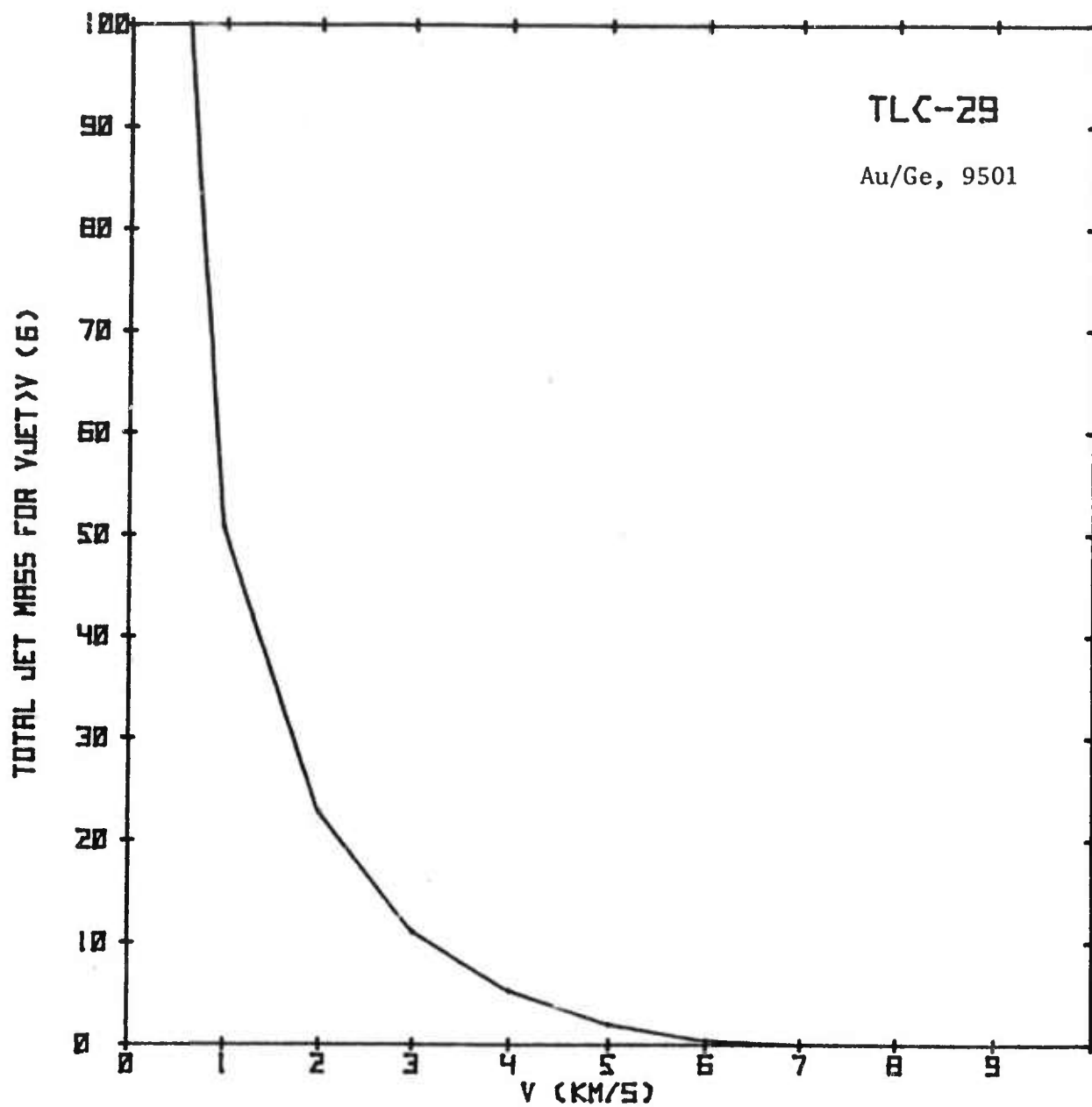
UNCLASSIFIED



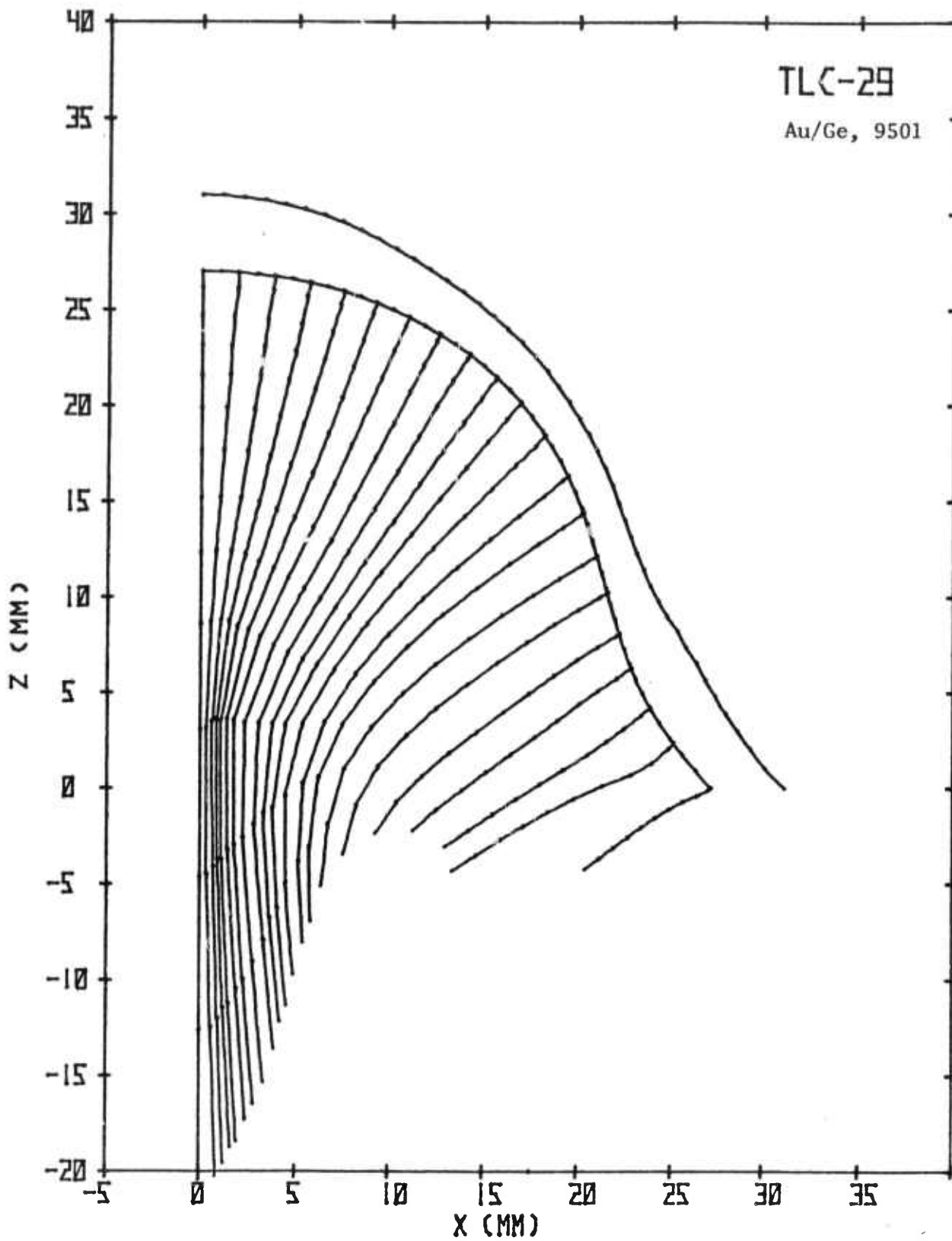
UNCLASSIFIED



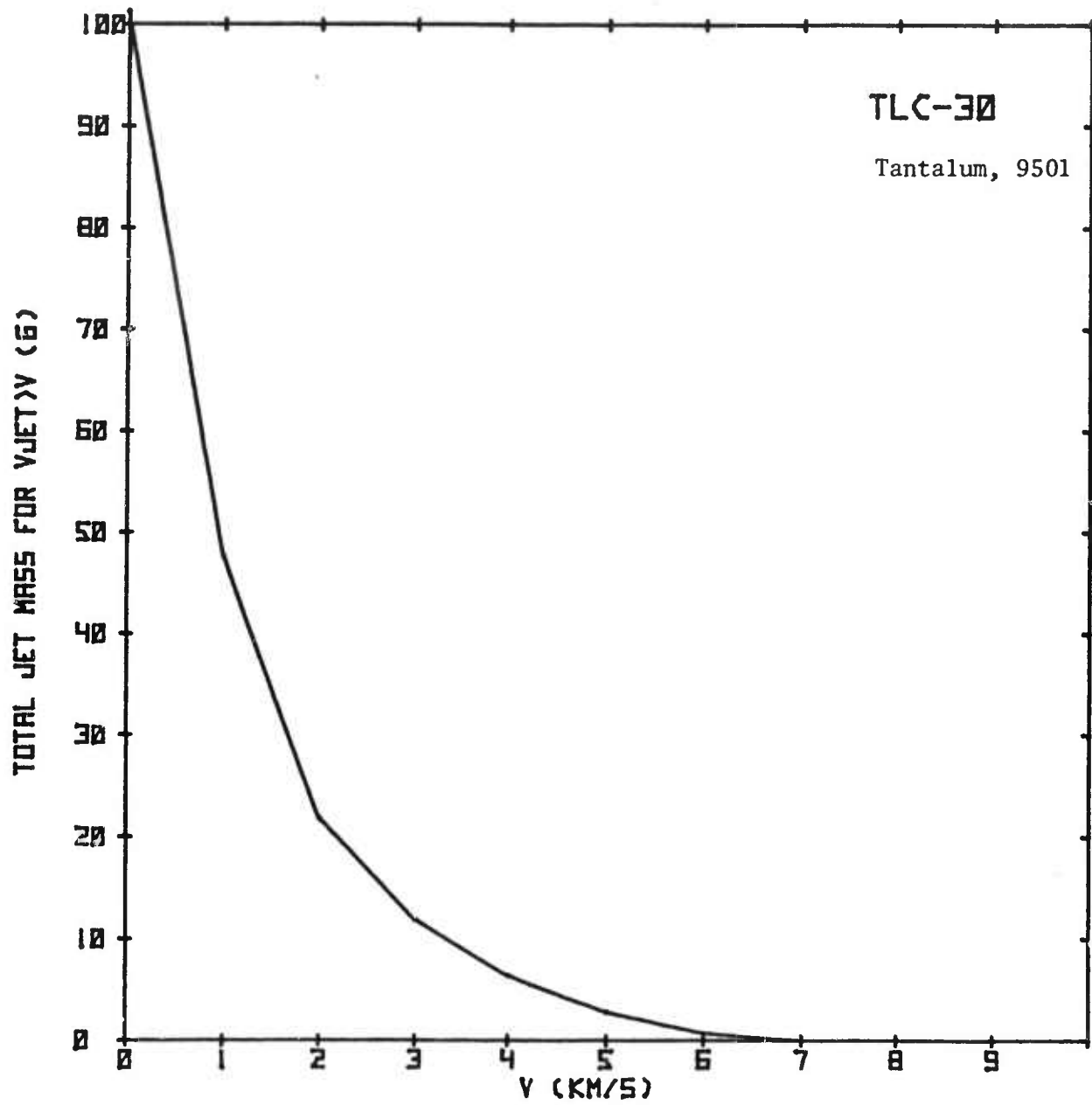
UNCLASSIFIED



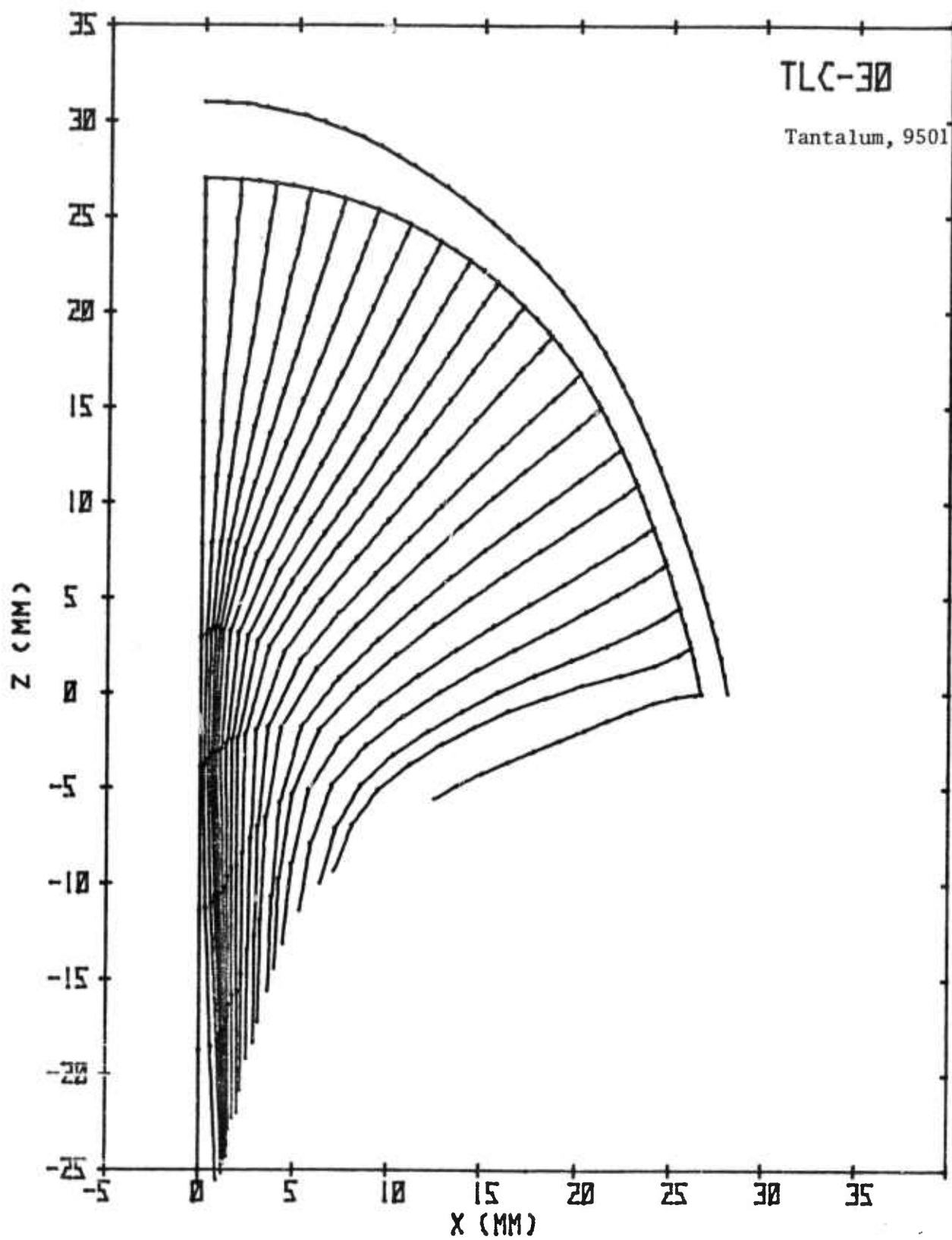
UNCLASSIFIED

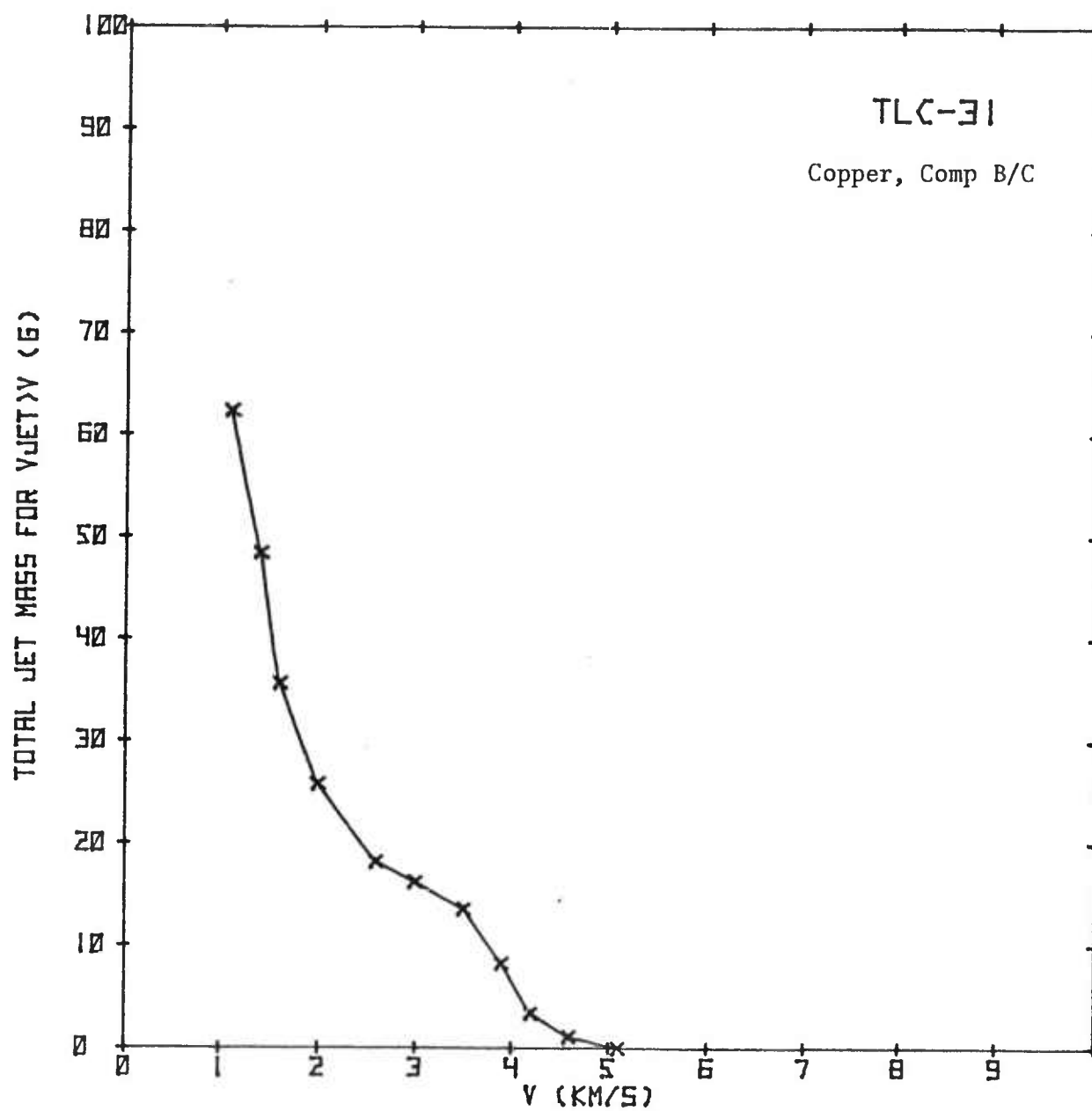
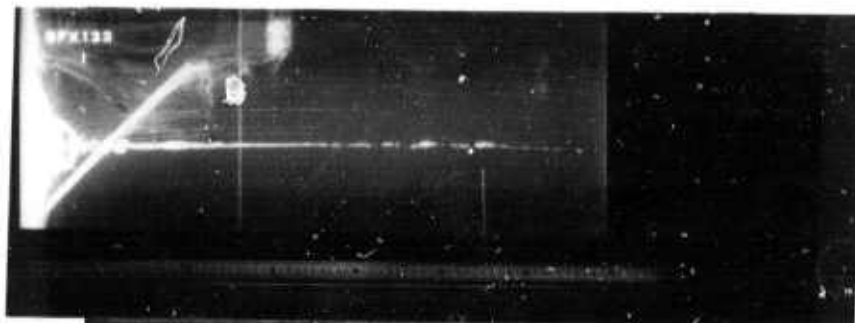


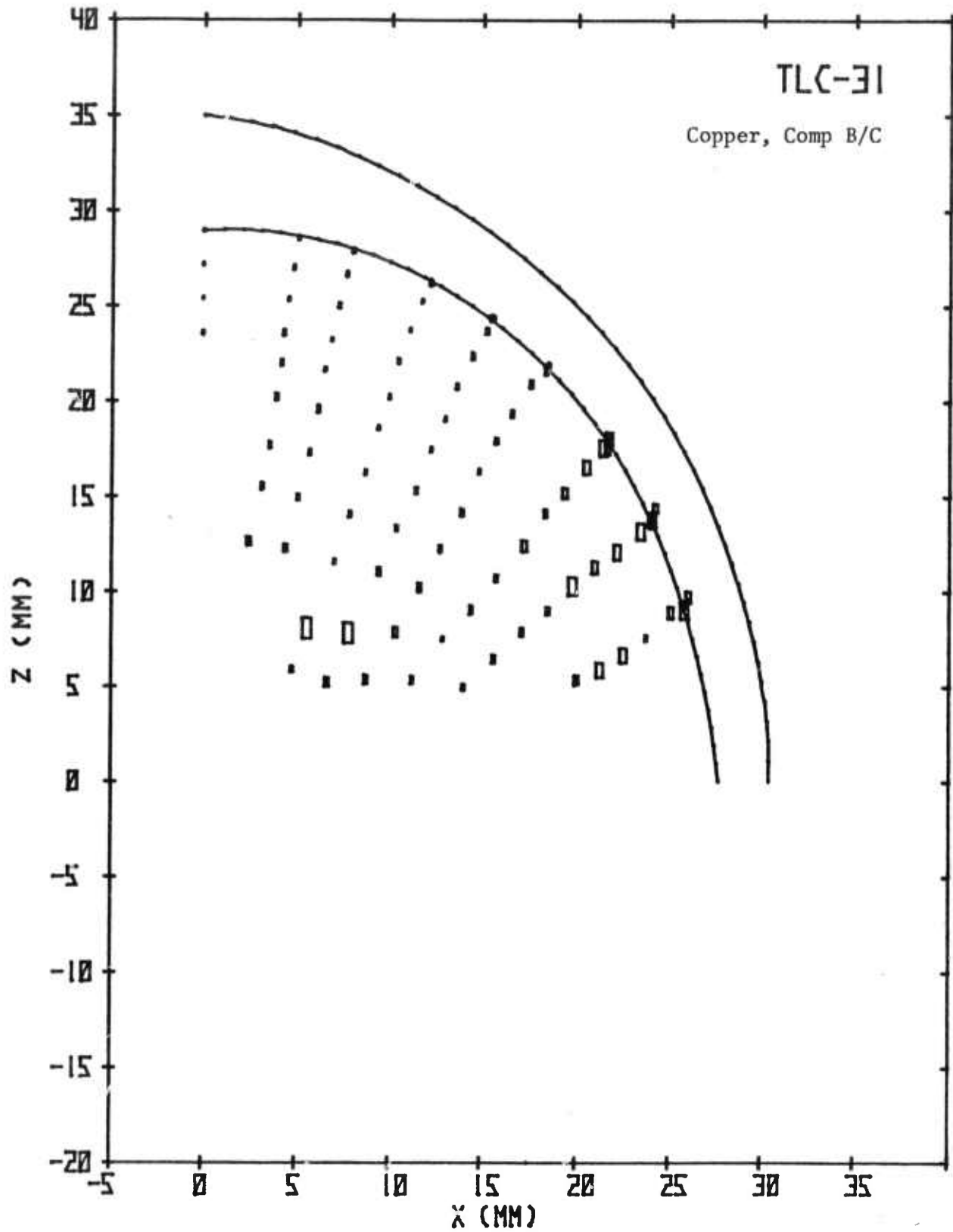
UNCLASSIFIED



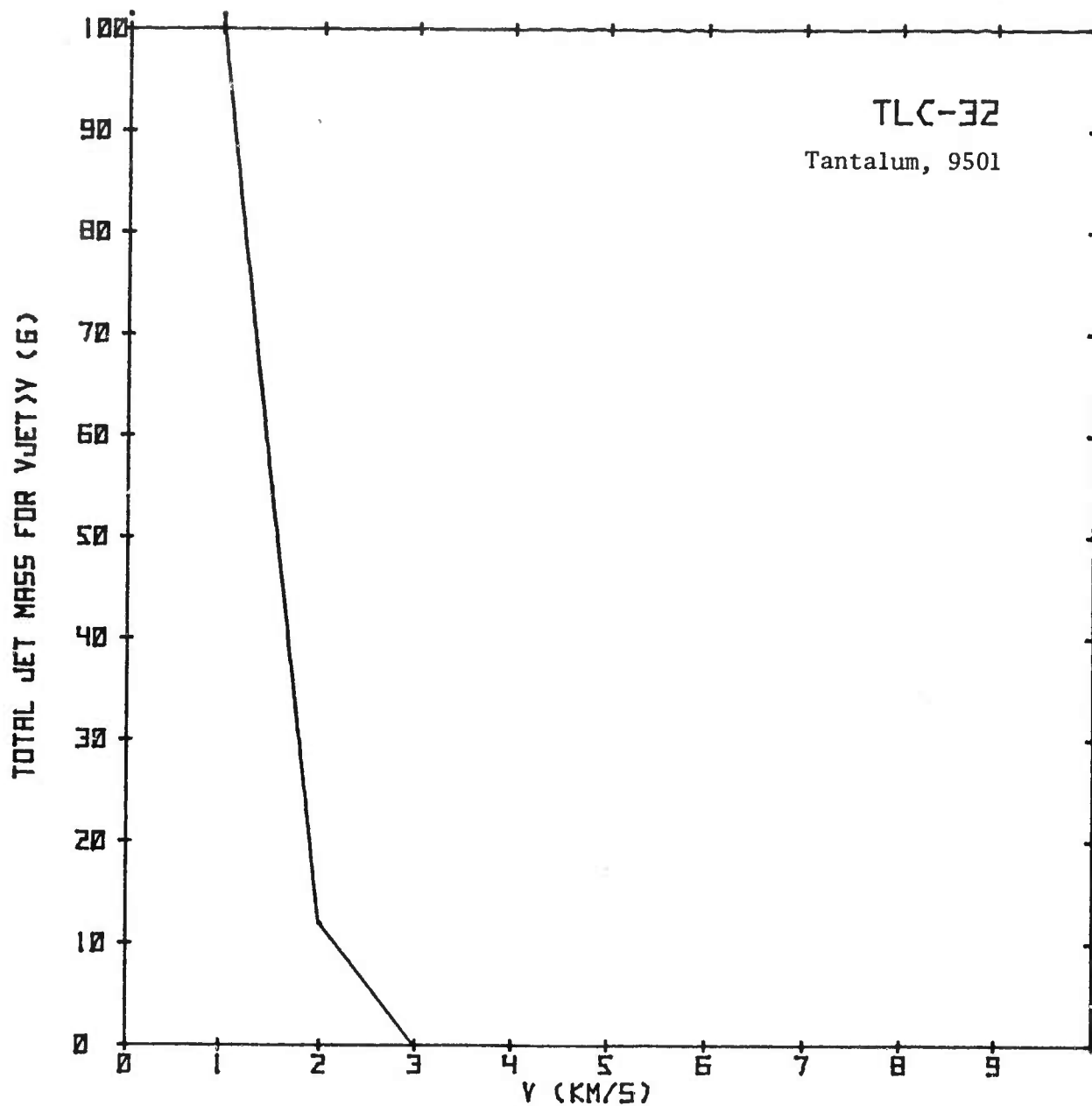
UNCLASSIFIED



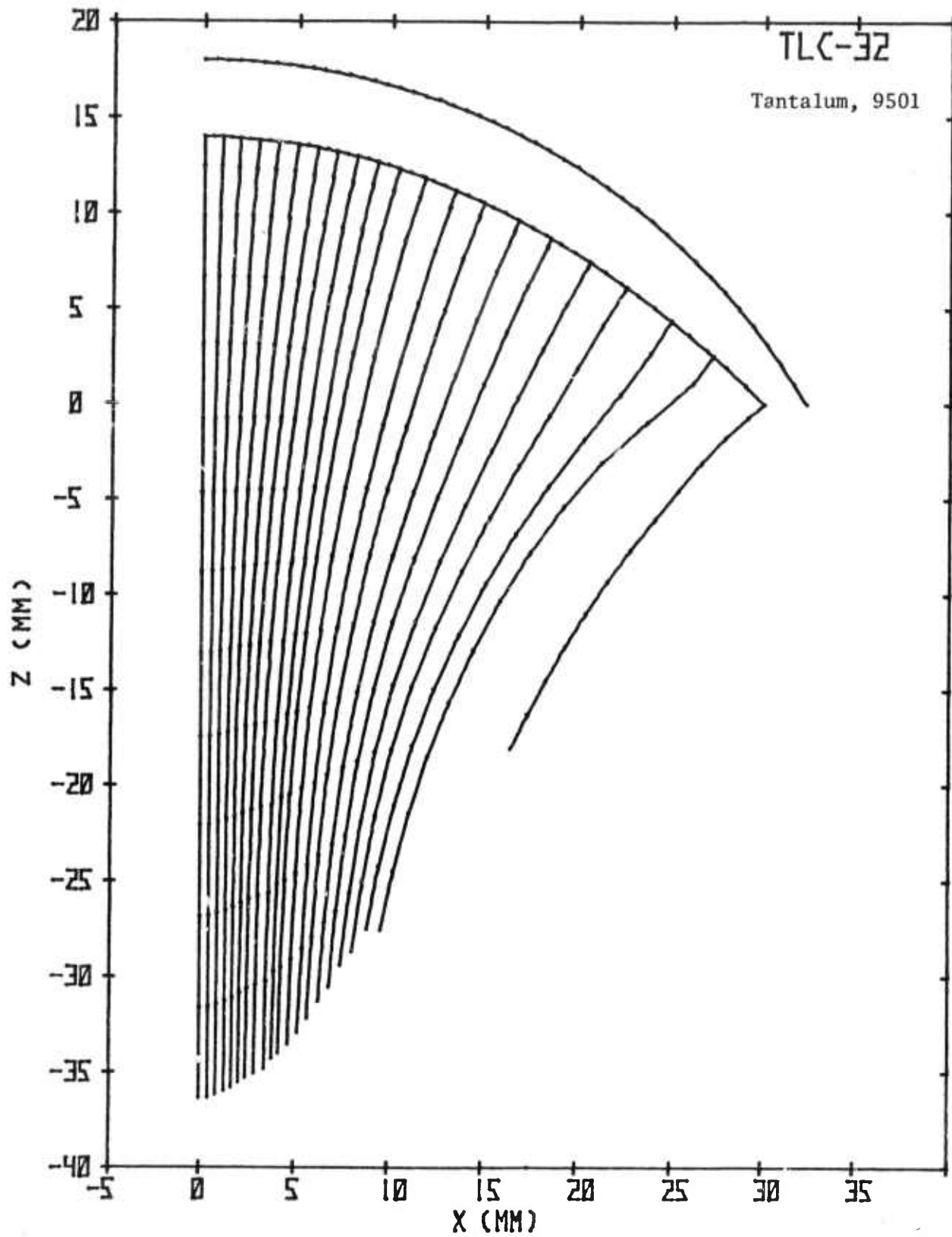




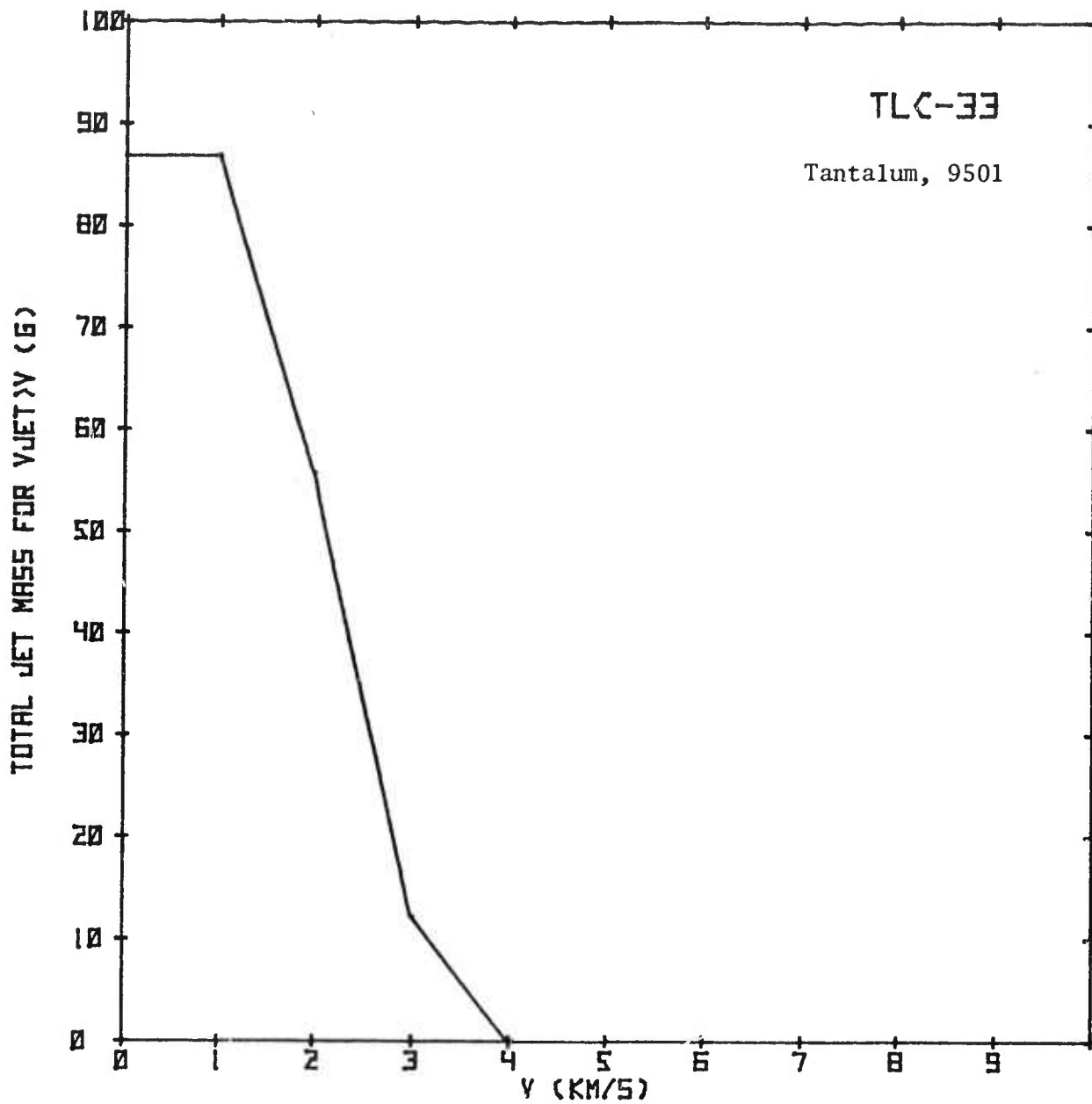
UNCLASSIFIED



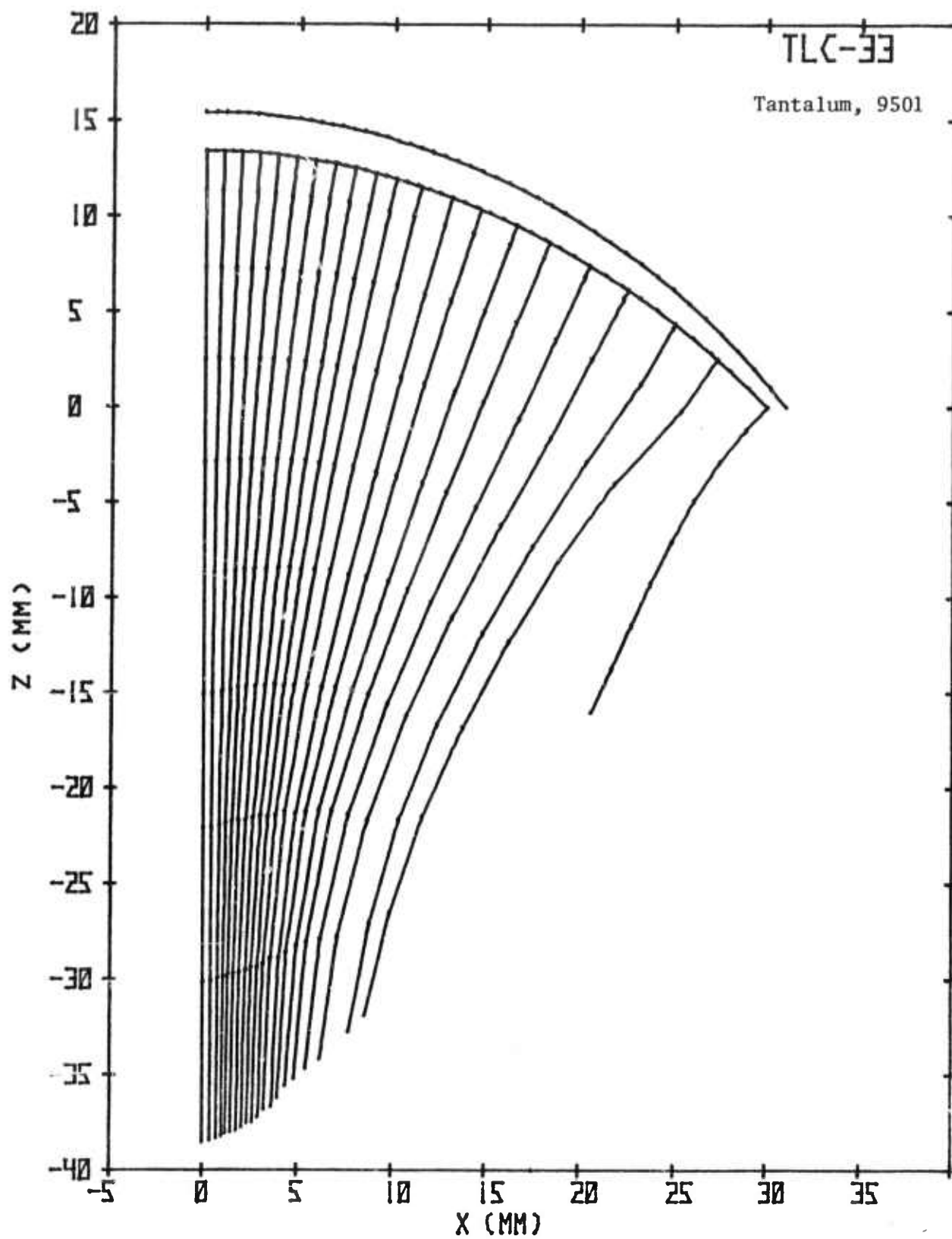
UNCLASSIFIED



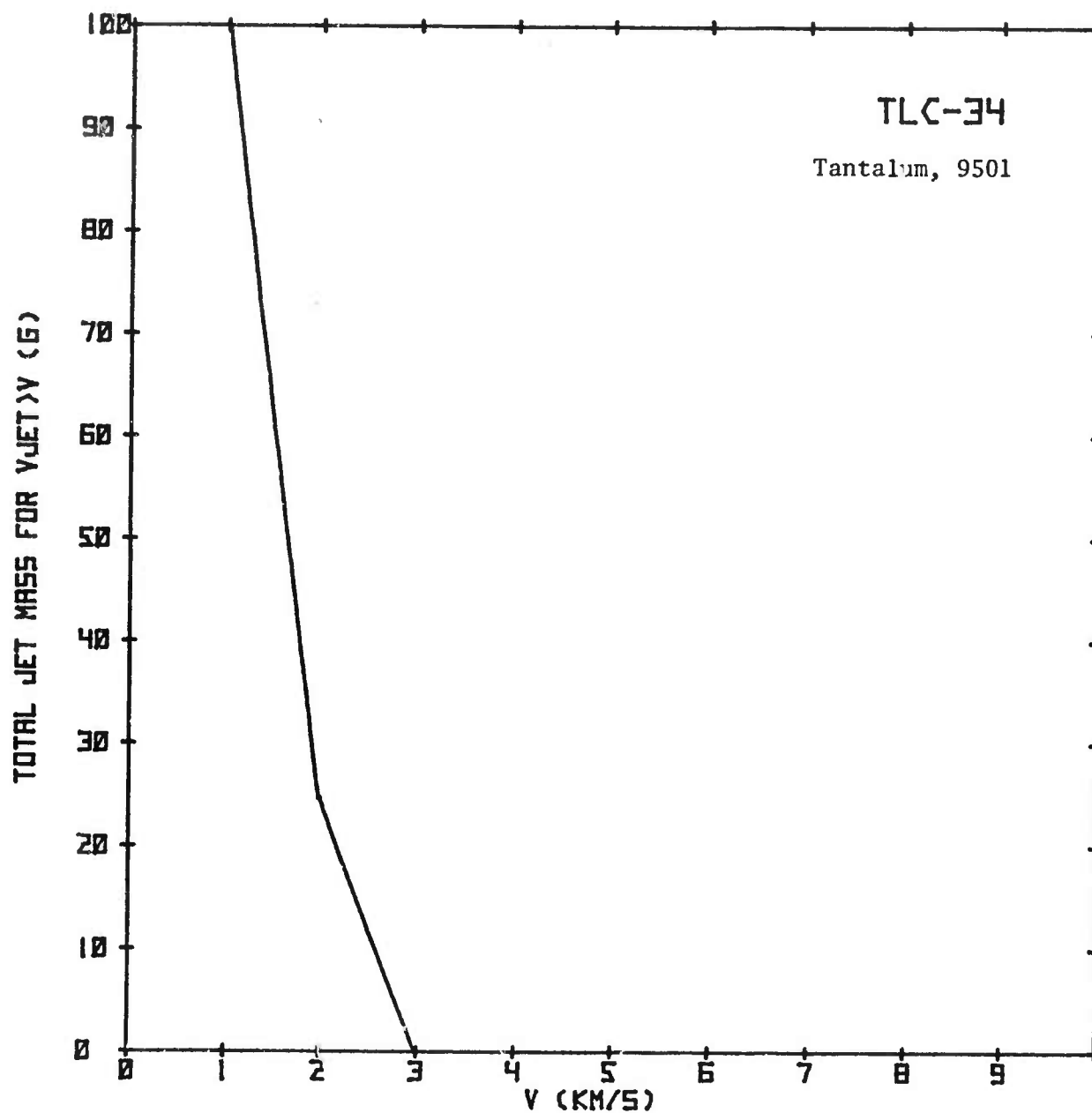
UNCLASSIFIED



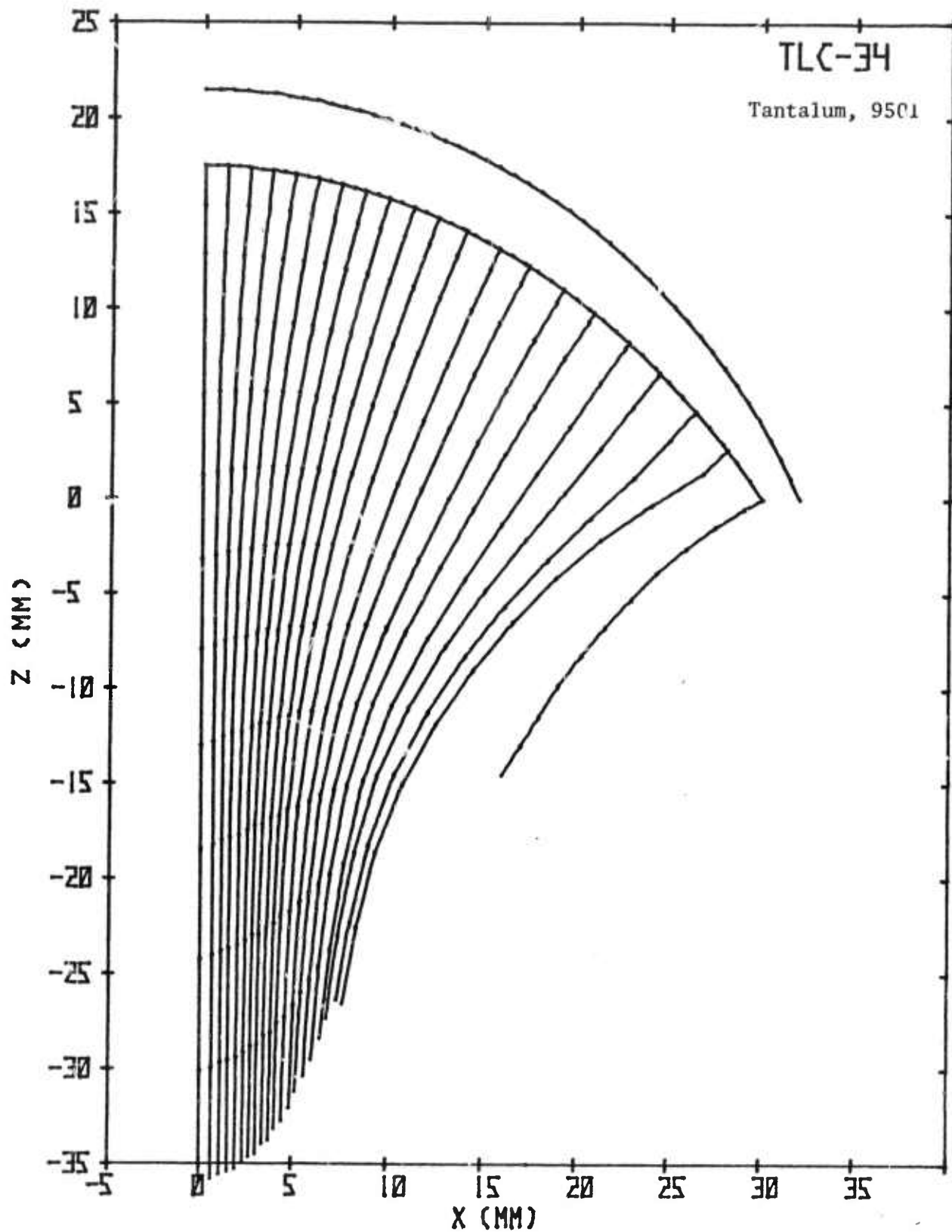
UNCLASSIFIED



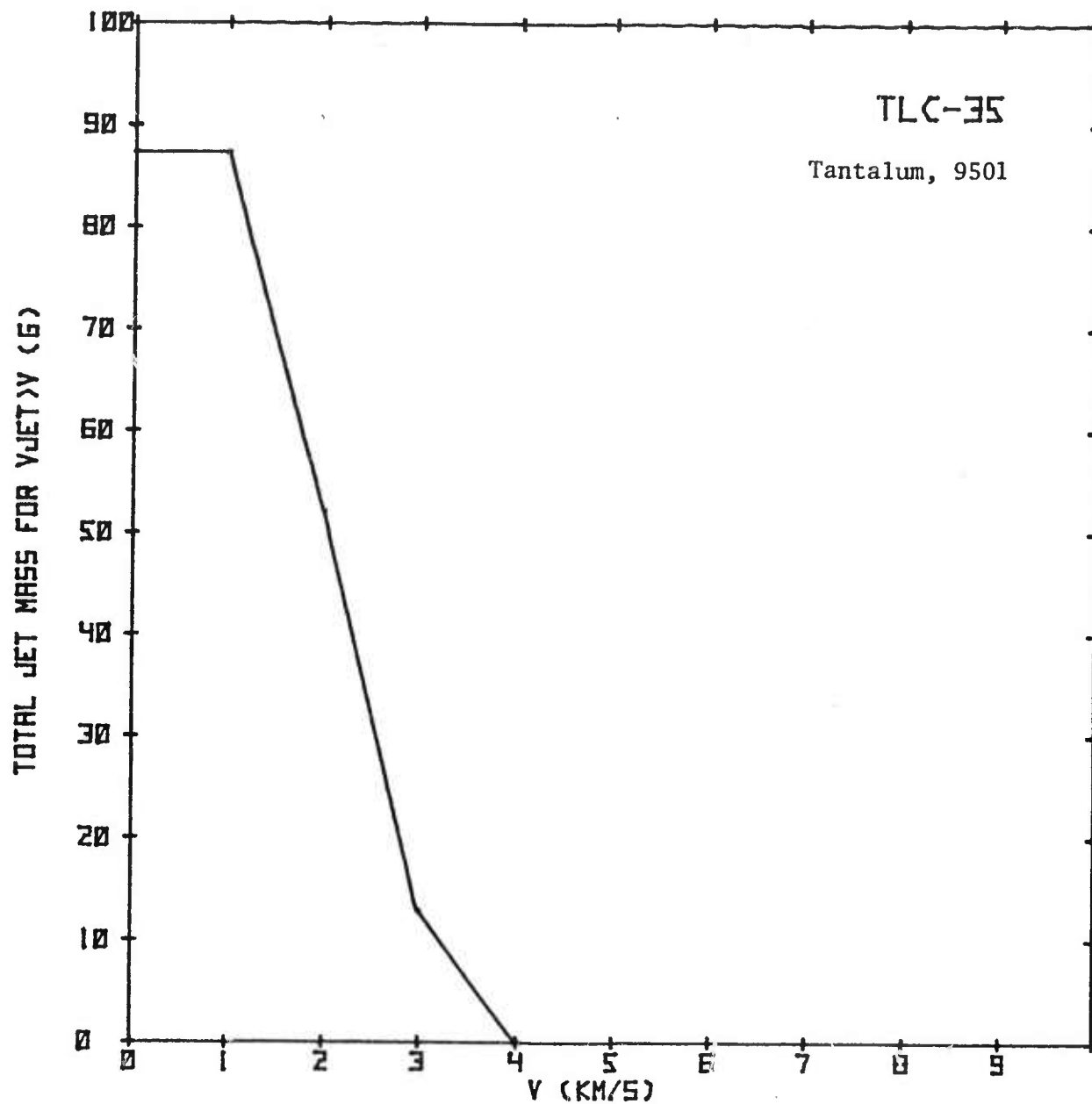
UNCLASSIFIED



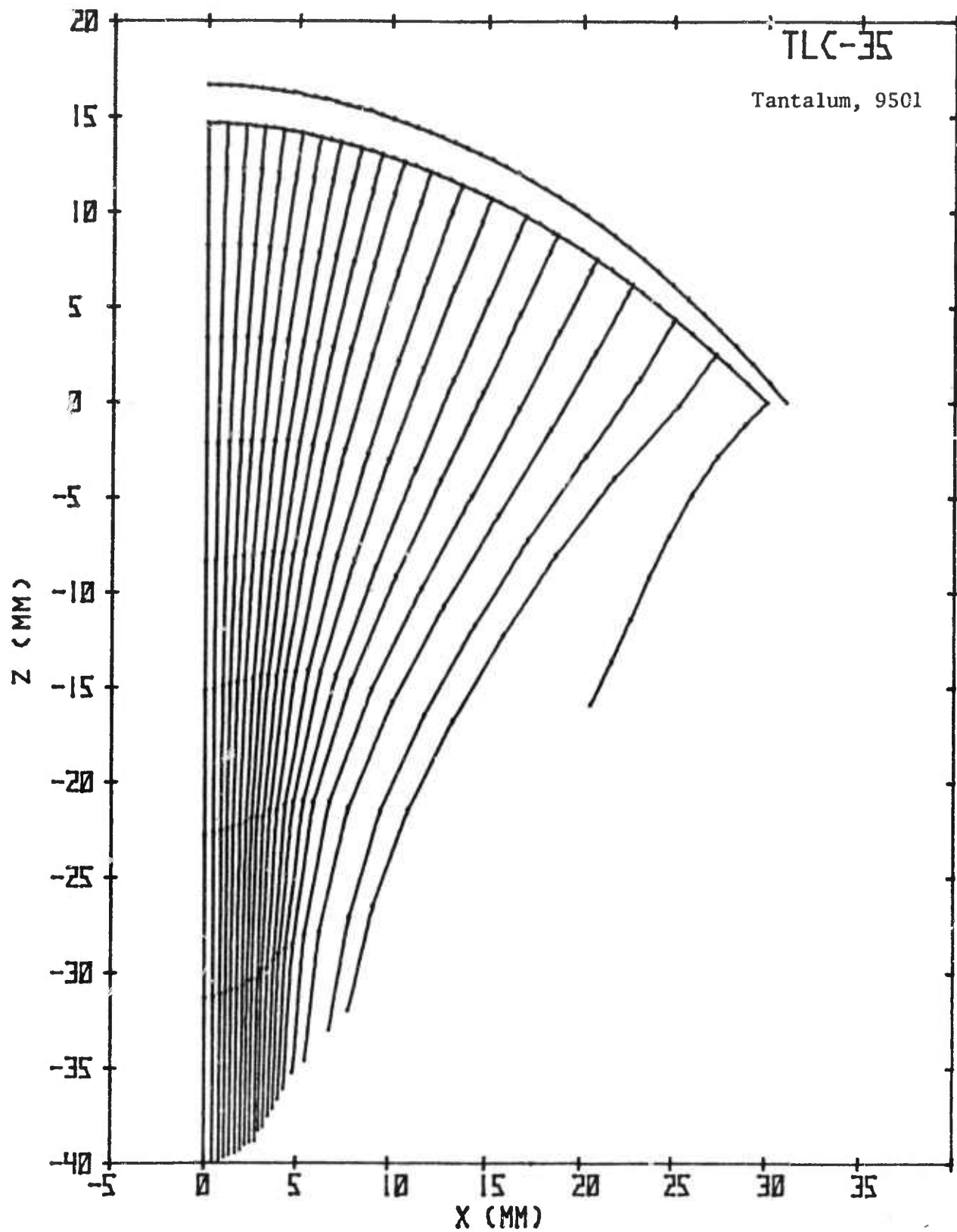
UNCLASSIFIED



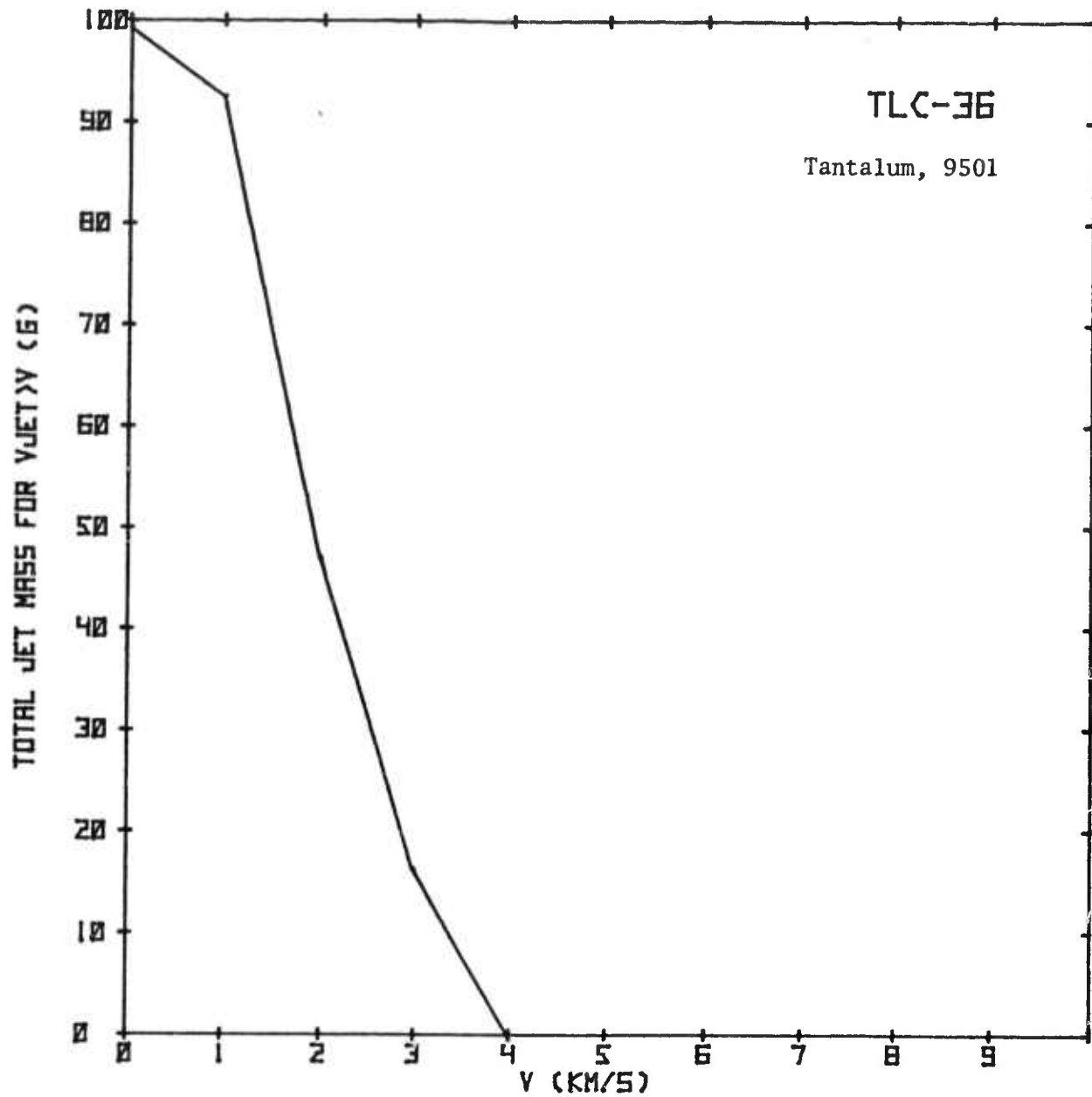
UNCLASSIFIED



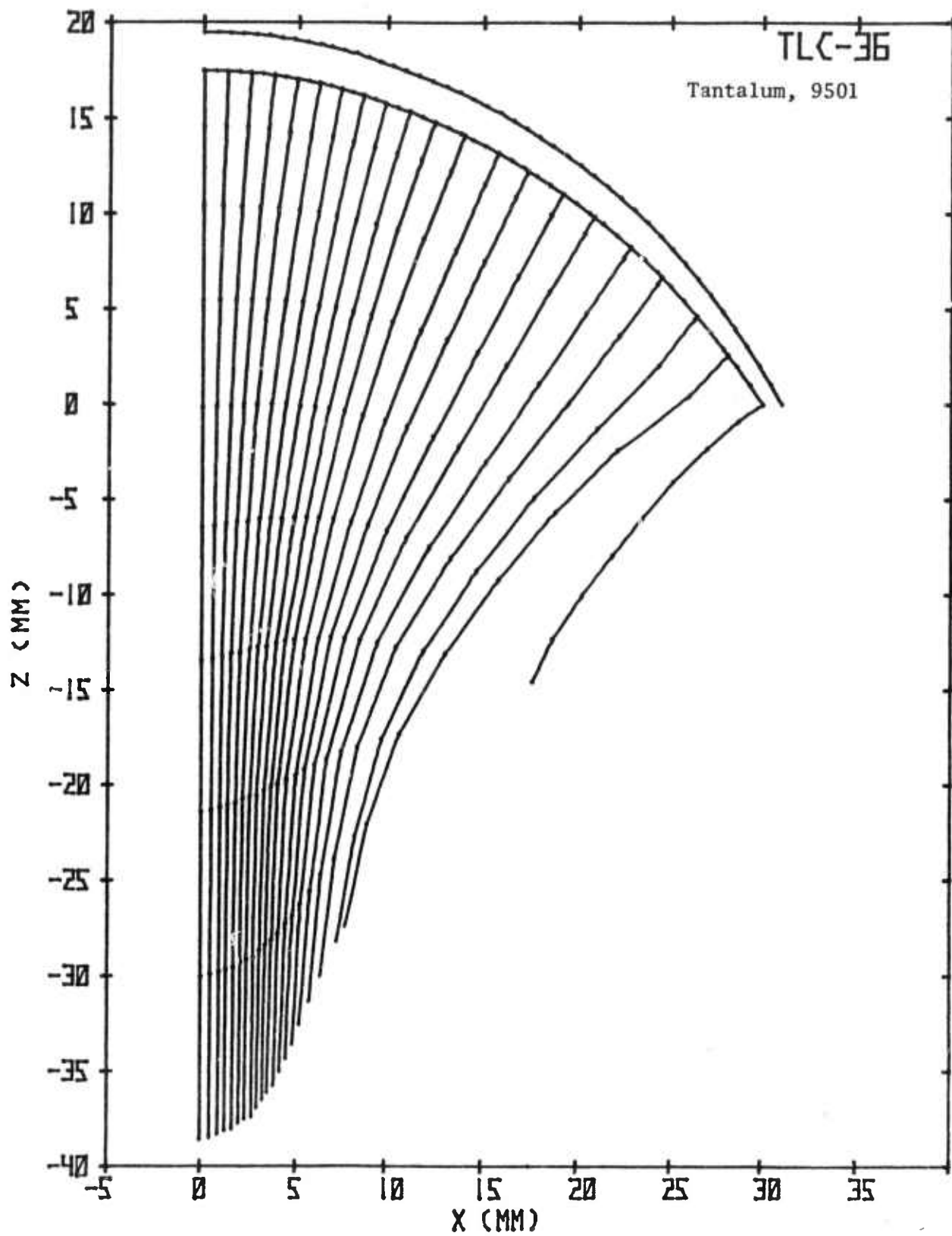
UNCLASSIFIED



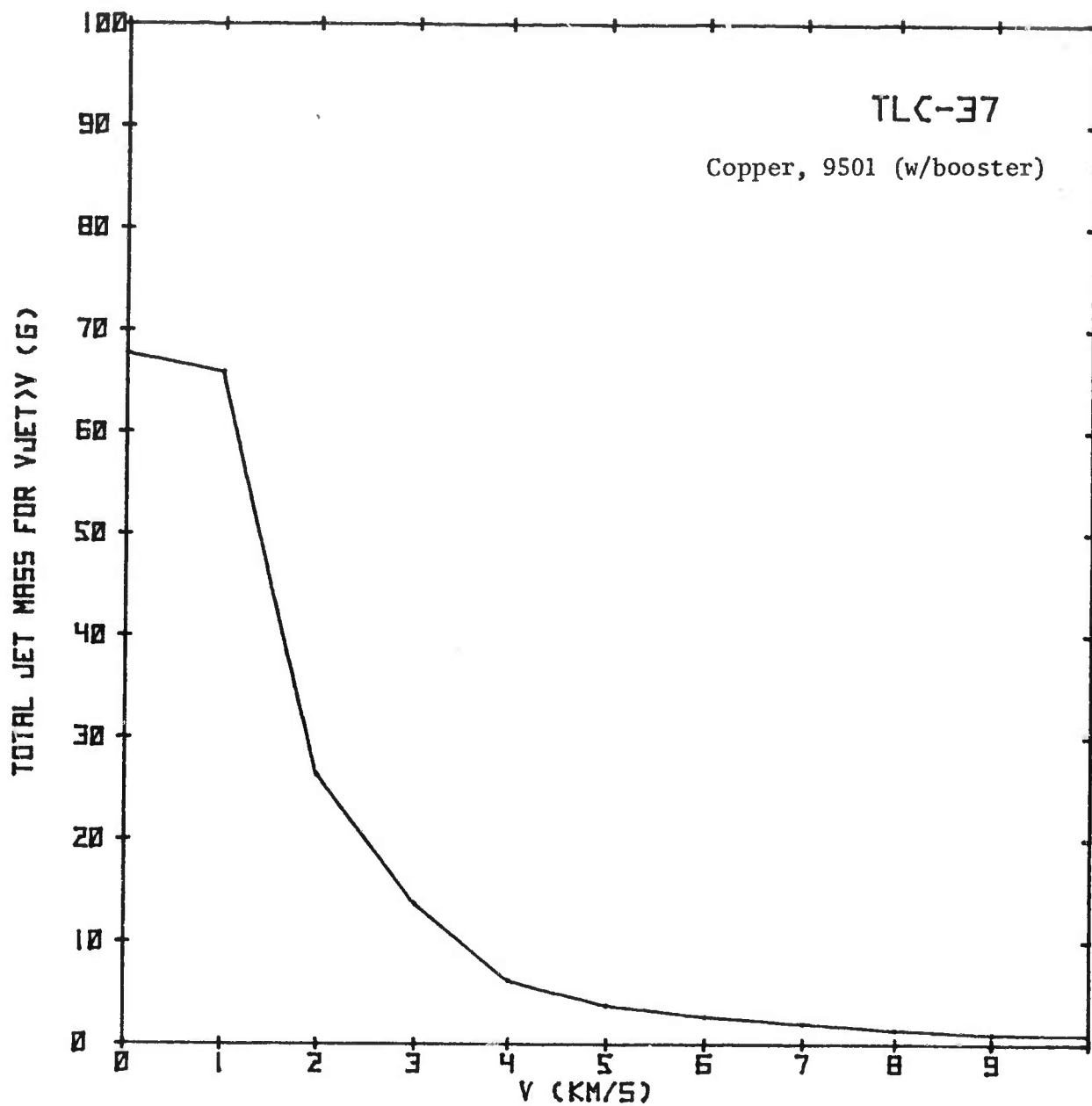
UNCLASSIFIED



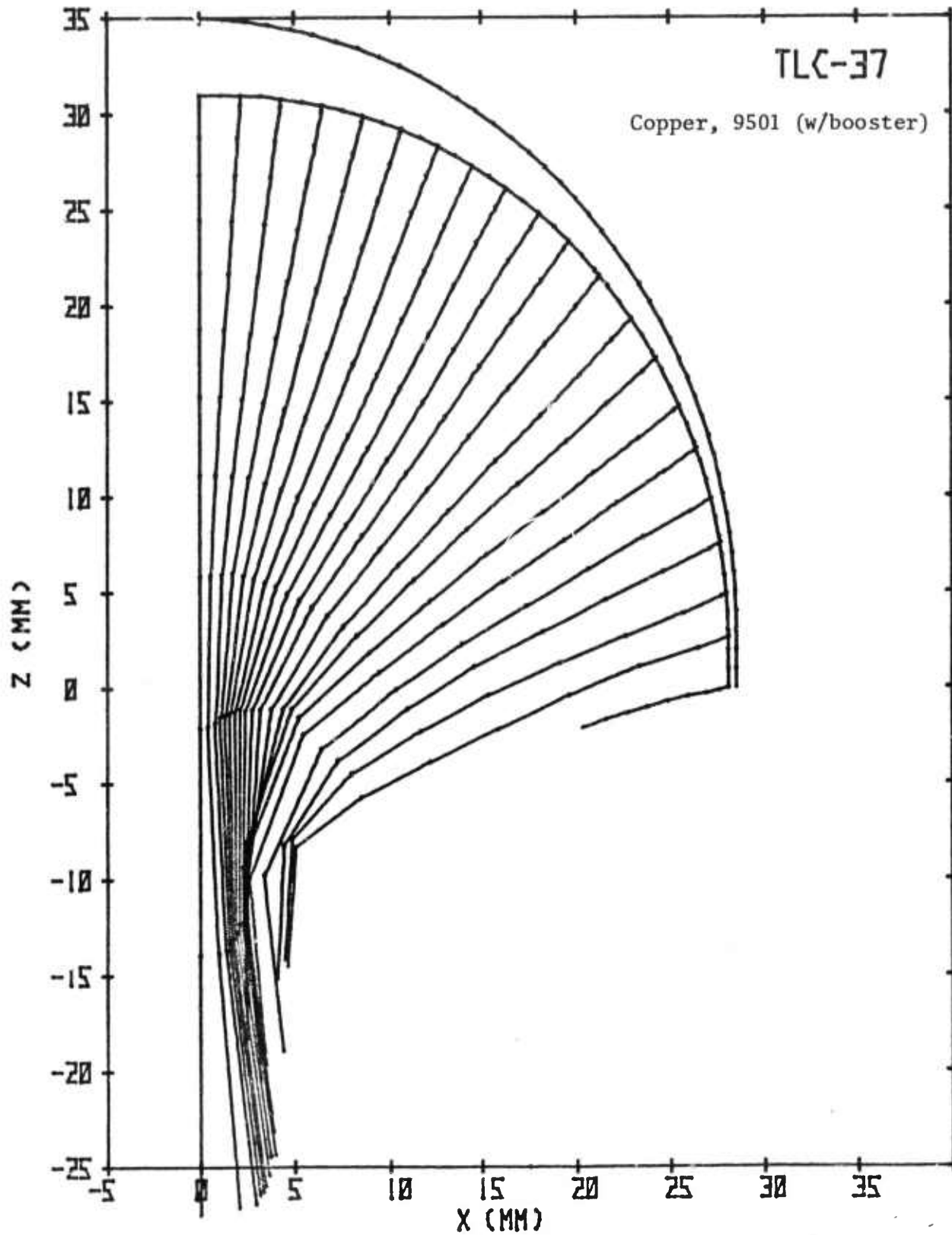
UNCLASSIFIED



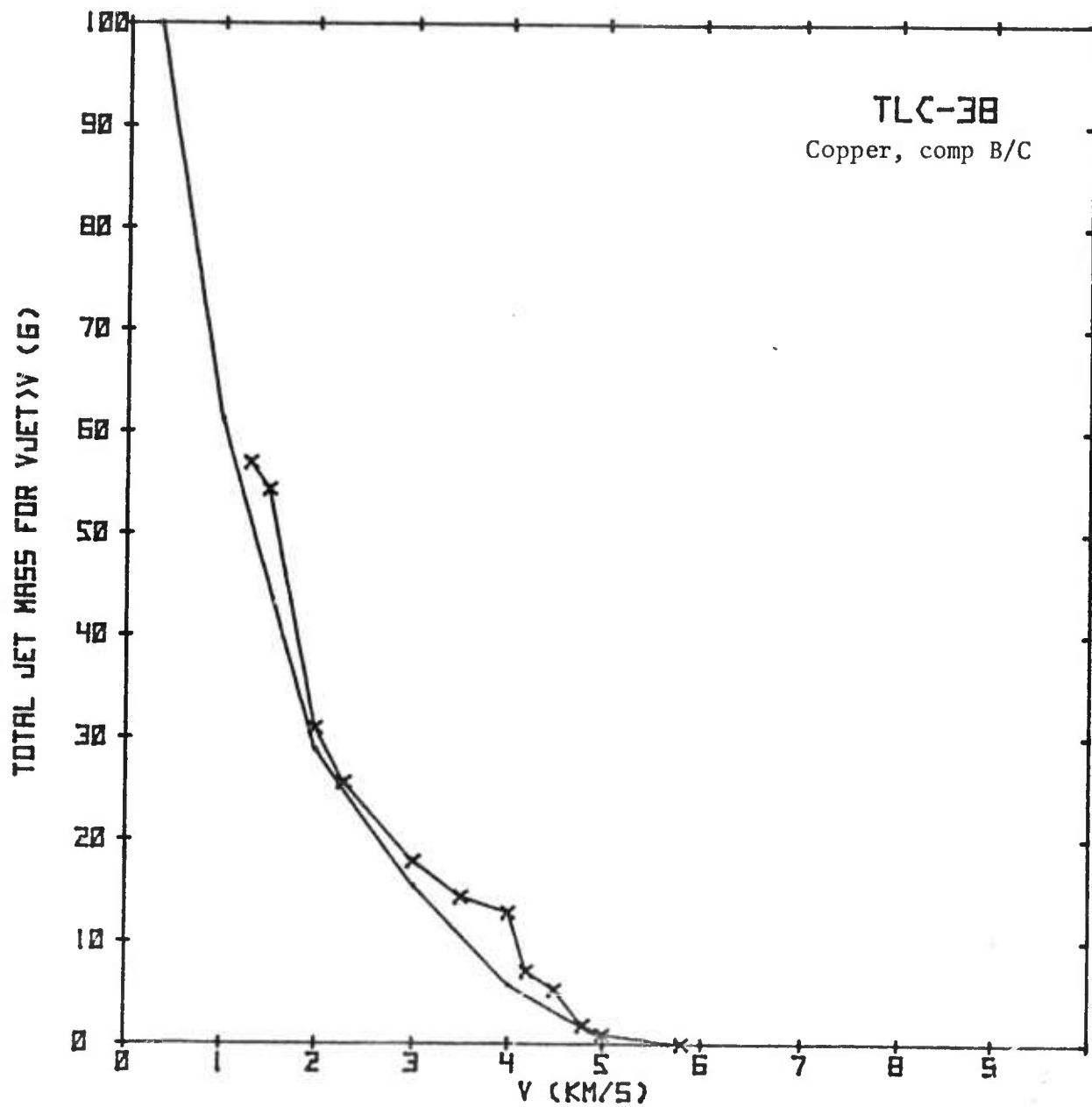
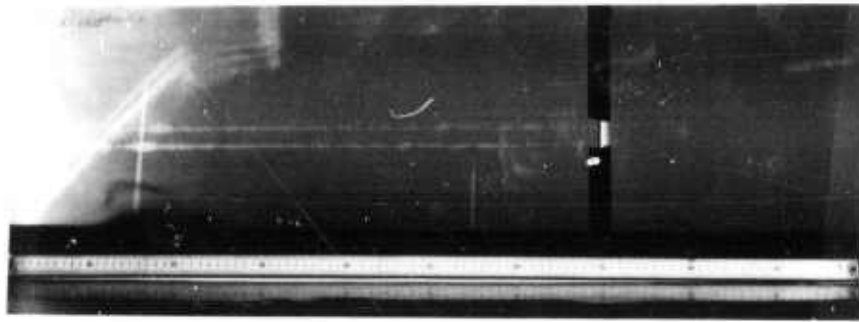
UNCLASSIFIED



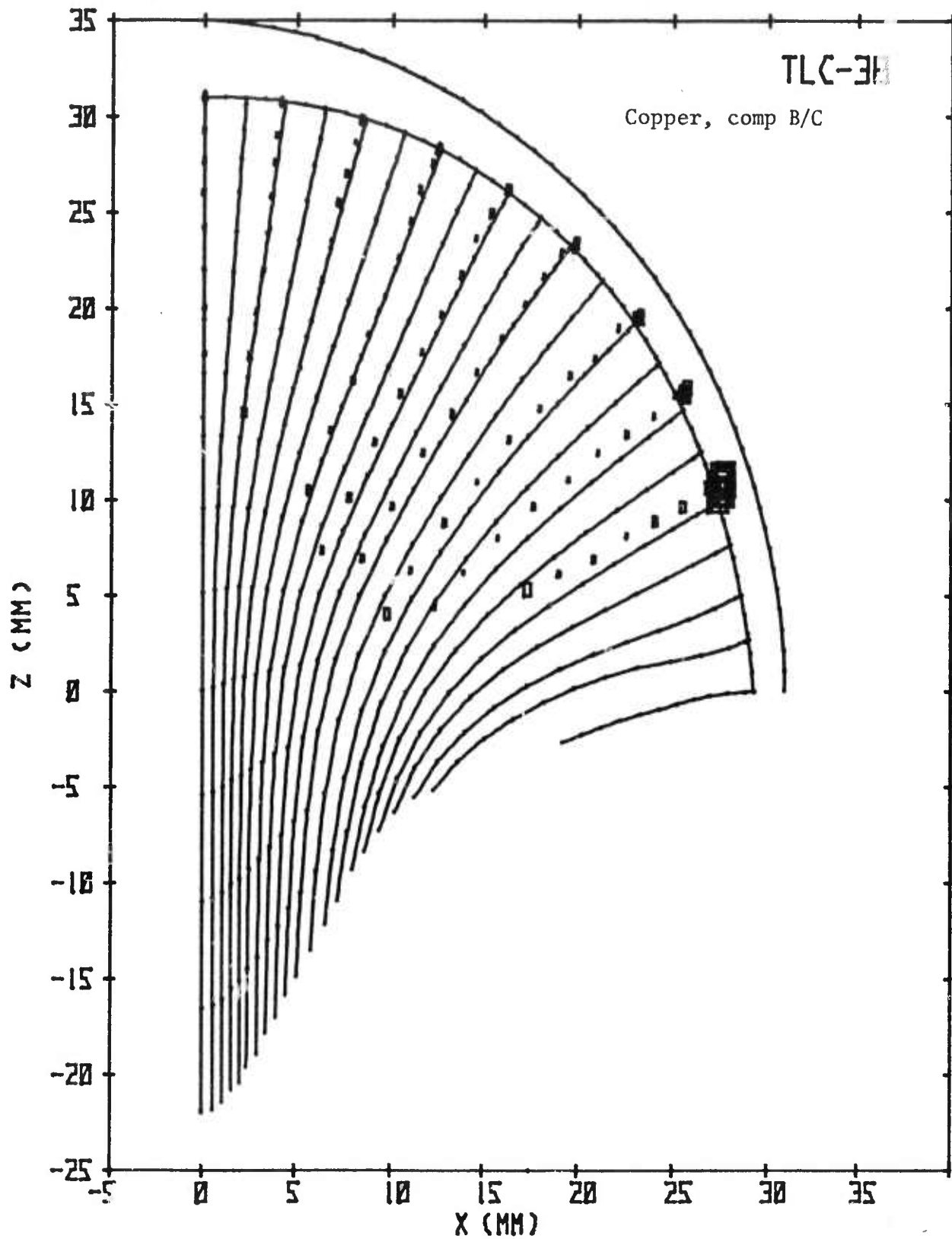
UNCLASSIFIED

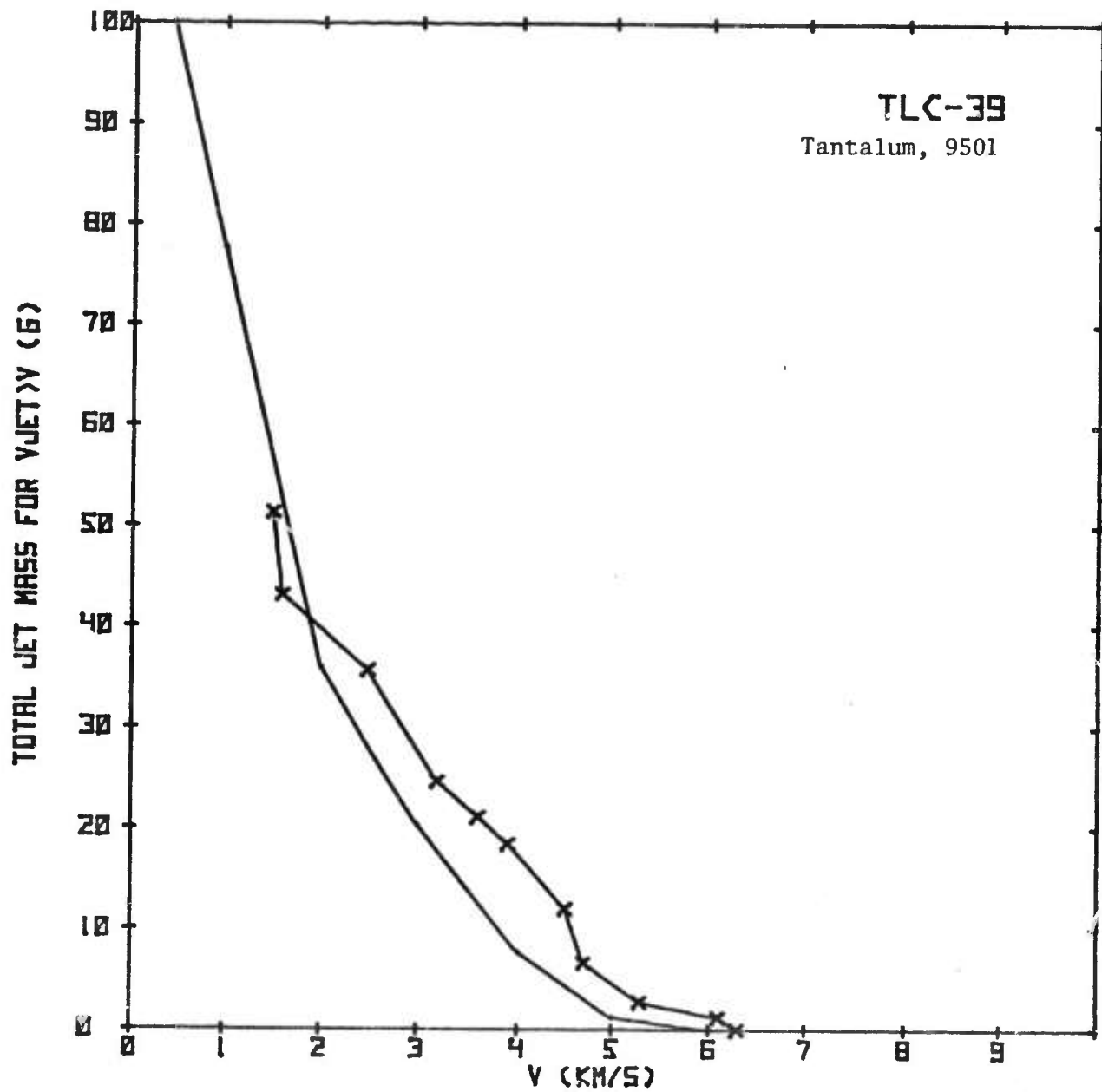
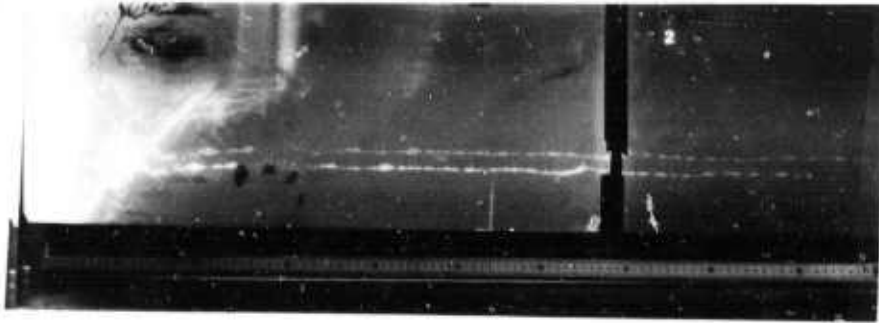


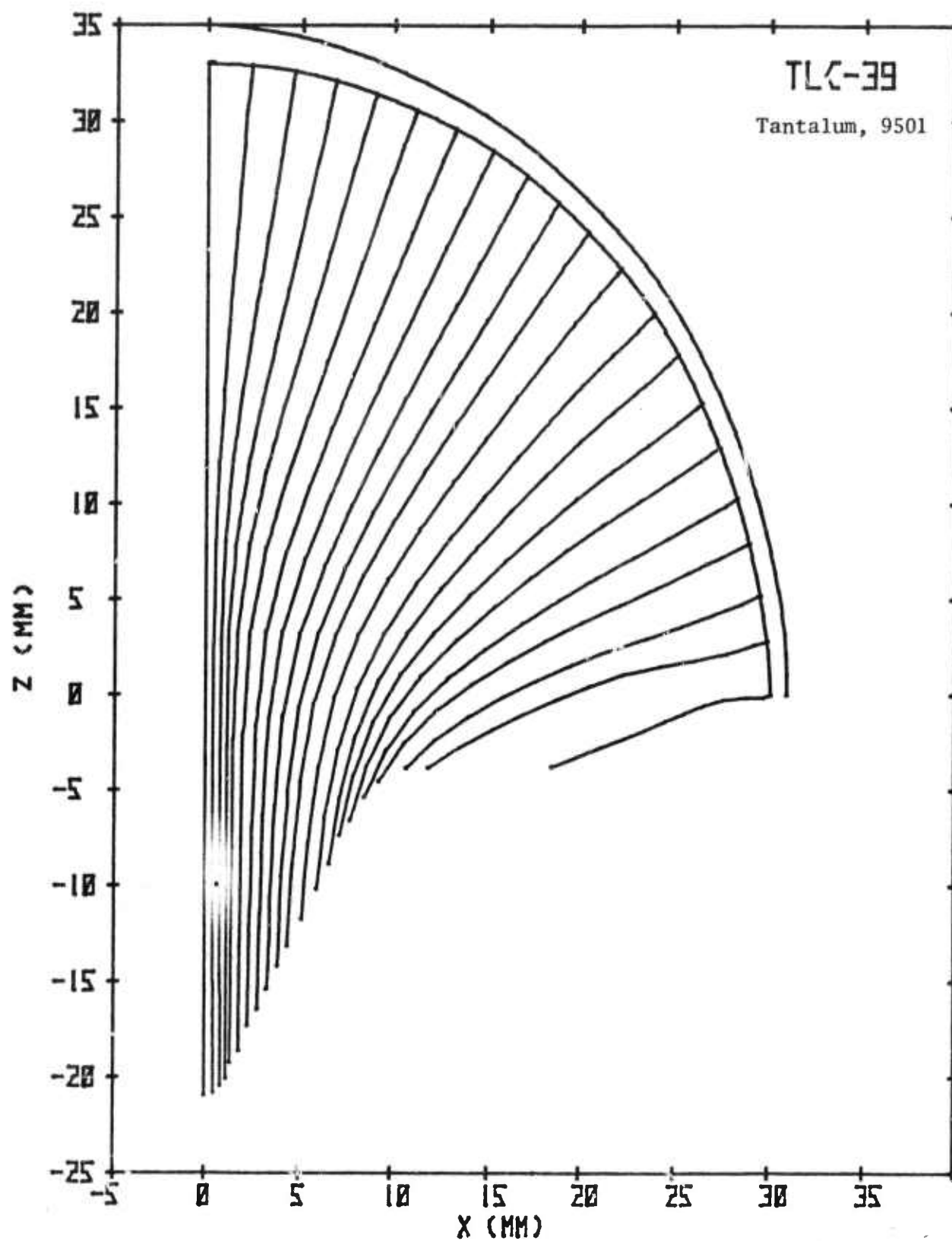
UNCLASSIFIED



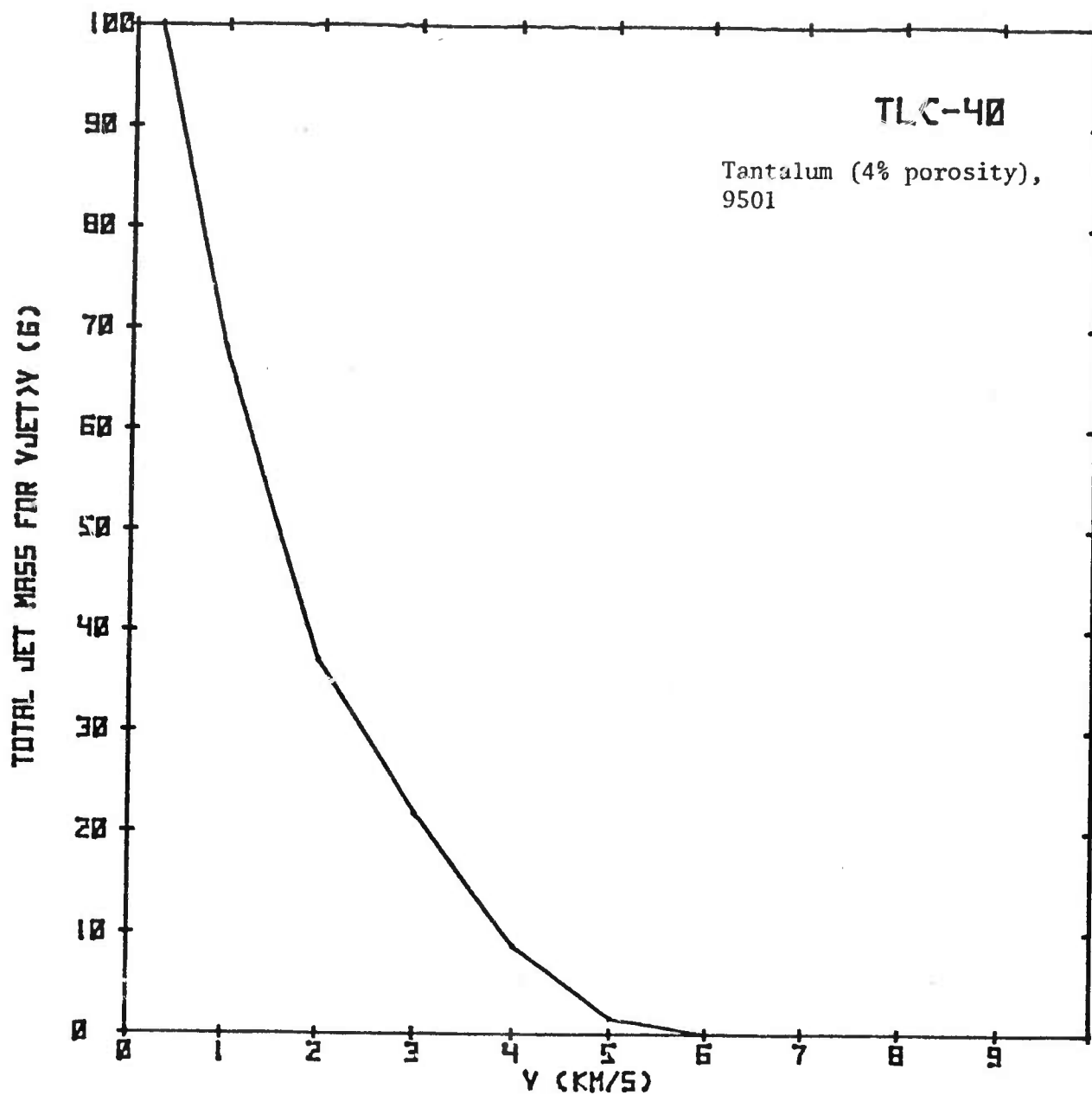
UNCLASSIFIED



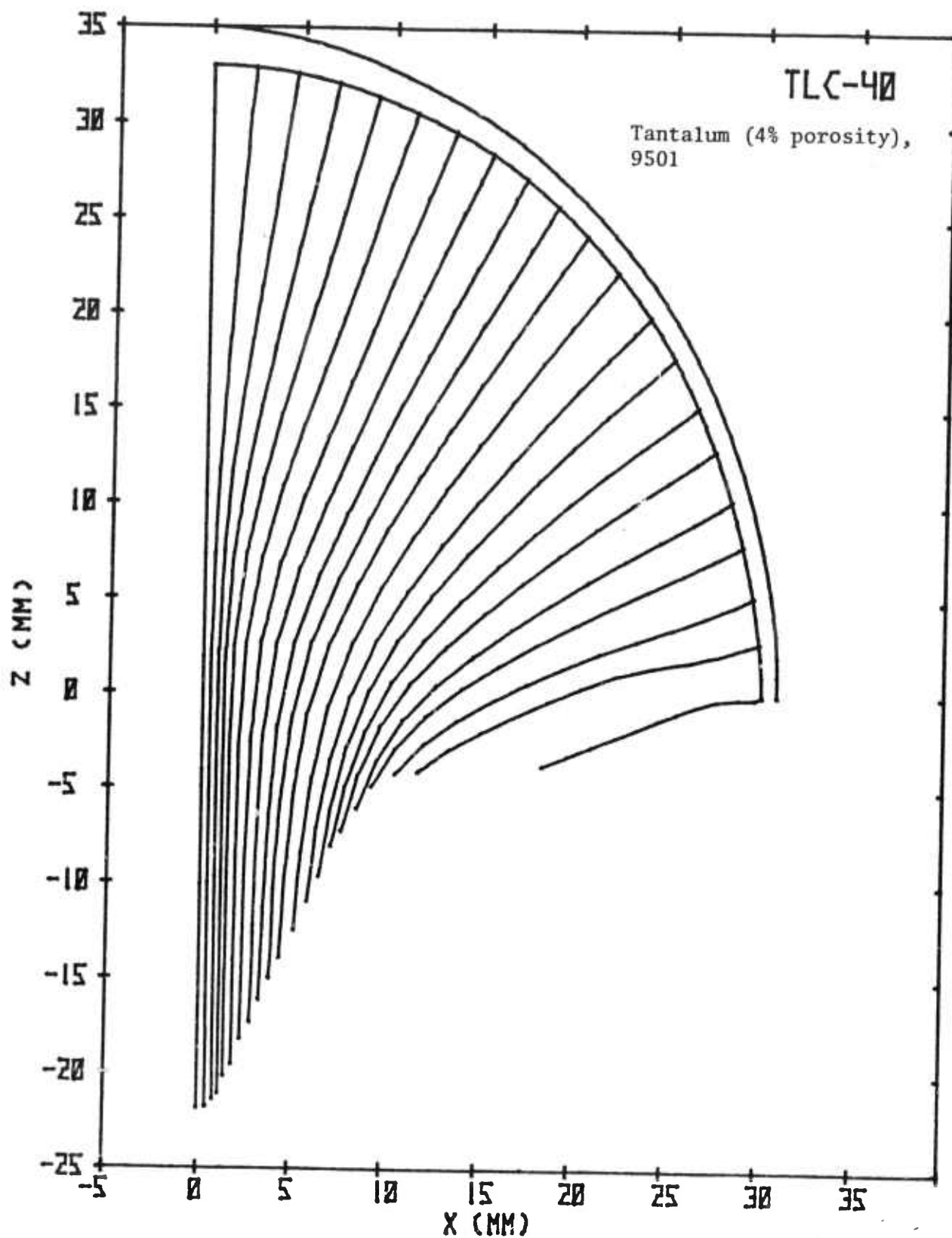


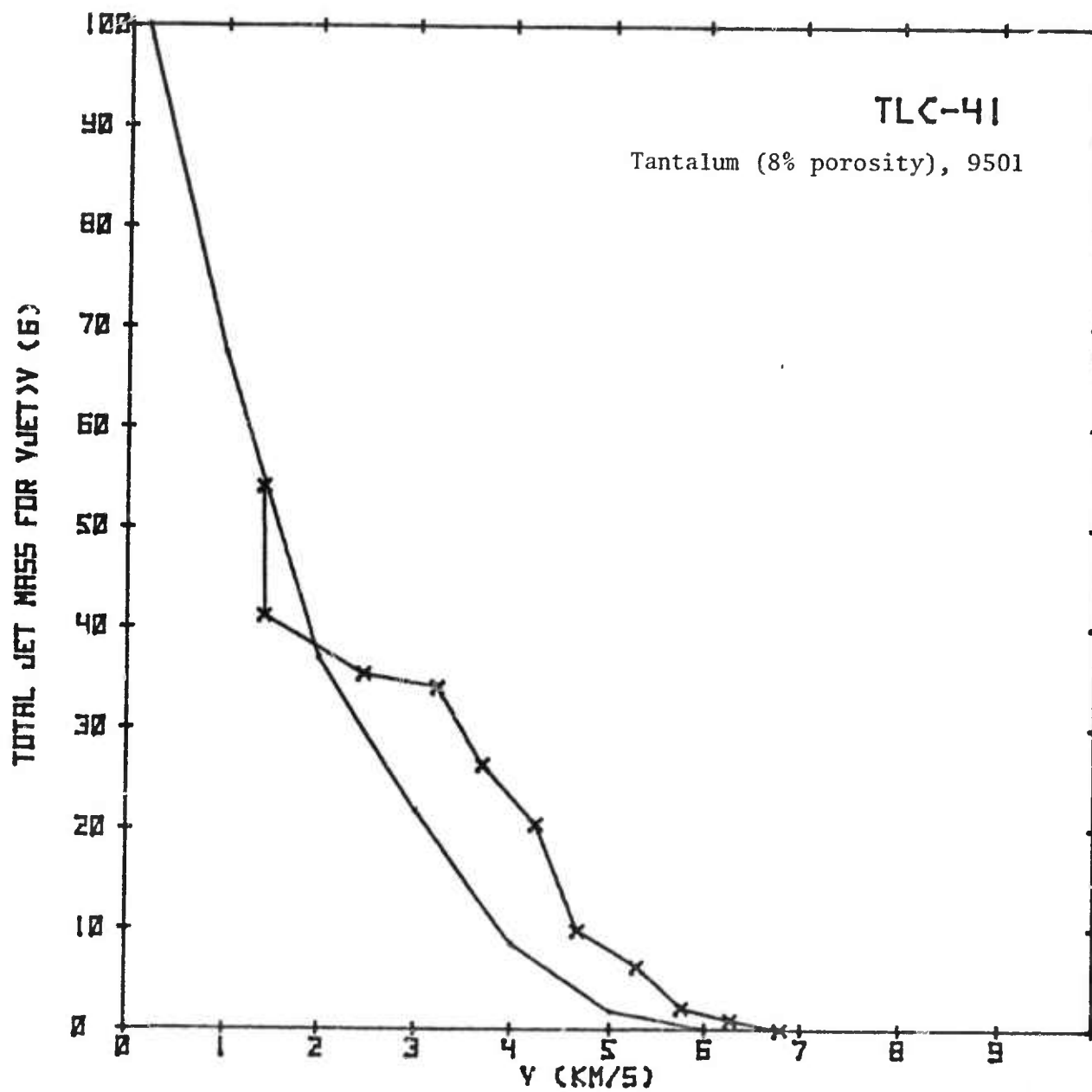
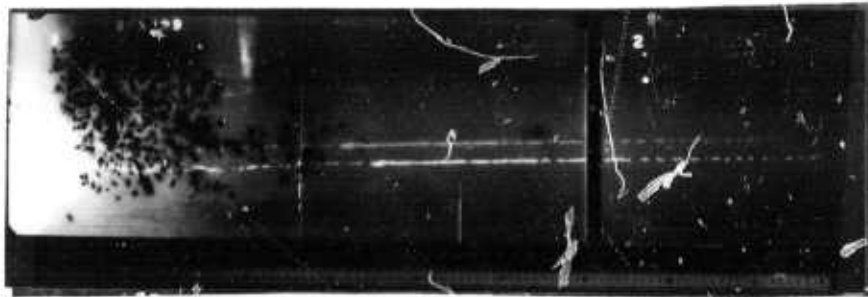


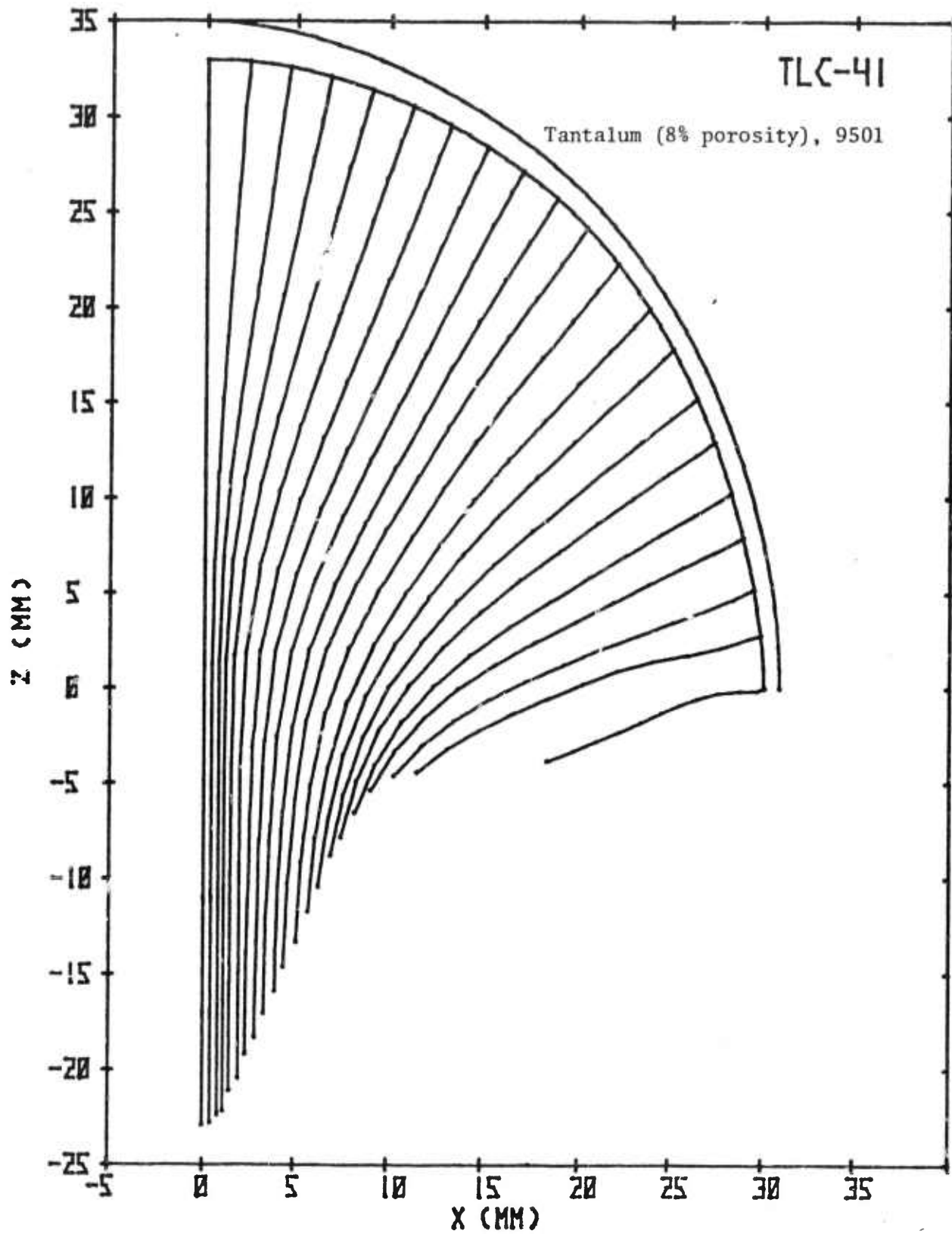
UNCLASSIFIED



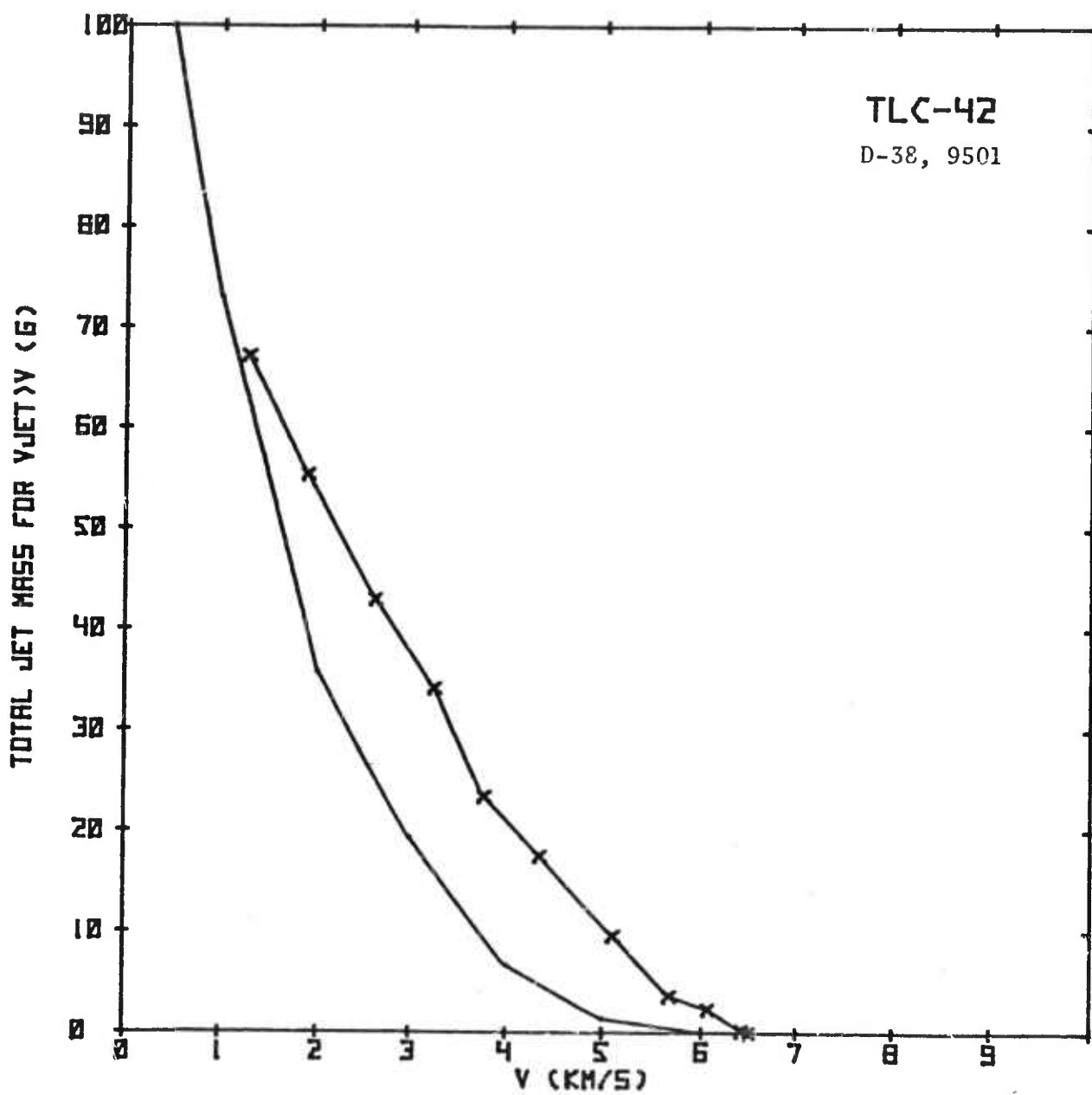
UNCLASSIFIED



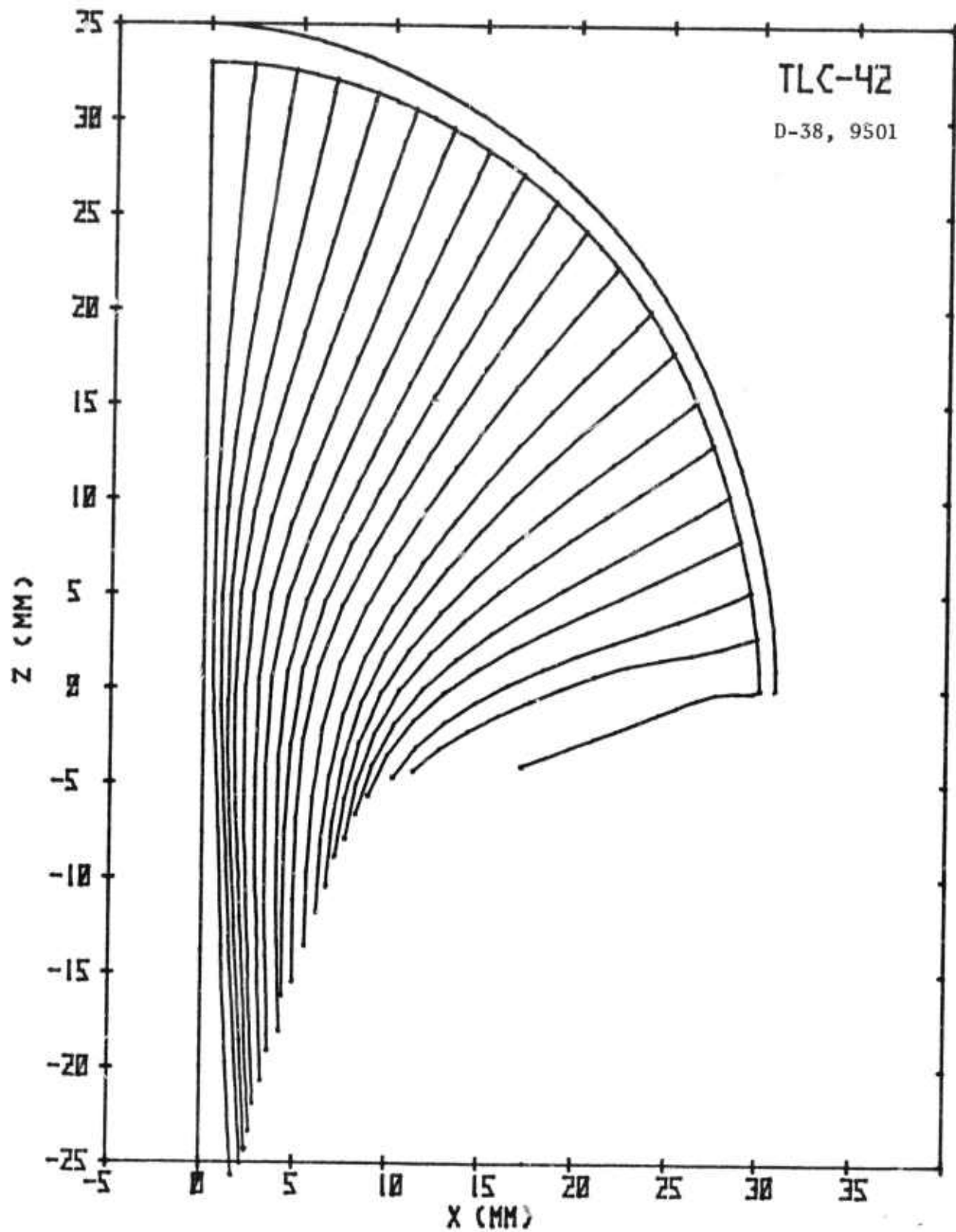




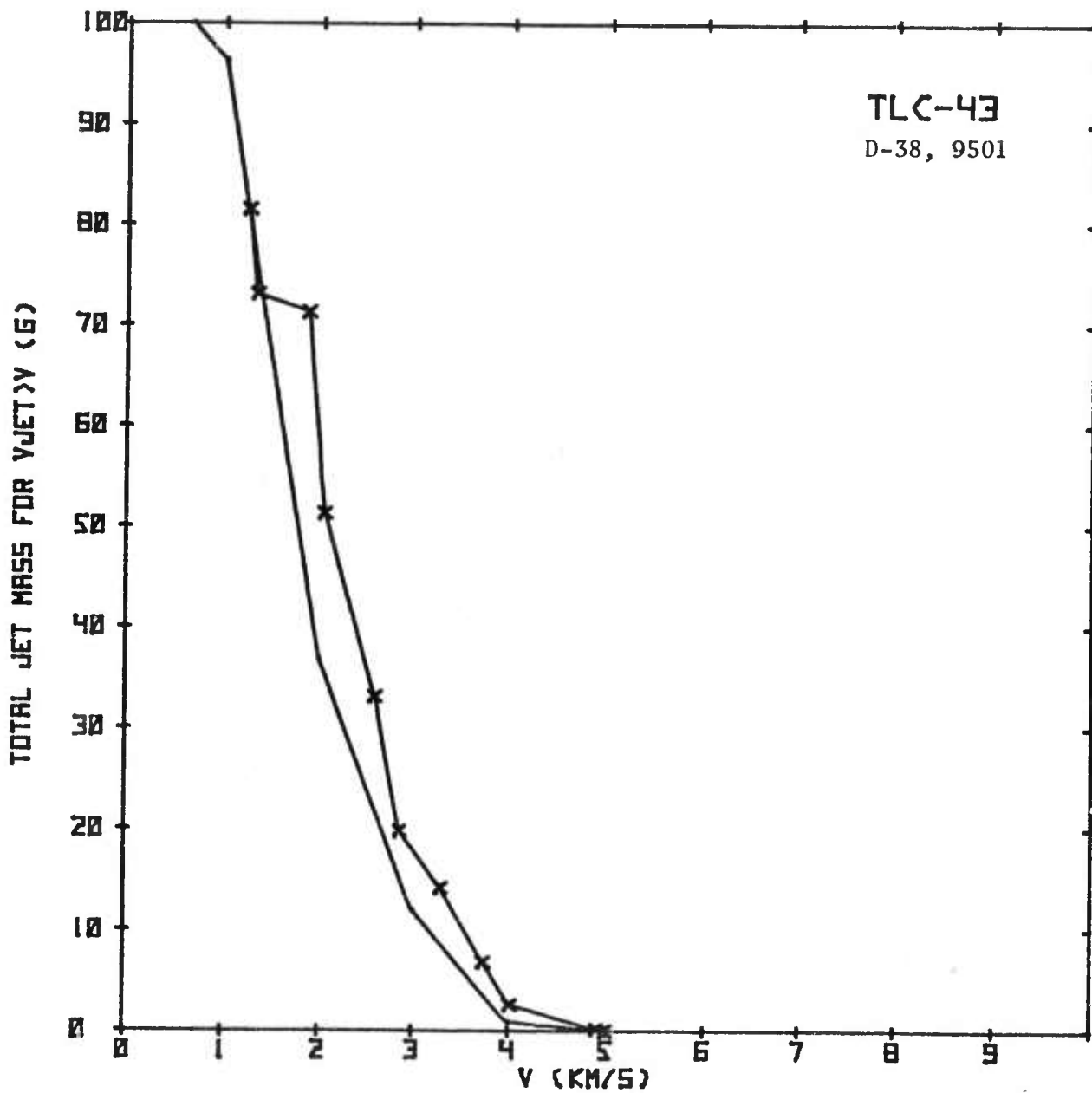
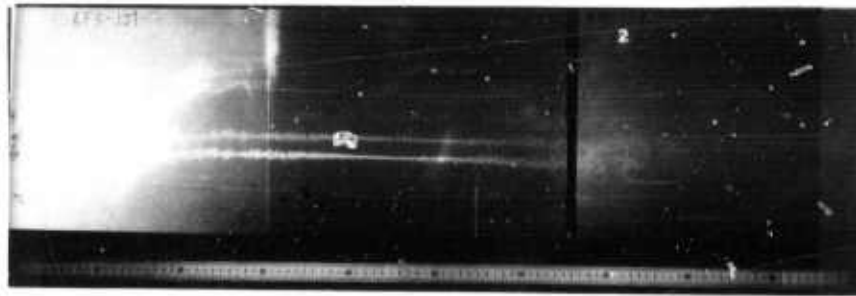
UNCLASSIFIED



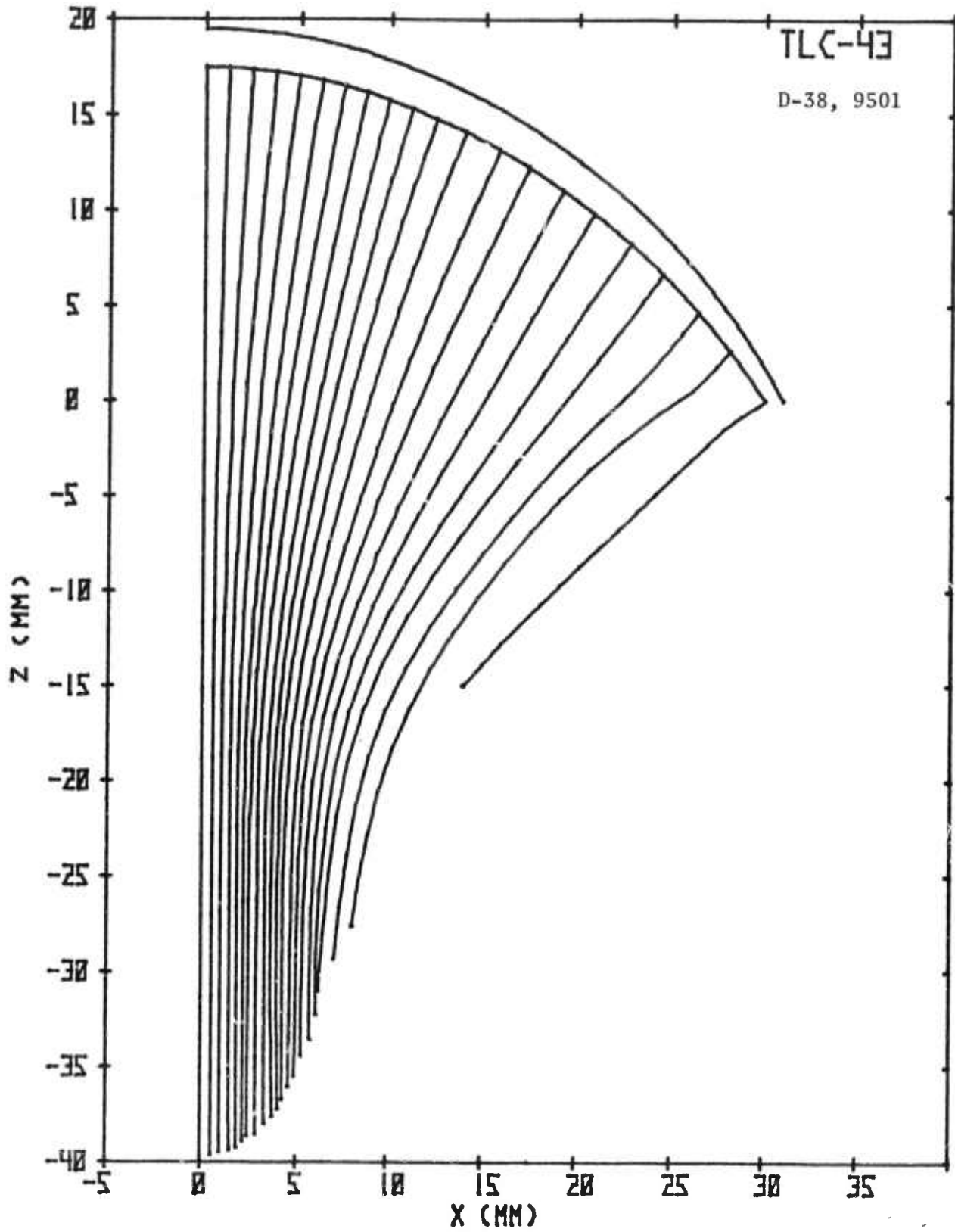
UNCLASSIFIED

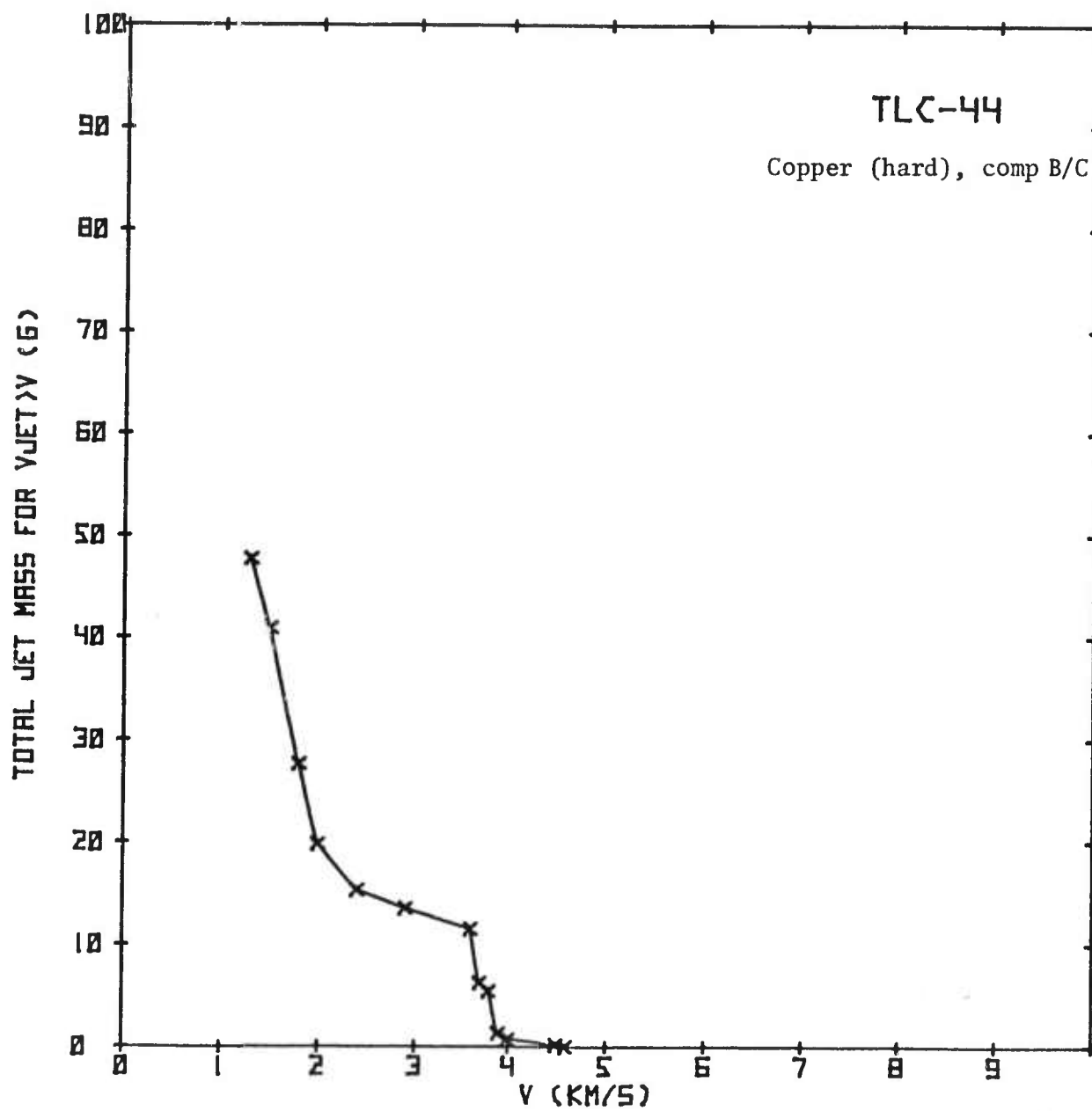
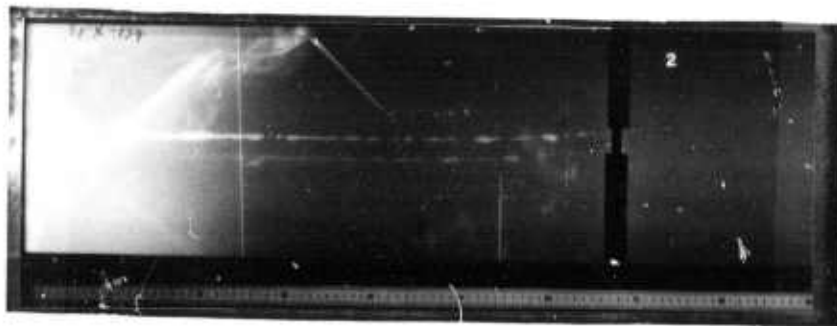


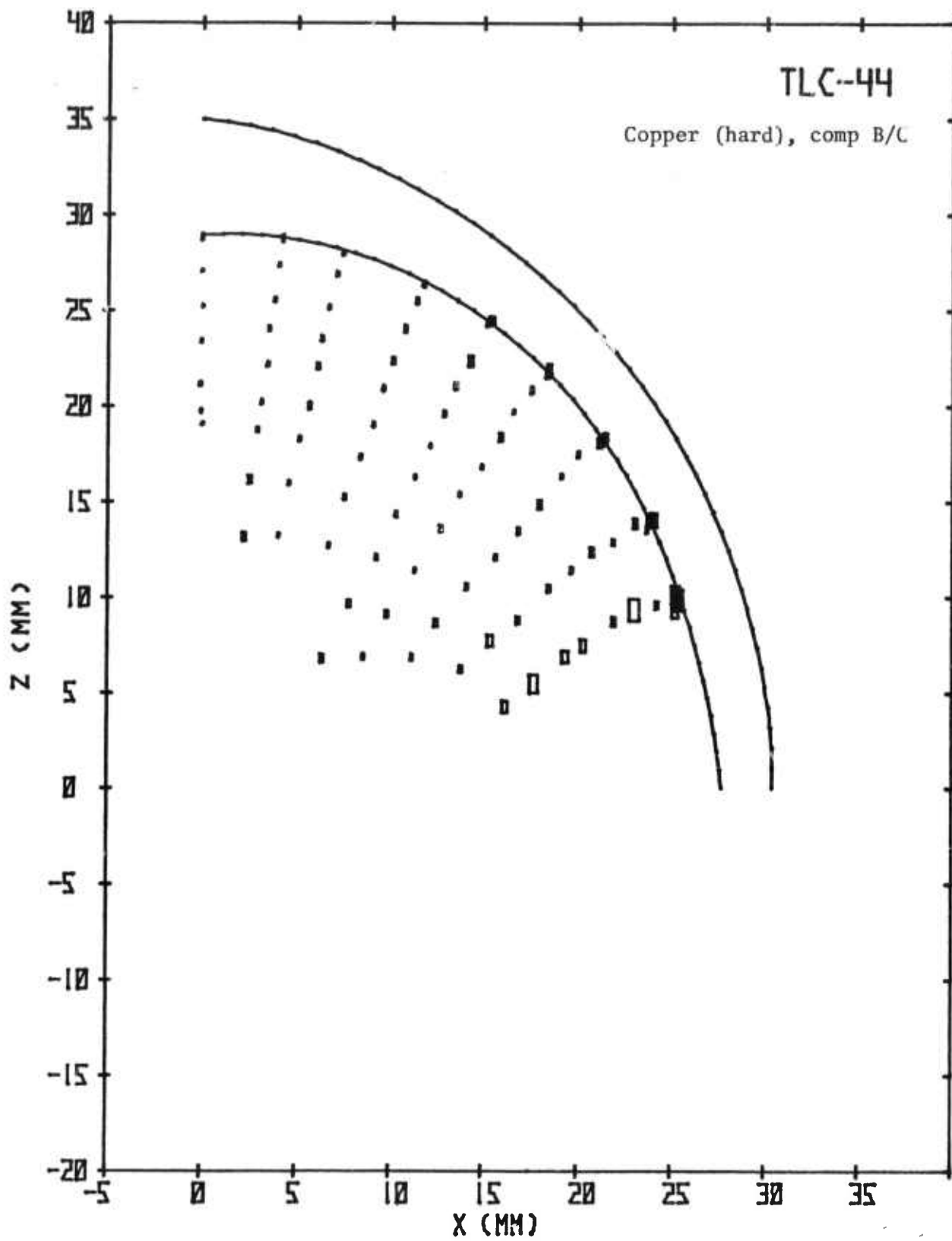
UNCLASSIFIED



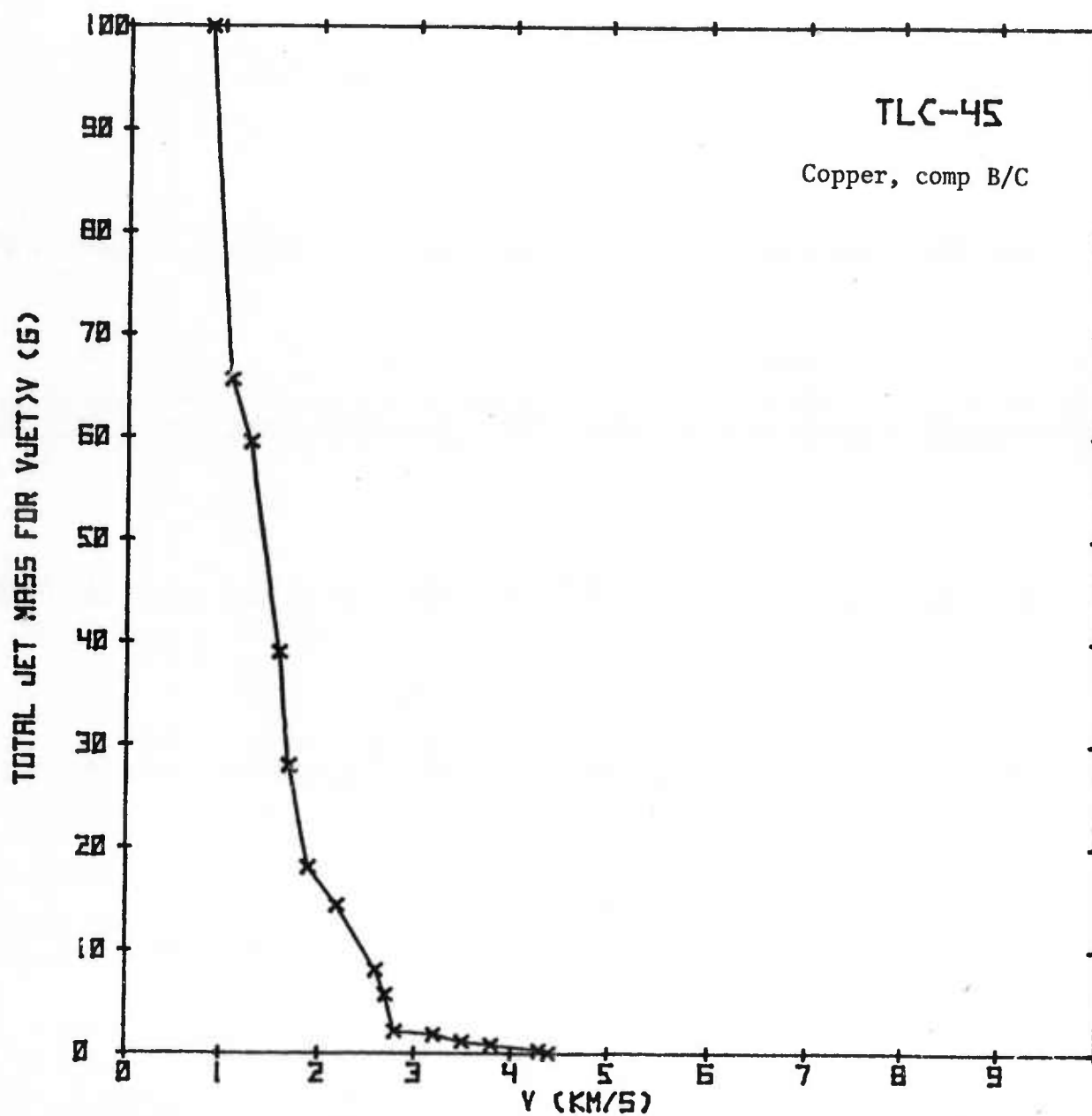
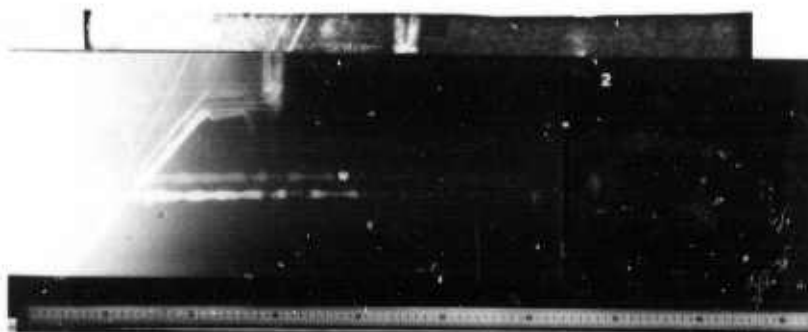
UNCLASSIFIED



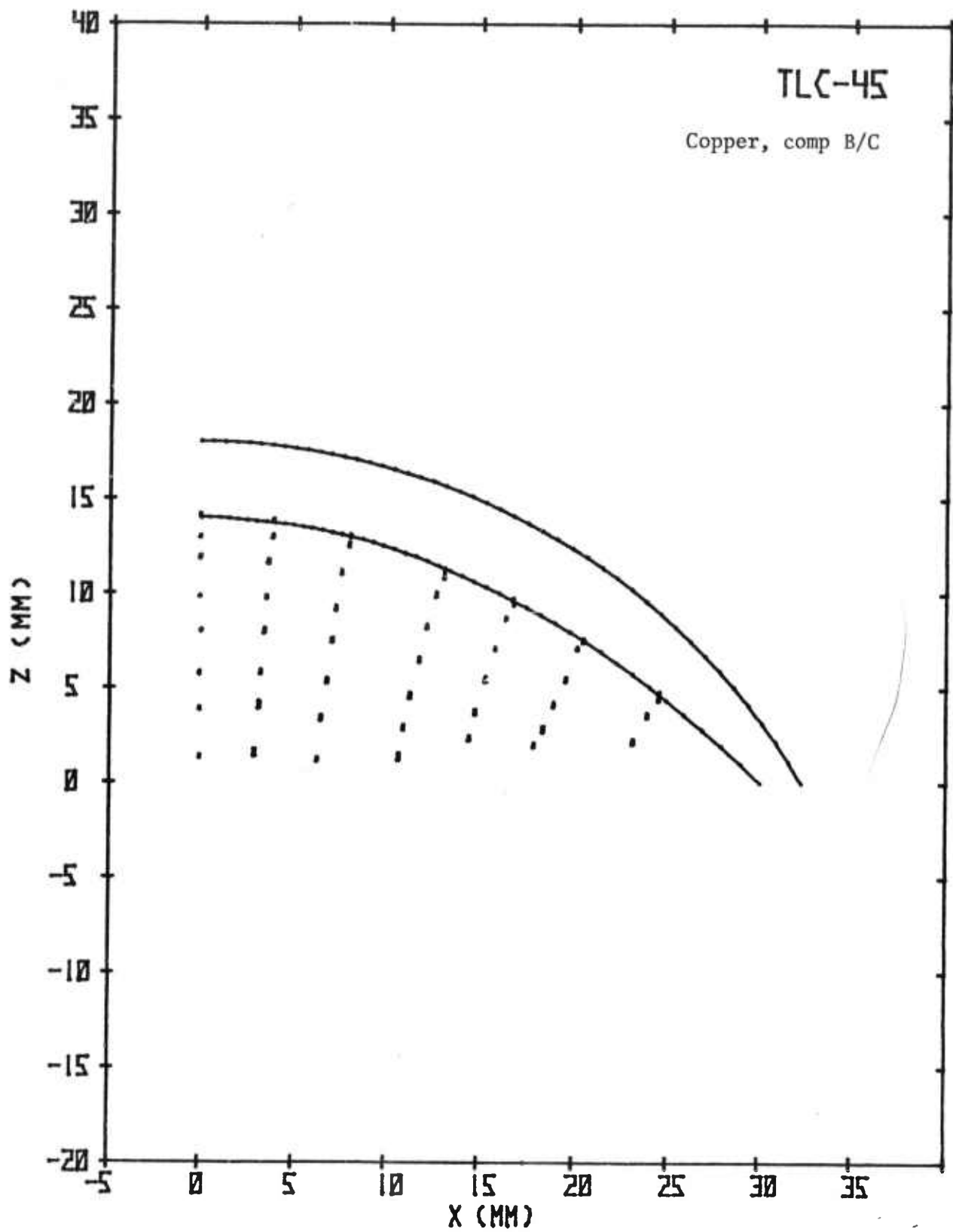




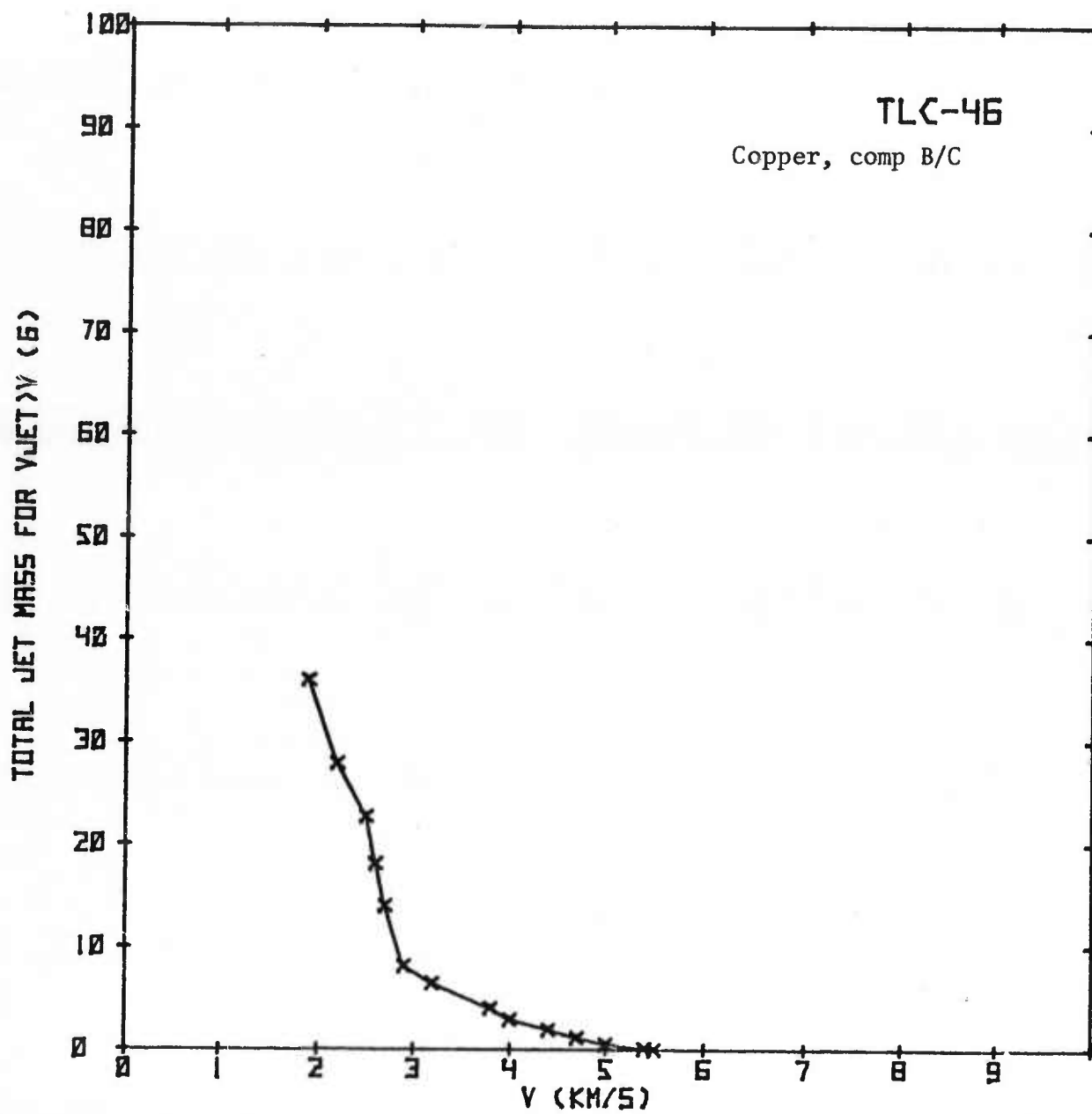
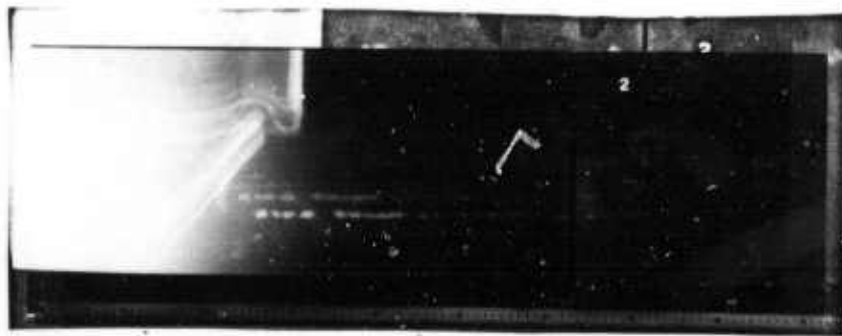
UNCLASSIFIED



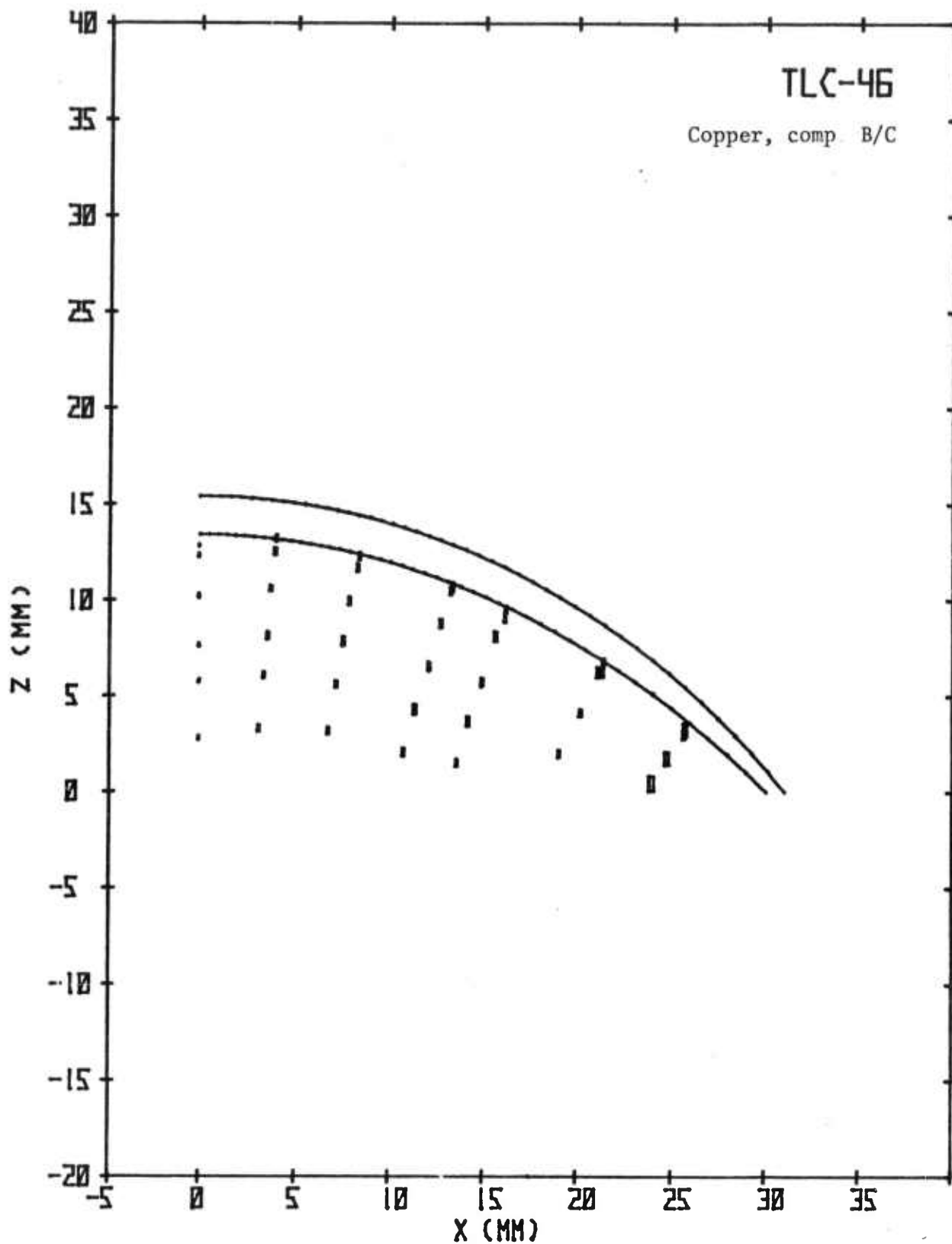
UNCLASSIFIED



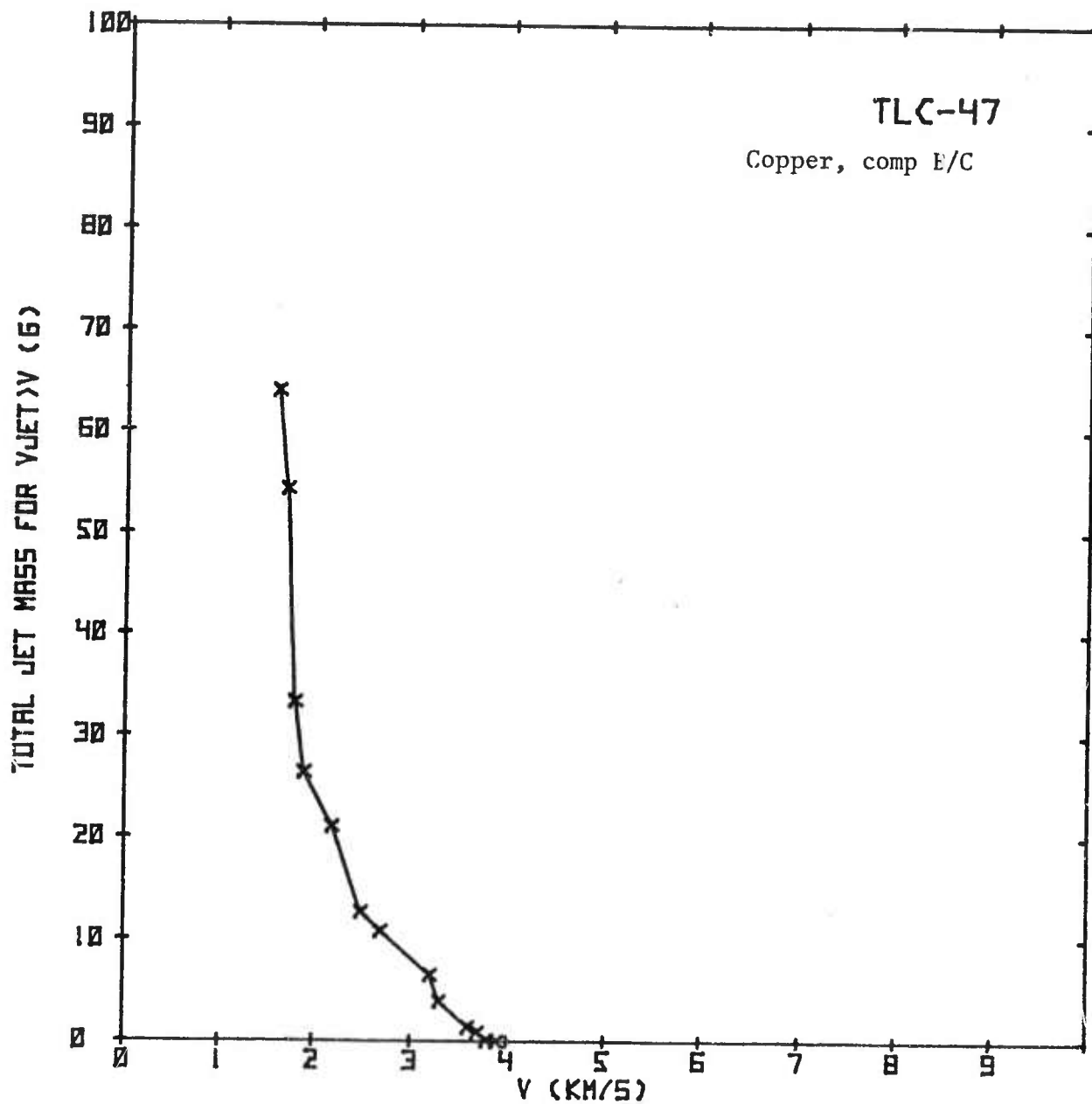
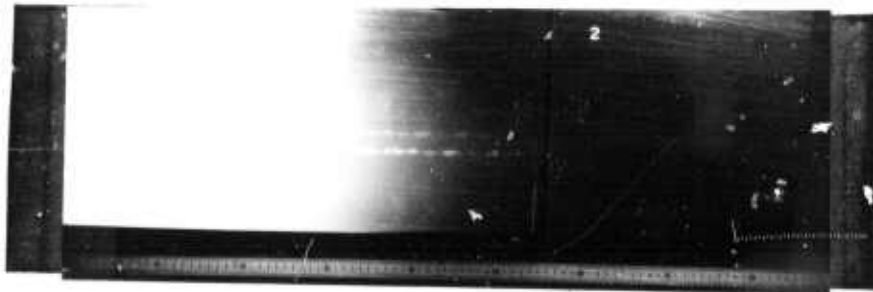
UNCLASSIFIED



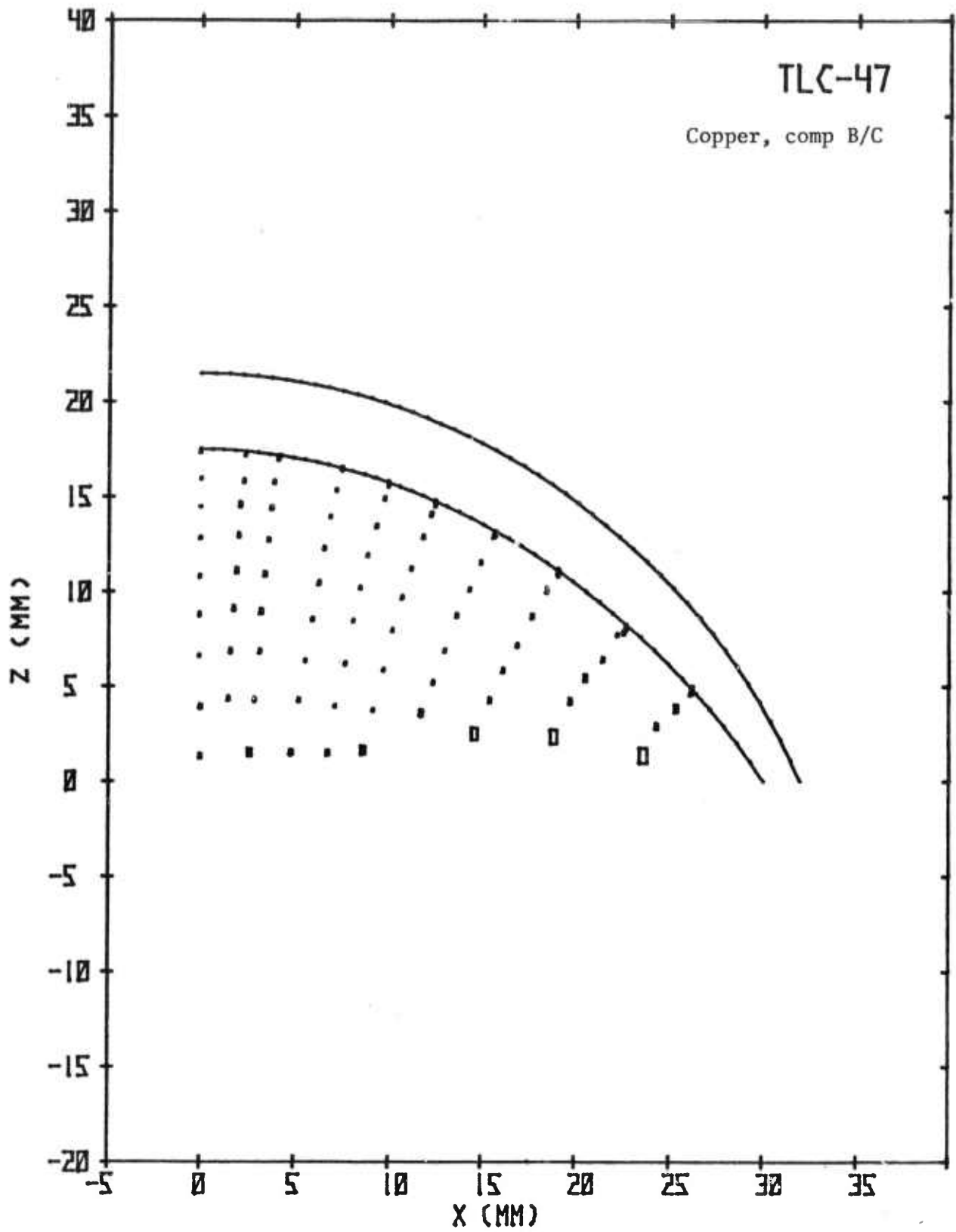
UNCLASSIFIED



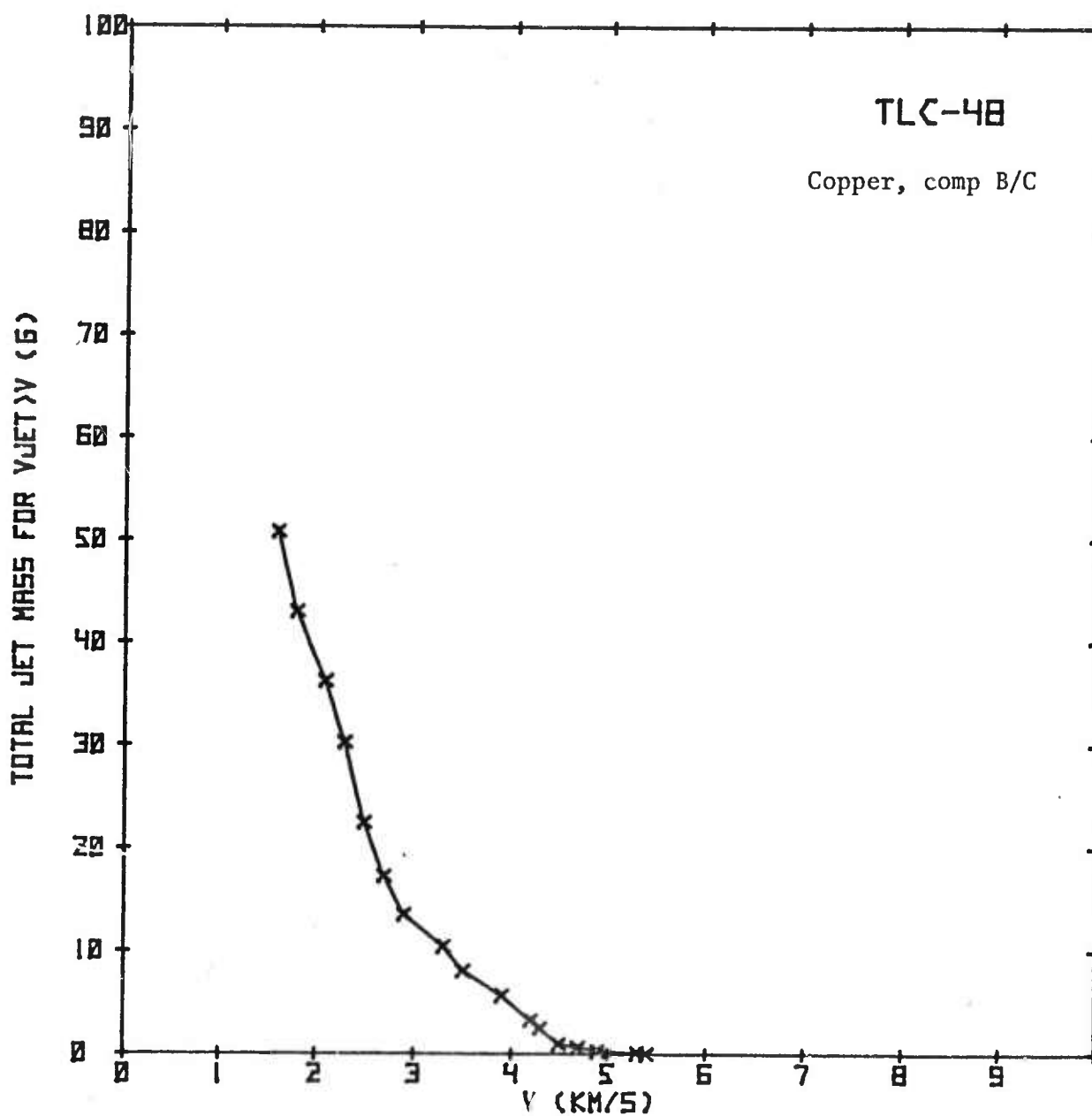
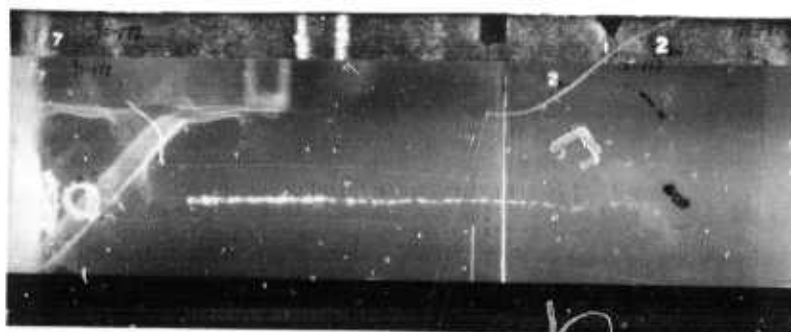
UNCLASSIFIED



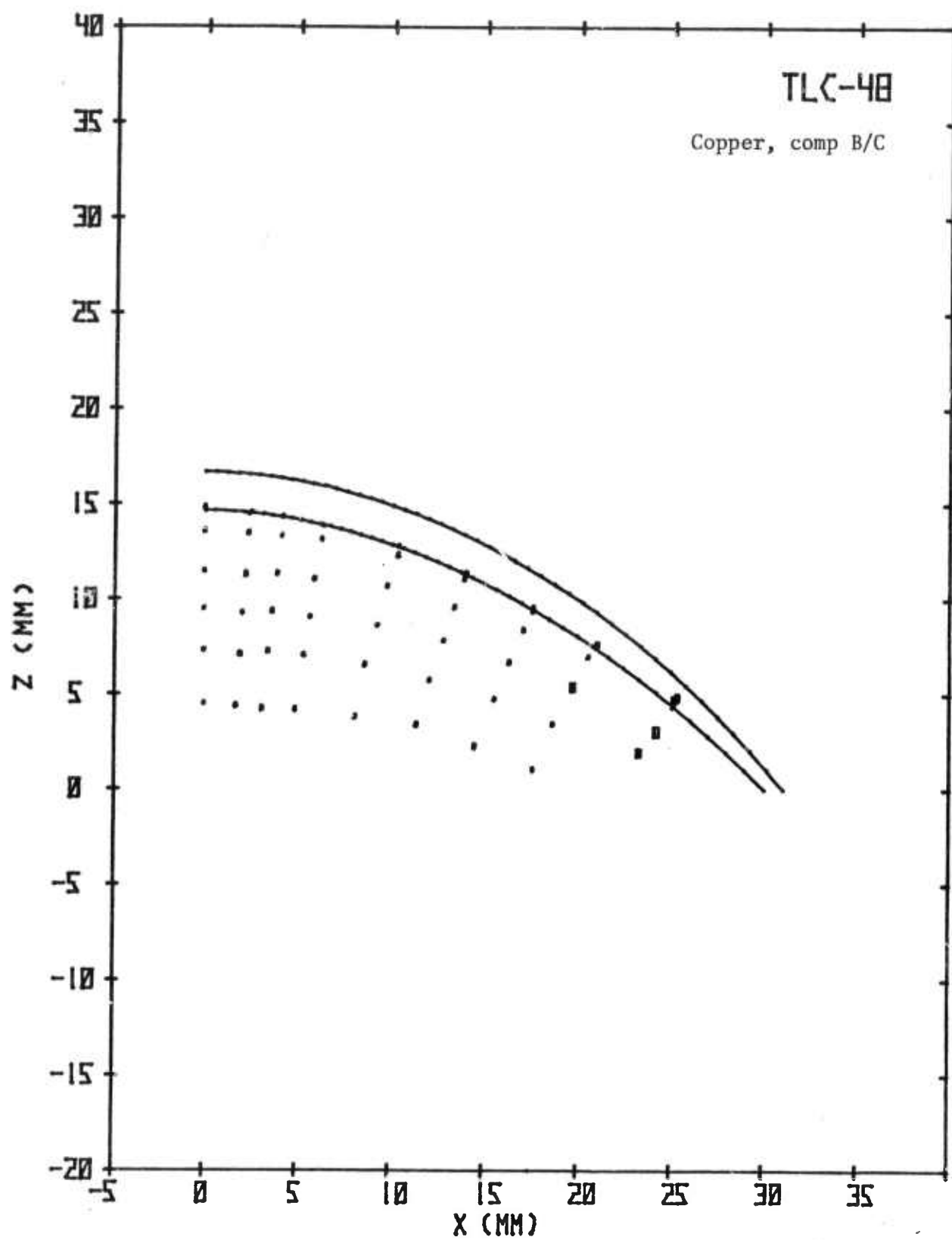
UNCLASSIFIED

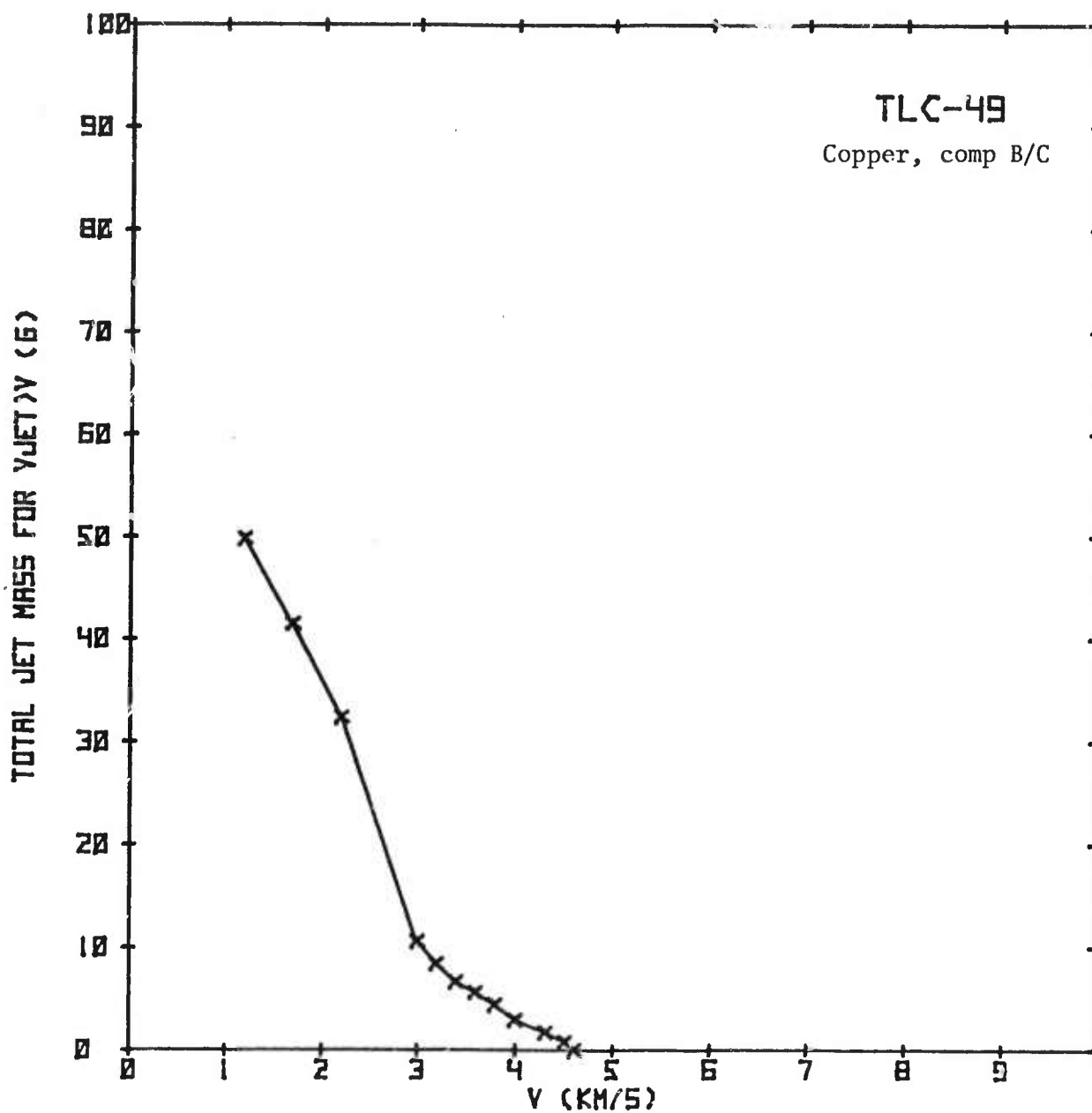
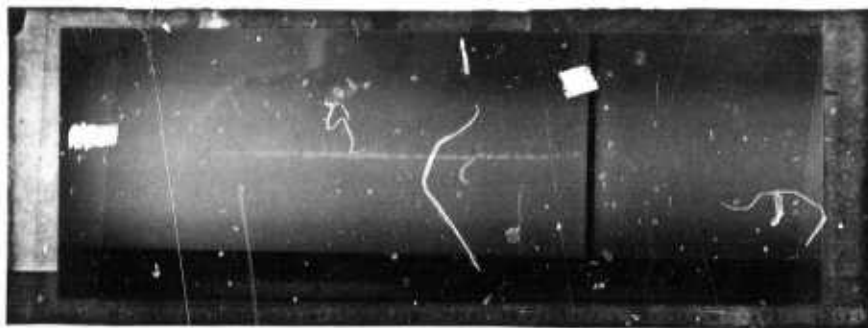


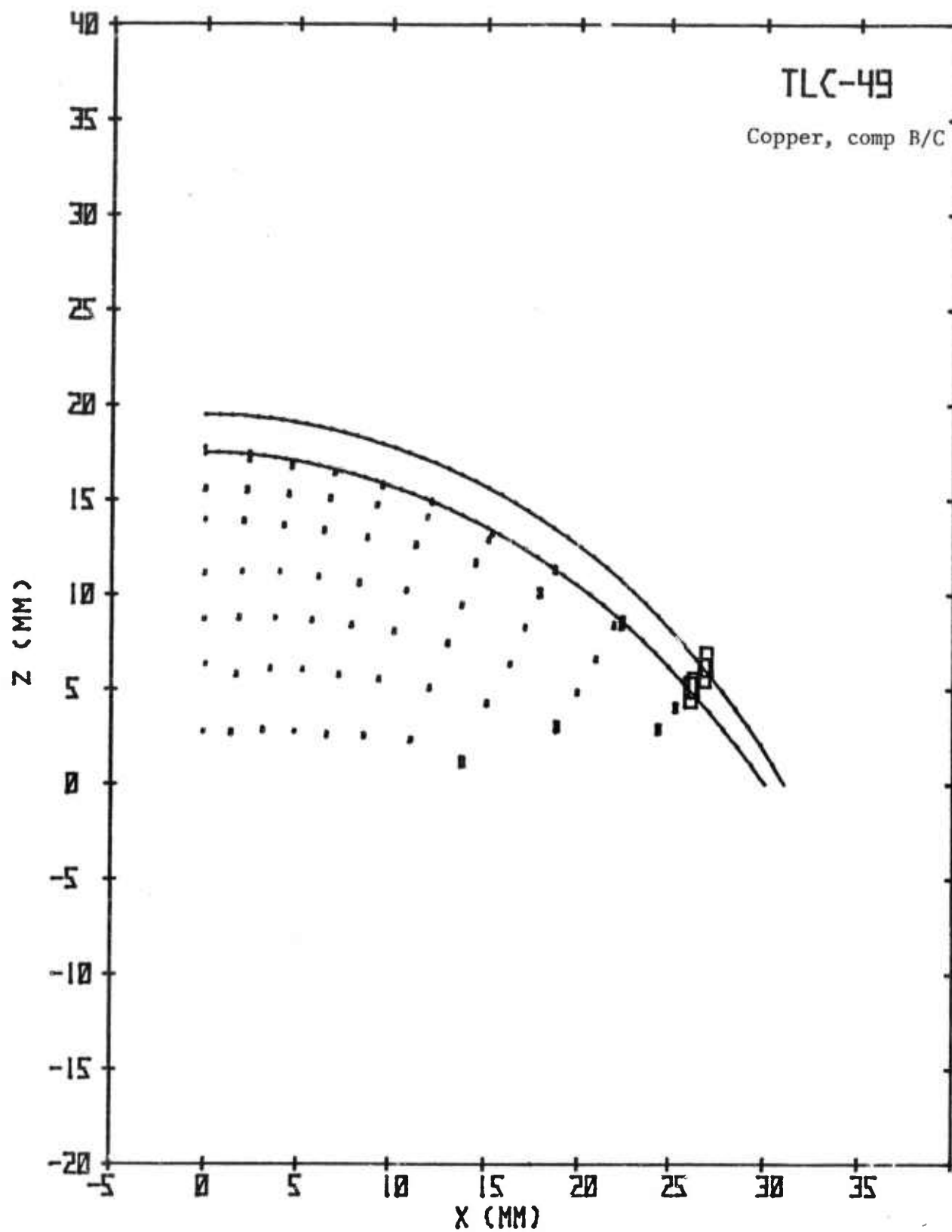
UNCLASSIFIED

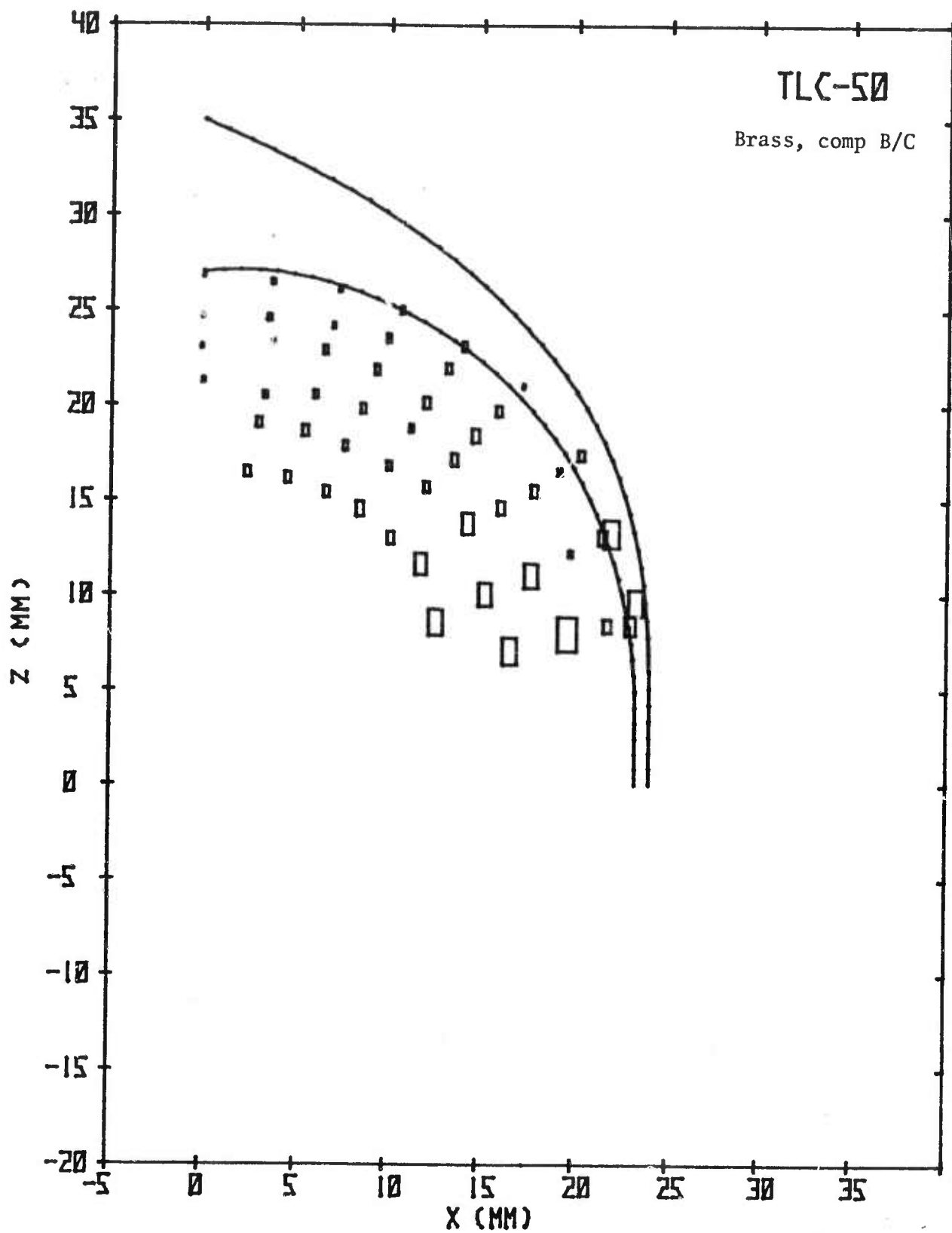


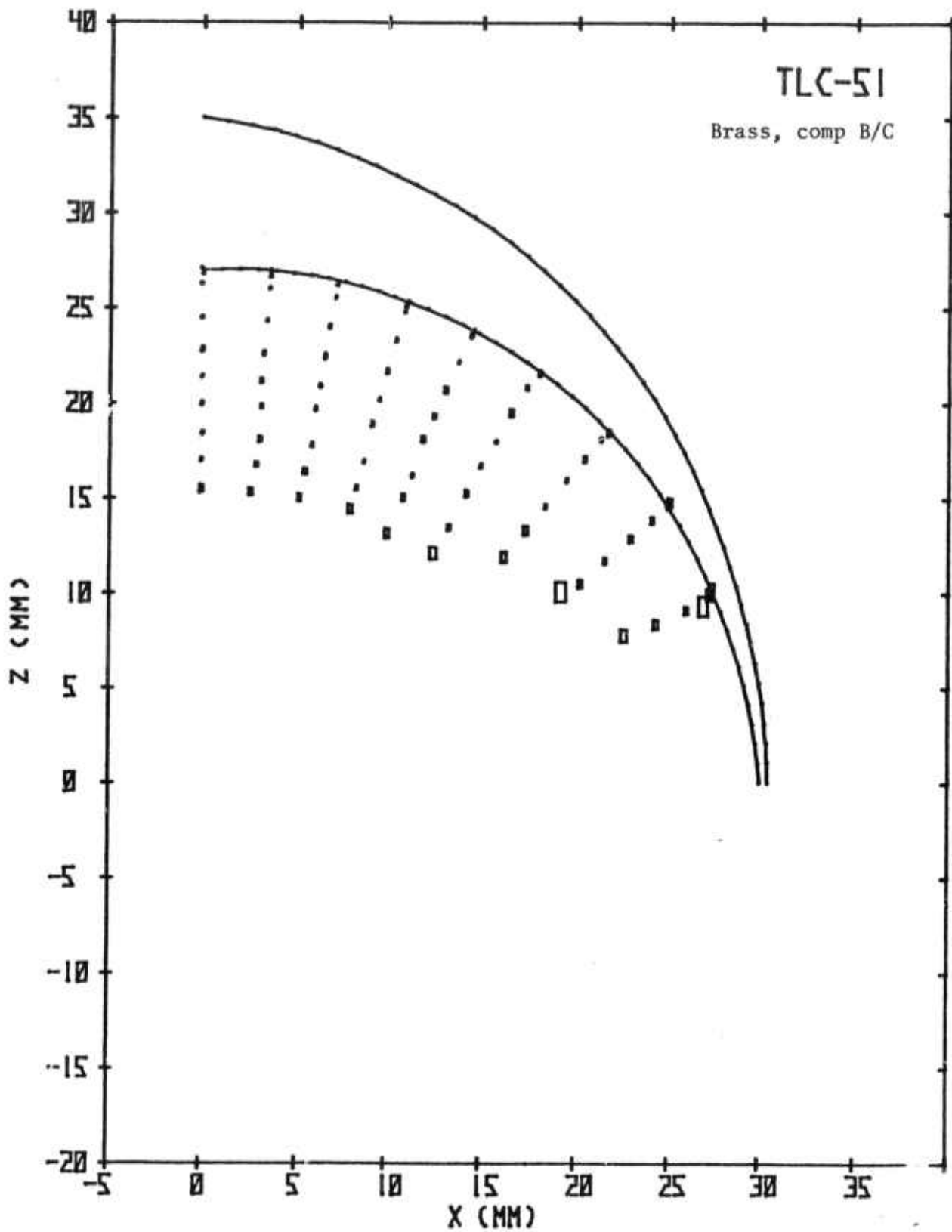
UNCLASSIFIED











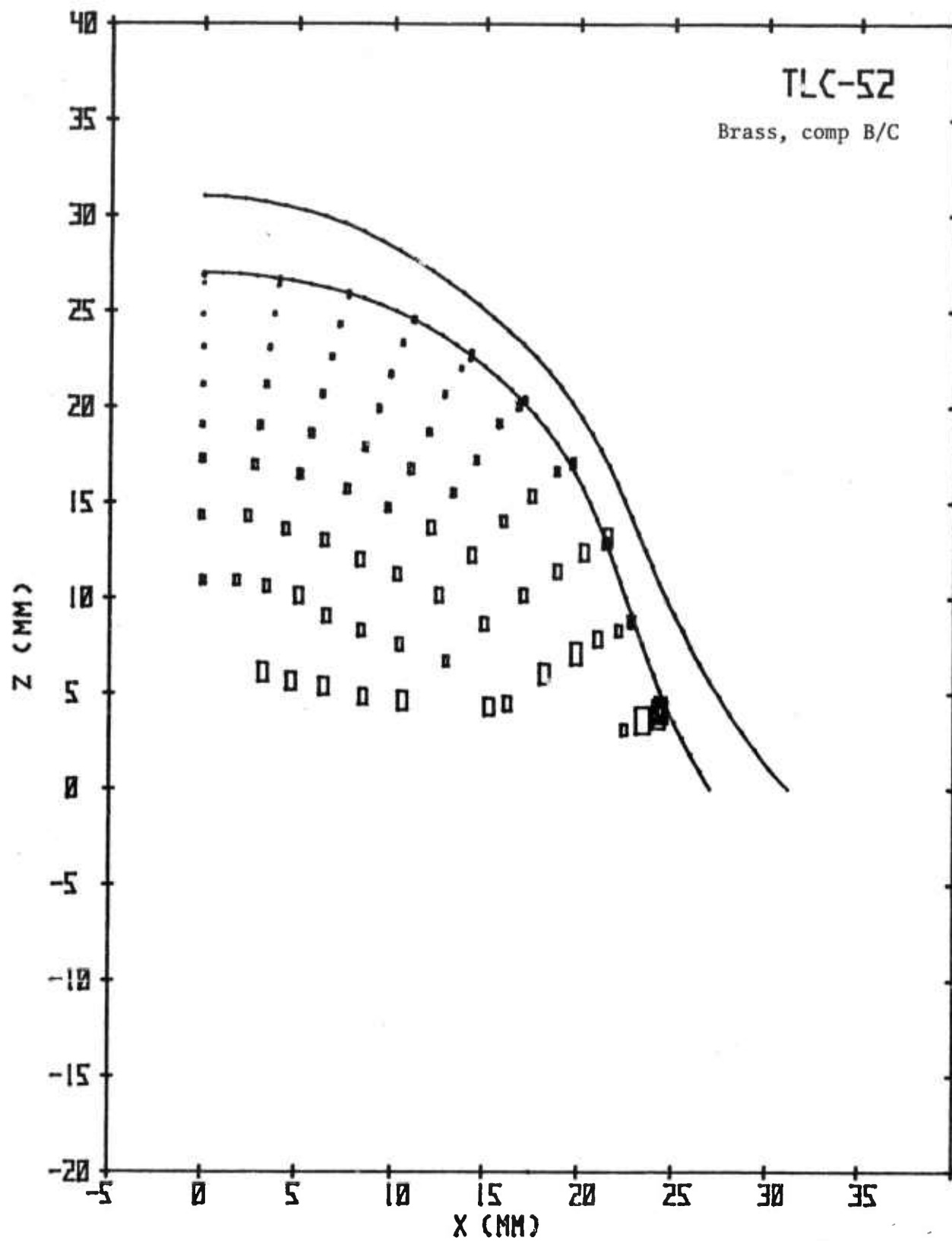
UNCLASSIFIED



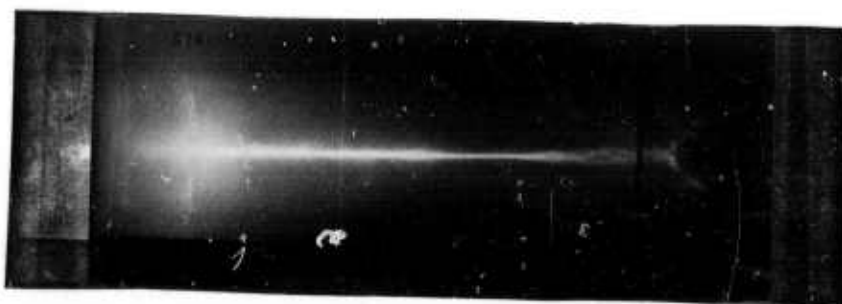
TLC-52

Brass, comp B/C

UNCLASSIFIED



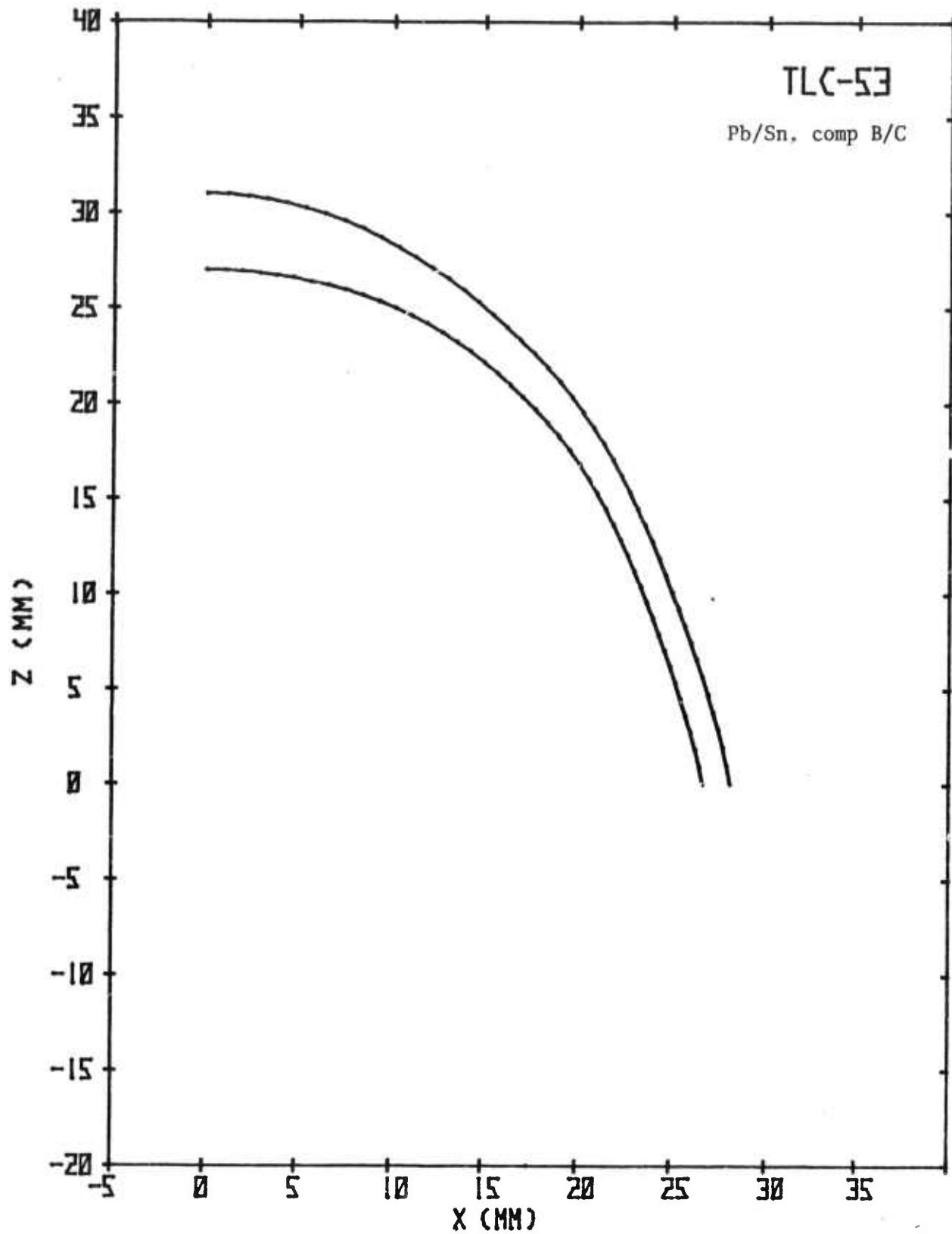
UNCLASSIFIED



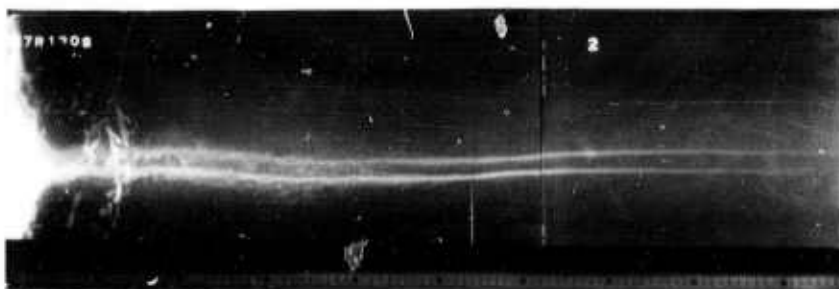
TLC-53

Pb/Sn, comp B/C

UNCLASSIFIED



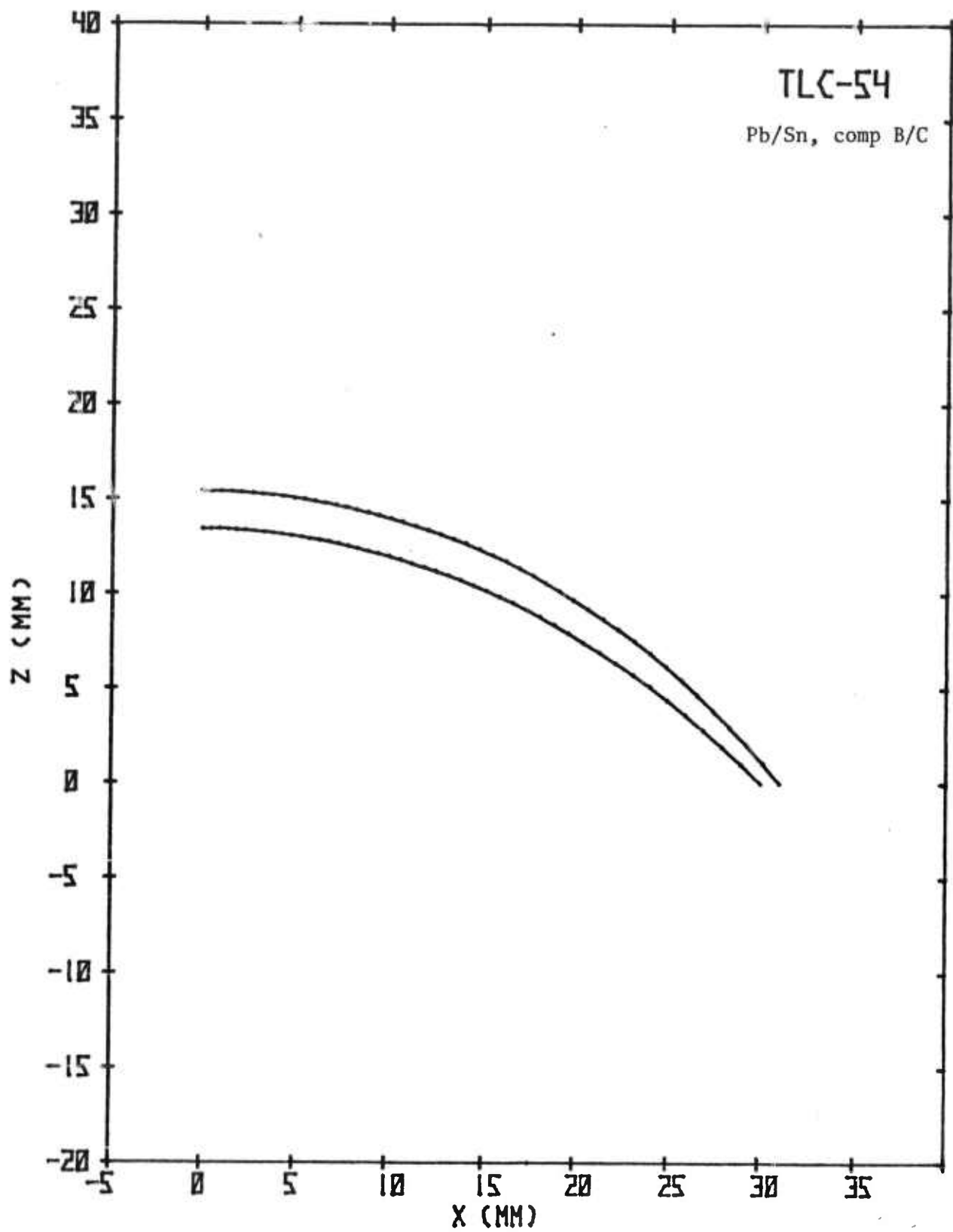
UNCLASSIFIED



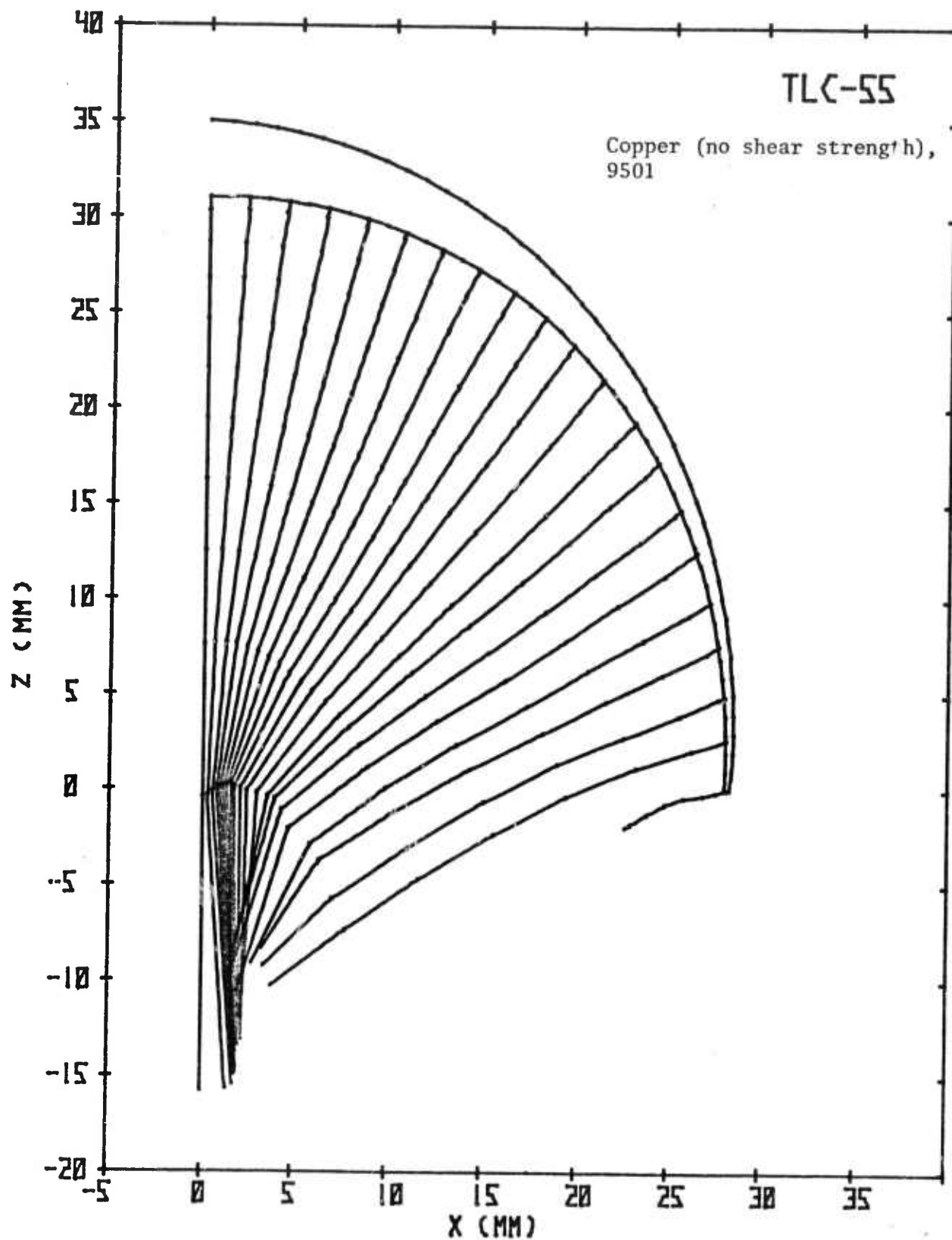
TLC-54

Pb/Sn, comp B/C

UNCLASSIFIED



CONFIDENTIAL
(This page is unclassified)

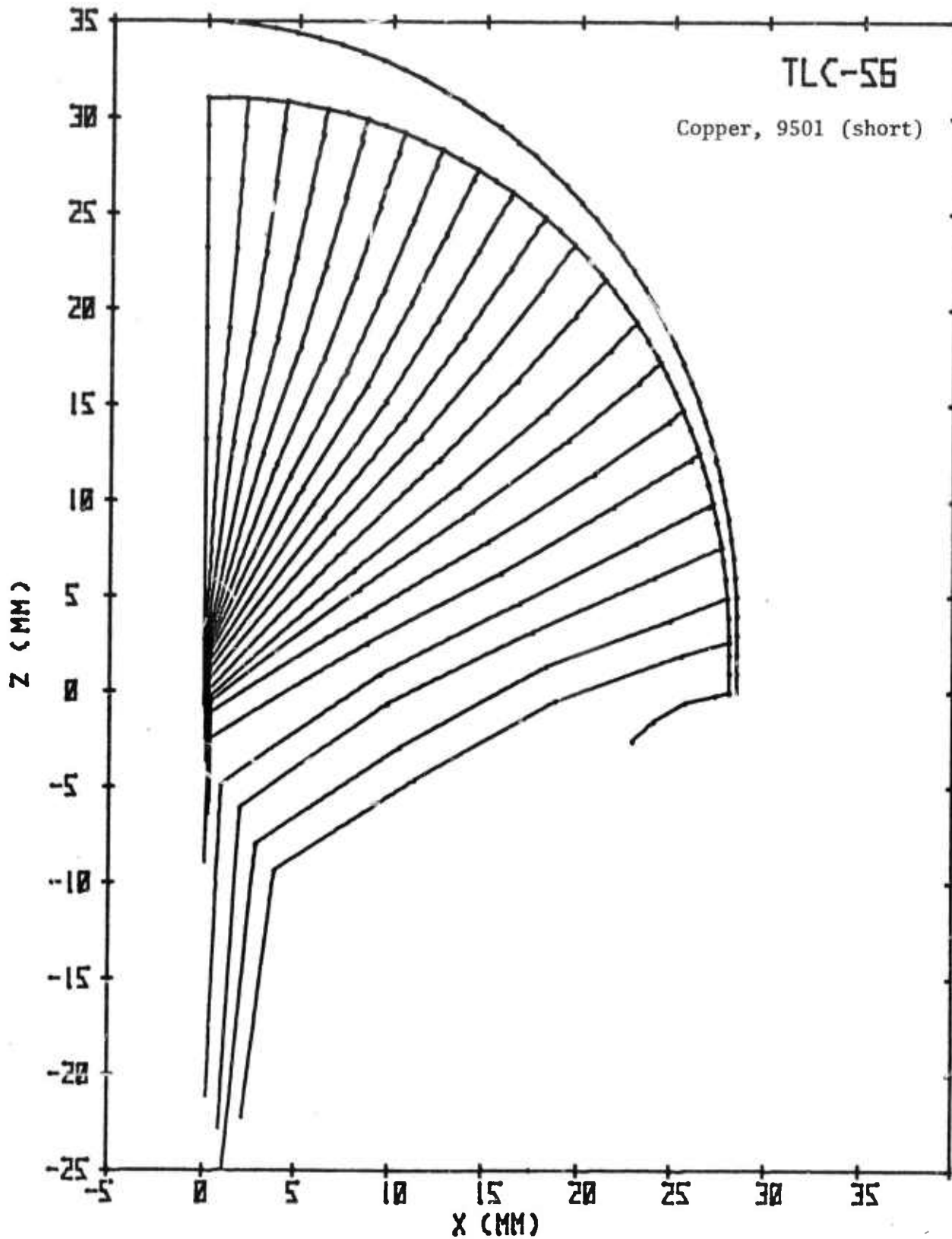


CONFIDENTIAL
(This page is unclassified)

UNCLASSIFIED

CONFIDENTIAL

(This page is unclassified)

**CONFIDENTIAL**

UNCLASSIFIED

(This page is unclassified)

THIS REPORT HAS BEEN DELIMITED
AND CLEARED FOR PUBLIC RELEASE
UNDER DOD DIRECTIVE 5200.20 AND
NO RESTRICTIONS ARE IMPOSED UPON
ITS USE AND DISCLOSURE.

DISTRIBUTION STATEMENT A

APPROVED FOR PUBLIC RELEASE,
DISTRIBUTION UNLIMITED.